

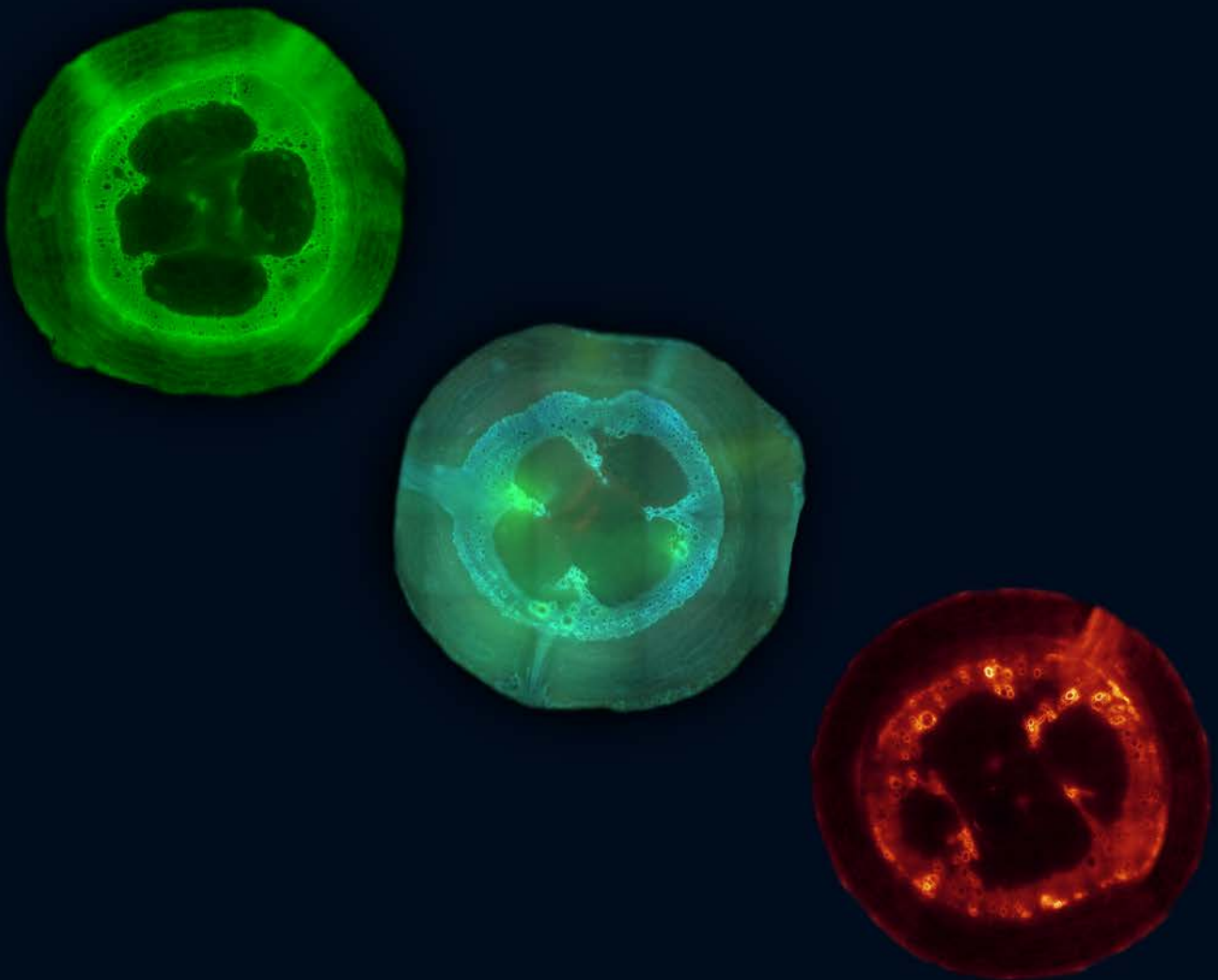
**ADVERTIMENT.** L'accés als continguts d'aquesta tesi queda condicionat a l'acceptació de les condicions d'ús establertes per la següent llicència Creative Commons:  [http://cat.creativecommons.org/?page\\_id=184](http://cat.creativecommons.org/?page_id=184)

**ADVERTENCIA.** El acceso a los contenidos de esta tesis queda condicionado a la aceptación de las condiciones de uso establecidas por la siguiente licencia Creative Commons:  <http://es.creativecommons.org/blog/licencias/>

**WARNING.** The access to the contents of this doctoral thesis it is limited to the acceptance of the use conditions set by the following Creative Commons license:  <https://creativecommons.org/licenses/?lang=en>

# PhD Thesis

## *Ralstonia solanacearum*-triggered defense responses at the tomato root xylem vasculature: Insights on the suberin pathway



**Anurag Kashyap**  
**2021**



Universitat Autònoma  
de Barcelona

***Ralstonia solanacearum*-triggered defense responses at the tomato root  
xylem vasculature: Insights on the suberin pathway**

**Anurag Kashyap**

Sota la direcció de: **Dra. Núria Sánchez Coll**

Tutoritzada per: **Dra. Roser Tolrà Pérez**

PER ACCEDIR AL GRAU DE DOCTOR DINS EL PROGRAMA DE DOCTORAT  
EN BIOLOGIA I BIOTECNOLOGIA VEGETAL DEL DEPARTAMENT DE  
BIOLOGIA ANIMAL, BIOLOGIA VEGETAL I ECOLOGIA

**Bellaterra, Abril 2021**

**Núria Sánchez Coll**, directora de la present tesi i científic titular del Consejo Superior de Investigaciones Científicas (CSIC), i **Roser Tolrà Pérez**, tutora de la present tesi i professora titular del Department de Biologia Animal, Biologia Vegetal i Ecologia a la Facultat de Biociències de la Universitat Autònoma de Barcelona, certifiquen:

Que la memòria titulada ***“Ralstonia solanacearum-triggered defense responses at the tomato root xylem vasculature: Insights on the suberin pathway”***, presentada per Anurag Kashyap amb la finalitat d’optar al grau de Doctor en Biologia i Biotecnologia Vegetal, ha estat realitzada sota la seva direcció i, considerant-la acabada, autoritzen la seva presentació perquè sigui jutjada per la comissió correspondent.

I perquè consti als efectes oportuns, signa la present a Bellaterra, a 23 de Abril de 2021.



Dra. Núria Sánchez Coll  
(Directora de la Tesi)



Dra. Roser Tolrà Pérez  
(Tutora de la de la Tesi)



Anurag Kashyap  
(Doctorand)





This PhD programme was funded by Netaji Subhas - Indian Council of Agricultural Research - International Fellowship. The work was also supported by a study leave granted to the author by Assam Agricultural University, Jorhat, Assam , India. Research work was funded by the Spanish Ministry of Economy and Competitiveness with grants 2016-78002-R (AGL) and RyC 2014-16158 (NSC), by the Ministry of Science and Innovation and Innovation State Research Agency PID2019-108595RB-I00/AEI/10.13039/501100011033, and through the “Severo Ochoa Programme for Centres of Excellence in R&D” (SEV-2015-0533 and and CEX2019-000902-S).

## ACKNOWLEDGEMENT

This doctoral dissertation would not have been possible without the guidance and the help of several individuals who in one way or another contributed and extended their valuable assistance in the preparation and completion of this study.

I express my sincere appreciation to my adviser, **Dr. Núria Sánchez Coll**, CSIC Scientist, Centre for Research in Agricultural Genomics (CRAG) for providing me all the support, guidance and resources to accomplish my research work. Many thanks for giving me the opportunity to do PhD study in her research group and for offering professional advice as well as encouragement.

I am thankful to **Dr. Marc Valls**, Associate Professor, University of Barcelona for sharing all his experiences and guiding me throughout the study.

I would like to express my gratitude to **Dr. Montserrat Capellades** for sharing her experiences and helping me in various technical aspects of the project.

**The Lab:** This work would not be possible without the support, help and guidance of all the fellow PhD students and post-doctoral scholars at Bacterial plant diseases and Plant cell death Lab, CRAG. The fond memories with all the lab mates will always be cherished. **Marc Planas**, he is gem of a person and his contribution towards my all-round well-being in Spain is immense. Things would have been tougher for me, if I haven't had his support. I am thankful to him for the numerous techniques that he demonstrated to me in my initial days in the lab. **Eugenia**, she is one of the kindest person I have ever known. She is extremely cheerful and her presence brings good vibes to the lab atmosphere. So many things I learnt from her regarding research and above all the art of staying motivated. I wish her the best for the remaining time in her PhD program. **Pau**, I thank him for being a true companion in my times in Spain. He is a highly motivated person, full of ideas. So many wonderful moments we shared together as we sailed through our PhD journey. **Roger**, he is an excellent team player. Many thanks to him for help in statistics and R program. I wish him all the best for his PhD research, which I am sure, will be a very productive one. **Jose**, so many enchanting discussions during our breaks from lab works, on science and life beyond PhD. It's was a pleasure to work with him all these years and thankful to him for guiding me in molecular biology works. **Ujjal**, it's a great coincidence that we two Assamese (both from Jorhat town) got the opportunity to work together in Barcelona. I

am thankful to him for sharing his expertise in plant molecular biology and providing inputs in my project. **Nerea** and **Weiqi**, I thank them for all their help, it's been a great pleasure to work with them both. I wish all success in their respective PhD projects. I am also thankful to past members of the lab: **Alex**, **Saul**, **Marina**, **Liang Li**, **Liang Yang**, **Jonathan** and **Agnese**. It's been a great learning experience to work with all of them.

**CRAG services:** I would like to express my sincere thankfulness to **Montse Amenos** for her help in microscopy and CRAG Plant Growth services (**Gloria**, **Eva**, **Carlos** and entire team) for their help in growing and maintenance of the plants.

I would like also to express my gratitude to the collaborators **Dr. Jorge Rencoret** from Institute of Natural Resources and Agrobiology of Seville (IRNAS), CSIC, Seville, Spain and to **Dr. Anna Laromaine** and **Sumithra Srinivasan** from Institute of Material Science of Barcelona (ICMAB), CSIC, Campus UAB, Bellaterra, Spain.

**ICAR:** I would like to express my gratitude to Indian Council of Agricultural Research (ICAR) for awarding me with **Netaji Subhas ICAR International fellowship**. This fellowship has contributed a lot to my career in terms of knowledge gained and skills learnt.

**AAU:** I am thankful to **Assam Agricultural Univeristy** for providing me three years study leave, for completion of PhD studies. I am highly indebted to **Dr. B.C. Beka**, Vice- Chancellor, Assam Agricultural Univeristy and **Dr. K.M. Bujarbaruah**, Former Vice- Chancellor, Assam Agricultural Univeristy for their guidance and support during the entire PhD studies. My warm thanks are due to **Dr. J. Deka**, Dean, Faculty of Agriculture, AAU; **Dr. A. Bhattacharyya**, Director of Research (Agri.) for their help and support during my PhD studies. I owe my most sincere gratitude to **Dr P.D. Nath**, Professor, Department of Plant Pathology, AAU for his constant guidance, support and care all throughout my study period.

**Family:** My **mom** and **dad**, they are my constant source of support. Their love, care and untiring effort to ensure an all-round well-being to myself, cannot be adequately acknowledged in words. This work has seen the light of the day because of their blessings. My wife **Munmi**, her contribution towards this thesis is immense. She stood as a pillar of strength providing me moral support all throughout my stay abroad. I also thank my mother-in-law for her love and blessings. My brother **Supratim**, sister-in-law **Mitali** and nephew **Adreet**, they have been a constant source of support and thanks to their encouragement all throughout the study period. I

thank my uncles **Aparesh, Paramesh, Iswar** and Aunt **Rita** for regularly enquiring about my well-being, while my stay abroad.

Last but not the least, a heartfelt thanks goes to all other members of my family, friends and well-wishers, and to the Almighty God, for giving me the strength and showing me the right path.

Anurag Kashyap  
April, 2021

# SUMMARY

---

## SUMMARY IN ENGLISH

*Ralstonia solanacearum* is one of the world's most devastating bacterial pathogens of plants. This soil-borne bacterium is the causative agent of bacterial wilt on more than 450 plant species, and it causes severe devastation on Solanaceous crops like tomato. *R. solanacearum* gains access to the root system through wounds and lateral root emerging sites and then moves to the root vasculature, where it multiplies in the xylem and later spreads vertically within the xylem sap and horizontally between vessels and to the surrounding tissues. To date, the most reliable management strategy to control *R. solanacearum* has been the use of genetic resistance. In tomato, among the best resistance sources is the resistant cultivar Hawaii 7996 (H7996), which is commonly used as a rootstock in commercial tomato cultivation. This resistant cultivar has evolved effective defense mechanisms to prevent vessel colonization or movement between vessels once vascular colonization has occurred.

Recent reports show that the root xylem vascular cylinder acts as a predominant tissue for mounting an efficient defense response against vascular invaders, restricting onward movement of the pathogen to the aerial tissue. However, the mechanisms regulating this form of resistance remain elusive. Unravelling the mechanisms through which the plants block or slow down pathogen progression at the root xylem vasculature can be vital in the development of resistant cultivars by biotechnological interventions. Hence, in this thesis we attempted to shed light on the defense responses acting at the root xylem vasculature that effectively restrict colonization by the vascular bacterial pathogen *R. solanacearum* in tomato.

Comparative histopathological studies in resistant and susceptible tomato lines indicated that a ferulate vascular reinforcement, culminating into a ferulo-suberin zone, may act as a strong physico-chemical barrier against *R. solanacearum* invasion (Chapter 1). This phenolic- aliphatic barrier reinforces the walls of xylem vascular tissue in H7996 and may restrict movement of the bacterium from the xylem vessel lumen to the surrounding xylem

---

parenchyma cells and nearby vessels and inter-cellular spaces. Compositional changes in walls were studied using spectroscopy, which showed strong accumulation of suberin-compatible metabolites specifically in roots of resistant H7996, upon infection of *R. solanacearum* (Chapter 2). Differences in the polymerization state of lignin in roots were observed after infection between resistant and susceptible tomato. H7996 contained a higher proportion of G-type lignin, which is more resistant to degradation, whereas susceptible Marmande contained more S-type lignin, which is more prone to degradation. Expression of genes from the suberin fatty acid biosynthetic pathway was significantly upregulated in the taproot xylem vascular tissue of H7996 infected plants compared to the mock controls or susceptible tomato (Chapter 3). This indicates that upregulation of these genes is a specific response of resistant H7996 plants that takes place in suberizing vasculature upon *R. solanacearum* infection. Further, induction of *Pro<sub>SIFHT</sub>::GUS* was observed in taproot xylem vasculature of infected H7996 plants, as well as in tissues known to deposit suberin such as epidermis, exodermis and tissues undergoing wound healing.

Implications of overexpressing genes from pathway of suberin and the associated soluble phenolics synthesis, were evaluated in susceptible tomato background. Overexpression of suberin feruloyl transferase (*FHT*), which catalyzes the formation feruloyl esters showed limited restriction against *R. solanacearum*. In contrast, overexpression of tyramine N-hydroxycinnamoyltransferase (*THT 1-3*), responsible for synthesis of hydroxycinnamic acid amides (HCAA) such as feruloyl tyramine resulted in an increase of resistance against *R. solanacearum* with disease progressing remarkably slower in this line compared to wild type plants. Accumulation of such soluble aminated phenolics may act as a chemical barrier initially acting as phytoalexin but could also act as physical barrier if cross-linked to the lignin-like poly-aromatic domain of suberin. Hence, our data show that genes responsible for synthesis of HCAA can be used for metabolic engineering resistance against *R. solanacearum*.

---

## RESUMEN CATALÀ

*Ralstonia solanacearum* és un dels patògens bacterians de plantes més devastadors del món. Aquest bacteri és l'agent causant del marciment bacterià en més de 450 espècies de plantes i causa una devastació severa en cultius de solanàcies com la tomaquera. *R. solanacearum* accedeix a sistema radicular a través de ferides i llocs d'emergència d'arrels laterals i després es desplaça fins a la vasculatura radicular, on es multiplica al xilema i després es dissemina verticalment a través del xilema i horitzontalment entre els vasos i els teixits circumdants. Fins ara, l'estratègia de maneig més fiable per controlar *R. solanacearum* ha estat l'ús de resistència genètica. En tomàquet, entre les millors fonts de resistència es troba el conrear resistent Hawaii 7996 (H7996), que s'usa comunament com a patró en el cultiu comercial de tomàquet. Aquesta varietat resistent ha desenvolupat mecanismes de defensa efectius per prevenir la colonització de vasos o el moviment entre vasos un cop que ha passat la colonització vascular.

Publicacions recents mostren que el cilindre vascular del xilema de l'arrel actua com a teixit predominant per muntar una resposta de defensa eficaç contra els invasors vasculars, restringint l'avanç del patogen cap al teixit aeri. No obstant això, els mecanismes que regulen aquesta forma de resistència segueixen sent desconeguts en gran manera. Desentranyar els mecanismes a través dels quals les plantes bloquegen o alenteixen la progressió de patògens en la vasculatura del xilema de l'arrel pot ser vital en el desenvolupament de varietats resistents mitjançant intervencions biotecnològiques. Per tant, en aquesta tesi intentem aprofundir en les respostes de defensa que actuen en la vasculatura del xilema de l'arrel que restringeixen efectivament la colonització pel patogen bacterià vascular *R. solanacearum* en tomàquet.

Els estudis histopatològics comparatius en línies de tomàquet resistents i susceptibles indiquen que un reforç vascular compost de ferulats, que culmina en la formació d'una zona ferulo-suberínica que pot actuar com una forta barrera fisico-química contra la invasió de *R. solanacearum* (Capítol 1). Aquesta barrera fenòlic-alifàtica reforça les parets del teixit vascular del xilema en H7996 i pot restringir el moviment del bacteri des de l'interior del vas del xilema cap al xilema circumdant, cèl·lules de l'parènquima,



---

vasos propers i espais intercel·lulars. Els canvis de composició en les parets es van estudiar mitjançant espectroscòpia, la qual cosa va mostrar una intensa acumulació de metabòlits compatibles amb la suberina específicament en les arrels de H7996 resistent, després de la infecció de *R. solanacearum* (Capítol 2). Es van observar diferències en l'estat de polimerització de la lignina en les arrels després de la infecció entre tomàquet resistent i susceptible. L'H7996 contenia una major proporció de lignina de tipus G, que és més resistent a la degradació, mentre que Marmande susceptible contenia més lignina de tipus S, que és més propensa a degradar-se. L'expressió de gens de la via biosintètica d'àcids grassos de la suberina es va incrementar significativament en el teixit vascular de l'xilema de l'arrel primària de les plantes infectades amb H7996 en comparació amb els controls o el tomàquet susceptible (Capítol 3). Això indica que la regulació positiva d'aquests gens és una resposta específica de plantes H7996 resistents que té lloc a la vasculatura suberitzada després de la infecció per *R. solanacearum*. A més, es va observar inducció de *ProSIFHT::GUS* en la vasculatura del xilema de l'arrel principal de les plantes H7996 infectades, així com en teixits que se sap que dipositen suberina com ara epidermis, exodermis i teixits que experimenten cicatrització de ferides.

Es van avaluar les implicacions de la sobreexpressió de gens de la via de biosíntesi de la suberina i de la síntesi de fenòlics solubles associats, en varietats de tomàquet susceptible. La sobreexpressió de suberin feruloil transferasa (*FHT*), que catalitza la formació de feruloil èsters, va mostrar una restricció limitada contra *R. solanacearum*. Per contra, la sobreexpressió del tiramina N-hidroxicinamoiltransferasa (*THT 1-3*), responsable de la síntesi de amides d'àcid hidroxicinàmic (HCAA) com la feruloil tiramina, va donar com a resultat un augment molt marcat de la resistència contra *R. solanacearum* i la malaltia va progressar notablement més lentament en aquesta línia en comparació amb les plantes de tipus salvatge. L'acumulació d'aquests compostos fenòlics aminats solubles pot actuar com una barrera química que actua inicialment com fitoalexina, però també podria actuar com una barrera física si s'associés amb el domini poliaromàtic de la suberina. Per tant, les nostres dades mostren que l'augment controlat dels gens responsables de la síntesi de HCAA es pot utilitzar com a estratègia d'enginyeria metabòlica per augmentar la resistència contra *R. solanacearum* a tomaquera.

# INDEX

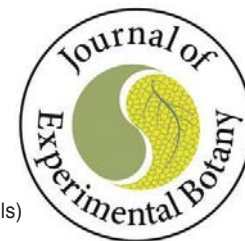
1. <b>Introduction</b> .....	1
Publication: Blocking intruders: inducible physico-chemical barriers against plant vascular wilt pathogens (Review)	
1.1 Invasion strategies used by vascular wilt pathogens.....	2
1.2 Immunity against vascular wilt pathogens .....	2
1.3 Inducible structural barriers to restrict the spread of vascular wilt pathogens.....	3
1.4 Vertical restriction of vascular colonization.....	4
1.4.1 Formation of tyloses .....	4
1.4.2 Deposition of gels .....	6
1.5 Horizontal restriction of vascular colonization .....	7
1.5.1 Deposition of lignin .....	7
1.5.2 Deposition of suberin.....	9
1.5.3 Deposition of callose.....	10
1.6 Concluding remarks and future prospects .....	11
1.7 Background of the study .....	16
<b>Objectives</b> .....	18
2. <b>Chapter 1:</b> Structural modifications of root xylem vasculature as defense response to <i>Ralstonia solanacearum</i> in tomato .....	19
2.1 Introduction .....	19
2.2 Results & discussion .....	21
3. <b>Chapter 2:</b> Spectroscopic analysis of physico-chemical barriers induced at roots upon <i>Ralstonia solanacearum</i> infection .....	48
3.1 Introduction .....	48
3.2 Results & discussion .....	49
4. <b>Chapter 3:</b> Characterization of genes responsible for ferulo-suberin barrier formation in tomato root defense against <i>Ralstonia solanacearum</i> .....	58

4.1 Results & discussion .....	58
<b>5. Discussion .....</b>	<b>92</b>
5.1 Thesis overview .....	92
5.2 <i>R. solanacearum</i> -triggers a phenolic wall reinforcement at root xylem vasculature of resistant H7996.....	94
5.3 A suberization zone at xylem vasculature acts as a physico-chemical barrier against <i>R. solanacearum</i> colonization .....	95
5.4 <i>R. solanacearum</i> infection induces a metabolic and genetic reprogramming towards vascular suberization in resistant H7996 .....	99
5.5 <i>FHT</i> overexpression in susceptible tomato had a minor effect on <i>R.</i> <i>solanacearum</i> colonization.....	101
5.6 <i>THT 1-3</i> overexpression in susceptible tomato background offers high degree of colonization restriction to <i>R. solanacearum</i> .....	102
<b>6. Conclusion .....</b>	<b>103</b>
<b>7. Materials &amp; Methods .....</b>	<b>106</b>
<b>References .....</b>	<b>115</b>
<b>Annex .....</b>	<b>125</b>
Publication : Four bottlenecks restrict colonization and invasion by the pathogen <i>Ralstonia solanacearum</i> in resistant tomato.....	125
Submitted article: A primary cell wall cellulose-dependent defense mechanism against vascular pathogens revealed by time-resolved dual-transcriptomics.....	140

## LIST OF ABBREVIATIONS

Abbreviation	Description of the term
2D	Two dimensional
BAR	Botany array resource
CFU	Colony forming unit
DAMP	Damage-associated molecular pattern
DPI	Days post inoculation
EPS	Exopolysaccharide
ETI	Effector-triggered immunity
FHT	Feruloyl transferase
FT-IR	Fourier transform infrared
GFP	Green fluorescent protein
GUS	$\beta$ -glucuronidase
H7996	Tomato cultivar 'Hawaii 7996'
HA	Hemagglutinin
HCAA	Hydroxycinnamic acid amides
HCl	Hydrochloric acid
HR	Hypersensitive response
HSQC	Heteronuclear single quantum coherence
KOH	Potassium hydroxide
MAMP	Microbe-associated molecular pattern
NLR	Nucleotide-binding leucine-rich repeat proteins
NMR	Nuclear magnetic resonance
PAMP	Pathogen-associated molecular pattern
Pro	Promoter
PRR	Pattern recognition receptor
PTI	PAMP-triggered immunity
qPCR	Quantitative Polymerase chain reaction
QTL	Quantitative trait loci
RLK	Receptor-like kinase
ROS	Reactive oxygen species
SEM	Scanning electron microscope
SEM-EDX	SEM- energy-dispersive X-ray
THT	Tyramine N-hydroxycinnamoyltransferase
UFs	Unsaturated fatty acids
UV	Ultraviolet
Wt	Wild type

# **INTRODUCTION**



*Journal of Experimental Botany*, Vol. 72, No. 2 pp. 184–198, 2021  
doi:10.1093/jxb/eraa444 Advance Access Publication 25 September 2020

This paper is available online free of all access charges (see <https://academic.oup.com/jxb/pages/openaccess> for further details)

DARWIN REVIEW

# Blocking intruders: inducible physico-chemical barriers against plant vascular wilt pathogens

Anurag Kashyap<sup>1</sup>, Marc Planas-Marquès<sup>1</sup>, Montserrat Capellades<sup>1</sup>, Marc Valls<sup>1,2</sup> and Núria S. Coll<sup>1,\*</sup>

<sup>1</sup> Centre for Research in Agricultural Genomics (CSIC-IRTA-UAB-UB), Bellaterra, Spain

<sup>2</sup> Genetics Department, Universitat de Barcelona, Barcelona, Spain

\* Correspondence: [nuria.sanchez-coll@cragenomica.es](mailto:nuria.sanchez-coll@cragenomica.es)

Received 29 July 2020; Editorial decision 11 September 2020; Accepted 16 September 2020

Editor: Donald Ort, University of Illinois, USA

## Abstract

Xylem vascular wilt pathogens cause devastating diseases in plants. Proliferation of these pathogens in the xylem causes massive disruption of water and mineral transport, resulting in severe wilting and death of the infected plants. Upon reaching the xylem vascular tissue, these pathogens multiply profusely, spreading vertically within the xylem sap, and horizontally between vessels and to the surrounding tissues. Plant resistance to these pathogens is very complex. One of the most effective defense responses in resistant plants is the formation of physico-chemical barriers in the xylem tissue. Vertical spread within the vessel lumen is restricted by structural barriers, namely, tyloses and gels. Horizontal spread to the apoplast and surrounding healthy vessels and tissues is prevented by vascular coating of the colonized vessels with lignin and suberin. Both vertical and horizontal barriers compartmentalize the pathogen at the infection site and contribute to their elimination. Induction of these defenses are tightly coordinated, both temporally and spatially, to avoid detrimental consequences such as cavitation and embolism. We discuss current knowledge on mechanisms underlying plant-inducible structural barriers against major xylem-colonizing pathogens. This knowledge may be applied to engineer metabolic pathways of vascular coating compounds in specific cells, to produce plants resistant towards xylem colonizers.

**Keywords:** Gels, inducible defenses, lignin, physico-chemical barriers, plant-pathogen interactions, structural defenses, suberin, tyloses, vascular pathogens, wilt

## Introduction

The plant immune system has been shaped by hundreds of millions of years of interactions with microbial pathogens that are constantly trying to evade or overcome host plant defense reactions. Pathogens that colonize the xylem - a vital component for transporting water and minerals from the roots to the aerial parts - are particularly pernicious, causing major destruction in numerous host plants worldwide (Yadeta and Thomma,

2013). Despite the xylem being nutritionally poor in comparison with other plant tissues, a select group of pathogens comprising a few genera of bacteria, fungi and oomycetes, have evolved to target this plant tissue as a niche for colonization. Proliferation of these wilt pathogens causes massive disruption in the xylem vessels through the production of toxins, exopolysaccharides, hyphal mass, conidia and other pathogen

propagules that cause destruction as well as physical occlusion of xylem elements, resulting in severe wilting and plant death (Zaini *et al.*, 2018).

### *Invasion strategies used by vascular wilt pathogens*

Vascular plant pathogens utilize diverse strategies to get access into the vessels. Vascular wilt pathogenic fungi (*Fusarium oxysporum*, *Verticillium albo-atrum*, *Verticillium dahliae*, *Ceratocystis fimbriata*, *Ophiostoma novo-ulmi*), oomycetes (*Pythium* spp) or the soil-borne bacterium *Ralstonia solanacearum* invade plant roots and advance inter- or intracellularly through the root cortex to reach the xylem, where they proliferate and spread systemically to aerial plant parts (Bae *et al.*, 2015). In order to get access into the vasculature, these pathogens generally target root extremities and the junction between primary and lateral roots where the epidermal barrier may be compromised, and the endodermis as well as Casparian strip are either not fully differentiated or reoriented by outgrowth of lateral roots (Vasse *et al.*, 1995; Álvarez *et al.*, 2010).

In contrast to these root invaders, many vascular bacteria, such as *Xylella fastidiosa*, are directly inoculated into the xylem by insect vectors that feed on the plant host (Wang *et al.*, 2017). Furthermore, a few species of vascular bacteria reach the xylem tissues via natural plant openings in the aerial parts of the plant, such as leaf hydathodes (*Xanthomonas oryzae* pv. *Oryzae*; Pradhan *et al.*, 2012), flower nectarhodes (*Erwinia amylovora*; Bubán *et al.*, 2003) or stem lenticels (*Pseudomonas syringae* pv. *actinidiae*; Renzi *et al.*, 2012). These bacteria multiply in intercellular spaces before eventually colonizing the xylem vessels. Moreover, there are vascular wilt pathogens which are transmitted through graft-infected rootstock/scion, as has been reported for the fungus *Ceratocystis fagacearum* on oak trees (Blaedow and Juzwik, 2010), or the bacterium *X. fastidiosa* on pecan (Sanderlin and Melanson, 2006). Another method of infection of vascular wilt pathogens occurs through the use of infected mother plants as a source for clonal propagation. This affects many plant species cultivated in nurseries, such as strawberry plants infected with *Fusarium oxysporum* f. sp. *fragariae* (Pastrana *et al.*, 2019), olive plants infected with *V. dahliae* (Morello *et al.*, 2016), and it is also common in grapevine mother plants that can harbor various vascular wilt fungi (Gramaje *et al.*, 2018).

### *Immunity against vascular wilt pathogens*

Plants are protected against pathogens by a well-orchestrated immune system (Jones and Dangl, 2006). Pattern-triggered immunity (PTI) is initiated upon recognition of conserved microbial features at the plasma membrane by pattern-recognition receptors (PRRs) in the plant. Effector-triggered immunity (ETI) is activated by recognition of pathogen-secreted effectors via intracellular nucleotide-binding leucine-rich repeat

proteins (NLRs). ETI is commonly known as a stronger immune response, while PTI offers durable and broad-spectrum resistance (Katagiri and Tsuda, 2010). Yet, these two layers of immunity operate synergistically, converging on several downstream responses including the oxidative burst, activation of kinase signaling cascades, expression of defense-related genes and accumulation of physico-chemical barriers (Thomma *et al.*, 2011; Ngou *et al.*, 2020, Preprint; Yuan *et al.*, 2020, Preprint).

Although PTI and ETI function in the interactions of plants with vascular pathogens, there are very few cases where these processes have been analyzed specifically in the xylem and surrounding tissues of infected plants. Several recent studies have shown that PTI can be triggered in plants by treatment or over-expression of conserved molecular patterns present in wilt pathogens. For example, an extracellular polysaccharide from the wilt bacterium *R. solanacearum* has been shown to act as a PTI elicitor in resistant tomato, leading to induced expression of defense response genes (Milling *et al.*, 2011; Prakasha *et al.*, 2017). Furthermore, in *Nicotiana benthamiana* and tomato, PTI is triggered upon perception of the COLD SHOCK PROTEIN 22 (csp22) peptide from *R. solanacearum* by the PRR COLD SHOCK PROTEIN RECEPTOR (CORE; Wang *et al.*, 2016). In accordance, treatment of tomato with csp22 conferred increased resistance to *R. solanacearum* in tomato plants. Additionally, transgenic *Arabidopsis thaliana* plants expressing the tomato csp22 receptor (SICORE) gained the ability to respond to csp22 and were more resistant to *R. solanacearum* infection (Wei *et al.*, 2018). Similarly, *V. dahliae*, possesses two cellulose-degrading glycoside hydrolase family 12 (GH12) proteins, namely VdEG1 and VdEG3, which in *N. benthamiana* are recognized by the PRR complexes LRR-RLP (Leucine Rich Repeat-Receptor-Like Protein)/SOBIR1/BAK1 (SUPPRESSOR OF BAK1-INTERACTING RECEPTOR-LIKE KINASE 1-1/BRASSINOSTEROID-INSENSITIVE 1-ASSOCIATED RECEPTOR KINASE) and LRR-RLKs (Receptor-Like Kinase)/BAK1, respectively, thereby triggering PTI responses (Gui *et al.*, 2017).

Concomitantly, some bacterial wilt pathogens have evolved modifications in the sequences of their conserved patterns, so that they are no longer recognizable by cognate PRRs. This occurs in *X. fastidiosa*, which contains a lipopolysaccharide featuring a masking motif that evades recognition by grapevine (Radicavoli *et al.*, 2018), or flagellin from *R. solanacearum*, with a polymorphic sequence that avoids perception by many host plants (Wei *et al.*, 2020).

An interesting emerging concept is that roots may be relatively insensitive to most conserved molecular patterns, which may prevent mounting defense responses against commensal organisms in an environment such as the soil, full of microbes. Underlying this phenomenon, it has been recently shown that root PTI is only activated upon local tissue damage (Zhou *et al.*, 2020). This work convincingly shows how localized cell



death upregulates PRR expression in the neighboring cells, leading to restricted responsiveness to conserved molecular patterns of root invaders (Zhou *et al.*, 2020).

ETI responses against vascular pathogens have also been documented in the literature. For instance, in the interaction between tomato and the vascular wilt fungus *F. oxysporum* f. sp. *lycopersici*, several R protein-effector pairs have been identified. The NLR I2 perceives the Avr2 effector; I, a receptor-like protein with an extracellular LRR domain (LRR-RLP) perceives Avr1; and I3, a S-receptor-like kinase (SRLK) perceives Avr3 (Houterman *et al.*, 2009; Catanzariti *et al.*, 2015, 2017). Interestingly, the I2 gene is primarily expressed in the xylem vascular tissue, probably partly explaining why the fungus reaches the vasculature before being contained in an incompatible interaction (van der Does *et al.*, 2019; Mes *et al.*, 2000). Similarly, effector AvrFom2 from *F. oxysporum* f. sp. *melonis* is perceived by the NLR Fom-2 in melon (Joobeur *et al.*, 2004). On the other hand, the effector Ave1 from *V. albo-atrum* induces resistance in several plant species, mediated by the receptor-like protein Ve1 (de Jonge *et al.*, 2012; Song *et al.*, 2018).

With respect to bacterial vascular wilt pathogens, the RRS1-R/RPS4 (Resistance to *Ralstonia solanacearum* 1-Recessive/Resistant to *Pseudomonas syringae* 4) NLR pair in Arabidopsis mediates immunity against *R. solanacearum* carrying the PopP2 effector (Deslandes *et al.*, 2002; Le Roux *et al.*, 2015; Sarris *et al.*, 2015). The rice LRR-RLK protein Xa21 confers broad-spectrum immunity to *X. oryzae* pv. *oryzae*, mediated through recognition of the small protein Ax21 (Park and Ronald, 2012). In addition, the rice NLR Xo1 recognizes the transcription activator-like effector Tal2H from *X. oryzae* pvs. *oryzicola* and *oryzae* (Triplett *et al.*, 2016). Similarly, the NLR Bs4 in tomato perceives the avirulence protein AvrBs4 from *Xanthomonas campestris* pv. *vesicatoria* (Schornack *et al.*, 2004). Furthermore, the Arabidopsis NLR ZAR1 (HOPZ-ACTIVATED RESISTANCE 1) recognizes the *X. campestris* effector AvrAC/XopAC by forming a complex with PBL2 (PROBABLE SERINE/THREONINE-PROTEIN KINASE 2), which acts as a decoy, and RKS1 (RESISTANCE-RELATED kinase 1), a pseudokinase (Wang *et al.*, 2015).

Besides individual examples of *R* genes, quantitative traits have been shown to underscore immunity against xylem colonizers in many different hosts. Stable resistance towards *R. solanacearum* in tomato is controlled by two major quantitative trait loci (QTLs), namely *Bwr-6* and *Bwr-12*, located in chromosomes six and twelve, respectively, and three minor QTLs, *Bwr-3*, *Bwr-4* and *Bwr-8* (Thoquet *et al.*, 1996; Mangin *et al.*, 1999; Wang *et al.*, 2000, 2013; Carmeille *et al.*, 2006). Some of these loci have been shown to be strain and/or environment-specific, and involve an extremely complex genetic basis of resistance. Similarly, QTLs for *Fusarium* wilt resistance have been mapped in several hosts such as chickpea (Sabbavarapu *et al.*, 2013), cotton (Ulloa *et al.*, 2013; Wang *et al.*,

2018), and watermelon (Lambel *et al.*, 2014). QTLs termed RESISTANCE TO FUSARIUM (*RFO1-RFO7*) have been identified in Arabidopsis that provide broad spectrum immunity to multiple *formae speciales* of *F. oxysporum* (Chen *et al.*, 2014). *RFO1* was found to encode a wall-associated kinase-like kinase 22 (WAKL22) and *RFO2* encodes a receptor-like protein (Diener and Ausubel, 2005). Likewise, resistance to *Verticillium* correlates with mapping of QTLs in several hosts such as strawberry (Antanaviciute *et al.*, 2015) and cotton (Palanga *et al.*, 2017). A major QTL conferring resistance to *X. fastidiosa* was identified in a *Vitis arizonica* linkage map and named as ‘Pierce’s disease resistance 1’ (PdR1), which has been introgressed into commercial cultivars (Krivanek *et al.*, 2006). However, the majority of available QTL mapping data for wilt resistance traits lack resolution. This may be partly due to the high sensitivity of wilt development to temperature variation, and also due to the fact that wilt resistance comprises a complex array of multilayered mechanisms involving the coordinated action of different plant tissues or cell types (Bani *et al.*, 2018). Importantly, this extremely complex polygenic and quantitative resistance underscores the structural physico-chemical defense mechanisms induced by vascular pathogens in resistant plants.

### Inducible structural barriers to restrict the spread of vascular wilt pathogens

Inducible structural barriers formed at and around the vasculature upon colonization constitute one of the most important defense components against wilt diseases. If a pathogen manages to reach the xylem, this transport system becomes an excellent channel of inoculum dissemination throughout the plant. As a consequence, plants have evolved effective structural defense mechanisms to prevent vessel colonization or movement between vessels once vascular colonization has occurred (Beckman and Roberts, 1995). Timely formation of these physico-chemical vascular barriers early upon pathogen perception can lead to confinement of the vascular pathogen at the infected vessel, avoiding the spread of wilt diseases (Robb *et al.*, 2007; Zaini *et al.*, 2018; Planas-Marquès *et al.*, 2019).

Some of these structural reinforcements induced by pathogens were already reported in classic botanical studies in the 19th century (Zimmermann, 1979). Moreover, during the 1980s and 1990s, they were intensely studied from anatomical and biochemical points of view, as they were recognized as important components of defense reactions (Newcombe and Robb, 1988; Nicholson, 1992; Niemann, 1994). In trees, the sequential response to confine fungal pathogen progression or tissue damage at the site of infection or injury was initially explained by the CODIT model (compartmentalization of decay in trees; Shigo and Marx, 1977). The model described four “walls” or barriers pre-formed or formed in response to wounding, that restrict pathogen colonization. In particular,



wall 1 defined vessel plugging structures formed as a response to vascular wilt pathogen invasion.

However, most of the research in the field of plant-pathogen interactions started refocusing during the 1990s when *Arabidopsis* gained momentum as a model species. This led to the identification of striking similarities between plant and animal immune systems, the type III secretion system in bacteria being discovered, and *avr-R* gene pairs being identified as a corollary of Flor's gene-for-gene model (Nishimura and Dangl, 2010). We now think it is time to revisit the role of inducible structural defenses in plant-pathogen interactions. These defenses are extremely important to block progression of the devastating vascular pathogens, and we are far from understanding how these types of defense mechanisms are controlled.

In this review, we summarize how inducible vascular structures compartmentalize the vascular wilt pathogens leading to resistance. For this, we classify inducible structural barriers using a bi-dimensional perspective. We define a vertical and a horizontal component of resistance as those structures that restrict the vertical and horizontal movement of the pathogen, respectively, within the xylem vascular tissue (Fig. 1, Table 1). Furthermore, we review current knowledge on mechanisms underlying plant-inducible structural defenses against major xylem-colonizing pathogens, highlighting their correlation with biochemical changes and genetic interactions. Finally, we discuss future perspectives in the study of inducible vascular structural defenses, taking into account recent technological advances and how this may be translated into increasing resistance to vascular wilt pathogens in the field. Such physico-chemical defense responses are key traits desired for effective management of vascular wilt pathogens (Ferreira *et al.*, 2017).

### Vertical restriction of vascular colonization

Once they reach the xylem, different lumen occlusions constitute vertical barriers to the anti-gravitational movement of vascular pathogens. Vascular occlusion is an effective means of slowing down vertical progression of the pathogen, or even confining it to the infection site, preventing systemic infection. The most prominent of these occlusions are tyloses and gels, which we will review in this section, focusing on the aspects related to plant defense. As an important defense strategy by vascular pathogens, mechanisms to evade or subvert vertical occlusions and secure colonization have evolved on the pathogen side, as part of the evolutionary arms race. Inhibition of vertical occlusions has been reported for various wilt fungi, although the mechanisms for this virulence mechanism are not fully understood (Beckman and Roberts, 1995; Pouzoulet *et al.*, 2017).

### Formation of tyloses

Tyloses (singular tylosis) are balloon-like overgrowths of the protoplast of adjacent living parenchyma cells that protrude

into xylem vessels through its pits (Fig. 1; Bonsen and Kucera, 1990). Tyloses are considered inducible defense structures against xylem intruders because their formation can prevent spreading of the pathogen and also protect healthy parts of the plant by blocking the infected vessels (Leśniewska *et al.*, 2017). However, formation of tyloses is not only linked to pathogen attack, as they can be induced by several other environmental stimuli, such as pruning, wounding, flooding and frost (Davison and Tay, 1985; Cochard and Tyree, 1990; Sun *et al.*, 2007; De Micco *et al.*, 2016). The process of tylosis formation is tightly controlled and has certain commonalities with regular cell enlargement (Bishop and Cooper, 1984). Hormones such as auxin, ethylene and jasmonate seem to have a prominent role in the formation of these structures (Vander Molen *et al.*, 1987; Leśniewska *et al.*, 2017).

The formation of tyloses in response to pathogen attack has been extensively reported (Table 1; Cooper and Williams, 2004; Sun *et al.*, 2013; Ferreira *et al.*, 2017; Rioux *et al.*, 2018). Restricted formation of tyloses has been observed and specifically induced in the infected vessels of resistant tomato and potato varieties, effectively restricting *R. solanacearum* to the infected vascular bundles (Grimault *et al.*, 1994; Ferreira *et al.*, 2017). Such specific induction was not observed in susceptible tomato cultivars infected with *R. solanacearum*, where the formation of tyloses appeared delayed and less focused, with numerous non-colonized vessels occluded by tyloses, and pathogen growth unrestricted (Grimault *et al.*, 1994). Tylosis formation in resistant tomato cultivars has also been observed upon inoculation with the pathogenic fungus *F. oxysporum* f. sp. *lycopersici* and *V. albo-atrum* (Hutson and Smith, 1980). Similarly, in a banana cultivar resistant to race 1 of *F. oxysporum* f. sp. *cubense*, tylosis initially appeared as early as within two days post-inoculation in the lumen of xylem vessels of the root (Vander Molen *et al.*, 1987).

In addition to acting as structural barriers, tyloses can act as storage organs of antimicrobial compounds. Although they are predominantly composed of pectic substances (Rioux *et al.*, 1998; Eynck *et al.*, 2009), fungicidal compounds such as elemental sulfur have been detected in tyloses of tomato lines resistant to *V. albo-atrum*, which was thought to inhibit spore germination (Williams *et al.*, 2002). In addition, a fully developed tylosis also develops a lignified and/or suberized cell wall, which may protect the exposed cell from the xylem pathogen (Pouzoulet *et al.*, 2013).

However, the formation of tyloses is not always linked to resistance. For instance, a tomato variety susceptible to *V. albo-atrum* formed a few miniature tyloses in response to infection that the fungal hyphae were able to easily surpass within the vessel (Tjamos and Smith, 1975). More important than the quantity or frequency of tyloses formed, the successful restriction of a vascular pathogen depends on synchronization and specificity of tylose production to pathogen-colonized vessels (Bishop and Cooper, 1984). Sun *et al.*, (2013) reported tyloses as the predominant type of occlusion that formed in

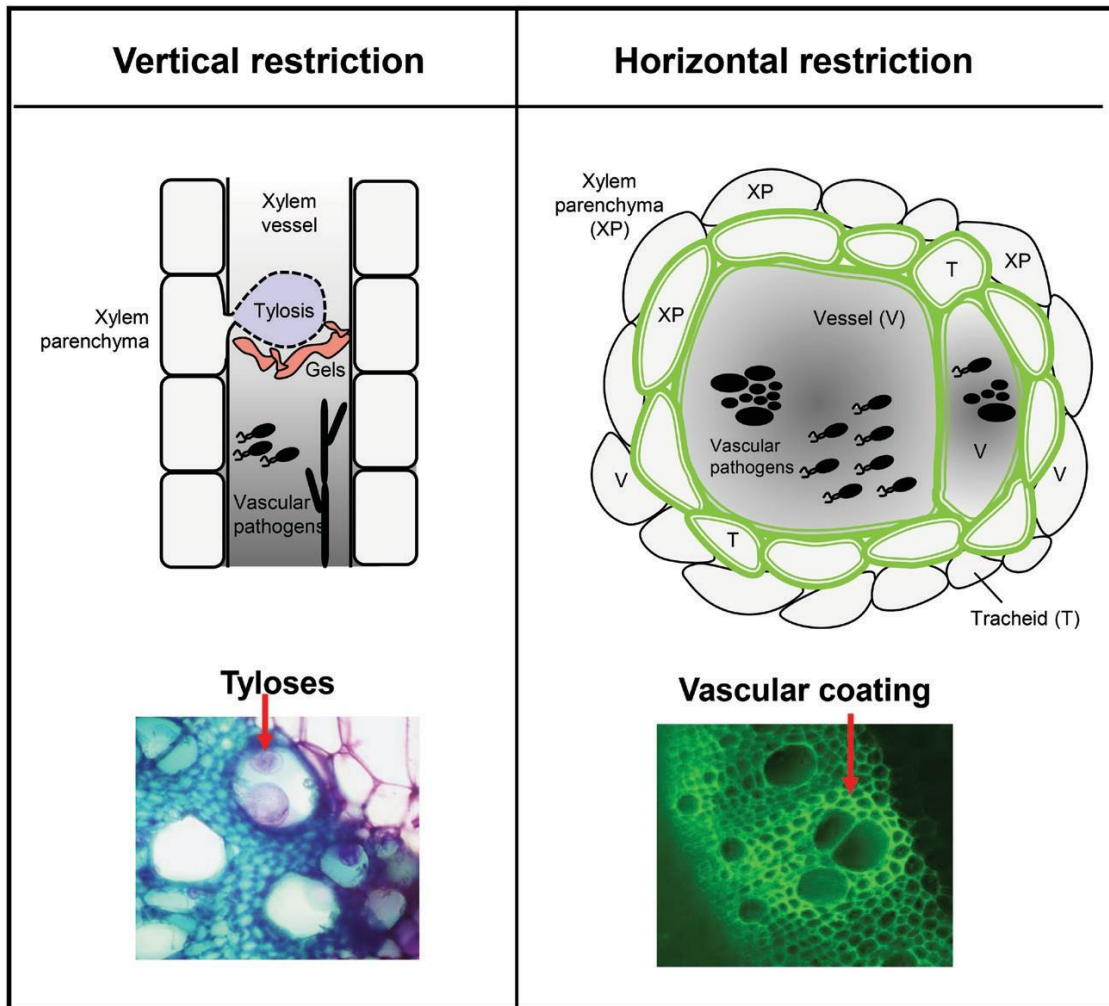


**Fig. 1. The two dimensions of plant physico-chemical barriers induced against xylem vascular wilt pathogens.** To counter invasion by xylem vascular wilt pathogens, resistant plants induce two-dimensional physico-chemical defenses that restrict vertical and horizontal movement of the pathogen. Vertical spread within the vessel lumen is mainly restricted by tyloses and gels (left). In contrast, horizontal spread of the pathogen to surrounding healthy vessels is prevented by reinforcement of the walls of colonized vessels (V) and the surrounding xylem parenchyma (XP) and tracheids (T), through vascular coating with mainly lignin and suberin (shown as a green color in the diagram). Synchronized formation of vertical and horizontal barriers early after pathogen invasion results in compartmentalization of the pathogen inoculum at the site of infection, thereby preventing wilt, and constitute a major component of resistance. To visualize tyloses and vascular coating (panels below), tomato root cross-sections were obtained after *R. solanacearum* soil soak inoculation, and fixed in 70% ethanol. For tyloses, cross-sections were stained with 0.1% toluidine blue and observed using a Leica DM6B-Z microscope under bright field conditions, and images were recorded through a MC190-HD-0518131623 camera. To visualize phenolic vascular coating, the cross-sections were illuminated by UV using a Leica DM6B-Z microscope, and the auto-fluorescence emitted from phenolic deposits was observed using a HC PL FLUOTAR objective. Images were captured using a Leica-DFC9000GT-VSC07341 camera. In the left panel, the arrow points towards *R. solanacearum*-induced formation of tyloses inside vessel lumen, which appear pink to violet color upon staining with 0.1% toluidine blue. In the right panel, the arrow points towards *R. solanacearum*-induced auto-fluorescence emitted from phenolics, deposited in the walls of vessels and the surrounding tracheids and parenchyma cells. Scale bar=120  $\mu$ m.

grapevines with differing resistance to *X. fastidiosa*. Excessive tylosis formation in response to *X. fastidiosa* infection in the susceptible grapevine cultivar led to heavy blockage of vessels and development of wilting symptoms, and did not significantly affect pathogen spread. In contrast, in resistant grapevines, tylosis development was specific and mainly limited to a few internodes close to the point of inoculation, impacting less of the vessels and indicating that timing and localization

are key (Sun *et al.*, 2013). Interestingly, the anatomy of xylem vessels also plays a role in augmenting pathogen compartmentalization by tyloses. Cultivars of grapevine having larger vessel size are known to be susceptible to vascular wilt pathogens such as *X. fastidiosa*, *Eutypa lata*, *Phaeoacremonium aleophilum*, *Phaeomoniella chlamydospora*, *Diplodia seriata*, and *Neofusicoccum parvum* (Pouzoulet *et al.*, 2017, 2019, 2020; Deyett *et al.*, 2019). Likewise, Dutch elm cultivars having larger vessel diameters

**Table 1.** List of plant pathosystems in which (I) vertical or (II) horizontal restriction of pathogen movement inside the plant has been shown.

I. Vertical restriction			
Structure	Host	Pathogen	Reference
Tylose formation	Banana	<i>Fusarium oxysporum</i> f.sp. <i>cubense</i>	(Vander Molen <i>et al.</i> , 1987)
	Butternut	<i>Ophiognomonia clavignenti-juglandacearum</i>	(Rioux <i>et al.</i> , 2018)
	Cotton	<i>Fusarium oxysporum</i> f. sp. <i>vasinfectum</i>	(Shi <i>et al.</i> , 1991)
	Cucurbits	<i>Fusarium oxysporum</i> f. sp. <i>melonis</i>	(Seo and Kim, 2017)
	Elm	<i>Ophiostoma novo-ulmi</i>	(Plichta <i>et al.</i> , 2016)
	Grapevine	<i>Xylella fastidiosa</i>	(Sun <i>et al.</i> , 2013)
		<i>Phaeomoniella chlamydospora</i>	(Pouzoulet <i>et al.</i> , 2013)
	Potato	<i>Rasltonia solanacearum</i>	(Ferreira <i>et al.</i> , 2017)
	Tomato	<i>Rasltonia solanacearum</i>	(Grimault <i>et al.</i> , 1994)
		<i>Verticillium albo-atrum</i>	(Hutson and Smith, 1980)
<i>Verticillium dahliae</i>		(Tjamos and Smith, 1975)	
Gel deposition		<i>Fusarium oxysporum</i> f. sp. <i>lycopersici</i>	(Hutson and Smith, 1980)
	Banana	<i>Fusarium oxysporum</i> f.sp. <i>cubense</i>	(Vander Molen <i>et al.</i> , 1987)
	Butternut	<i>Ophiognomonia clavignenti-juglandacearum</i>	(Rioux <i>et al.</i> , 2018)
	Carnation	<i>Fusarium oxysporum</i> f.sp. <i>dianthi</i>	(Baayen and Elgersma, 1985)
	Elm	<i>Ophiostoma novo-ulmi</i>	(Plichta <i>et al.</i> , 2016)
	Grapevine	<i>Xylella fastidiosa</i>	(Sun <i>et al.</i> , 2013)
	Pea	<i>Fusarium oxysporum</i> f. sp. <i>pisi</i>	(Bishop and Cooper, 1983)
	Plane tree	<i>Ceratocystis fimbriata</i> f. sp <i>platani</i>	(Clérivet <i>et al.</i> , 2000)
	Tomato	<i>Rasltonia solanacearum</i>	(Grimault <i>et al.</i> , 1994; Kim <i>et al.</i> , 2016)
		<i>Verticillium albo-atrum</i>	(Hutson and Smith, 1980)
		<i>Fusarium oxysporum</i> f. sp. <i>lycopersici</i>	(Hutson and Smith, 1980)
II. Horizontal restriction			
Structure	Host	Pathogen	Reference
Lignin deposition	Banana	<i>Fusarium oxysporum</i> f. sp. <i>cubense</i>	(De Ascensao and Dubery, 2000)
	Cotton	<i>Verticillium dahliae</i>	(Xu <i>et al.</i> , 2011; Bu <i>et al.</i> , 2014)
	Dutch elm	<i>Ophiostoma novo-ulmi</i>	(Martin <i>et al.</i> , 2007)
	Flax	<i>Fusarium oxysporum</i> f. sp. <i>lini</i>	(Galindo-González and Deyholos, 2016)
	Oilseed rape	<i>Verticillium longisporum</i>	(Eynck <i>et al.</i> , 2009)
	Olive	<i>Xylella fastidiosa</i>	(Sabella <i>et al.</i> , 2018)
	Pepper	<i>Verticillium dahliae</i>	(Novo <i>et al.</i> , 2017)
	Potato	<i>Rasltonia solanacearum</i>	(Ferreira <i>et al.</i> , 2017)
	Tomato	<i>Verticillium dahliae</i>	(Street <i>et al.</i> , 1986; Hu <i>et al.</i> , 2019)
		<i>Rasltonia solanacearum</i>	(Ishihara <i>et al.</i> , 2012; Ferreira <i>et al.</i> , 2017)
Suberin deposition	Alfalfa	<i>Verticillium albo-atrum</i>	(Newcombe and Robb, 1988)
	Butternut	<i>Ophiognomonia clavignenti-juglandacearum</i>	(Rioux <i>et al.</i> , 2018)
	Dutch elm	<i>Ophiostoma novo-ulmi</i>	(Martin <i>et al.</i> , 2008)
	Grapevine	<i>Phaeomoniella chlamydospora</i>	(Pouzoulet <i>et al.</i> , 2013)
	Tomato	<i>Verticillium albo-atrum</i>	(Street <i>et al.</i> , 1986; Robb <i>et al.</i> , 1991)

are susceptible to *Ophiostoma novo-ulmi* (Pouzoulet *et al.*, 2014; Venturas *et al.*, 2014). Across the grapevine genotypes, it has been observed that the extent of *P. chlamydospora* compartmentalization is a function of the diameter of the host xylem vessels. Genotypes with increased number of xylem vessels above 100 µm in diameter resulted in increased infection of host tissue (Pouzoulet *et al.*, 2020). Though numerous tyloses are formed in large vessels of susceptible grapevine cultivars in response to the wilt pathogen *P. chlamydospora*, the compartmentalization process is not as efficient as in narrow diameter vessels, due to the presence of large escape routes (Pouzoulet *et al.*, 2017).

### Deposition of gels

Deposition of electrodense material corresponding to gels or gums in the lumen of the xylem vessels is another feature commonly observed during xylem invasion by vascular pathogens, and acts as one of the multiple factors that contribute to induced structural defense (Vander Molen *et al.*, 1977). Besides its role in immunity, these occluding structures also form in response to other stimuli such as wounding or aging (Ratnayake *et al.*, 2013).

Gels are commonly secreted by xylem parenchyma cells and they are transported across pit membranes into vessel elements



(Fig. 1; Bishop and Cooper, 1984). Tyloses have also been observed to secrete gels into the lumen of vessels, thereby multiplying the clogging effect (Bonsen and Kucera, 1990; Rioux *et al.*, 1998). Gels appear fibrillar, forming thin networks of varying electron density that ultimately fill and clog the vessel lumen (Sun *et al.*, 2008). Gels initially appear as translucent fibres arising from several places along lateral walls of vessels, and later form a continuous layer with wavy edges toward the vessel lumen. Subsequently, gels turn yellow and are interspersed with small particles, coinciding with vessel occlusions (Sun *et al.*, 2008). Although the main component of gels are pectic substances such as partially esterified pectic polysaccharides (Rioux *et al.*, 1998; Cl  rivet *et al.*, 2000), they may also accumulate antimicrobial compounds such as elemental sulfur and phytoalexins (Cooper and Williams, 2004; Sun *et al.*, 2008). Furthermore, these gels are strengthened by deposition of lignin and other phenolic compounds, which make these plugs strong physical barriers (Kpemoua *et al.*, 1996; Rioux *et al.*, 1998).

Formation of vascular gels is considered an important part of resistance towards several wilt diseases (Table 1). For example, *F. oxysporum* f. sp. *dianthi* colonization is restricted due to the formation of gels in the vascular lumen of carnation plants (Baayen and Elgersma, 1985). Moreover, in most resistant cultivars these gels are often observed together with tyloses (Vander Molen *et al.*, 1987; Grimault *et al.*, 1994). In banana plants resistant to *F. oxysporum* f. sp. *cubense*, formation of vascular occlusions including both gels and tyloses have been observed (Vander Molen *et al.*, 1977). Gel formation in the xylem lumen is also a trait of tomato cultivars resistant towards the vascular bacterium *R. solanacearum* (Grimault *et al.*, 1994). In other cases, such as pea plants resistant to *F. oxysporum* f. sp. *pisi*, vascular gels, but not tyloses, are observed after infection (Bishop and Cooper, 1984).

#### Horizontal restriction of vascular colonization

The mechanisms mentioned above are part of host responses that restrict vertical movement of vascular pathogens to healthy regions of the host. In addition, resistant plants can often develop a protective vascular coating upon invasion by vascular pathogens, posing a horizontal barrier to further colonization of adjacent healthy tissues. Vascular coating involves physico-chemical structural modifications in the cell walls of xylem tissues that result in confinement of the pathogen to the infected vessels (Figs 1, 2A).

Xylem pits are the primary routes of vessel-to-vessel and vessel-to-parenchyma cell water transport. Pits are covered by a pit membrane, which is impermeable to particulate matter like bacteria and other pathogens (Choat *et al.*, 2008). For a pathogen to achieve successful horizontal transfer into vessels, it has to either form openings in vessel walls or degrade pit membranes, thereby reaching the adjacent parenchyma cells and vessels (Nakaho *et al.*, 2000). To avoid the breach by

pathogens, resistant plants with altered composition and structure of homogalacturonans (HGs) and xyloglucans (XyGs) in pit membranes have evolved; however, these compounds are potential targets of the pathogen's cell wall degrading enzymes. Grapevine genotypes resistant to *X. fastidiosa* lacked fucosylated XyGs and weakly methylesterified HGs (ME-HGs), and contained a small amount of heavily ME-HGs. In contrast, pit membranes of susceptible genotypes all had substantial amounts of fucosylated XyGs and weakly ME-HGs, but lacked heavily ME-HGs (Sun *et al.*, 2011).

In addition, reinforcement occurs at vessel walls, parenchyma cells and pit membranes, to confine the spread of vascular pathogens. Ultra-microscopic studies showed that the pit membranes, as well as vessels walls and parenchyma cells, form a conspicuously thick coating in the form of an electron dense amorphous layer, as part of the defense response against vascular pathogens (Street *et al.*, 1986; Benhamou, 1995; Daayf *et al.*, 1997; Nakaho *et al.*, 2000; Araujo *et al.*, 2014). Such reinforcement acts to limit the horizontal movement of the pathogen from the protoxylem or the primary xylem to the surrounding cells (Street *et al.*, 1986; Benhamou, 1995; Daayf *et al.*, 1997; Nakaho *et al.*, 2000; Araujo *et al.*, 2014). Besides, its deposition acts as a shield against pathogen-derived metabolites such as toxins and enzymes, and makes water and nutrients inaccessible for pathogens, thereby impeding their growth (Araujo *et al.*, 2014).

Importantly, the timing of synthesis of the vascular coating plays a crucial role in immunity. Even if vascular coating can be observed in response to vascular pathogens in susceptible plants, these structures form at late time points, compared with their induction in resistant plants (Shi *et al.*, 1991; Daayf *et al.*, 1997). The specific composition of vascular deposits varies depending on the particular host-pathogen interaction. However, phenolics are the most important compounds, as they act as building blocks of the secondary cell wall, and they also have direct antimicrobial activity (Eynck *et al.*, 2009). Among the phenolic polymers constituting vascular coating structures, the principal players are lignin and suberin, described in further detail below. We also outline the role of callose, a non-phenolic compound that plays an important role in the formation of horizontal vascular barriers in certain interactions.

#### Deposition of lignin

Lignin is a complex phenolic polymer that constitutes a major component of secondary cell walls in vascular plants. Lignin imparts strength to secondary cell walls, being deposited in spaces between cellulose, hemicellulose and pectin (Kang *et al.*, 2019; Fig. 2A). The building blocks of the lignin polymer are monolignols, synthesized from phenylalanine via the phenylpropanoid pathway, where numerous enzymes are involved (Fig. 2B). Monolignols are then transported from the cytosol into the apoplast, where they are polymerized to lignin units by the oxidative activities of laccases and peroxidases.

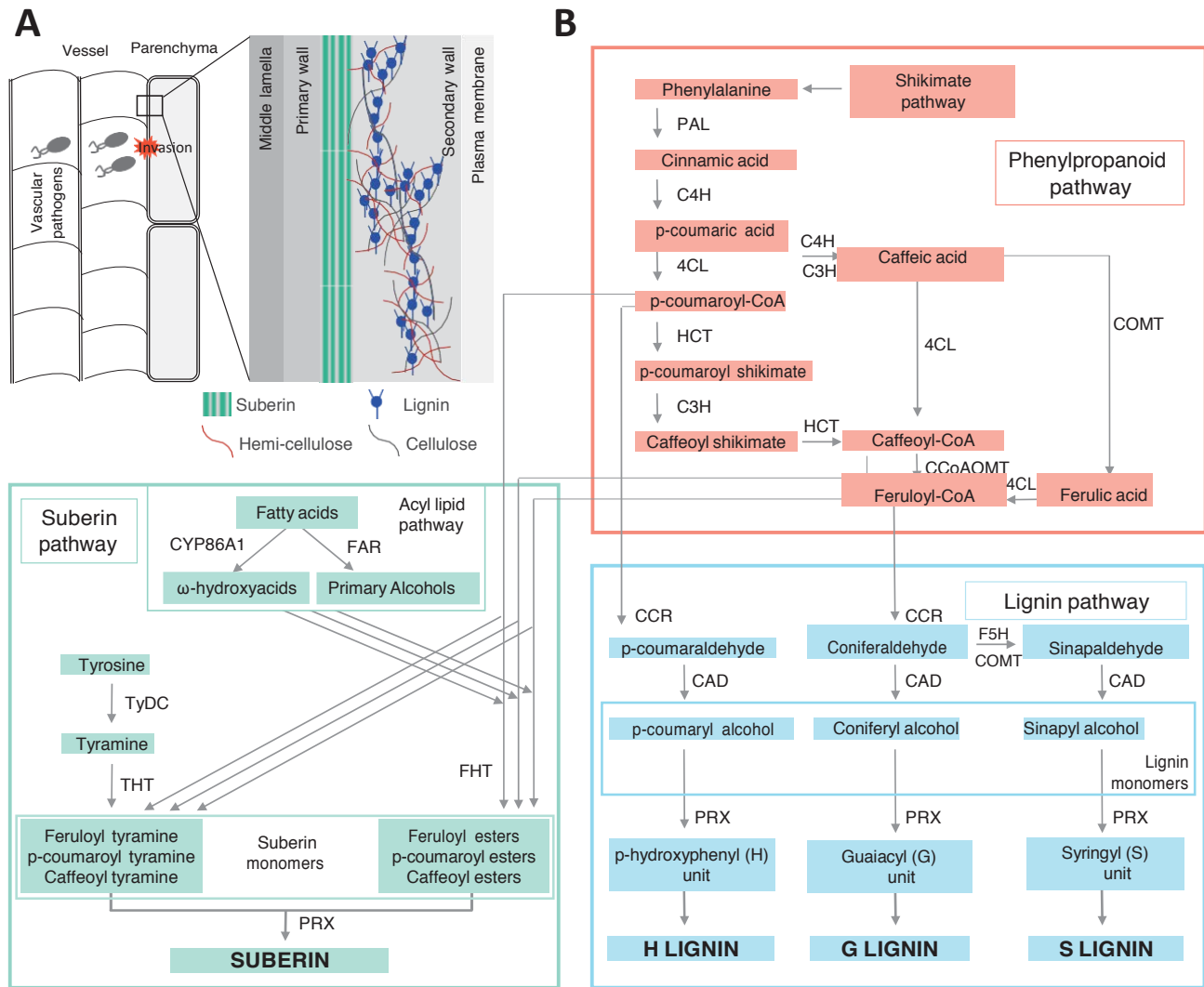


**Fig. 2. Lignin and suberin have a major role in vascular coating induced by xylem vascular wilt pathogens.** A. Schematic structure of reinforced cell walls of xylem vessels and parenchyma cells in resistant plants upon infection with xylem vascular wilt pathogens. B. The phenylpropanoid pathway provides precursors for both lignin and suberin biosynthesis. Phenylalanine, derived from the shikimate pathway, undergoes several enzymatic reactions as part of the phenylpropanoid pathway. The resulting precursors yield the monolignols *p*-coumaryl alcohol, coniferyl alcohol and sinapyl alcohol, which are the building blocks of lignin. In parallel, the phenylpropanoid metabolites feruloyl-CoA, caffeoyl-CoA, and *p*-coumaroyl-CoA bifurcate into the suberin pathway. In the suberin pathway, these metabolites can be conjugated to aromatic amine compounds such as tyramine by the action of THT, or can be linked to aliphatic compounds by the action of FHT, to yield suberin monomers. Lignin and suberin monomers are then transported to the cell wall, where they are subsequently polymerized into the reinforcing matrices that constitute vascular coating structures. Abbreviations: PAL: phenylalanine ammonia-lyase; C4H: cinnamate-4-hydroxylase; C3H: coumarate 3-hydroxylase; 4CL: 4-coumarate-CoA ligase; HCT: hydroxycinnamoyl-CoA shikimate/quinate hydroxycinnamoyl transferase; COMT: caffeic acid 3-O-methyltransferase; CCoAOMT: caffeoyl CoA 3-O-methyltransferase; CCR: cinnamoyl CoA reductase; CAD: cinnamoyl alcohol dehydrogenase; PRX: peroxidase; CYP86A1: fatty acid cytochrome P450 oxidases; FAR: fatty acyl-CoA reductase; TyDC: tyrosine decarboxylase; FHT: feruloyl transferase; THT: tyramine hydroxycinnamoyl transferase.

Lignin is a particularly important element in cell walls of xylem tissue cells, not only because of its structural function, but also because it facilitates water retention in vascular bundles due to its hydrophobic nature. In addition, lignin is resistant to biodegradation and acts as a potent structural barrier against pathogens. Although lignin is an integral part of pre-existing structural barriers in plants, its deposition can also be induced in the xylem upon pathogen attack to form additional

reinforcements that further restrict pathogen colonization. This inducible deposition of lignin as a vascular coating can be an important component of resistance towards certain pathogens (Table 1).

Restriction of pathogen colonization by lignin has been elegantly shown using a non-vascular pathogen, the leaf-infecting bacterium *Pseudomonas syringae* pv *tomato* (*Pto*) on *Arabidopsis thaliana* (Lee et al., 2019). It was shown that infection with

either virulent or avirulent strains of the pathogen induced localized lignification at the site of pathogen attack. However, lignin deposition was more conspicuous upon avirulent *Pto* recognition, leading to confinement of the pathogen, and restricting hypersensitive response cell death to the infection site. In contrast, virulent strains could overcome induced lignification, as the deposition in this case was milder, leading to unrestricted disease progression.

Interestingly, Casparian strip membrane domain proteins (CASPs), were shown to be involved in pathogen-induced lignin deposition (Lee *et al.*, 2019). The Casparian strip acts as a diffusion barrier that controls the uptake of water and molecules from the soil into the water-conducting tissues, and prevents the entry of pathogens and other harmful substances. Both the Casparian strip and the above-mentioned pathogen-induced lignification mechanism involve lignin-containing structures that function as anti-pathogenic physical barriers, serving parallel functions. In addition to lignin, suberin (discussed in detail later) is a chief component of the Casparian strip (Doblas *et al.*, 2017). Recent findings show that the Casparian strip possesses a barrier surveillance pathway comprised of the receptor-like cytoplasmic kinase SCHENGEN1 and the LRR-RLK SCHENGEN3, hence bearing a striking resemblance to signaling pathways for perception of pathogen-associated molecular patterns (Alassimone *et al.*, 2016; Fujita *et al.*, 2020). These receptors in the Casparian strip domain interact with peptides (CASPARIAN STRIP INTEGRITY FACTORS, CIF1/2) expressed in the stele, leading to Casparian strip formation. This spatial separation of receptor and ligand constitutes a surveillance system where interaction stops after effective sealing by the strip, but any breach in the barrier leads to re-interaction and further strengthening (Doblas *et al.*, 2017).

Lignin deposits seem to also play a crucial role in spatial growth restriction of vascular pathogens. There are several examples showing a pronounced transcriptional upregulation of genes involved in lignin biosynthesis in resistant plants following infection with various vascular pathogens (Table 1). This occurs, for example, in cotton after *V. dahliae* infection, flax after infection with *F. oxysporum*, tomato after infection with *R. solanacearum*, or olive tree after *X. fastidiosa* infection (Xu *et al.*, 2011; Ishihara *et al.*, 2012; Galindo-González and Deyholos, 2016; Sabella *et al.*, 2018). Furthermore, there are several examples showing that resistance/tolerance to vascular pathogens is accompanied by an increase in lignin content and enhanced cell wall lignification upon infection. This includes examples of different pathosystems such as *V. dahliae*—pepper, *O. novoulmi*—*Ulmus minor*, *V. longisporum*—rapeseed, *F. oxysporum*—banana or tomato, and *R. solanacearum*—potato (Street *et al.*, 1986; De Ascensao and Dubery, 2000; Martín *et al.*, 2005; Martín *et al.*, 2007; Eynck *et al.*, 2009; Ferreira *et al.*, 2017; Novo *et al.*, 2017).

Nevertheless, the mechanisms that orchestrate timely and effective induction of lignin deposition in resistant plants upon vascular colonization remain vastly unknown. Some progress has been made using cotton plants infected with *V. dahliae*. In this pathosystem, two proteins potentially regulating *V. dahliae*-induced vascular lignin deposition have been identified. GhUMC1, a copper-binding protein, is involved in resistance mediated by lignin deposition and jasmonate signaling (Zhu *et al.*, 2018). *GhUMC1* knock-down plants are more susceptible to the pathogen, and lignin vascular coating is drastically reduced. On the other hand, the proline-rich protein GhHyPRP1 acts as a negative regulator of defense against *V. dahliae*, and was shown to induce lignin deposition (Zhu *et al.*, 2018). In accordance, *GhHyPRP1* knock-down plants displayed more lignin deposition upon infection and were more resistant to the pathogen. Interestingly, PevD1, a *V. dahliae* secreted protein, has been shown to activate defenses in cotton, triggering the expression of phenylpropanoid genes and lignin accumulation (Bu *et al.*, 2014). This may indicate that PevD1 acts as an avirulence effector in cotton triggering a defense reaction that includes lignin deposition in the vasculature, which may lead to pathogen confinement into infected vessels. It remains to be determined whether the differential lignin deposition phenotypes observed in resistant cultivars is a direct consequence of pathogen effector recognition via its secreted effectors, and if so, to what degree the mechanisms are conserved between different pathosystems. Moreover, the molecular players involved also need to be identified.

### Deposition of suberin

Suberin is a heteropolymer that deposits as a poly-lamellar structure between the plasma membrane and the cell wall, forming a hydrophobic protective barrier (Fig. 2A). Suberin is deposited in specialized tissues such as root and tuber epidermis, root endodermis, and seed coats. In addition, suberin is formed in response to several stresses such as wounding, salt injury and pathogen attack (Dixon and Paiva, 1995; Bernards, 2002). Besides providing strength to the cell wall, suberin prevents water loss and pathogen entry by sealing off the layer of suberized cells.

Suberin consists of a polyphenolic and a polyaliphatic domain. The polyphenolic domain is predominantly formed by esters and amides of ferulic acid, as well as other hydroxycinnamic acids, such as caffeic acid and *p*-coumaric acid (Negrel *et al.*, 1995; Lashbrooke *et al.*, 2016; Woolfson *et al.*, 2011; Woolfson, 2018). The aliphatic domain consists of a glycerol-based fatty acid-derived polyester comprised primarily of  $\omega$ -hydroxyacids,  $\alpha$ ,  $\omega$ -dicarboxylic acids, fatty alcohols, and small amounts of hydroxycinnamic acids (mainly alkyl ferulates; Beisson *et al.*, 2012). Ferulic esters composed of ferulic acid esterified to fatty acids are considered as one of the monomers of suberin polymer (Negrel *et al.*, 1995).



Significant progress elucidating suberin biosynthesis has been achieved in the last two decades using molecular genetics approaches, especially in the model species *A. thaliana* and in potato tuber periderm (Ranathunge *et al.*, 2011). Suberin shares the phenylpropanoid pathway with lignin (Fig. 2B). This pathway provides the precursors for its polyphenolic domain, which are used by downstream suberin-specific enzymes such as tyramine N-feruloyltransferase (THT) and feruloyl transferase (FHT; Fig. 2B; Serra *et al.*, 2010; Woolfson, 2018; Woolfson *et al.*, 2011). Similarly, several genes involved in the aliphatic metabolism of suberin have been described, such as fatty acid cytochrome P450 oxidases (CYP86A1), fatty acyl-CoA reductase (FARs),  $\beta$ -ketoacyl-CoA synthases (KCS2/Daisy and KCS20), glycerol-3-phosphate acyltransferase5 (GPAT5), as well as *ATP-BINDING CASSETTE G* (*ABCG*) genes involved in the delivery of suberin monomers to the site of suberization (*ABCG2*, *ABCG6*, and *ABCG20*; Beisson *et al.*, 2007; Höfer *et al.*, 2008; Franke *et al.*, 2009; Vishwanath *et al.*, 2013; Yadav *et al.*, 2014). In addition, a few upstream regulators of the suberin biosynthetic pathway have been identified in *A. thaliana*, such as the MYB transcription factors MYB41, MYB107 and SUBERMAN (MYB39; Kosma *et al.*, 2014; Gou *et al.*, 2017; Cohen *et al.*, 2020).

Suberin reinforcement in the xylem vascular tissue has been long recognized as a potent barrier to colonization by pathogens (Robb *et al.*, 1991). There are numerous studies reporting that suberin deposition in the xylem tissue upon infection contributes to resistance (Table 1). For example, vascular deposits have been observed after infection with *V. albo-atrum* in resistant tomato and alfalfa (Street *et al.*, 1986; Newcombe and Robb, 1988; Robb *et al.*, 1991). Similarly, induction of suberin deposition is an important line of defense in *Ulmus minor* against *O. novo-ulmi* (Martín *et al.*, 2008). Interestingly, exogenous application of phenolic compounds further increased resistance of trees to this pathogen through formation of suberin-like compounds in xylem tissues (Martín *et al.*, 2008). Another example of xylem tissue suberization induced by a vascular pathogen is provided by the histological characterization of grapevine infection by the wilt fungus *Phaeomonilla chlamydospora* (Pouzoulet *et al.*, 2013, 2017). It was shown that deposition of suberin in paravascular parenchyma cells is an effective barrier against horizontal *P. chlamydospora* colonization from one vessel to the adjacent vessel. Suberin was also shown to form deposits in tyloses induced by infection with this pathogen (Pouzoulet *et al.*, 2013). Interestingly, inhibition of tylose formation in grapevine by *P. chlamydospora* led to vascular coating of surrounding parenchyma cells with phenolic compounds, including suberin (Pouzoulet *et al.*, 2017). This indicates that sequential/superimposed defense mechanisms are in place to restrict pathogen progression to the infection site, once it has reached the vasculature.

Although suberin deposition seems to be an important component of defense responses against vascular pathogens, very

little is known about its regulation. Similar to lignin, the effectiveness of vascular suberization as a structural barrier against horizontal colonization by vascular pathogens largely depends on the spatio-temporal control of its deposition, i.e. formation of suberin deposits early after pathogen detection at the site of vascular invasion. The phytohormones abscisic acid (ABA) and ethylene have both been shown to regulate suberization (Soliday *et al.*, 1978; Cottle and Kolattukudy, 1982; Barberon *et al.*, 2016). Since these two hormones are involved in defense against various vascular pathogens, a possibility exists that pathogen-induced vascular suberization correlates with an increase of hormone concentrations during immune responses. However, the mechanistic links between these hormonal pathways and suberin biosynthesis during pathogen-triggered suberin vascular coating remain to be established.

### Deposition of callose

Callose is a linear amorphous cell wall polysaccharide formed by hundreds of glucose units linked by  $\beta$ -1,3 glucosidic bonds (Stone, 2009). This homopolysaccharide is synthesized from uridine diphosphate glucose by callose synthases (also known as CalS or GSL for glucan synthase-like), large multisubunit complexes at the plasma membrane (Ellinger and Voigt, 2014). Callose is not a particularly abundant polymer in the cell wall, but has very relevant regulatory roles in development, plasmodesmata function, as well as in immunity (Schneider *et al.*, 2016). Pathogen-induced callose deposition has been shown to be localized to callosic papillae, providing structural defense against various pathogens (Schneider *et al.*, 2016). In addition, callose can constitute a matrix for accumulation of antimicrobial compounds, thereby providing targeted delivery of chemical defenses at the sites of pathogen attack (Luna *et al.*, 2011).

In the vasculature, callose has also been shown to act as a structural barrier against fungal wilt pathogens, restricting their horizontal vessel-to-vessel movement. Tomato plants resistant to *F. oxysporum* f. sp. *lycopersici* form callose deposits in paravascular parenchyma cells and at pit membranes in response to infection by this pathogen (Beckman *et al.*, 1982; Mueller and Beckman, 1988). In addition, application of the microbe-associated molecular pattern chitosan, a derivative of chitin, restricts colonization of *F. oxysporum* f. sp. *lycopersici* by inducing a vascular coating composed of callose and phenolic compounds (Benhamou *et al.*, 1994). Furthermore, cotton roots infected with *V. dahliae* showed reinforcement with callose deposits (Daayf *et al.*, 1997). In contrast, infection by the bacterial wilt pathogen *R. solanacearum* caused deposition of callose in both tolerant and susceptible potato plants, indicating that in this interaction callose may not be as important for resistance towards the pathogen (Ferreira *et al.*, 2017). Additional research is needed to clarify the precise role and regulation of callose as a structural defense mechanism induced upon perception of vascular wilt pathogens.

## Concluding remarks and future prospects

During the last few decades, much evidence has accumulated showing the importance of physico-chemical barriers as a crucial component of resistance towards xylem vascular pathogens. From all the research until now in this field, it becomes clear that the localization and timing of formation of these vascular structures is key for their effectiveness as barriers for pathogen confinement. Resistant plants are able to form vertical and horizontal barriers quickly upon pathogen invasion of the vasculature, confining them to infected vessels and avoiding spread to the rest of the plant. In susceptible plants, formation of the same vascular structures is observed, but not targeted to infected vessels, and later in time, once the pathogen has spread throughout the plant they have no effect on disease progression. However, the mechanisms regulating the spatial and temporal formation of vascular structures leading to effective pathogen confinement, and their precise composition, are old questions that remain unanswered. In fact, it remains unclear as to how vascular wilt pathogens are perceived at the vasculature, and how this perception is transduced into timely and restricted formation of structural defenses. Since effective mechanisms of resistance are very much sought after in breeding programs, in the coming years it will be important to make an effort to advance knowledge in this area, even though inducible structural defenses are governed by complex polygenic traits.

Major technological advances in the last few years have placed plant molecular biologists in a privileged position to make significant advances. Of particularly relevance is the CRISPR-Cas9 technology, which has proven extremely efficient for Solanaceous crops such as tomato, pepper and eggplant, which are severely affected by wilt diseases caused by xylem vascular pathogens (Hu *et al.*, 2019; Li *et al.*, 2019; Wang *et al.*, 2019). Importantly, an array of technologies have emerged that allow the study of specific processes in a cell, or in a tissue-specific manner. These techniques will become instrumental in the study of plant-pathogen interactions, which constitute a localized phenomenon by its very nature. This is particularly the case for colonization of vascular cells by vascular pathogens, since the ability to confine the invading agent is a key feature of resistant plants. With the advent of single-cell technologies it will be possible to attain astonishing resolution when investigating the processes occurring at infected cells and surrounding areas. For instance, RNA sequencing of laser-dissected areas or single cells allows profiling of the transcriptomic landscape after infection at relevant sites. In turn, this will allow the identification of marker genes associated with the formation of structural defenses and the subsequent generation of transgenic marker lines, to be able to track relevant cells/tissues at early time points after infection for their analysis. In addition, extremely sensitive analytical techniques have been developed in recent years that allow the identification and quantification of proteins, small molecules and metabolites, and the interactions between them. This includes

Raman spectroscopy or MALDI (matrix-assisted laser desorption/ionization) spectrometry imaging, both of which can be extremely useful in zonal responses such as structural resistance. All this knowledge could lead in the future to the engineering of metabolic pathways of vascular coating compounds in specific cells, to produce resistant plants against xylem colonizers.

With this article we hope to contribute towards raising awareness of the importance of attaining a better understanding of the structural physico-chemical barriers as a crucial component of resistance towards xylem vascular pathogens. Disease management through host resistance is the most efficient and eco-friendly approach to control pathogens. However, a lot has to be learnt about the complex genetic interactions which govern induced structural resistance in various hosts, to be able to deploy this trait in future cultivars and fight vascular pathogens, agents of the most devastating plant diseases in the field.

## Acknowledgements

The authors would like to thank all members of the Bacterial plant diseases and cell death lab for helpful comments. We apologize to all authors whose work has been omitted because of space limitations. Research in the lab is funded by the Spanish Ministry of Economy and Competitiveness with grants 2016-78002-R (AGL) and RyC 2014-16158 (NSC), by the Ministry of Science and Innovation / Spanish State Research Agency PID2019-108595RB-I00 / AEI / 10.13039/501100011033, and through the “Severo Ochoa Programme for Centres of Excellence in R&D” (SEV-2015-0533). AK is the recipient of a Netaji Subhas—Indian Council of Agricultural Research (ICAR) International Fellowship. This work was also supported by the CERCA Programme / Generalitat de Catalunya.

## Author contribution

AK, MP-M, MC, MV, and NSC conceptualized and wrote the article, and obtained funds.

## References

- Alassimone J, Fujita S, Doblaz VG, et al.** 2016. Polarly localized kinase SGN1 is required for Casparian strip integrity and positioning. *Nature Plants* **2**, 16113.
- Álvarez B, Biosca EG, López MM.** 2010. On the life of *Ralstonia solanacearum*, a destructive bacterial plant pathogen. In: Méndez-Vilas A, ed. Technology and education topics in applied microbiology and microbial biotechnology. Current Research, Technology and Education Topics in Applied Microbiology. Badajoz: Formatex, 267–279.
- Antanaviciute L, Šurbanovski N, Harrison N, McLeary KJ, Simpson DW, Wilson F, Sargent DJ, Harrison RJ.** 2015. Mapping QTL associated with *Verticillium dahliae* resistance in the cultivated strawberry (*Fragaria × ananassa*). *Horticulture Research* **2**, 15009.
- Araujo L, Bispo WM, Cacique IS, Moreira WR, Rodrigues FÁ.** 2014. Resistance in mango against infection by *Ceratocystis fimbriata*. *Phytopathology* **104**, 820–833.
- Baayen RP, Elgersma DM.** 1985. Colonization and histopathology of susceptible and resistant carnation cultivars infected with *Fusarium oxysporum* f. sp. *dianthi*. *Netherlands Journal of Plant Pathology* **91**, 119–135.



- Bae C, Han SW, Song YR, Kim BY, Lee HJ, Lee JM, Yeam I, Heu S, Oh CS. 2015. Infection processes of xylem-colonizing pathogenic bacteria: possible explanations for the scarcity of qualitative disease resistance genes against them in crops. *Theoretical and Applied Genetics* **128**, 1219–1229.
- Bani M, Pérez-De-Luque A, Rubiales D, Rispail N. 2018. Physical and chemical barriers in root tissues contribute to quantitative resistance to *Fusarium oxysporum* f. sp. *pisi* in pea. *Frontiers in Plant Science* **9**, 199.
- Barberon M, Vermeer JEM, De Bellis D, Wang P, Naseer S, Andeersen TG, Humbel BM, Nawrath C, Takano J, Salt DE. 2016. Adaptation of root function by nutrient-induced plasticity of endodermal differentiation. *Cell* **164**, 447–459.
- Beckman CH, Mueller WC, Tessier BJ, Harrison NA. 1982. Recognition and callose deposition in response to vascular infection in *Fusarium* wilt-resistant or susceptible tomato plants. *Physiological Plant Pathology* **20**, 1–10.
- Beckman CH, Roberts EM. 1995. On the nature and genetic basis for resistance and tolerance to fungal wilt diseases of plants. *Advances in Botanical Research* **21**, 35–77.
- Beisson F, Li Y, Bonaventure G, Pollard M, Ohlrogge JB. 2007. The acyltransferase GPAT5 is required for the synthesis of suberin in seed coat and root of *Arabidopsis*. *The Plant cell* **19**, 351–368.
- Beisson F, Li-Beisson Y, Pollard M. 2012. Solving the puzzles of cutin and suberin polymer biosynthesis. *Current Opinion in Plant Biology* **15**, 329–337.
- Benhamou N, Lafontaine P, Nicole M. 1994. Induction of systemic resistance to *Fusarium* crown and root rot in tomato plants by seed treatment with chitosan. *Phytopathology* **84**, 1432–1444.
- Benhamou N. 1995. Ultrastructural and cytochemical aspects of the response of eggplant parenchyma cells in direct contact with *Verticillium*-infected xylem vessels. *Physiological and Molecular Plant Pathology* **46**, 321–338.
- Bernards MA. 2002. Demystifying suberin. *Canadian Journal of Botany* **80**, 227–240.
- Bernards MA. 2018. Differential induction of polar and non-polar metabolism during wound-induced suberization in potato (*Solanum tuberosum* L.) tubers. *The Plant Journal* **93**, 931–942.
- Bishop CD, Cooper RM. 1983. An ultrastructural study of root invasion in three vascular wilt diseases. *Physiological Plant Pathology* **22**, 15–27.
- Bishop CD, Cooper RM. 1984. Ultrastructure of vascular colonization by fungal wilt pathogens. II. Invasion of resistant cultivars. *Physiological Plant Pathology* **24**, 277–289.
- Blaedow RA, Juzwik J. 2010. Spatial and temporal distribution of *Ceratocystis fagacearum* in roots and root grafts of oak wilt affected red oaks. *Arboriculture and Urban Forestry* **36**, 28–34.
- Bonsen KJM, Kucera LJ. 1990. Vessel occlusions in plants: morphological, functional and evolutionary aspects. *IAWA Bulletin* **11**, 393–399.
- Bu B, Qiu D, Zeng H, Guo L, Yuan J, Yang X. 2014. A fungal protein elicitor PevD1 induces *Verticillium* wilt resistance in cotton. *Plant Cell Reports* **33**, 461–470.
- Bubán T, Orosz-Kovács Z, Farkas Á. 2003. The nectary as the primary site of infection by *Erwinia amylovora* (Burr.) Winslow *et al.*: A mini review. *Plant Systematics and Evolution* **238**, 183–194.
- Carmeille A, Caranta C, Dintinger J, Prior P, Luisetti J, Besse P. 2006. Identification of QTLs for *Ralstonia solanacearum* race 3-phylo type II resistance in tomato. *Theoretical and Applied Genetics* **113**, 110–121.
- Catanzariti AM, Do HT, Bru P, de Sain M, Thatcher LF, Rep M, Jones DA. 2017. The tomato *I* gene for *Fusarium* wilt resistance encodes an atypical leucine-rich repeat receptor-like protein whose function is nevertheless dependent on SOBIR1 and SERK3/BAK1. *The Plant Journal* **89**, 1195–1209.
- Catanzariti AM, Lim GT, Jones DA. 2015. The tomato *I-3* gene: a novel gene for resistance to *Fusarium* wilt disease. *New Phytologist* **207**, 106–118.
- Chen YC, Wong CL, Muzzi F, Vlaardingerbroek I, Kidd BN, Schenk PM. 2014. Root defense analysis against *Fusarium oxysporum* reveals new regulators to confer resistance. *Scientific Reports* **4**, 5584.
- Choat B, Cobb AR, Jansen S. 2008. Structure and function of bordered pits: new discoveries and impacts on whole-plant hydraulic function. *New Phytologist* **177**, 608–625.
- Clérivet A, Déon V, Alami I, Lopez F, Geiger JP, Nicole M. 2000. Tyloses and gels associated with cellulose accumulation in vessels are responses of plane tree seedlings (*Platanus x acerifolia*) to the vascular fungus *Ceratocystis fimbriata* f. sp. *platani*. *Trees* **15**, 25–31.
- Cochard H, Tyree MT. 1990. Xylem dysfunction in *Quercus*: vessel sizes, tyloses, cavitation and seasonal changes in embolism. *Tree Physiology* **6**, 393–407.
- Cohen H, Fedyuk V, Wang C, Wu S, Aharoni A. 2020. SUBERMAN regulates developmental suberization of the *Arabidopsis* root endodermis. *The Plant Journal* **102**, 431–447.
- Cooper RM, Williams JS. 2004. Elemental sulphur as an induced antifungal substance in plant defence. *Journal of Experimental Botany* **55**, 1947–1953.
- Cottle W, Kolattukudy PE. 1982. Abscissic acid stimulation of suberization: induction of enzymes and deposition of polymeric components and associated waxes in tissue cultures of potato tuber. *Plant Physiology* **70**, 775–780.
- Daayf F, Nicole M, Boher B, Pando A, Geiger JP. 1997. Early vascular defense reactions of cotton roots infected with a defoliating mutant strain of *Verticillium dahliae*. *European Journal of Plant Pathology* **103**, 125–136.
- Davison EM, Tay FCS. 1985. The effect of waterlogging on seedlings of *Eucalyptus marginata*. *New Phytologist* **101**, 743–753.
- De Ascensao AR, Dubery IA. 2000. Panama disease: cell wall reinforcement in banana roots in response to elicitors from *Fusarium oxysporum* f. sp. *cubense* race four. *Phytopathology* **90**, 1173–1180.
- de Jonge R, van Esse HP, Maruthachalam K, *et al.* 2012. Tomato immune receptor Ve1 recognizes effector of multiple fungal pathogens uncovered by genome and RNA sequencing. *Proceedings of the National Academy of Sciences, USA* **109**, 5110–5115.
- De Micco V, Balzano A, Wheeler EA, Baas P. 2016. Tyloses and gums: a review of structure, function and occurrence of vessel occlusions. *IAWA Journal* **37**, 186–205.
- Deslandes L, Olivier J, Theulieres F, Hirsch J, Feng DX, Bittner-Eddy P, Beynon J, Marco Y. 2002. Resistance to *Ralstonia solanacearum* in *Arabidopsis thaliana* is conferred by the recessive *RRS1-R* gene, a member of a novel family of resistance genes. *Proceedings of the National Academy of Sciences, USA* **99**, 2404–2409.
- Deyett E, Pouzoulet J, Yang JI, Ashworth VE, Castro C, Roper MC, Rolshausen PE. 2019. Assessment of Pierce's disease susceptibility in *Vitis vinifera* cultivars with different pedigrees. *Plant Pathology* **68**, 1079–1087.
- Diener AC, Ausubel FM. 2005. RESISTANCE TO FUSARIUM OXYSPORUM 1, a dominant *Arabidopsis* disease-resistance gene, is not race specific. *Genetics* **171**, 305–321.
- Dixon RA, Paiva NL. 1995. Stress-induced phenylpropanoid metabolism. *The Plant Cell* **7**, 1085–1097.
- Doblas VG, Smakowska-Luzan E, Fujita S, Alassimone J, Barberon M, Madalinski M, Belkhadir Y, Geldner N. 2017. Root diffusion barrier control by a vasculature-derived peptide binding to the SGN3 receptor. *Science* **355**, 280–284.
- Ellinger D, Voigt CA. 2014. Callose biosynthesis in *Arabidopsis* with a focus on pathogen response: what we have learned within the last decade. *Annals of Botany* **114**, 1349–1358.
- Eynck C, Koopmann B, Karlovsky P, von Tiedemann A. 2009. Internal resistance in winter oilseed rape inhibits systemic spread of the vascular pathogen *Verticillium longisporum*. *Phytopathology* **99**, 802–811.
- Ferreira V, Pianzola MJ, Vilaró FL, Galván GA, Tondo ML, Rodríguez MV, Orellano EG, Valls M, Siri MI. 2017. Interspecific potato breeding lines display differential colonization patterns and induced defense responses after *Ralstonia solanacearum* infection. *Frontiers in Plant Science* **8**, 1424.
- Franke R, Höfer R, Briesen I, Emsermann M, Efremova N, Yephremov A, Schreiber L. 2009. The DAISY gene from *Arabidopsis*

encodes a fatty acid elongase condensing enzyme involved in the biosynthesis of aliphatic suberin in roots and the chalaza-micropyle region of seeds. *The Plant Journal* **57**, 80–95.

**Fujita S, De Bellis D, Edel KH, et al.** 2020. SCHENGEN receptor module drives localized ROS production and lignification in plant roots. *The EMBO Journal* **39**, e103894.

**Galindo-González L, Deyholos MK.** 2016. RNA-seq transcriptome response of flax (*Linum usitatissimum* L.) to the pathogenic fungus *Fusarium oxysporum* f. sp. *lini*. *Frontiers in Plant Science* **7**, 1766.

**Gou M, Hou G, Yang H, Zhang X, Cai Y, Kai G, Liu CJ.** 2017. The MYB107 transcription factor positively regulates suberin biosynthesis. *Plant Physiology* **173**, 1045–1058.

**Gramaje D, Úrbez-Torres JR, Sosnowski MR.** 2018. Managing grapevine trunk diseases with respect to etiology and epidemiology: current strategies and future prospects. *Plant Disease* **102**, 12–39.

**Grimault V, Gélie B, Lemattre M, Prior P, Schmit J.** 1994. Comparative histology of resistant and susceptible tomato cultivars infected by *Pseudomonas solanacearum*. *Physiological and Molecular Plant Pathology* **44**, 105–123.

**Gui YJ, Chen JY, Zhang DD, et al.** 2017. *Verticillium dahliae* manipulates plant immunity by glycoside hydrolase 12 proteins in conjunction with carbohydrate-binding module 1. *Environmental Microbiology* **19**, 1914–1932.

**Höfer R, Briesen I, Beck M, Pinot F, Schreiber L, Franke R.** 2008. The Arabidopsis cytochrome P450 CYP86A1 encodes a fatty acid omega-hydroxylase involved in suberin monomer biosynthesis. *Journal of Experimental Botany* **59**, 2347–2360.

**Houterman PM, Ma L, van Ooijen G, de Vroomen MJ, Cornelissen BJ, Takken FL, Rep M.** 2009. The effector protein Avr2 of the xylem-colonizing fungus *Fusarium oxysporum* activates the tomato resistance protein I-2 intracellularly. *The Plant Journal* **58**, 970–978.

**Hu N, Xian Z, Li N, Liu Y, Huang W, Yan F, Su D, Chen J, Li Z.** 2019. Rapid and user-friendly open-source CRISPR/Cas9 system for single- or multi-site editing of tomato genome. *Horticulture Research* **6**, 7.

**Hutson RA, Smith IM.** 1980. Phytoalexins and tyloses in tomato cultivars infected with *Fusarium oxysporum* f.sp. *lycopersici* or *Verticillium albo-atrum*. *Physiological Plant Pathology* **17**, 245–257.

**Ishihara T, Mitsuhashi I, Hideki T, Kazuhiro N.** 2012. Transcriptome analysis of quantitative resistance- specific response upon *Ralstonia solanacearum* infection in tomato. *PLoS Pathogens* **7**, e46763.

**Jones JD, Dangl JL.** 2006. The plant immune system. *Nature* **444**, 323–329.

**Joobeur T, King JJ, Nolin SJ, Thomas CE, Dean RA.** 2004. The *Fusarium* wilt resistance locus Fom-2 of melon contains a single resistance gene with complex features. *The Plant Journal* **39**, 283–297.

**Kang X, Kirui A, Dickwella Widanage MC, Mentink-Vigier F, Cosgrove DJ, Wang T.** 2019. Lignin-polysaccharide interactions in plant secondary cell walls revealed by solid-state NMR. *Nature Communications* **10**, 347.

**Katagiri F, Tsuda K.** 2010. Understanding the plant immune system. *Molecular Plant-Microbe Interactions* **23**, 1531–1536.

**Kim SG, Hur OS, Ro NY, Ko HC, Rhee JH, Sung JS, Ryu KY, Lee SY, Baek HJ.** 2016. Evaluation of resistance to *Ralstonia solanacearum* in tomato genetic resources at seedling stage. *The Plant Pathology Journal* **32**, 58–64.

**Kosma DK, Murmu J, Razeq FM, Santos P, Bourgault R, Molina I, Rowland O.** 2014. AtMYB41 activates ectopic suberin synthesis and assembly in multiple plant species and cell types. *The Plant Journal* **80**, 216–229.

**Kpemoua K, Boher B, Nicole M, Calatayud P, Geiger J.** 1996. Cytochemistry of defense responses in cassava infected by *Xanthomonas campestris* pv. *manihotis*. *Canadian Journal of Microbiology* **42**, 1131–1143.

**Krivanek AF, Riaz S, Walker MA.** 2006. Identification and molecular mapping of *PdR1* a primary resistance gene to Pierce's disease in *Vitis*. *Theoretical and Applied Genetics* **112**, 1125–1131.

**Lambel S, Lanini B, Vivoda E, Fauve J, Patrick Wechter W, Harris-Shultz KR, Massey L, Levi A.** 2014. A major QTL associated with *Fusarium oxysporum* race 1 resistance identified in genetic populations derived from closely related watermelon lines using selective genotyping and genotyping-by-sequencing for SNP discovery. *Theoretical and Applied Genetics* **127**, 2105–2115.

**Lashbrooke J, Cohen H, Levy-Samocha D, et al.** 2016. MYB107 and MYB9 homologs regulate suberin deposition in angiosperms. *The Plant Cell* **28**, 2097–2116.

**Le Roux C, Huet G, Jauneau A, et al.** 2015. A receptor pair with an integrated decoy converts pathogen disabling of transcription factors to immunity. *Cell* **161**, 1074–1088.

**Lee MH, Jeon HS, Kim SH, Chung JH, Roppolo D, Lee HJ, Cho HJ, Tobimatsu Y, Ralph J, Park OK.** 2019. Lignin-based barrier restricts pathogens to the infection site and confers resistance in plants. *The EMBO Journal* **38**, e101948.

**Leśniewska J, Öhman D, Krzesłowska M, Kushwah S, Barciszewska-Pacak M, Kleczkowski LA, Sundberg B, Moritz T, Mellerowicz EJ.** 2017. Defense responses in aspen with altered pectin methylesterase activity reveal the hormonal inducers of tyloses. *Plant Physiology* **173**, 1409–1419.

**Li R, Liu C, Zhao R, Wang L, Chen L, Yu W, Zhang S, Sheng J, Shen L.** 2019. CRISPR/Cas9-Mediated SINPR1 mutagenesis reduces tomato plant drought tolerance. *BMC Plant Biology* **19**, 1–13.

**Luna E, Pastor V, Robert J, Flors V, Mauch-Mani B, Ton J.** 2011. Callose deposition: a multifaceted plant defense response. *Molecular Plant-Microbe Interactions* **24**, 183–193.

**Mangin B, Thoquet P, Olivier J, Grimsley NH.** 1999. Temporal and multiple quantitative trait loci analyses of resistance to bacterial wilt in tomato permit the resolution of linked loci. *Genetics* **151**, 1165–1172.

**Martín JA, Solla A, Coimbra MA, Gil L.** 2005. Metabolic distinction of *Ulmus minor* xylem tissues after inoculation with *Ophiostoma novo-ulmi*. *Phytochemistry* **66**, 2458–2467.

**Martín JA, Solla A, Domingues MR, Coimbra MA, Gil L.** 2008. Exogenous phenol increase resistance of *Ulmus minor* to Dutch elm disease through formation of suberin-like compounds on xylem tissues. *Environmental and Experimental Botany* **64**, 97–104.

**Martín JA, Solla A, Woodward S, Gil L.** 2007. Detection of differential changes in lignin composition of elm xylem tissues inoculated with *Ophiostoma novo-ulmi* using fourier transform-infrared spectroscopy. *Forest Pathology* **37**, 187–191.

**Mes JJ, van Doorn AA, Wijbrandi J, Simons G, Cornelissen BJ, Haring MA.** 2000. Expression of the *Fusarium* resistance gene I-2 colocalizes with the site of fungal containment. *The Plant Journal* **23**, 183–193.

**Milling A, Babujee L, Allen C.** 2011. *Ralstonia solanacearum* extracellular polysaccharide is a specific elicitor of defense responses in wilt-resistant tomato plants. *PLoS One* **6**, e15853.

**Morello P, Diez CM, Codes M, Rallo L, Barranco D, Trapero A, Moral J.** 2016. Sanitation of olive plants infected by *Verticillium dahliae* using heat treatments. *Plant Pathology* **65**, 412–421.

**Mueller W, Beckman C.** 1988. Correlated light and electron microscope studies of callose deposits in vascular parenchyma cells of tomato plants inoculated with *Fusarium oxysporum* f.sp. *lycopersici*. *Physiological and Molecular Plant Pathology* **33**, 201–208.

**Nakaho K, Hibino H, Miyagawa H.** 2000. Possible mechanisms limiting movement of *Ralstonia solanacearum* in resistant tomato tissues. *Journal of Phytopathology* **148**, 181–190.

**Negrel J, Lotfy S, Javelle F.** 1995. Modulation of the activity of two hydroxycinnamoyl transferases in wound-healing potato tuber discs in response to pectinase or abscisic acid. *Journal of Plant Physiology* **146**, 318–322.

**Newcombe G, Robb J.** 1988. The function and relative importance of the vascular coating response in highly resistant, moderately resistant and susceptible alfalfa infected by *Verticillium albo-atrum*. *Physiological and Molecular Plant Pathology* **33**, 47–58.



- Ngou BPM, Ahn H, Ding P, Jones JDG. 2020. Mutual potentiation of plant immunity by cell-surface and intracellular receptors. *BioRxiv* doi: [doi:10.1101/2020.04.10.034173](https://doi.org/10.1101/2020.04.10.034173) 1–29. [Preprint].
- Nicholson RL. 1992. Phenolic compounds and their role in disease resistance. *Annual Reviews in Phytopathology* **30**, 369–389.
- Niemann AH. 1994. A crucial role of phenolic metabolism in resistance of carnations to wilt diseases. *Acta Horticulturae* **381**, 565–571.
- Nishimura MT, Dangl JL. 2010. Arabidopsis and the plant immune system. *The Plant Journal* **61**, 1053–1066.
- Novo M, Silvar C, Merino F, Martínez-Cortés T, Lu F, Ralph J, Pomar F. 2017. Deciphering the role of the phenylpropanoid metabolism in the tolerance of *Capsicum annuum* L. to *Verticillium dahliae* Kleb. *Plant Science* **258**, 12–20.
- Palanga KK, Jamshed M, Rashid MHO, et al. 2017. Quantitative Trait Locus mapping for *Verticillium* wilt resistance in an upland cotton recombinant inbred line using SNP-based high density genetic map. *Frontiers in Plant Science* **8**, 382.
- Park CJ, Ronald PC. 2012. Cleavage and nuclear localization of the rice XA21 immune receptor. *Nature Communications* **3**, 920.
- Pastrana AM, Watson DC, Gordon TR. 2019. Transmission of *Fusarium oxysporum* f. sp. *fragariae* through stolons in strawberry plants. *Plant Disease* **103**, 1249–1251.
- Planas-Marqués M, Kressin JP, Kashyap A, Panthee DR, Louws FJ, Coll NS, Valls M. 2019. Four bottlenecks restrict colonization and invasion by the pathogen *Ralstonia solanacearum* in resistant tomato. *Journal of Experimental Botany* **71**, 2157–2171.
- Plichta R, Urban J, Gebauer R, Dvořák M, Ďurkovič J. 2016. Long-term impact of *Ophiostoma novo-ulmi* on leaf traits and transpiration of branches in the Dutch elm hybrid 'Dodoens'. *Tree Physiology* **36**, 335–344.
- Pouzoulet J, Jacques A, Besson X, Dayde J, Mailhac N. 2013. Histopathological study of response of *Vitis vinifera* 'Cabernet Sauvignon' to bark and wood injury with and without inoculation by *Phaeomoniella chlamydospora*. *Phytopathologia Mediterranea* **52**, 313–323.
- Pouzoulet J, Pivovarov AL, Santiago LS, Rolshausen PE. 2014. Can vessel dimension explain tolerance toward fungal vascular wilt diseases in woody plants? Lessons from Dutch elm disease and esca disease in grapevine. *Frontiers in Plant Science* **5**, 253.
- Pouzoulet J, Rolshausen P, Charbois R, Chen J, Guillaumie S, Ollat N, Gambetta GA, Delmas CEL. 2020. Behind the curtain of the compartmentalization process: exploring how xylem vessel diameter impacts vascular pathogen resistance. *Plant, Cell & Environment*, doi: [10.1111/pce.13848](https://doi.org/10.1111/pce.13848).
- Pouzoulet J, Scudiero E, Schiavon M, Rolshausen PE. 2017. Xylem vessel diameter affects the compartmentalization of the vascular pathogen *Phaeomoniella chlamydospora* in grapevine. *Frontiers in Plant Science* **8**, 1442.
- Pouzoulet J, Scudiero E, Schiavon M, Santiago LS, Rolshausen PE. 2019. Modeling of xylem vessel occlusion in grapevine. *Tree Physiology* **39**, 1438–1445.
- Pradhan BB, Ranjan M, Chatterjee S. 2012. XadM, a novel adhesin of *Xanthomonas oryzae* pv. *oryzae*, exhibits similarity to Rhs family proteins and is required for optimum attachment, biofilm formation, and virulence. *Molecular Plant-Microbe Interactions* **25**, 1157–1170.
- Prakash A, Darren Grice I, Vinay Kumar KS, Sadashiva MP, Shankar HN, Umesha S. 2017. Extracellular polysaccharide from *Ralstonia solanacearum*; a strong inducer of eggplant defense against bacterial wilt. *Biological Control* **110**, 107–116.
- Ranathunge K, Schreiber L, Franke R. 2011. Suberin research in the genomics era—new interest for an old polymer. *Plant Science* **180**, 399–413.
- Rapicavoli JN, Blanco-Ulate B, Muszyński A, Figueroa-Balderas R, Morales-Cruz A, Azadi P, Dobruchowska JM, Castro C, Cantu D, Roper MC. 2018. Lipopolysaccharide O-antigen delays plant innate immune recognition of *Xylella fastidiosa*. *Nature Communications* **9**, 390.
- Ratnayake K, Joyce DC, Webb RI. 2013. Cu<sup>2+</sup> inhibition of gel secretion in the xylem and its potential implications for water uptake of cut *Acacia holosericea* stems. *Physiologia Plantarum* **148**, 538–548.
- Renzi M, Copini P, Taddei AR, Rossetti A, Gallipoli L, Mazzaglia A, Balestra GM. 2012. Bacterial canker on kiwifruit in Italy: anatomical changes in the wood and in the primary infection sites. *Phytopathology* **102**, 827–840.
- Rioux D, Blais M, Nadeau-Thibodeau N, Lagacé M, DesRochers P, Klimaszewska K, Bernier L. 2018. First extensive microscopic study of butternut defense mechanisms following inoculation with the canker pathogen *Ophiognomonia clavignenti-juglandacearum* reveals compartmentalization of tissue damage. *Phytopathology* **108**, 1237–1252.
- Rioux D, Nicole M, Simard M, Ouellette GB. 1998. Immunocytochemical evidence that secretion of pectin occurs during gel (Gum) and tylosis formation in trees. *Phytopathology* **88**, 494–505.
- Robb J, Lee B, Nazar RN. 2007. Gene suppression in a tolerant tomato-vascular pathogen interaction. *Planta* **226**, 299–309.
- Robb J, Lee SW, Mohan R, Kolattukudy PE. 1991. Chemical characterization of stress-induced vascular coating in tomato. *Plant Physiology* **97**, 528–536.
- Sabbavarapu MM, Sharma M, Chamarthi SK, et al. 2013. Molecular mapping of QTLs for resistance to *Fusarium* wilt (race 1) and *Ascochyta* blight in chickpea (*Cicer arietinum* L.). *Euphytica* **193**, 121–133.
- Sabella E, Luvisi A, Aprile A, Negro C, Vergine M, Nicoli F, Miceli A, De Bellis L. 2018. *Xylella fastidiosa* induces differential expression of lignification related-genes and lignin accumulation in tolerant olive trees 'Leccino'. *Journal of Plant Physiology* **220**, 60–68.
- Sanderlin RS, Melanson RA. 2006. Transmission of *Xylella fastidiosa* through pecan rootstock. *HortScience* **41**, 1455–1456.
- Sarris PF, Duxbury Z, Huh SU, et al. 2015. A plant immune receptor detects pathogen effectors that target WRKY transcription factors. *Cell* **161**, 1089–1100.
- Schneider R, Hanak T, Persson S, Voigt CA. 2016. Cellulose and callose synthesis and organization in focus, what's new? *Current Opinion in Plant Biology* **34**, 9–16.
- Schornack S, Ballvora A, Göllebeck D, Peart J, Baulcombe D, Ganai M, Baker B, Bonas U, Lahaye T. 2004. The tomato resistance protein Bs4 is a predicted non-nuclear TIR-NB-LRR protein that mediates defense responses to severely truncated derivatives of AvrBs4 and overexpressed AvrBs3. *The Plant Journal: for cell and molecular biology* **37**, 46–60.
- Seo Y, Kim YH. 2017. Pathological interrelations of soil-borne diseases in Cucurbits caused by *Fusarium* species and *Meloidogyne incognita*. *The Plant Pathology Journal* **33**, 410–423.
- Serra O, Hohn C, Franke R, Prat S, Molinas M, Figueras M. 2010. A feruloyl transferase involved in the biosynthesis of suberin and suberin-associated wax is required for maturation and sealing properties of potato periderm. *The Plant journal* **62**, 277–290.
- Shi J, Mueller WC, Beckman CH. 1991. Ultrastructural responses of vessel contact cells in cotton plants resistant or susceptible to infection by *Fusarium oxysporum* f. sp. *vasinfectum*. *Physiological and Molecular Plant Pathology* **38**, 211–222.
- Shigo AL, Marx HG. 1977. Compartmentalization of decay in trees. U. S. Department of Agriculture. Agriculture Information Bulletin. **405**, 1–73.
- Soliday CL, Dean BB, Kolattukudy PE. 1978. Suberization: inhibition by washing and stimulation by abscisic acid in potato disks and tissue culture. *Plant Physiology* **61**, 170–174.
- Song Y, Liu L, Wang Y, Valkenburg DJ, Zhang X, Zhu L, Thomma BPHJ. 2018. Transfer of tomato immune receptor Ve1 confers Ave1-dependent *Verticillium* resistance in tobacco and cotton. *Plant Biotechnology Journal* **16**, 638–648.
- Stone BA. 2009. Chemistry of  $\beta$ -glucans. In: Bacic A, Fincher G, Stone B, eds. *Chemistry, biochemistry and biology of 1–3 Beta glucans and related polysaccharides*. San Diego, USA: Academic press, 5–46.
- Street PFS, Robb J, Ellis BE. 1986. Secretion of vascular coating components by xylem parenchyma cells of tomatoes infected with *Verticillium albo-atrum*. *Protoplasma* **132**, 1–11.

- Sun Q, Greve LC, Labavitch JM. 2011. Polysaccharide compositions of intervessel pit membranes contribute to Pierce's disease resistance of grapevines. *Plant Physiology* **155**, 1976–1987.
- Sun Q, Rost TL, Matthews MA. 2008. Wound-induced vascular occlusions in *Vitis vinifera* (Vitaceae): tyloses in summer and gels in winter. *American Journal of Botany* **95**, 1498–1505.
- Sun Q, Rost TL, Reid MS, Matthews MA. 2007. Ethylene and not embolism is required for wound-induced tylose development in stems of grapevines. *Plant Physiology* **145**, 1629–1636.
- Sun Q, Sun Y, Walker MA, Labavitch JM. 2013. Vascular occlusions in grapevines with Pierce's disease make disease symptom development worse. *Plant Physiology* **161**, 1529–1541.
- Thomma BPHJ, Nürnberger T, Joosten MHJ. 2011. Of PAMPs and effectors: The blurred PTI-ETI dichotomy. *Plant Cell* **23**, 4–15.
- Thoquet P, Olivier J, Sperisen C, Rogowsky P, Laterrot H, Grimsley N. 1996. Quantitative trait loci determining resistance to bacterial wilt in tomato 'Hawaii7996'. *Molecular Plant-Microbe Interactions* **9**, 826–836.
- Tjamos EC, Smith IM. 1975. The expression of resistance to *Verticillium albo-atrum* in monogenically resistant tomato varieties. *Physiological Plant Pathology* **6**, 215–225.
- Triplett LR, Cohen SP, Heffelfinger C, Schmidt CL, Huerta AI, Tekete C, Verdier V, Bogdanove AJ, Leach JE. 2016. A resistance locus in the American heirloom rice variety Carolina Gold Select is triggered by TAL effectors with diverse predicted targets and is effective against African strains of *Xanthomonas oryzae* pv. *oryzicola*. *The Plant Journal* **87**, 472–483.
- Ulloa M, Hutmacher RB, Roberts PA, Wright SD, Nichols RL, Michael Davis R. 2013. Inheritance and QTL mapping of *Fusarium* wilt race 4 resistance in cotton. *Theoretical and Applied Genetics* **126**, 1405–1418.
- van der Does HC, Constantin ME, Houterman PM, Takken FLW, Cornelissen BJC, Haring MA, van den Burg HA, Rep M. 2019. *Fusarium oxysporum* colonizes the stem of resistant tomato plants, the extent varying with the *R*-gene present. *European Journal of Plant Pathology* **154**, 55–65.
- Vander Molen GE, Beckman CH, Rodehorst E. 1987. The ultrastructure of tylose formation in resistant banana following inoculation with *Fusarium oxysporum* f.sp. *cubense*. *Physiological and Molecular Plant Pathology* **31**, 185–200.
- Vander Molen GE, Beckman CH, Rodehorst E. 1977. Vascular gelation: a general response phenomenon following infection. *Physiological Plant Pathology* **11**, 95–100.
- Vasse J, Frey P, Trigalet A. 1995. Microscopic studies of intercellular infection and protoxylem invasion of tomato roots by *Pseudomonas solanacearum*. *Molecular Plant-Microbe Interactions* **8**, 241–251.
- Venturas M, López R, Martín JA, Gascó A, Gil L. 2014. Heritability of *Ulmus minor* resistance to Dutch elm disease and its relationship to vessel size, but not to xylem vulnerability to drought. *Plant Pathology* **63**, 500–509.
- Vishwanath SJ, Kosma DK, Pulsifer IP, Scandola S, Pascal S, Joubès J, Dittrich-Domergue F, Lessire R, Rowland O, Domergue F. 2013. Suberin-associated fatty alcohols in Arabidopsis: distributions in roots and contributions to seed coat barrier properties. *Plant Physiology* **163**, 1118–1132.
- Wang C, Ulloa M, Duong T, Roberts PA. 2018. Quantitative Trait Loci mapping of multiple independent loci for resistance to *Fusarium oxysporum* f. sp. *vasinfectum* Races 1 and 4 in an interspecific cotton population. *Phytopathology* **108**, 759–767.
- Wang G, Roux B, Feng F, et al. 2015. The decoy substrate of a pathogen effector and a pseudokinase specify pathogen-induced modified-self recognition and immunity in plants. *Cell Host & Microbe* **18**, 285–295.
- Wang JF, Ho FI, Truong HTH, Huang SM, Balatero CH, Dittapongpich V, Hidayati N. 2013. Identification of major QTLs associated with stable resistance of tomato cultivar 'Hawaii 7996' to *Ralstonia solanacearum*. *Euphytica* **190**, 241–252.
- Wang JF, Olivier J, Thoquet P, Mangin B, Sauviac L, Grimsley NH. 2000. Resistance of tomato line Hawaii7996 to *Ralstonia solanacearum* Pss4 in Taiwan is controlled mainly by a major strain-specific locus. *Molecular Plant-Microbe Interactions* **13**, 6–13.
- Wang L, Albert M, Einig E, Fürst U, Krust D, Felix G. 2016. The pattern-recognition receptor CORE of Solanaceae detects bacterial cold-shock protein. *Nature Plants* **2**, 16185.
- Wang P, Lee Y, Igo MM, Roper MC. 2017. Tolerance to oxidative stress is required for maximal xylem colonization by the xylem-limited bacterial phytopathogen, *Xylella fastidiosa*. *Molecular Plant Pathology* **18**, 990–1000.
- Wang T, Zhang H, Zhu H. 2019. CRISPR technology is revolutionizing the improvement of tomato and other fruit crops. *Horticulture Research* **6**, 77.
- Wei Y, Balaceanu A, Rufian JS, Segonzac C, Zhao A, Morcillo RJL, Macho AP. 2020. An immune receptor complex evolved in soybean to perceive a polymorphic bacterial flagellin. *Nature Communications* **11**, 3763.
- Wei Y, Caceres-Moreno C, Jimenez-Gongora T, Wang K, Sang Y, Lozano-Duran R, Macho AP. 2018. The *Ralstonia solanacearum* csp22 peptide, but not flagellin-derived peptides, is perceived by plants from the Solanaceae family. *Plant Biotechnology Journal* **16**, 1349–1362.
- Williams JS, Hall SA, Hawkesford MJ, Beale MH, Cooper RM. 2002. Elemental sulfur and thiol accumulation in tomato and defense against a fungal vascular pathogen. *Plant Physiology* **128**, 150–159.
- Woolfson KN, Haggitt ML, Zhang Y, et al. 2011. Lignin metabolism has a central role in the resistance of cotton to the wilt fungus *Verticillium dahliae* as revealed by RNA-seq-dependent transcriptional analysis and histochemistry. *Journal of Experimental Botany* **62**, 5607–5621.
- Woolfson KN. 2018. Suberin biosynthesis and deposition in the wound-healing potato (*Solanum tuberosum* L.) tuber model. PhD thesis, The University of Western Ontario, London, Canada. <https://ir.lib.uwo.ca/cgi/viewcontent.cgi?article=8075&context=etd>. Accessed July 2020.
- Xu L, Zhu L, Tu L, Liu L, Yuan D, Jin L, Long L, Zhang X. 2011. Lignin metabolism has a central role in the resistance of cotton to the wilt fungus *Verticillium dahliae* as revealed by RNA-Seq-dependent transcriptional analysis and histochemistry. *Journal of Experimental Botany* **62**, 5607–5621.
- Yadav V, Molina I, Ranathunge K, Castillo IQ, Rothstein SJ, Reed JW. 2014. ABCG transporters are required for suberin and pollen wall extracellular barriers in Arabidopsis. *The Plant Cell* **26**, 3569–3588.
- Yadeta KA, J Thomma BP. 2013. The xylem as battleground for plant hosts and vascular wilt pathogens. *Frontiers in Plant Science* **4**, 97.
- Yuan M, Jiang Z, Bi G, Nomura K, Liu M, He SY, Zhou J-M, Xin X-F. 2020. Pattern-recognition receptors are required for NLR-mediated plant immunity. *BioRxiv* doi.org/10.1101/2020.04.10.031294. [Preprint].
- Zaini PA, Nascimento R, Gouran H, Cantu D, Chakraborty S, Phu M, Goulart LR, Dandekar AM. 2018. Molecular profiling of Pierce's disease outlines the response circuitry of *Vitis vinifera* to *Xylella fastidiosa* infection. *Frontiers in Plant Science* **9**, 771.
- Zhou F, Emonet A, Dénervaud Tendon V, Marhavy P, Wu D, Lahaye T, Geldner N. 2020. Co-incidence of damage and microbial patterns controls localized immune responses in roots. *Cell* **180**, 440–453.e18.
- Zhu W, Gao E, Shaban M, Wang Y, Wang H, Nie X, Zhu L. 2018. GhUMC1, a blue copper-binding protein, regulates lignin synthesis and cotton immune response. *Biochemical and Biophysical Research Communications* **504**, 75–81.
- Zimmermann MH. 1979. The discovery of tylose formation by a Viennese lady in 1845. *IAWA BULLETIN*, 2–3, 51–56.

## 1.7 Background of the study

The soil borne vascular wilt pathogen *Ralstonia solanacearum* causes wilt disease in more than 450 plant species (Sakthivel *et al.*, 2016). The pathogen invades through plant roots and advances inter-cellularly through the root cortex to reach the xylem, where it proliferates and spreads systemically to aerial plant parts (Bae *et al.*, 2015). In order to get access into the vasculature, the pathogen generally target root extremities and the junction between primary and lateral roots where the epidermal barrier may be compromised, and the endodermis as well as casparian strip are either not fully differentiated or reoriented by outgrowth of lateral roots (Álvarez *et al.*, 2010). Hence, colonization of the root xylem vasculature is critical, as in this particular tissue the bacterium multiplies and moves vertically to the stem. However, plants have evolved mechanisms in the roots to sense invading pathogens and mount a defense response against this aggressor. Root resistance against soil borne vascular pathogens has been identified in germplasms of several plant species, which are used as rootstocks for grafting commercially important varieties (Caldwell *et al.*, 2017; Cháves-Gómez *et al.*, 2020). The resistant tomato cultivar Hawaii 7996 (H7996) imposes severe restriction in colonization by *R. solanacearum* at the root cortex and compartmentalizes the pathogen at the xylem vasculature (Planas-Marquès *et al.*, 2019). Similarly, in incompatible interactions of tomato with the phytopathogenic fungus *Fusarium oxysporum* f.sp. *lycopersici*, the pathogen reaches the vasculature but its colonization is drastically confined thereafter (van der Does *et al.*, 2019).

Inducible structural barriers formed at and around the root vasculature upon colonization constitute one of the most important defense components against *R. solanacearum* (Ishihara *et al.*, 2012). Plants have evolved effective structural defense mechanisms to prevent vessel colonization or movement between vessels once vascular colonization has occurred (Beckman and Roberts, 1995). During pathogen progression through the root cortex and vasculature, cell walls stand as the first barrier of defense against soil borne vascular pathogens (Novo *et al.*, 2017; Kashyap *et al.*, 2021). *R. solanacearum* induced reinforcements in secondary cell wall of vascular tissue act as a potent barrier against colonization of the bacterium (Ferreira *et al.*, 2017). Timely formation of these physico-chemical vascular barriers early upon pathogen perception

can lead to confinement of the vascular pathogen at the infected vessel, avoiding the spread of wilt diseases (Robb *et al.*, 2008; Zaini *et al.*, 2018; Planas-Marquès *et al.*, 2019). However, lack of in depth characterization on such vascular reinforcements act as bottleneck in deploying these traits of interest for crop improvement. Hence, in this thesis we attempted to characterize by comparative histological studies the key physico-chemical barriers induced in tomato root xylem vascular defense against *R. solanacearum* (Chapter 1). Changes in secondary wall components of root induced by *R. solanacearum* infection were characterized by spectroscopic techniques (Chapter 2). Further, differential transcript accumulation in resistant and susceptible tomato root xylem vasculature was evaluated for the pathway genes of secondary wall polymers. We also delve into the possibility of metabolic engineering resistance in susceptible tomato against *R. solanacearum*, by conducting infection assays in overexpressing lines of suberin and hydroxycinnamic acid amide pathway genes (Chapter 3).

# **OBJECTIVES**

## OBJECTIVES

---

The main goals of this thesis are described below:

### Objectives:

#### **I. Characterization of the xylem vascular wall reinforcements induced by *Ralstonia solanacearum* infection in resistant Hawaii 7996 tomato**

- To characterize and compare histopathologically the responses of resistant and susceptible tomato lines against *Ralstonia solanacearum* to identify key defense-associated structural changes in the root vasculature.
- To characterize root vascular wall modifications against *Ralstonia solanacearum* in resistant tomato.

#### **II. Exploring the suberin pathway for resistance against *Ralstonia solanacearum* in tomato**

- To analyse differential expression of suberin poly-aromatic and aliphatic pathway genes in the root vasculature of resistant and susceptible tomato upon *Ralstonia solanacearum* infection.
- To study the *R. solanacearum* induced suberization in xylem vascular tissue spatiotemporally using reporter gene system.
- To characterize the impact of overexpressing ligno-suberin pathway genes in susceptible tomato background in relation to *R. solanacearum* colonization and disease development.



# **CHAPTER I**

## **2. Structural modifications of root xylem vasculature as defense response to *Ralstonia solanacearum* in tomato**

### **2.1 Introduction**

Plants have a robust multi-layered immune system to protect themselves from pathogens (Jones and Dangl, 2006). The pre-existing barriers such as cuticle and epidermis present in plants, act as a first line of defense to pathogens (Serrano *et al.*, 2014; Falter *et al.*, 2015). Further, several physico-chemical barriers are formed *de novo* to prevent pathogenic invasion, composition of which varies depending on the patho-system and tissue under attack (Dixon and Paiva, 1995). Inducible physico-chemical barriers are particularly important as a defense response to compartmentalize infection sites and prevent systemic spread of vascular wilt pathogens, which are highly pernicious agents (Kashyap *et al.*, 2021). These wilt pathogens colonize the xylem vasculature and their unrestrained multiplication may cause devastating diseases in plants (Potter *et al.*, 2011; Scortichini, 2020).

The soil borne bacterial wilt pathogen *Ralstonia solanacearum* causes disease in more than 450 plant species and it is an aggressive pathogen of important crop species of Solanaceae family such as tomato (Peeters *et al.*, 2013). However, there are resistant accessions of tomato which are known to strongly hinder this invasive strategy of *R. solanacearum*. Among the different resistant germplasms of tomato, the cultivar Hawaii 7996 (H7996) is the most effective natural source of resistance against *R. solanacearum*, proven to resist various strains of the bacterium under different environmental conditions (Grimault *et al.*, 1994a; Nakaho *et al.*, 2004). In this cultivar, resistance to *R. solanacearum* is a complex polygenic trait involving two major quantitative trait loci (QTLs) located in chromosomes 12 and 6 (Bwr-12 and Bwr-6), accounting for 18–56% and 11–22% of the phenotypic variation, respectively (Wang *et al.*, 2013), and three minor loci (Bwr-3, Bwr-4, and Bwr-8) (Thoquet *et al.*, 1996; Mangin *et al.*, 1999; Wang *et al.*, 2000). This cultivar offers severe restriction in root colonization, vertical movement from roots to shoots as well as circular vascular bundle invasion, and radial apoplastic spread in the cortex (Planas-Marquès *et al.*, 2019).

In case of vascular wilt diseases, host xylem vascular tissue acts as an important battleground for pathogens, consequences of which determine the outcome of the infection (Yadeta and Thomma, 2013). To prevent the spread of pathogenic propagules, the xylem vasculature of resistant plants undergoes intense structural and metabolic modifications. If a pathogen manages to reach the xylem, this transport system becomes an excellent channel of inoculum dissemination throughout the plant. Hence, the resistant plants form vertical barriers such as tyloses and gels inside the vessel lumen, which is an effective means of slowing down vertical progression of the pathogen, or even confining it to the infection site, preventing systemic infection (VanderMolen *et al.*, 1987; Rioux *et al.*, 2018). Further, for a successful vascular colonization the pathogen has to proliferate inside vessel lumen and later move from xylem vessel lumen to the surrounding xylem parenchyma cells and nearby vessels and intercellular spaces by degeneration of vessel pit membranes or by a breach in the walls (Nakaho *et al.*, 2000; Dignonnet *et al.*, 2012). To facilitate this process, the pathogen's cell wall degrading enzymes come into play, which are important pathogenicity determinants of wilt pathogens (Liu *et al.*, 2005; Pérez-Donoso *et al.*, 2010; Lowe-Power *et al.*, 2018). However, in resistant plants, this horizontal movement of pathogens is restricted by reinforcing the walls of xylem vasculature preventing pathogenic degradation (Street *et al.*, 1986; Benhamou, 1995). Such reinforcement acts to limit the horizontal movement of the pathogen from the colonized vessel (Daayf *et al.*, 1997). Besides, its deposition acts as a shield against pathogen-derived metabolites such as toxins and enzymes, and makes water and nutrients inaccessible for pathogens, thereby impeding their growth (Fig. 1) (Araujo *et al.*, 2014).

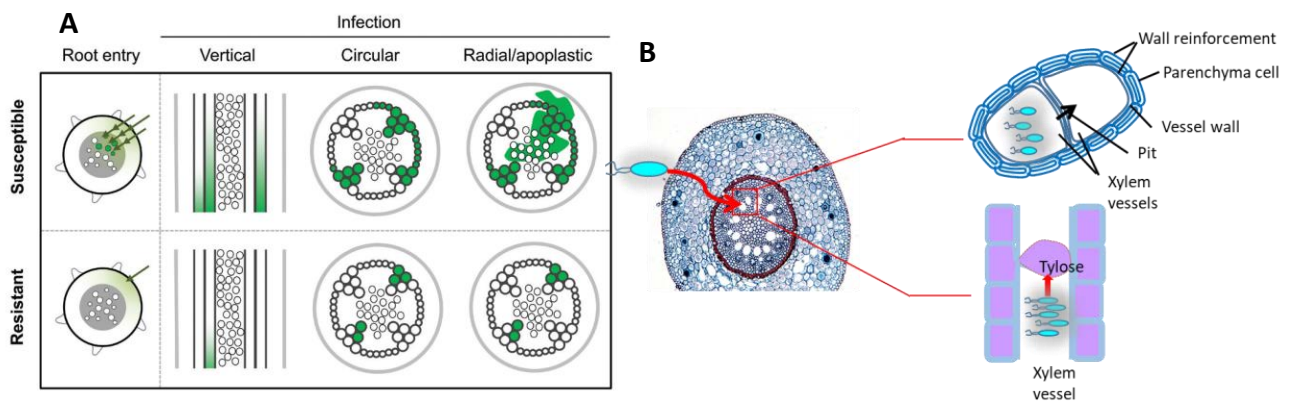


**Figure 1: Structural restriction of *R. solanacearum* colonization in resistant tomato.** (A) Schematic representation of the tissue levels where *R. solanacearum* (shown in green) undergoes colonization restriction

in resistant tomato H7996. This cultivar offers severe restriction in root colonization, vertical movement from roots to shoots as well as circular vascular bundle invasion, and radial apoplastic spread in the cortex. (B) Tyloses and gels could act as a structural barrier in vertical movement of *R. solanacearum* in colonized vessel and wall reinforcements may act in restricting horizontal movement of the pathogen. (A) Adapted from Planas-Marquès et al., (2019).

These vascular wall reinforcements seem to play an important role in confining *R. solanacearum* at the xylem vascular bundles of resistant H7996. Ultra-microscopic studies in quantitatively resistant tomato cultivars showed that the pit membranes, as well as vessels walls and parenchyma cells, form a conspicuously thick coating in the form of an electron dense amorphous layer, as part of the defense response against *R. solanacearum* (Nakaho *et al.*, 2000; Kim *et al.*, 2016). However, the type of barriers involved in this interaction remains mostly elusive. Understanding the underlying mechanisms of restriction can give vital clues in management of the pathogen by biotechnological interventions. In the current chapter, we discuss about a detailed histopathological investigation to identify the anatomical and physico-chemical modification in the vasculature of H7996 after infection with *R. solanacearum* compared to a susceptible cultivar Marmande.

## **2.2 Results & discussion**

### **2.2.1 Resistant H7996 tomato restricts *R. solanacearum* colonization at the root xylem vasculature**

Inoculation assays with *R. solanacearum* GMI100 showed that resistant tomato cultivar H7996 offered a high degree of resistance against *R. solanacearum*, thereby exhibiting extremely mild symptoms upon infection as compared to susceptible tomato Marmande. Soil soak inoculation of *R. solanacearum* GMI1000 resulted in wilting of most plants of susceptible Marmande at 10 days post inoculation (10 dpi), while H7996 plants remained mostly asymptomatic (Fig 2A). Progress of wilting was assayed in both cultivars by rating plants daily on a 0 to 4 disease index scale where 0 = healthy and 4 =100% wilted (Planas-Marquès *et al.*, 2019). At 12 dpi most Marmande plants were 100% wilted, whereas H7996

plants were free from wilting showing occasionally yellowing on lowermost leaves (Fig 2B).

To unravel the mechanisms of colonization restriction and the patterns of invasion, resistant tomato cultivar H7996 and susceptible cultivar Marmande were inoculated using luminescent and fluorescent reporter strain *R. solanacearum* GMI1000 carrying a *PpsbA::LuxCDABE* and *PpsbA::GFPuv* fusion, respectively (Cruz *et al.*, 2014). These reporter strains allow a direct and precise visualization of luminescent and fluorescent bacterial cells in plant tissues by luminometry and microscopy (Ferreira *et al.*, 2017). Plants were inoculated through the roots by soil drench in both H7996 and Marmande and analyzed for differences in colonization. Using the luminescent reporter strain, we investigated the colonization pattern in the taproot of both the cultivars over time. The luminescent readings obtained from taproot tissues were converted to colony forming units per gram tissue (CFU g<sup>-1</sup>) as described in Planas-Marquès *et al.*, (2019). Bacterial load in taproot rises from ~10<sup>3</sup> CFU g<sup>-1</sup> at 2DPI to 10<sup>8</sup> CFU g<sup>-1</sup> in Marmande at 12 DPI. In contrast, bacterial load in taproot of H7996 remained at <10<sup>6</sup> CFU g<sup>-1</sup> at 12 DPI, showing remarkable restriction in invasion (Fig 2C).

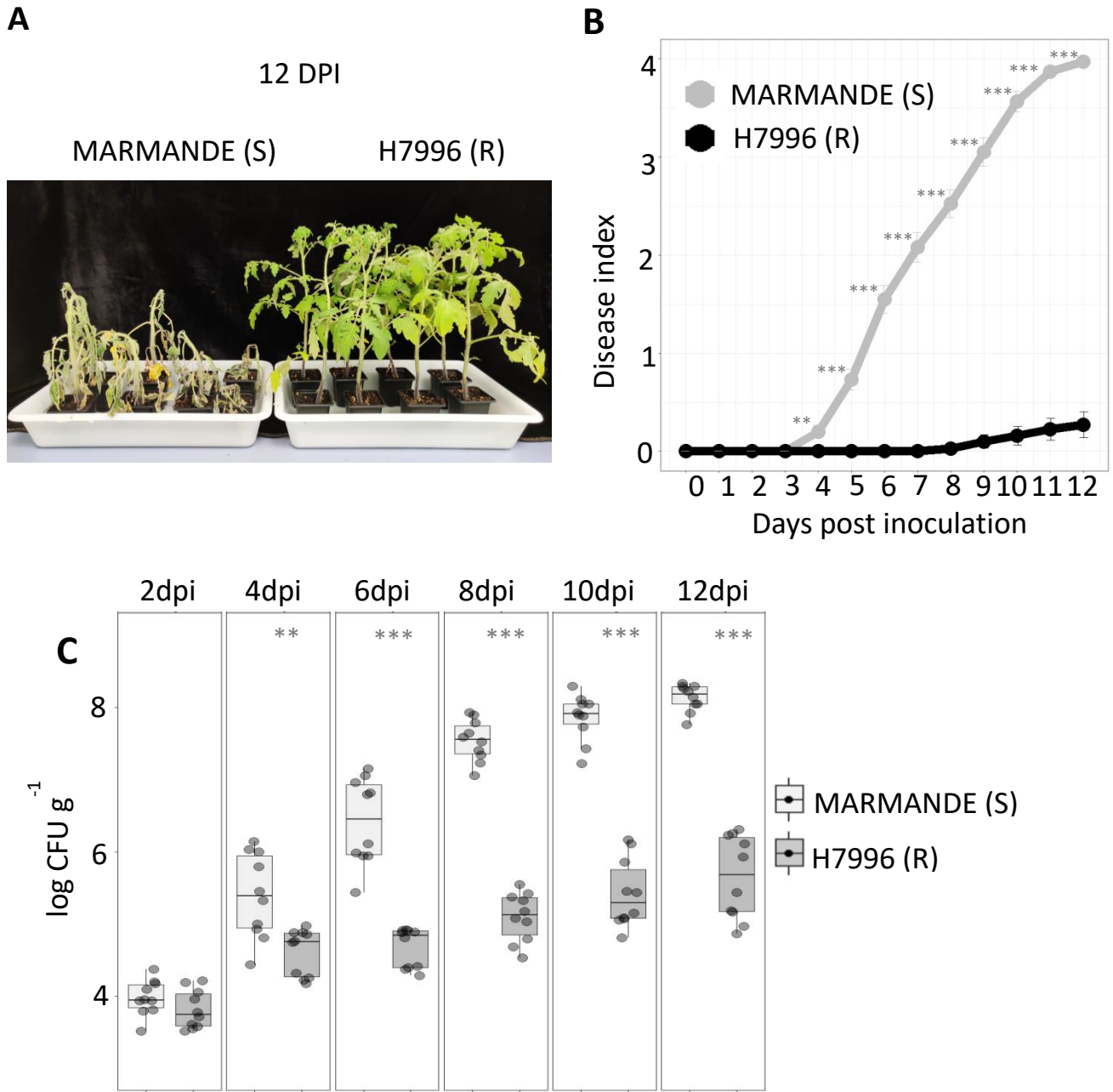


**Figure 2: Tomato cultivar H7996 shows high degree of resistance to *R. solanacearum* and restricts colonization at the root.** Susceptible (Marmande) and resistant (H7996) 5-week-old tomato plants were root-inoculated with a *R. solanacearum* GMI1000 luciferase reporter strain at a concentration of  $\sim 1 \times 10^7$  CFU/ml (A) At 12 days post inoculation (DPI) most plants of Marmande show severe wilting symptom, whereas H7996 remain mostly symptomless. (B) Progress of wilting was assayed in both cultivars by rating plants daily on a 0 to 4 disease index scale where 0 = healthy and 4 = 100% wilted. (C) The level of *in planta* colonization by *R. solanacearum* was calculated as colony forming units per gram of fresh taproot tissue (CFU·g<sup>-1</sup>) at the indicated days post-infection (dpi). Data presented are of a representative experiment with n=10 plants for each time point each cultivar out of a total of 3 experiments. Asterisks indicate statistically



significant difference between Marmande and H7996 in a paired Student's t-test (\*\* p-value of  $p < 0.01$  and \*\*\* p-value of  $p < 0.001$ )

To spatially determine the colonization restriction pattern of *R. solanacearum* in root tissue of H7996, we infected H7996 plants alongside Marmande with the strain constitutively expressing GFPuv and observed the cross-sections of the taproot with a fluorescence stereomicroscope. It was observed that H7996 imposes severe restriction in movement of the bacterium within the xylem vascular ring. H7996 confined bacterial multiplication to isolated regions of vascular tissue and in many cases restricted to one xylem pole of the vascular ring. The pathogen upon reaching the vasculature, remains confined to the vessel lumen and its movement from vessel to vessel, to surrounding parenchyma cells and apoplast is severely restricted (Fig 3B). In contrast, the bacteria multiplied intensively in Marmande, filling the xylem vessels as well as surrounding parenchyma cells and apoplastic spaces at 9 DPI (Fig 3A). These observations corroborated our previous study where we identified four distinct spatiotemporal phases where resistant tomato cultivar H7996 is able to restrict the bacterium *in planta* (Planas-Marquès *et al.*, 2019). The pathogen was observed to encounter severe restriction in root colonization, vertical movement from roots to shoots as well as circular vascular bundle invasion, and radial apoplastic spread in the cortex.

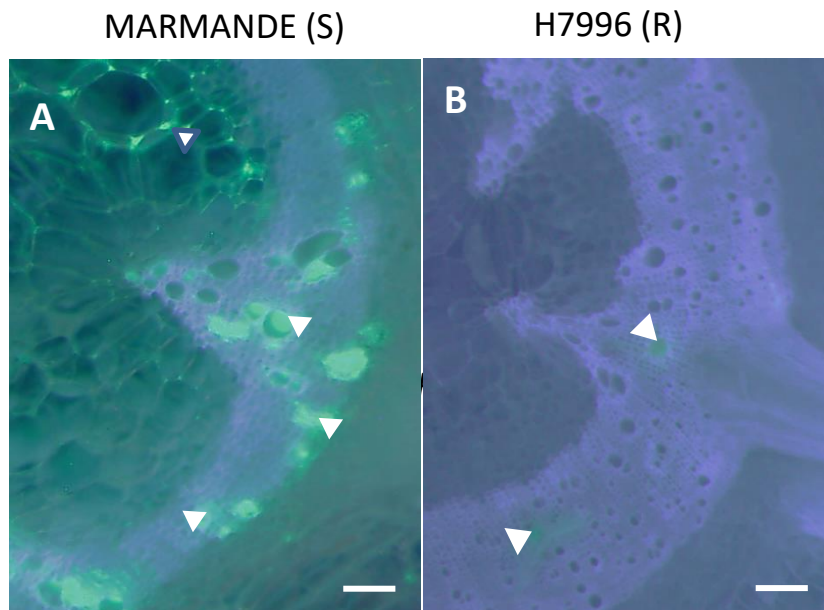


**Figure 3: Resistant H7996 tomato restricts *R. solanacearum* colonization at the root xylem vasculature.** Susceptible (Marmande) and resistant (H7996) 5-week-old tomato plants were root-inoculated with a *R. solanacearum* GMI1000 GFP reporter strain at a concentration of  $\sim 1 \times 10^7$  CFU/ml. (A) Microscopic

observation showed that in Marmande at 9 dpi bacteria multiplied intensively filling the xylem vessels as well as surrounding parenchyma cells and apoplastic spaces. (B) However, in H7996 *R. solanacearum* at 9 dpi remained confined to the vessel lumen and its movement from vessel to vessel, to surrounding parenchyma cells and apoplast is severely restricted.

### **2.2.2 Resistant H7996 tomato induces deposition of a vascular coating of phenolic nature at the roots in response to *R. solanacearum***

To understand the mechanisms controlling this restriction in the xylem vasculature, we performed histological investigations to identify any physico-chemical barrier formed as a result of this interaction. Taproots of *R. solanacearum*-soil drench inoculated or water-treated plants were used for obtaining transverse cross-sections with a sterile razor blade and kept in 70 % ethanol at room temperature for 5-7 days. By treating with ethanol it removes all soluble components, which also contain phenolics but not wall-bound, and that can be a component of defense, but not structural. Epi-fluorescence microscopy of transverse taproot cross-sections, indicated that xylem vascular tissue of resistant H7996 structurally responded to *R. solanacearum* by reinforcing the walls of xylem vascular tissue with cell wall bound phenolic materials. Phenolic deposits at the wall are known to emit auto-fluorescence signal upon illumination with UV under an epi-fluorescence microscope (Pouzoulet *et al.*, 2013; Araujo *et al.*, 2014). As an indication of phenolic polymers in wall reinforcements, we observed a strong auto-fluorescence signal emitted from walls of vessels, surrounding xylem parenchyma cells and tracheids upon infection of *R. solanacearum* in resistant H7996 (Fig 4D, F). *R. solanacearum* colonize xylem tissue by moving from vessel to vessel as well as into surrounding xylem parenchyma cells and inter-cellular spaces by degeneration of vessel pit membranes or by a breach in the vessel walls by enzymatic degradation (Nakaho *et al.*, 2000; Kim *et al.*, 2016). Hence, this vascular coating with wall bound phenolic compounds might play a role in restricting horizontal spread of the bacterium. Phenolic deposits in H7996 may strengthen the vascular walls restricting pathogenic degradation, and also might act as an antimicrobial barrier. In contrast, susceptible Marmande is not able to induce such vascular coatings (Fig. 4 C,E). Absence of such reinforcements in the wall and pit membranes might make the vascular tissue prone to pathogenic degradation.

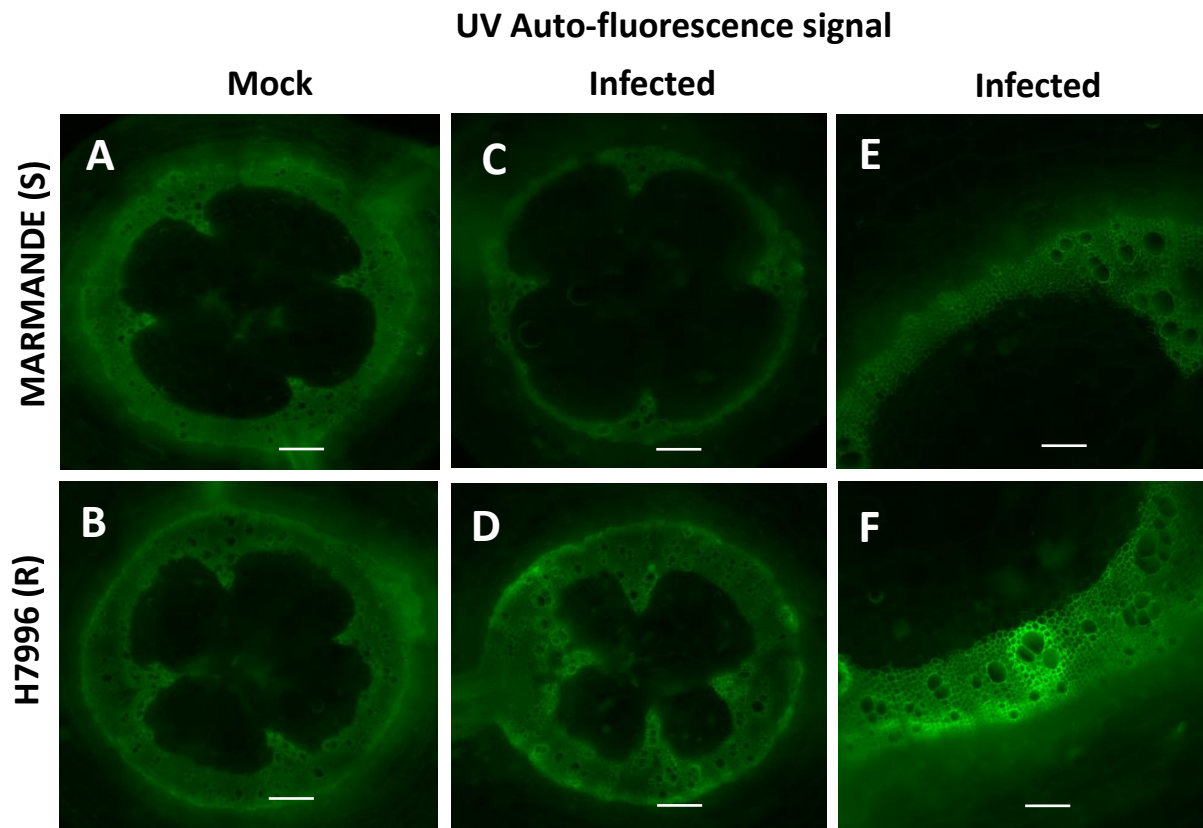


**Figure 4: Resistant H7996 induce a vascular coating with wall bound phenolics as defense response to *R. solanacearum*.** Marmande and H7996 plants were soil-soak inoculated with  $\sim 1 \times 10^7$  CFU/ml of *Ralstonia solanacearum* GMI1000 and incubated at 28°C. Taproot cross-sections were obtained at 9 dpi. UV microscopy showed a strong auto-fluorescence signal emitted from the walls of vessels and surrounding parenchyma cells in (D,F) infected H7996 plants, corresponding to phenolic deposits, compared to (C,E) Marmande or (A,B) the mock controls. Images from a representative experiment with  $n=6$  plants per variety. Scale bar = 500  $\mu$ m.

### 2.2.3 Differential lignin deposition response in root vasculature of resistant H7996 and susceptible Marmande against *R. solanacearum*

Lignin is a phenolic polymer that constitutes an integral part of the secondary cell wall of the xylem vasculature that has been shown to act as a common structural defense response

against vascular wilt pathogens (Novo *et al.*, 2017). To test whether lignin was a major component of the strong auto-fluorescence induced in H7996 in response to *R. solanacearum*, we used the Phloroglucinol-HCl staining technique (Baayen and Elgersma, 1985; Rioux *et al.*, 1998; Pouzoulet *et al.*, 2013). Phloroglucinol-HCl binds with lignin and stains it magenta. Phloroglucinol-HCl staining did not show any rise in lignification in H7996 upon infection. However, in Marmande *R. solanacearum* infection seemed to have a detrimental effect on lignification of xylem vasculature (Figure 5). Observation of Phloroglucinol-HCl stained sections under brightfield microscopy, showed that mock and infected H9776 (resistant) as well as mock Marmande (susceptible) samples showed a red purple color characteristic of the reaction of phloroglucinol HCl in vessels and fibers, indicative of lignin (Fig 5 A,C,D); in contrast, infected Marmande tap root sections exhibit phloroglucinol staining primarily in the xylem with less staining in the interfascicular fiber, suggesting that lignin in the cell walls of fibers might be less cross-linked due to a different composition of lignin and/or may have been degraded by *R. solanacearum* (Fig. 5B). Lignin is deposited in the cell wall between cellulose, hemicellulose and pectin. Although it is not known whether *R. solanacearum* can directly target lignin by enzymatic degradation, the bacterium has several cell-wall-modifying proteins such as cellulases, expansin and pectinases, which may participate in disintegration of the cell wall matrix (Liu *et al.*, 2005; Pérez-Donoso *et al.*, 2010; Lowe-Power *et al.*, 2018; Kang *et al.*, 2019).

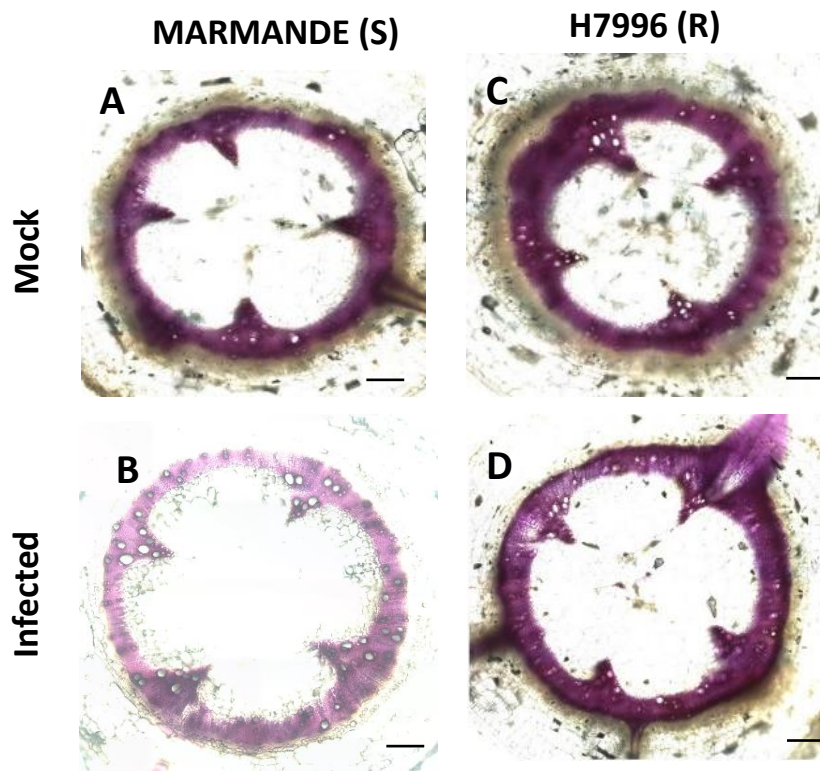


**Figure 5: *R. solanacearum* infection showed a detrimental effect on xylem vasculature lignification in Marmande, but not in H7996.** Phloroglucinol-HCl staining of taproot xylem vasculature of Marmande and H7996 water treated or *R. solanacearum* inoculated at 9 dpi, showed reduced lignin staining in (B) Marmande infected in comparison to (A) water treated plants. In H7996, no visible differences in lignin content of xylem vasculature was observed between (C) water treated and (D) infected plants. Images from a representative experiment with  $n=6$  plants per variety. Scale bar = 500  $\mu\text{m}$ .

Also, Phloroglucinol-HCl has a property wherein upon staining lignin, it quenches the UV auto-fluorescence signal emitted from the phenolic polymer (Biggs, 1984; Aoun *et al.*, 2009; Pouzoulet *et al.*, 2013). Utilizing this property, we analyzed taproot cross-sections of mock and *R. solanacearum*-inoculated plants of both Marmande and H7996. Phloroglucinol-HCl staining could quench the UV auto-fluorescence from xylem vasculature of susceptible Marmande mock water treated plants (Fig 6A) and *R. solanacearum* infected plants (Fig 6B), as well as resistant H7996 water treated plants (Fig 6C). In contrast, in *R. solanacearum* infected resistant H7996 (Fig 6D) strong UV auto-fluorescence could be observed in walls of xylem vessels, surrounding xylem

parenchyma cells and tracheids, indicating reinforcement of walls of vascular tissue with phenolics formed *de novo* upon infection. The fact that this auto-fluorescence could not be quenched by lignin binding phloroglucinol-HCl stain, indicated the non-lignin nature of these structural phenolics. Phenolic auto-fluorescence from walls, which cannot be quenched by phloroglucinol-HCl treatment is attributed to suberin polymer (Aoun *et al.*, 2009; Pouzoulet *et al.*, 2013). The UV auto-fluorescence signal emitted from xylem vessel walls and the surrounding parenchyma cells, tracheids was measured using the LAS X Leica software after the Phloroglucinol-HCl treatment. *R. solanacearum* induced rise in auto-fluorescence signal was observed specifically in resistant H7996 (Fig 6E).

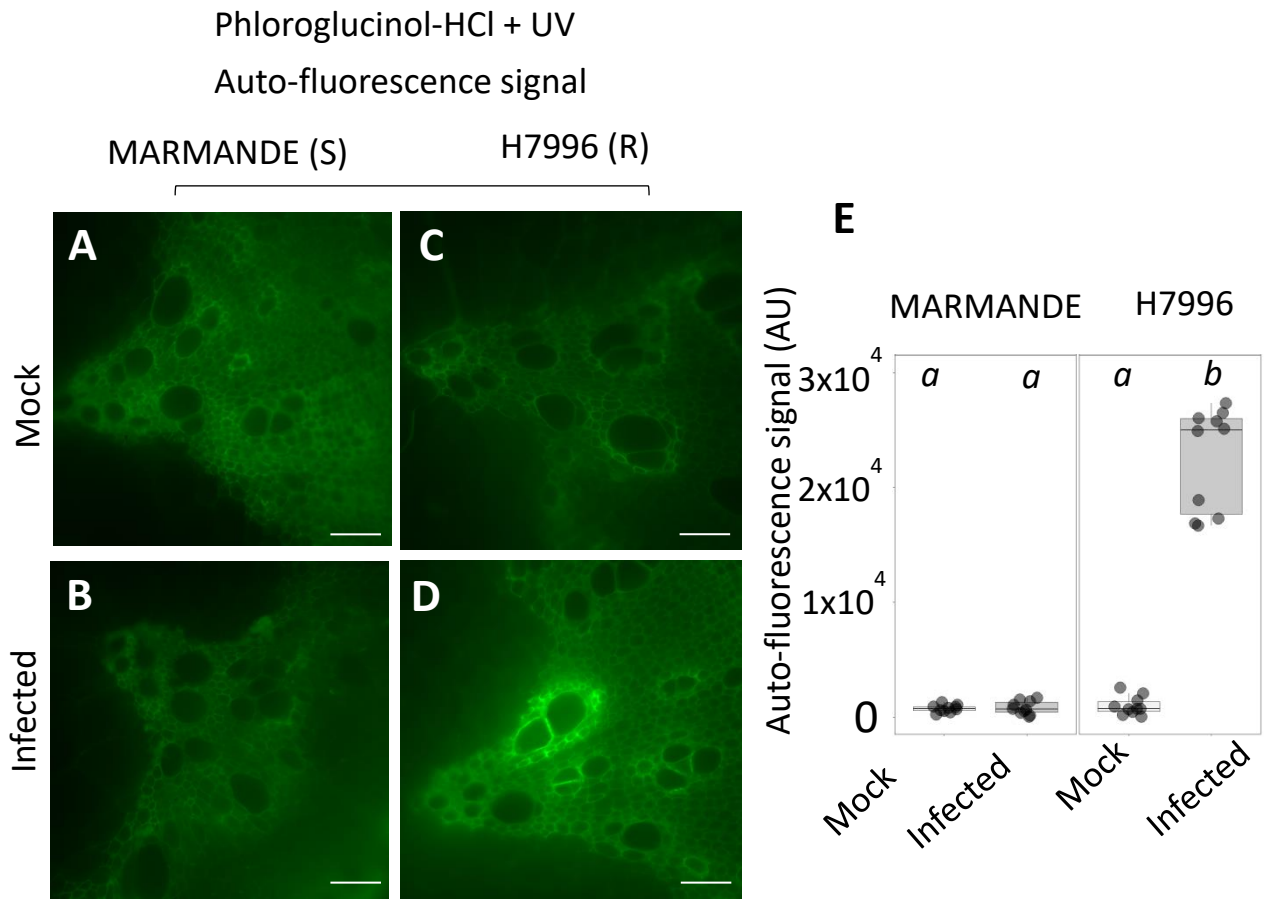


**Figure 6: Phenolic deposits at xylem vessel walls and surrounding parenchyma cells formed in resistant H7996 in response to *R. solanacearum* infection, cannot be quenched by phloroglucinol-HCl treatment.** Susceptible (Marmande) and resistant (H7996) 5-week-old tomato plants were root-inoculated with a *R. solanacearum* GMI1000 at a concentration of  $\sim 1 \times 10^7$  CFU/ml (B,D,E) or water mock (A,C,E). (A,B,C,D) Quenching of lignin UV autofluorescence was analyzed after phloroglucinol-HCl staining of



taproot cross-sections containing  $10^5$  CFU g<sup>-1</sup> of *R. solanacearum*. (D) In infected H7996 strong UV auto-fluorescence could be observed in the walls of xylem vessels surrounding xylem parenchyma cells and tracheids, indicating reinforcement of walls of vascular tissue with phenolics formed *de novo* upon infection. This auto-fluorescence could not be quenched by the lignin-binding Phloroglucinol-HCl stain. (E) The UV auto-fluorescence signal was measured using the LAS X Leica software after the phloroglucinol-HCl treatment described in (A,B,C,D). Data presented correspond to a representative experiment out of 3 each with n=6 plants per variety. Different letters indicate statistically significant differences ( $\alpha=0.05$ , Fisher's least significant difference test). Scale bar = 100  $\mu$ m.

### **2.2.4 Ferulates accumulate in vascular coating of resistant H7996 as defense response to *R. solanacearum***

Ferulic acid derivatives, such as conjugates with amides and esters (ferulates), are known to deposit in cell walls during wounding, pathogen attack and elicitor treatments (Bernards and Lewis, 1992; Negrel *et al.*, 1995; Franke *et al.*, 1998; King and Calhoun, 2005; Novo *et al.*, 2017). These compounds cross-link with cell wall polysaccharides, contribute towards formation of a phenolic barrier and make cell wall resilient to pathogenic degradation. Further, they act as important precursors of the suberin poly-phenolic domain (Bernards and Lewis, 1992; Negrel *et al.*, 1995). To analyze whether the pathogen-induced coating of vessels observed in H7996 corresponded to an increase in ferulates we used a technique whereby ferulates can be detected by emission of blue fluorescence with UV excitation at neutral pH that characteristically changes to a stronger green emission under conditions of high pH such as in the presence of alkali (Carnachan and Harris, 2000; Harris and Trethewey, 2010; Donaldson and Williams, 2018).

Interestingly, we observed that the UV autofluorescence detected in vascular coatings in response to *R. solanacearum* infection in resistant H7996 changed from blue to a strong green color upon treatment with alkali (1N KOH pH above 10) (Fig. 7,8), indicating the presence of ferulates in these coatings. This *R. solanacearum*-induced xylem vasculature feruloylation is specific to resistant H7996, as in susceptible Marmande any blue autofluorescence observed does not change to green upon alkali treatment both at earlier stage of infection when bacterial colonization level is  $\sim 1 \times 10^5$  CFU g<sup>-1</sup> taproot tissue (Fig. 8) or late stages of infection (9 dpi) when bacterial colonization level crossed  $\sim 1 \times 10^7$  CFU g<sup>-1</sup> taproot tissue and plants showing wilting symptoms (Fig. 7). Also, constitutive ferulate

accumulation is not observed in xylem vascular tissue of mock-treated tomato plants of neither cultivar (Fig. 7 and 8).

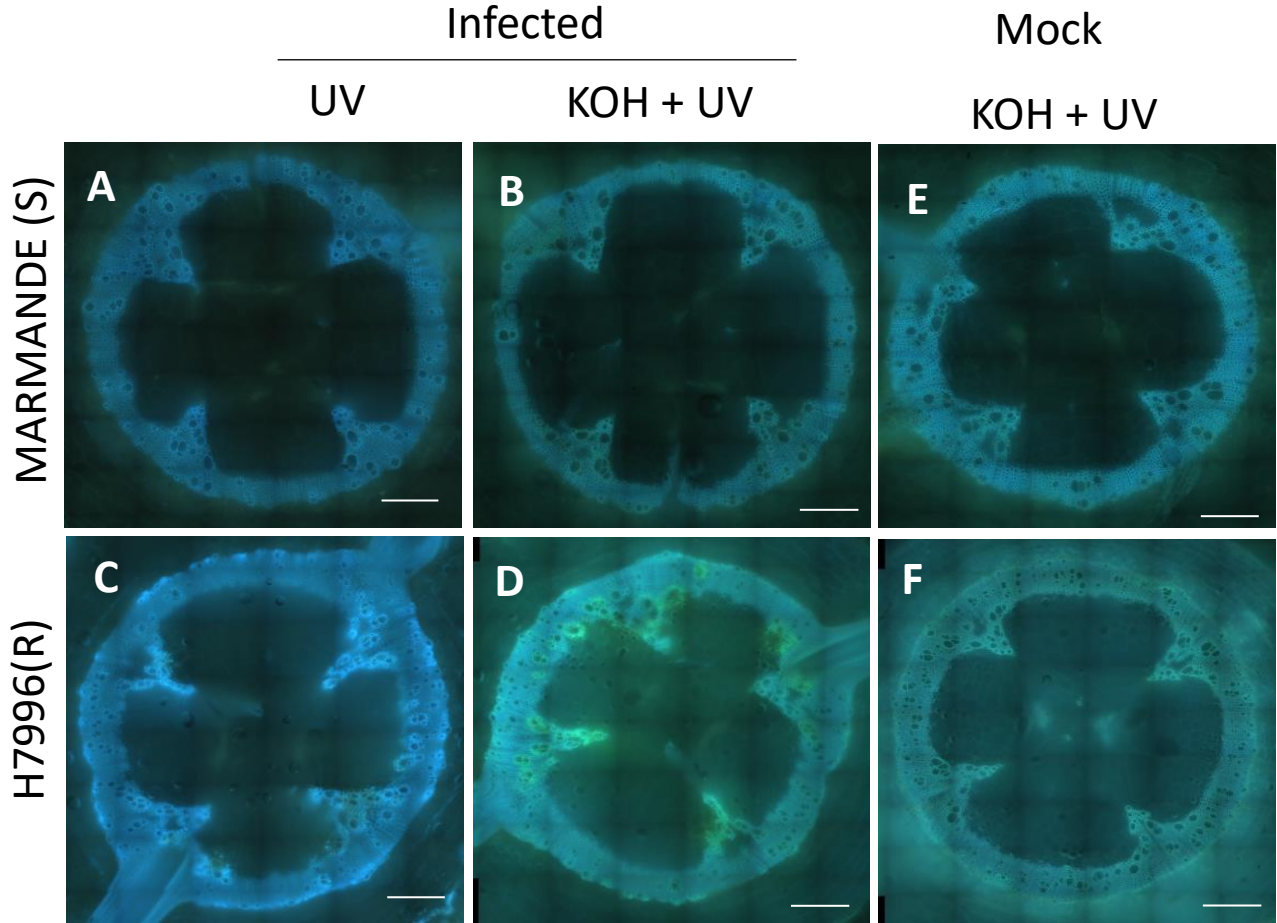


**Figure 7: Ferulates accumulate in walls of xylem vascular tissue of resistant H7996 as defense response to *R. solanacearum*.** Ferulates deposited in walls can be detected by emission of a blue fluorescence with UV excitation at neutral pH, that characteristically changes to stronger green emission under conditions of high pH such as in the presence of alkali. (A,B) In susceptible Marmande plants infected with *R. solanacearum*, ferulate deposition is either not observed or change due to infection is minimum as no UV auto-fluorescence could be seen which showed pH dependent colour conversion from blue to green. Whereas, in (C,D) resistant H7996 post *R. solanacearum* infection, UV auto-fluorescence of vessel wall, the surrounding xylem parenchyma cells and tracheid changed from blue to green or turquoise colour on treatment with KOH alkali (high pH above 10). Ferulates were also not observed in (E) Marmande water-treated plants and (F) H7996 water-treated plants. 40 ml of *Ralstonia solanacearum* strain GMI1000 suspension per plant with a concentration of  $\sim 1 \times 10^7$  CFU/ml was inoculated by soil soak and incubated at 28°C. Taproot cross-sections were made at 9DPI. Data presented correspond to a representative experiment out of 3 each with n=6 plants per variety. Scale bar = 500  $\mu$ m.

Specific deposition of ferulates in the vessel walls and surrounding parenchyma cells and tracheids of H7996 may presumably act as a physico-chemical barrier against *R. solanacearum*, either by preventing the enzymatic degradation of the cell wall, by directly inhibiting the growth of pathogen, or both. This barrier would also prevent the spread of the bacterium from the colonized vessel.

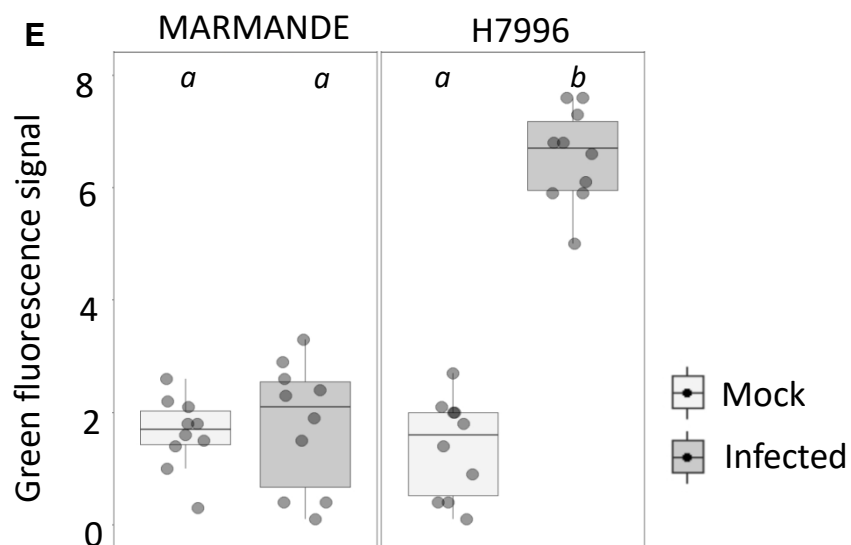
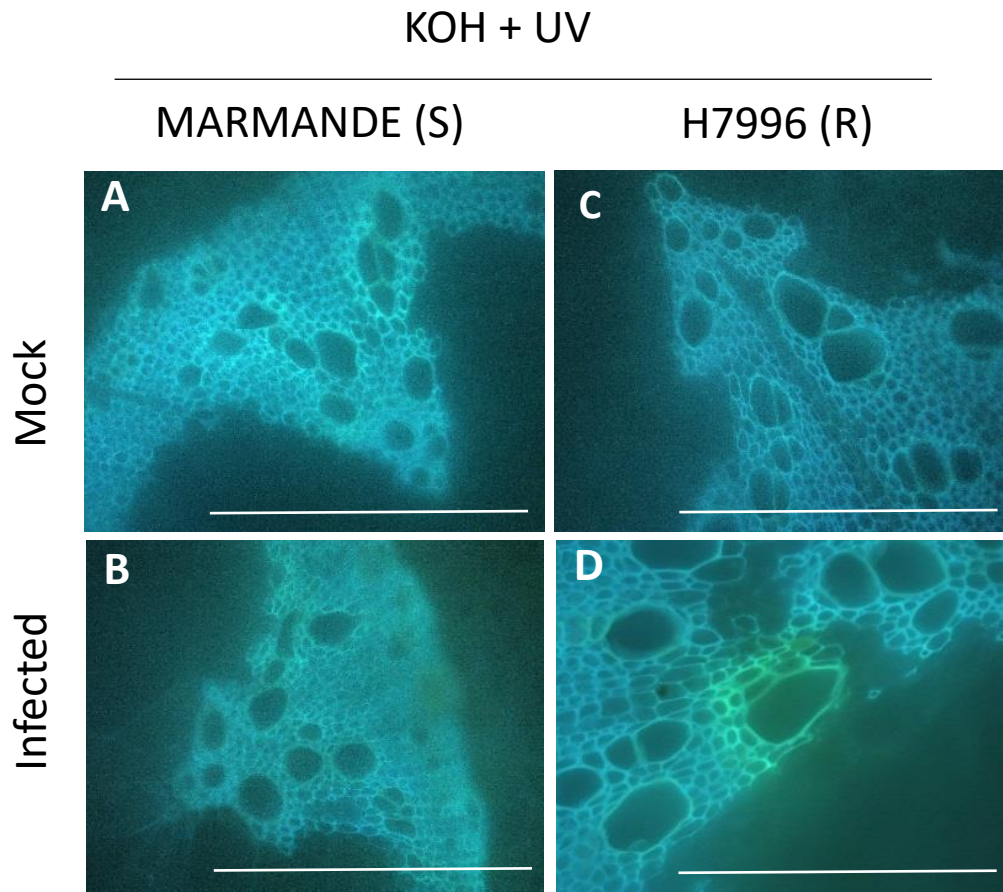


**Figure 8: *R. solanacearum* induced xylem vasculature feruloylation is specific to resistant H7996 and respond at early stage of colonization.** Taproot cross-sections containing  $10^5$  CFU g<sup>-1</sup> of *R. solanacearum* and mock plants were treated with 1N KOH alkali (pH above 10) and observed under UV to detect green ferulate depositions. Representative image of (A) water-treated; (B) *R. solanacearum* inoculated susceptible Marmande cross-sections and (C) water-treated and (D) *R. solanacearum* inoculated resistant H7996 cross-sections are shown. Scale bar = 500  $\mu$ m. (E) Green fluorescence from ferulate deposits in xylem and surrounding parenchyma cells was measured using ImageJ. Data presented correspond to a representative experiment out of 3 each with n=6 plants per variety.. (E) Box-and-whisker plots show data from a single representative experiment (n =6). Different letters in box-plot indicate statistically significant differences ( $\alpha=0.05$ , Fisher's least significant difference test).

### **2.2.5 Vascular feruloylation may be an intrinsic part of *R. solanacearum*-induced suberization in resistant H7996**

Ferulates are a major component of suberin, a cell wall polymer deposited in specialized tissues (root/tuber epidermis, root endodermis and seed coats) or in response to several stresses including pathogen attack. Suberin is comprised of a poly-phenolic/aromatic domain and a poly-aliphatic domain, deposited between the plasma membrane and the cell wall forming a hydrophobic protective barrier. The poly-phenolic domain of suberin is predominantly composed of ferulates, along with presence of other hydroxycinnamate such as p-coumarate and sinapate (Negrel *et al.*, 1995; Graça, 2010). The aliphatic domain consists of long chain fatty acids as well as small amounts of p-hydroxycinnamic acids (mainly ferulate) (Cohen *et al.*, 2020). The early accumulation of ferulates at suberization sites is a critical aspect for the coupling of the aromatic and aliphatic suberin domains (Boher *et al.*, 2013). Still, the process of suberization in response to pathogen invasion remains poorly defined.

To determine whether the ferulate accumulation in infected H7996 tomato was related with a vascular suberization process, we combined the ferulate-specific UV-alkali technique described above with Sudan IV staining, which binds to the aliphatic domain of suberin to produce a reddish-brown coloration upon UV illumination. In the taproot of *R. solanacearum*-infected H7996 plants, xylem vessel walls as well as the layers of vessels,

parenchyma cells and tracheids in the immediate vicinity could be seen suberized (reddish-brown signal from Sudan IV, Fig. 9, 10). In the periphery of suberized cells, feruloylated cells could be observed (green signal from UV-alkali, Fig. 9,11), which may indicate a preceding stage towards suberization. In comparison, no positive Sudan IV or UV-alkali staining could be detected in infected Marmande or mock-treated tomato plants. Our data suggest that walls of xylem parenchyma cells, vessels and tracheids present in the immediate vicinity of colonized vessels might respond by depositing ferulates in the beginning of infection that later become suberized. In later stages of infection, this layer of feruloylated walls expand towards more distal layers of cells in the immediate vicinity (Fig 9,11). Together, suberized and feruloylated layers of parenchyma cells, vessels and tracheids might form a “suberization zone” creating a strong physico-chemical barrier to limit *R. solanacearum* spread from the colonized xylem vessel lumen.



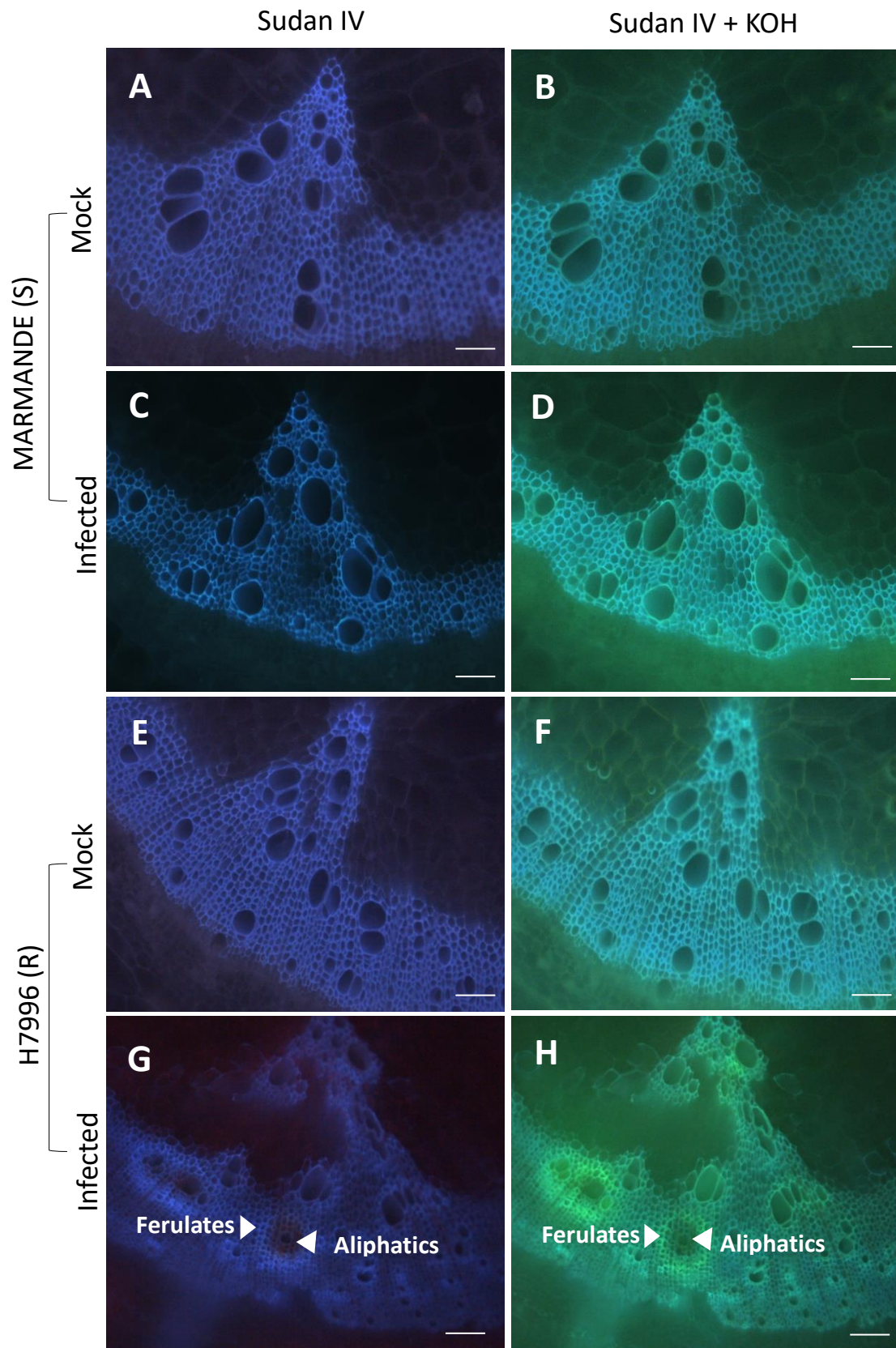


**Figure 9: Resistant H7996 tomato shows vascular deposition of ferulates as an intrinsic part of *R. solanacearum*-induced suberization.** Susceptible Marmande or resistant H7996 tomato plants were soil-



inoculated with a  $\sim 1 \times 10^7$  CFU/ml suspension of *Ralstonia solanacearum* GMI1000 or mock-inoculated with water and incubated at 28°C. Cross-sections were obtained from taproot tissue containing  $10^5$  CFU  $\text{g}^{-1}$  of *R. solanacearum*. For comparison taproot sections of mock plants from both cultivars of a similar age were used. Sections were stained with Sudan IV to visualize suberin aliphatics and subsequently treated with 1N KOH (pH above 10) to visualize ferulates. Sudan IV positive staining (reddish-brown coloration) was observed around xylem vessels specifically in infected H7996, indicating accumulation of suberin aliphatics. Accumulation of ferulates (blue-green coloration) appears also specifically in infected H7996 resistant tomato, surrounding sudan IV-stained areas. White arrowheads indicate the sites of accumulation of ferulates and aliphatic compounds. Representative images from one experiment out of three with  $n=6$  plants each were taken. Scale bar = 100  $\mu\text{m}$

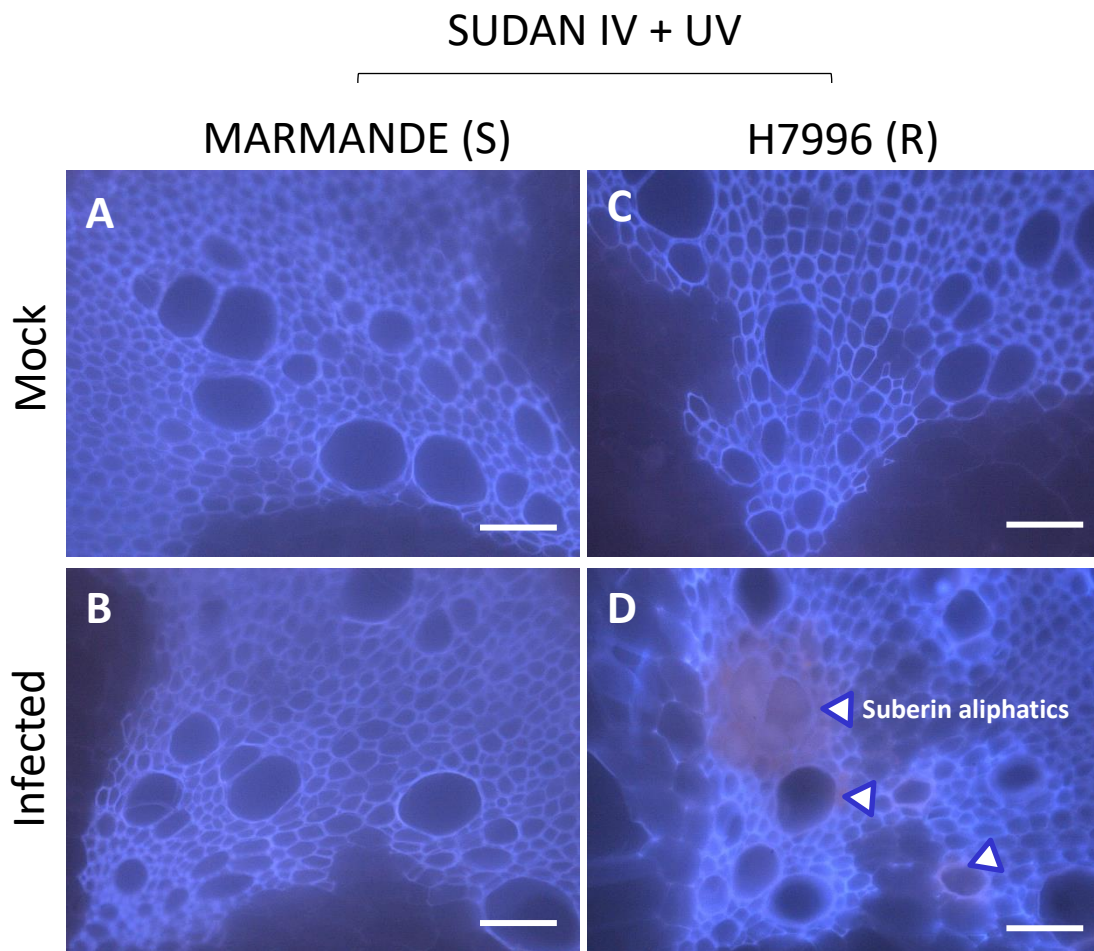


**Figure 10: Deposition of suberin aliphatics in walls of xylem vessel and the surrounding parenchyma cells and tracheids specifically in *R. solanacearum* infected resistant H7996.** Sudan IV stain binds to the aliphatic domain of suberin to produce a reddish-brown coloration when observed under UV. Images from a representative experiment with  $n=6$  plants. Susceptible (Marmande) and horizontally resistant (H7996), 5 week old tomato plants were inoculated through roots by soil-soak with 40 ml of *Ralstonia solanacearum*

strain GMI1000 suspension per plant with a concentration of  $\sim 1 \times 10^7$  CFU/ml and incubated at 28°C. Cross-sections of taproots containing *R. solanacearum* at a level of  $10^5$  CFU g<sup>-1</sup> tissue were used for microscopic observation. Scale bar = 100 µm

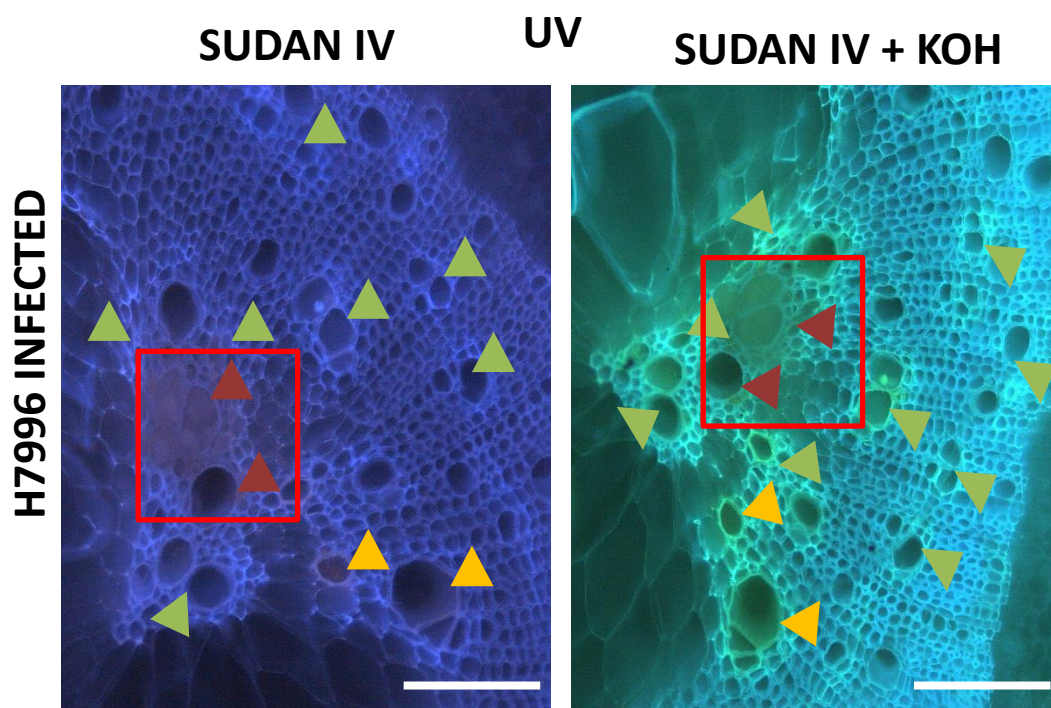


**Figure 11: Vascular feruloylation as a preceding step towards suberin aliphatics deposition.** Infected H7996 taproot cross-sections show vessels in three stages of vascular reinforcements, firstly there are vessels with ferulate deposits (green arrow heads). Secondly, there are vessels where the walls give Sudan IV positive signal (suberin aliphatics) and surrounding layers are ferulate positive (yellow arrow head). Thirdly, there are vessels where a Sudan IV positive signal from both vessel walls and surrounding parenchyma layers could be observed and also ferulate layers outside (red arrow heads). Scale bar = 200µm

The combined ferulate-specific UV-alkali and Sudan IV UV technique was found to be very sensitive in studying suberization in well characterized suberin model namely, potato tuber periderm. Potato tuber periderm consists of outer 6-12 outer layers of suberized cells called phellem, beneath which is a layer of metabolically active cells called phellogen,

undergoing cell wall thickening/suberization during periderm maturation process. Sudan IV stains reddish brown the walls of suberized phellem cells on UV illumination (Fig 12A). Upon KOH alkali treatment of sections, followed by UV illumination, walls of phellogen cells emitted green auto-florescence, indicating strong deposition of ferulate in its walls, showing the association of feruloylation as early suberization event (Fig 12B).

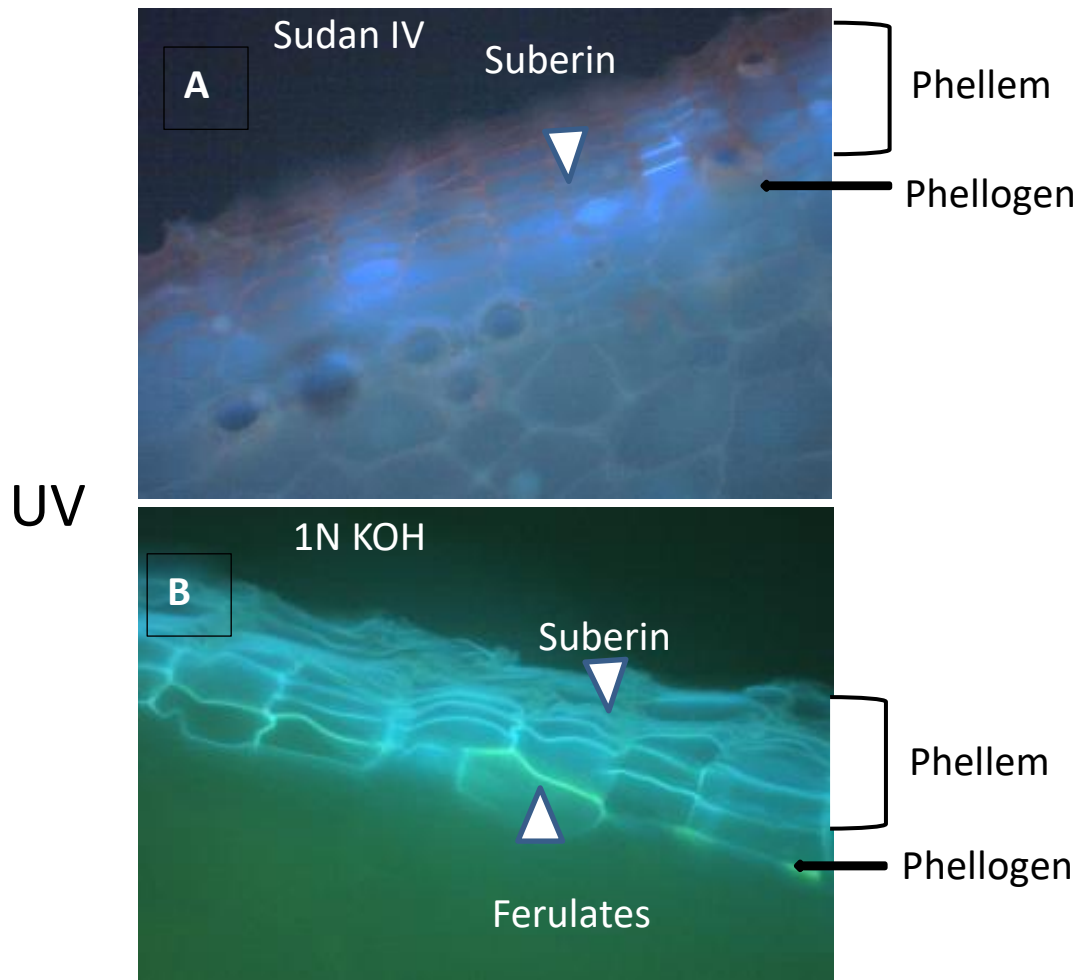


**Figure 12: The combined ferulate-specific UV-alkali and Sudan IV UV technique was found to be very sensitive in studying potato tuber periderm suberization.** (A) Sudan IV stains reddish brown the walls of suberized phellem cells on UV illumination. (B) Upon KOH alkali treatment of sections, followed by UV illumination, walls of phellogen cells emitted green auto-florescence, indicating strong deposition of ferulate in its walls.

The root xylem vasculature is one of the first sites of multiplication of *R. solanacearum* inside the host (Vasse *et al.*, 1995; Álvarez *et al.*, 2010; Digonnet *et al.*, 2012). Colonization of the xylem vasculature is critical, as in this particular tissue the pathogen

multiplies and moves vertically to the stem alongside the xylem fluid. In susceptible hosts, the pathogen also spreads horizontally from colonized vessels to the healthy neighboring tissues, including vessels and surrounding parenchyma cells (Nakaho *et al.*, 2000). To facilitate this process *R. solanacearum* secretes an array of cell wall degrading enzymes (Liu *et al.*, 2005; Pérez-Donoso *et al.*, 2010; Lowe-Power *et al.*, 2018). In parallel, plant cell walls also act as dynamic barriers against pathogens, acting as first line of defense by undergoing remodeling or strengthening upon pathogen recognition (Underwood, 2012). However, the precise role of cell walls in defense responses is far from being understood and has been mostly studied in the leaves.

In response to the vascular pathogen *R. solanacearum*, deposition of electron dense compounds on the pit membranes and cell walls from xylem vessels has been observed in resistant tomato varieties (Nakaho *et al.*, 2000; Kim *et al.*, 2018). In our study, resistant tomato (H7996) was observed to react aggressively to *R. solanacearum* infection by reinforcing the walls of vessels and the surrounding parenchyma cells with phenolic deposits (Fig 4). This vascular coating with wall-bound phenolic compounds may restrict horizontal spread of the bacterium at early stages of bacterial colonization (starting at  $\sim 10^5$  CFU g<sup>-1</sup> taproot tissue), before the plant shows any visible wilting symptom (Fig 2). These phenolic reinforcements in the xylem vasculature may in addition act as a shield against pathogen-derived metabolites such as toxins and enzymes, and make water and nutrients inaccessible for pathogens, thereby impeding their growth (Araujo *et al.*, 2014).

In comparison, susceptible tomato (Marmande) is either not able to induce such vascular coating upon *R. solanacearum* infection or induce a very weak and late response, predisposing its vascular walls to disruption by the pathogen's cell wall degrading enzymes. In absence of any reinforcements, the bacterium multiplies and colonizes abundantly moving out from vessel lumen into surrounding parenchyma cells and apoplastic spaces. At late stages of colonization, the xylem vasculature of Marmande appeared remarkably degraded, as evidenced from the reduced lignin staining (Fig 5).

The strong UV auto-florescence emitted from xylem vessel walls and the surrounding parenchyma cells observed in resistant H7996 against *R. solanacearum* could not be quenched by phloroglucinol-HCl (Fig. 6), suggesting the presence of suberin deposits in the observed vascular coatings (Pouzoulet *et al.*, 2013). In line with this, the walls of



vessels and surrounding parenchyma cells bound Sudan IV, which strongly indicated presence of aliphatic domain of suberin (Fig. 9,10,11). Interestingly, in the periphery of the aliphatic-binding layers we could observe cells with intense accumulation of phenolics where Sudan IV did not bind, potentially acting as further cell wall reinforcements surrounding the suberized zone (Fig. 9,11). These peripheral phenolic reinforcements were identified as wall-bound ferulates, by means of the strong blue-to-green color conversion upon alkali treatment (Carnachan and Harris, 2000; Harris and Trethewey, 2010) (Fig. 7,8,9). Ferulates are a major component of the suberin poly-phenolic domain (Negrel *et al.*, 1995; Graça, 2010; Cohen *et al.*, 2020). Importantly, ferulates accumulate at early stages of suberization, while later other aliphatic compounds of suberin are deposited to form the mature suberin matrix (Bernards and Lewis, 1992; Negrel *et al.*, 1995; Serra *et al.*, 2010). The early accumulation of ferulates is a critical aspect for the formation of suberin lamellae through coupling the aromatic and aliphatic suberin domains, considering that ferulates are able to form covalent bonds with cell wall polysaccharides and polyphenolics while leaving the aliphatic chain ready for esterification (Boher *et al.*, 2013). In support of this view, transient overexpression in *Nicotiana benthamiana* of AtMYB39 (SUBERMAN), a transcription factor controlling endodermal suberization in roots, results in a dramatic increase of ferulates in leaves, accompanied by the formation of suberin lamellae and upregulation suberin biosynthesis pathway genes (Cohen *et al.*, 2020).

### **2.2.6 Formation of tyloses as defense response to *R. solanacearum***

Tyloses are balloon like overgrowths of the protoplast of adjacent living parenchymatous cells, which protrude into xylem vessel lumen through pits. Its development involves the expansion of the portions of the parenchyma cell wall that are shared with the neighbouring vessels, specifically the so-called pit membranes. Our previous study reported severe restriction in movement of *R. solanacearum* from root to shoot in resistant tomato H7996 (Planas-Marquès *et al.*, 2019). This vertical restriction, in part, could be attributed to the formation of tyloses as a defense response to the bacterium. Tyloses are described to be a defense strategy activated in resistant plants when they perceive an attack of invading pathogens in the xylem, presumably blocking or reducing the vertical

movement of the pathogen (Grimault *et al.*, 1994b). Restricted formation of tyloses has been observed and specifically induced in the infected vessels of resistant tomato and potato varieties, effectively restricting *R. solanacearum* to the infected vascular bundles (Grimault *et al.*, 1994b; Ferreira *et al.*, 2017). Such specific induction was not observed in susceptible tomato cultivars infected with *R. solanacearum*, where the formation of tyloses appeared delayed and less focused, with numerous non-colonized vessels occluded by tyloses, and pathogen growth unrestricted (Grimault *et al.*, 1994b). Tylosis formation in resistant tomato cultivars has also been observed upon inoculation with the pathogenic fungus *F. oxysporum* f. sp. *lycopersici* and *Verticillium albo-atrum* (Hutson and Smith, 1980). Similarly, in a banana cultivar resistant to race 1 of *F. oxysporum* f. sp. *cubense*, tylosis initially appeared as early as within two days post-inoculation in the lumen of xylem vessels of the root (VanderMolen *et al.*, 1987). However, the extent of tylose formation may not be directly linked to the degree of resistance in certain host pathogen interaction. Excessive tylosis formation in response to *X. fastidiosa* infection in the susceptible grapevine cultivar led to heavy blockage of vessels and development of wilting symptoms, and did not significantly affect pathogen spread. In contrast, in resistant grapevines, tylosis development was specific and mainly limited to a few internodes close to the point of inoculation, impacting less of the vessels and indicating that timing and localization are key (Sun *et al.*, 2013).

Our histopathological studies showed that post infection of *R. solanacearum* resistant H7996 forms abundant tyloses. In resistant H7996, which shows extremely mild symptoms at 9 dpi, xylem vessels are seen developing a lot of tyloses in the taproot. In contrast the susceptible Marmande forms either no tyloses or very little tylose in xylem vessels even when the plants are completely wilted at 9 dpi (Fig 13). This indicates that wilting symptoms observed in susceptible Marmande is predominantly caused by blockage in water conducting tissue by bacterial multiplication and production of exopolysaccharides rather than by formation of plant obstructing structures such as tyloses.



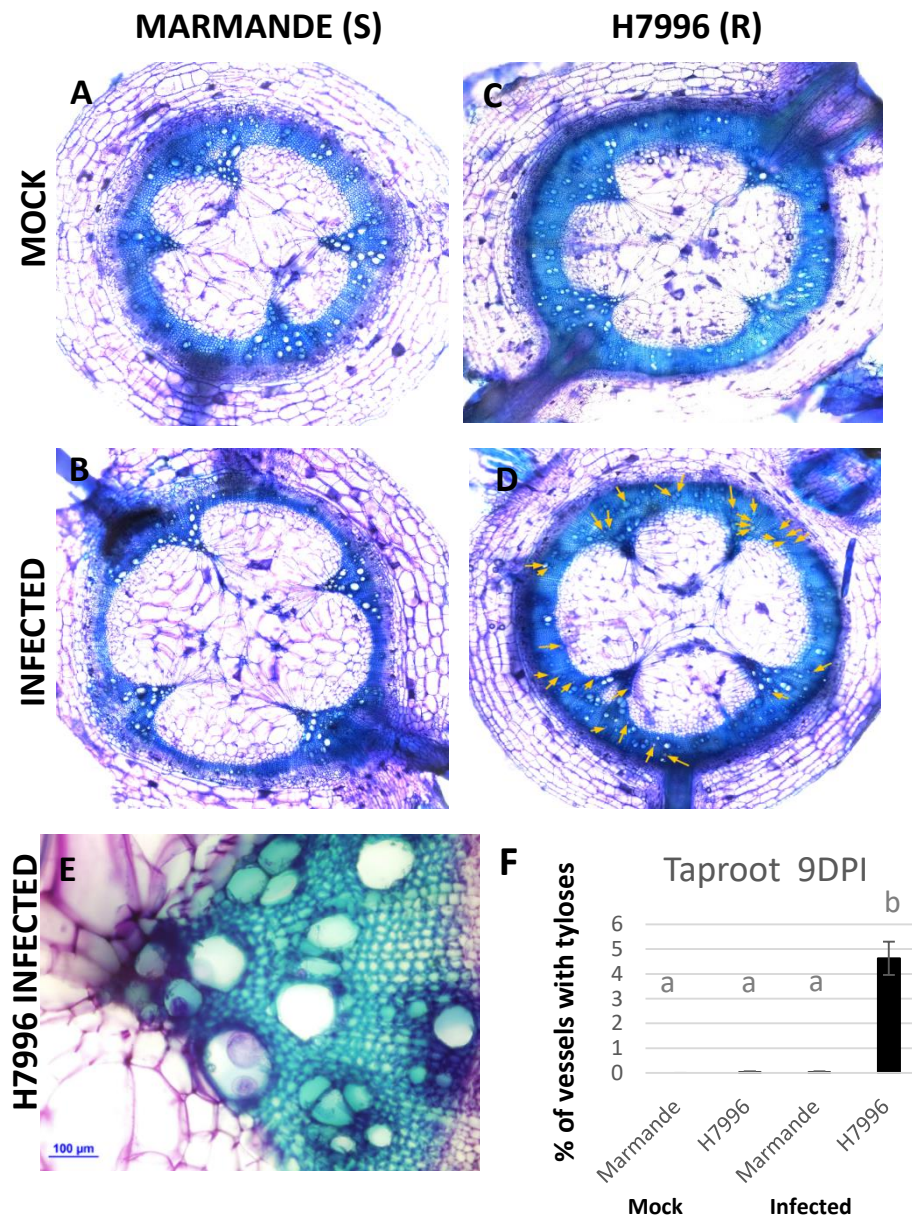


**Figure 13. *R. solanacearum* infection induces significantly high tyloses formation in resistant H7996 tomato, but not in susceptible Marmande.** Toluidine blue staining of taproot section cross-sections showed formation of tyloses in resistant H7996, after *R. solanacearum* infection whereas susceptible Marmande is mostly free from tyloses. Representative image of (A) water-treated; (B) *R. solanacearum* inoculated susceptible Marmande cross-sections and (C) water-treated and (D) *R. solanacearum* inoculated resistant H7996 cross-sections made at 9 dpi. (E) Tyloses observed in meta xylem of taproot in resistant H7996. (F) At 9 dpi percentage of vessels showing tyloses was quantified and significant induction of tyloses was observed in resistant H7996, post infection. Resistant H7996, 5 week old tomato plants were inoculated through roots by soil-soak with 40 ml of *R. solanacearum* strain GMI1000 suspension per plant with a concentration of  $\sim 1 \times 10^7$  CFU/ml and incubated at 28°C. Cross-sections of taproots at 9 dpi were used for microscopic observation.

Observations made in scanning electron microscope (SEM) of xylem vasculature, showed formation of globular tyloses in taproot xylem vasculature of resistant H7996 post infection of *R. solanacearum*, whereas the water-treated plants are free from tyloses (Fig 13). Further, SEM- energy-dispersive X-ray (SEM-EDX) detected intense deposition of calcium on the surface of tylose plasma membrane as well as in xylem vessel walls in taproot of H7996 post infection of *R. solanacearum*. Compared to infected plants, calcium accumulation was much less in water-treated plants (Fig 14). This spike in calcium deposition post *R. solanacearum* infection in H7996 might play a role in signalling defense responses. The information encoded in transient  $\text{Ca}^{2+}$  changes is decoded by an array of  $\text{Ca}^{2+}$ -binding proteins giving rise to a cascade of downstream effects, including altered protein phosphorylation and gene expression patterns (Rudd and Franklin-tong, 2001).

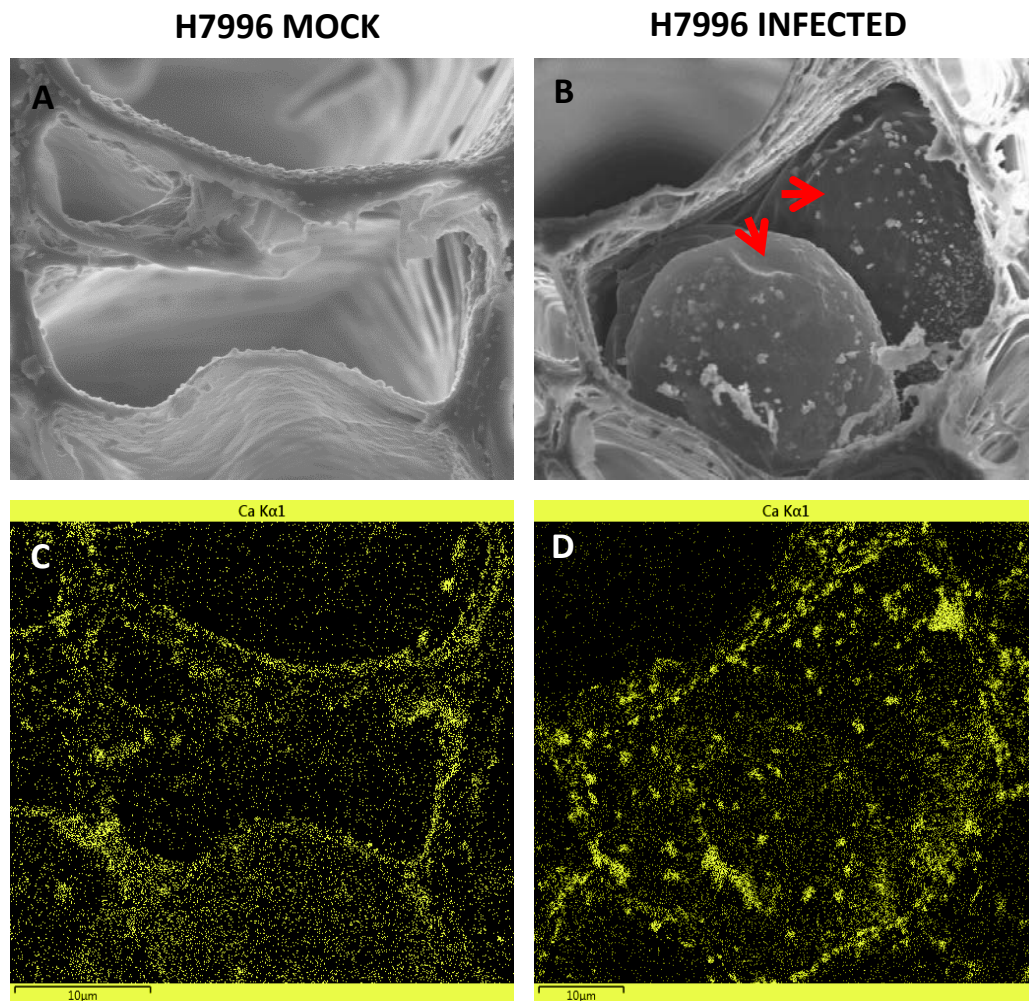


**Figure 14: Calcium accumulation in tyloses and vessel walls of resistant H7996 as defense response to *R. solanacearum*.** Representative SEM image showing (A) xylem vessels of taproot cross-section from water-treated plant which is devoid of tyloses. (B) In xylem vessel of taproot cross-section of infected plants,

globular tyloses were observed. (C,D) SEM-EDX showing accumulation of elemental calcium as yellow dots in the cross-sections obtained from taproot. (D) SEM-EDX detected intense deposition of calcium crystals (yellow dots) on the surface of tylose plasma membrane as well as in xylem vessel walls in taproot of H7996 plants post infection of *R. solanacearum*. Resistant H7996, 5 week old tomato plants were inoculated through roots by soil-soak with 40 ml of *R. solanacearum* strain GMI1000 suspension per plant with a concentration of  $\sim 1 \times 10^7$  CFU/ml and incubated at 28°C. Cross-sections of taproots at 9 dpi was used for SEM-EDX analysis.

Besides pathogen attack, formation of tyloses can be induced by several environmental stimuli, such as pruning, wounding, flooding and frost. However, the molecular triggers of tylose formation has been elusive. In aspen (*Populus tremula x tremuloides*) the activation of oxidative stress has been recently linked to the induction of tyloses. The study showed that downregulation of *PECTIN METHYLESTERASE1* (*PtxtPME1*) in aspen leads to higher peroxidase activity and hydrogen peroxide levels and this oxidative stress and the downstream hormones namely, jasmonates acting synergistically with ethylene are the key molecular triggers of tyloses (Fig. 15) (Leśniewska *et al.*, 2017).

Interestingly, oxidative stress and downstream hormonal signalling is a generalized response on pathogen perception events such as recognition of pathogen associated molecular patterns (PAMPs) by plant pattern recognition receptors (PRRs). Exopolysaccharide from *R. solanacearum* has been shown to act as a pattern-triggered immunity (PTI) elicitor in resistant tomato, leading to an oxidative burst and induced expression of defense response genes (Milling *et al.*, 2011; Prakasha *et al.*, 2017). This exopolysaccharide of *R. solanacearum* was observed to be recognized in resistant cultivar H7996, but not in susceptible cultivar. The exopolysaccharide mutant of *R. solanacearum* triggered noticeably less production of defense-associated reactive oxygen species in resistant tomato stems and leaves, despite attaining similar cell densities in planta (Milling *et al.*, 2011). Hence, we hypothesized that the exopolysaccharide mutant of *R. solanacearum* may induce less tyloses in H7996 due to a diminished oxidative burst response of resistant tomato against this mutant.

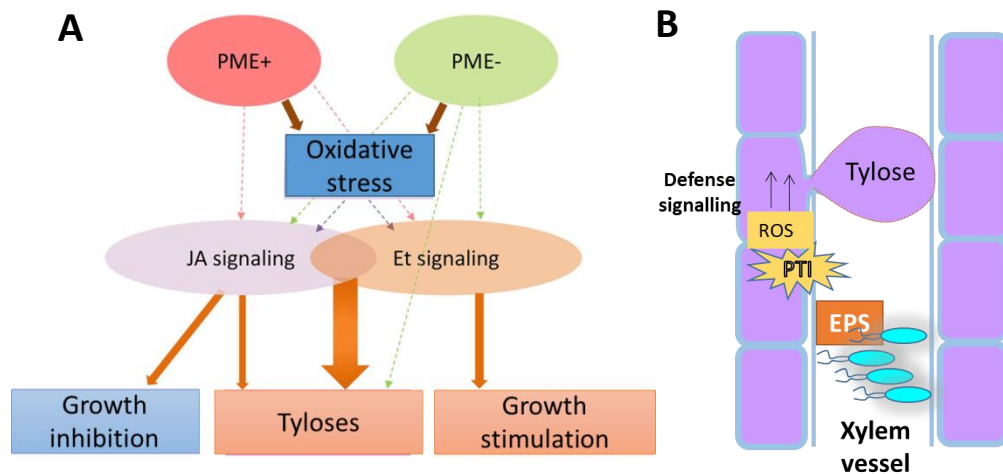


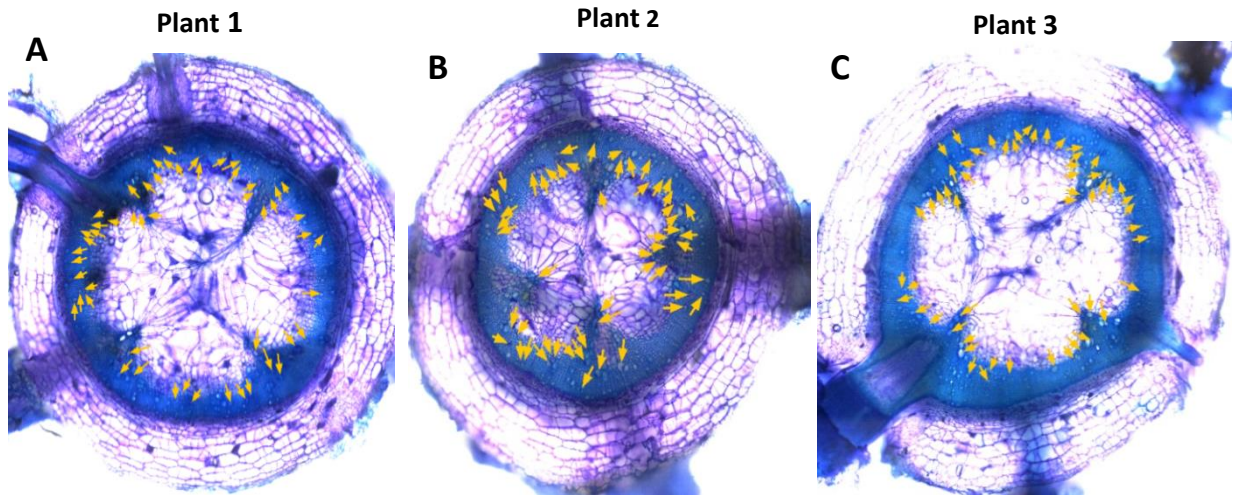
**Figure 15: Oxidative stress and the downstream hormonal signalling may act as possible inducers of tylose formation.** (A) Down-regulation of PECTIN METHYLESTERASE1 in aspen (*Populus tremula x tremuloides*) triggers the activation of oxidative stress and formation of tyloses, regulated by hormonal signalling. Adapted from Leśniewska *et al.*, (2017). (B) Our hypothesis regarding *R. solanacearum* induced tylose formation in resistant tomato line H7996. Tylose formation in H7996 may be a downstream event of pathogen recognition via conserved molecular patterns such as exopolysaccharide leading to a PTI response. Such response lead to activation oxidative burst, defense hormonal signalling and may also regulate tylose formation.

To test our hypothesis we infected resistant H7996 plants with either *R. solanacearum* GMI1000 Wt strain or its exopolysaccharide mutant by soil soak inoculation and taproot transverse cross-sections were obtained at 12 dpi. Toluidine blue staining of taproot showed that the exopolysaccharide mutant induced significantly low amount of tyloses compared to wild type GMI1000, even when the bacterial colonization at taproots were similar (Fig 16). Taproot xylem vessels of plants infected with Wt strain had almost 8 % of its vessels forming tyloses. In contrast plants infected with exopolysaccharide mutant had around 2 % of the taproot vessels showing tyloses. The bacterial colonization for both the strains crossed  $10^6$  CFU g<sup>-1</sup> taproot at 12 dpi. However, the decrease in tylose production by exopolysaccharide mutant may be also due to its hypovirulence effect. Therefore, though an indirect link between oxidative stress and tyloses was observed both in down-regulation of *PECTIN METHYLESTERASE1* in aspen and tomato H7996 plants infected with *R. solanacearum* exopolysaccharide mutant, the association in tomato needs



to be further validated by using chemical inhibitors of reactive oxygen species or in mutant plants.

**H7996 + *R. solanacearum* GMI1000**



**H7996 + *R. solanacearum* *epsB***

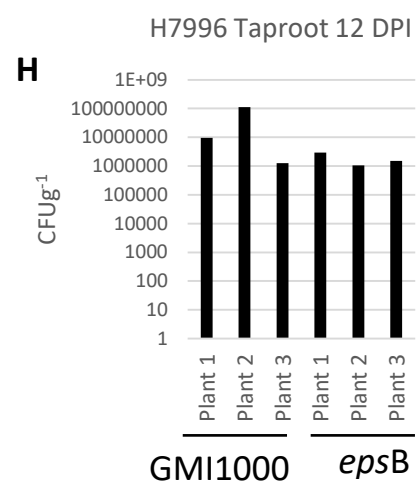
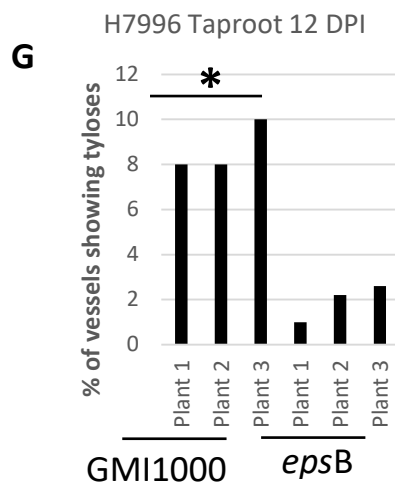
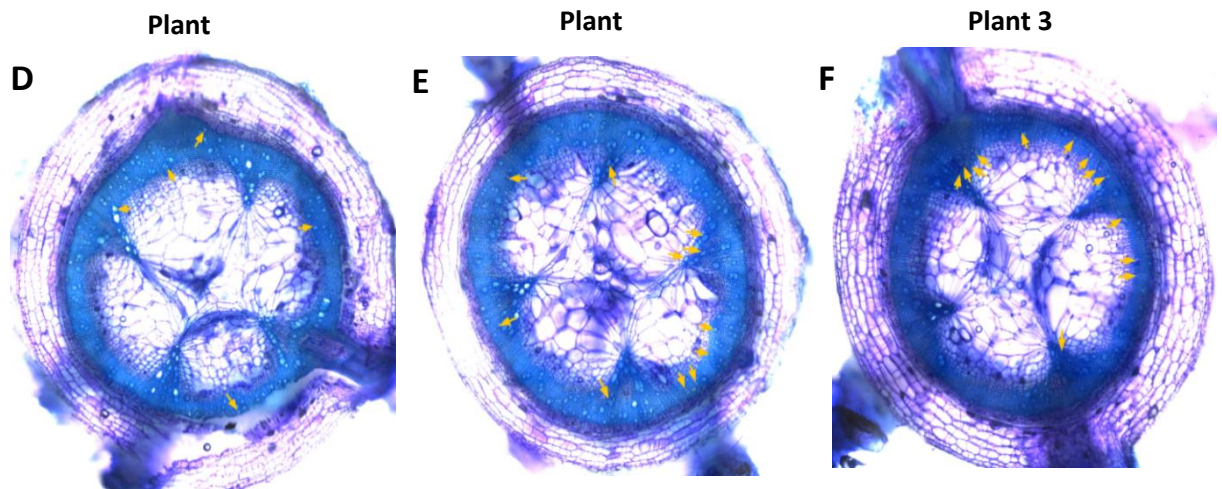


**Figure 16: *R. solanacearum* exopolysaccharide (epsB) mutant, which is known to elicit reduced oxidative burst in H7996 tomato, induce significantly low tyloses.** Toluidine blue staining of taproot cross-section of resistant H7996 made at 12 DPI of (A,B,C) *R. solanacearum* GMI1000 and (D,E,F) *R. solanacearum* epsB mutant. (G) Quantification of percentage of vessels showing tyloses, showed significantly higher amount of tyloses in plants inoculated with wild type (WT) *R. solanacearum* compared to epsB mutant. (H) Though *R. solanacearum* epsB mutant reached similar population densities as Wt. Resistant H7996, 5 week old tomato plants were inoculated through roots by soil-soak with 40 ml of *R. solanacearum* strain GMI1000 or epsB mutant suspension per plant with a concentration of  $\sim 1 \times 10^7$  CFU/ml and incubated at 28°C. Cross-sections of taproots at 12DPI were used for microscopic observation.



## **CHAPTER II**

### 3. Spectroscopic analysis of physico-chemical barriers induced at roots upon *Ralstonia solanacearum* infection

#### 3.1 Introduction

In order to gain in depth information on compositional changes in phenolic polymers of the walls involved in reinforcement and their role in bacterial restriction at the xylem vessels, we performed spectroscopic analysis of tomato roots. Spectroscopy offers an accurate and sensitive technique to study compositional changes in cell walls in response to external stimuli (Alonso-Simón *et al.*, 2011; Kim & Ralph, 2014). In plant–microbe interaction studies, nuclear magnetic resonance (NMR) and fourier transform infrared (FT-IR) spectroscopy can reveal accurately the compositional changes in cell wall constituents (Agrelli *et al.*, 2009; Taoutaou *et al.*, 2012). The heteronuclear single quantum coherence or heteronuclear single quantum correlation (HSQC 2D-NMR), is used frequently in analysis of organic samples and is of particular significance in biological systems (Rico *et al.*, 2015). 2D-NMR and the use of chemometric data analysis of NMR spectra have been proven to be highly effective at identifying changes in cell wall compositions (Rico *et al.*, 2015). Further, FT-IR spectroscopy is a non-destructive analytical technique that provides a snapshot of the metabolic composition of a tissue at a given time, offering extensive information on bio-chemical compositions and interactions (Alonso-Simón *et al.*, 2011). The FT-IR method measures predominantly the vibrations of bonds within chemical functional groups and generates a spectrum that can be regarded as a biochemical or metabolic “fingerprint” of a sample. In this chapter, using HSQC 2D-NMR and FT-IR we discuss about differential changes in secondary wall polymers of root tissue of resistant and susceptible cultivar against *R. solanacearum*. We tried to gain insights on the type of metabolites involved in cell wall reinforcement mechanisms of resistant H7996 tomato roots, as defense response to *R. solanacearum*.

## 3.2 Results & discussion

### 3.2.1 2D-HSQC NMR spectroscopy showed infected H7996 root xylem vasculature is enriched in suberin-compatible compounds

Histological studies indicated that wall reinforcements containing ferulates and suberin in the root vasculature were an important defense trait of resistant H7996 tomato against *R. solanacearum*. Hence, using 2D-HSQC NMR we delved into the compositional changes in phenolic polymers viz. lignin and suberin in walls of tomato roots in response to *R. solanacearum*. Infected or mock-treated tomato taproots of H7996 and Marmande tomato plants were subjected to 2D-HSQC NMR to detect modifications on lignin and suberin structures as previously reported (Rencoret *et al.*, 2011; Mansfield *et al.*, 2012; Lourenço *et al.*, 2016; Marques *et al.*, 2016). Lyophilized powders (300 mg) were obtained from tomato plant taproots, water-treated or *R. solanacearum*-inoculated by soil soak having a bacterial load of  $10^5$  CFU g<sup>-1</sup>. Samples were milled and extracted sequentially with solvents and the lignin/suberin fraction was enzymatically isolated as previously described by Rico *et al.*, (2015). Approximately 20 mg of enzymatic lignin/suberin preparation was used to obtain heteronuclear single quantum coherence (2D HSQC) spectra.

Results are illustrated in Fig. 1, where the main lignin and suberin substructures are depicted, while the main cross-signals assigned to the 2D HSQC spectra are shown in Table 1. Interestingly, the aliphatic region of the 2D-HSQC spectra revealed that H7996 infected plants were enriched in poly-aliphatic structures characteristic of suberin (Fig 1b), compared to its mock control (Fig 1a). Related to this, an olefinic cross-signal of unsaturated fatty acid structures (UF,  $\delta C/\delta H$  129.4/5.31), typical of suberin, was also found to be increased in the HSQC spectrum of the infected H7996 plants (Fig 1b). In plants, unsaturated fatty acids (UFs) are used as raw material to produce numerous aliphatic compounds, including suberin. These products, as well as UFs themselves, take part in plant defense against various biotic and abiotic stresses such as constructing physically and chemically resistant barriers (He & Ding, 2020).

Interestingly, signals compatible with feruloylamides at  $\delta C/\delta H$  138.6/7.31 (Mahmoud et al. 2020), and with tyramide-related structures ( $\delta C/\delta H$  129.3/6.92, 114.8/6.64, 40.5/3.29 and 34.2/2.62) were exclusively found in the spectrum of infected H7996 plants, indicating the presence of feruloyltyramine in these samples (Fig. 1b). Since tyramines are well established components of the suberization process (Bernards *et al.*, 1995; Bernards & Lewis, 1998), these data substantiate the hypothesis of suberin as an important defense element against *R. solanacearum* infection in resistant tomato plants. On the contrary, the 2D-HSQC spectra of the lignin/suberin fractions isolated from the Marmande variety did not display notable variations, between mock and infected plants in the signals corresponding to suberin (Fig 1 c,d).

2D-HSQC NMR also revealed significant structural modifications in the composition of lignin and the distribution of linkages in tomato plants after infection. The ratio between syringyl (S) and guaiacyl (G) units in lignin informs about its polymerization state, and hence its degradation propensity. Infection of susceptible Marmande plants resulted in an increase of the S/G ratio and a reduction of the major lignin linkages ( $\beta$ -O-4',  $\beta$ -5' and  $\beta$ - $\beta'$ ) (Fig. 1c,d). In contrast, infected H7996 tomato displayed a decrease of the S/G ratio (Fig. 1a,b). A higher cross-linking of cell wall polymers is related to reduced accessibility of the pathogen's hydrolytic enzymes to their substrates and contribute to cell wall strengthening and blocking ingress of pathogens (Iiyama *et al.*, 2020). In this context, the major reduction in lignin linkages ( $\beta$ -O-4',  $\beta$ -5' and  $\beta$ - $\beta'$ ) observed in Marmande after infection corroborates the decrease in lignin observed histochemically (Chapter 2, Fig 5), and explains, at least in part, its higher susceptibility to the pathogen.

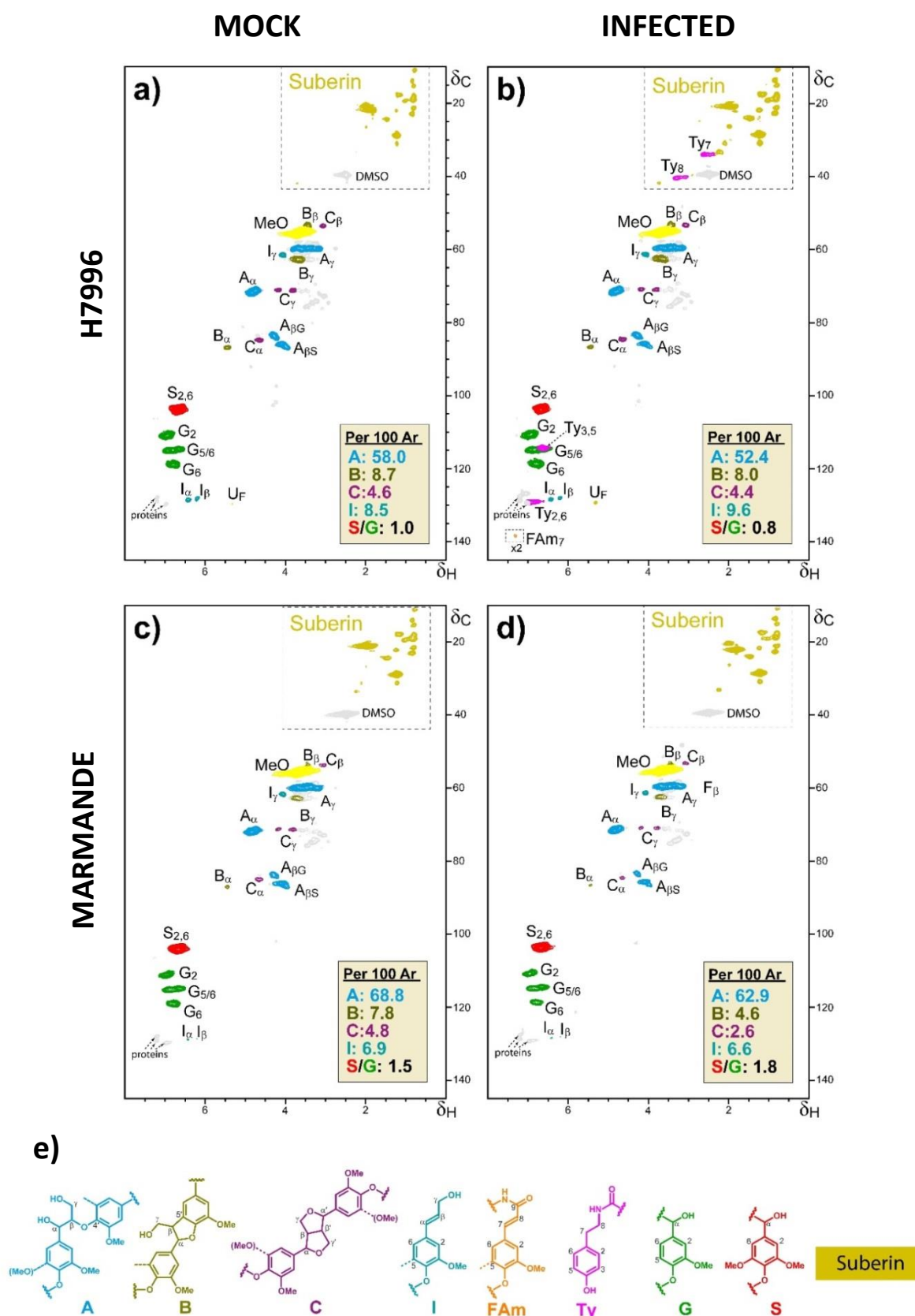


**Figure 1: Suberin-compatible compounds are specifically enriched in resistant H7996 tomato after infection with *R. solanacearum*.** Five-week-old tomato plants were inoculated soil-soak inoculated with  $\sim 1 \times 10^7$  CFU/ml *R. solanacearum* GMI1000 and incubated at 28°C. Taproots containing  $10^5$  CFU g<sup>-1</sup> of *R. solanacearum* were obtained from H7996 and Marmande, powdered in liquid nitrogen and lyophilized. For comparison taproot powder of mock plants from both cultivars of a similar age was used. (a,b) Upon

infection H7996 showed strong enrichment in poly-aliphatic structures characteristic of suberins. Also, olefinic cross-signal of unsaturated fatty acid structures was obtained, which is typical of suberin. Interestingly, correlation signals compatible with feruloylamides and with tyramide-related structures were obtained specifically in roots of resistant H7996 upon infection of *R. solanacearum*. (c,d) On the contrary, the 2D-HSQC spectra of the lignin/suberin fractions isolated from the Marmande variety did not display notable variations, between mock and infected plants, in the signals corresponding to suberin. (e) The structures of relevant suberin-related compounds displayed in (a,b,c,d) are represented.

**Table 1:** Assignments of the correlation signals in the 2D HSQC spectra.

Label	$\delta_C/\delta_H$ (ppm)	Assignment
Ty <sub>7</sub>	34.2/2.62	C <sub>7</sub> /H <sub>7</sub> in tyramide ( <b>Ty</b> )
Ty <sub>8</sub>	40.5/3.29	C <sub>8</sub> /H <sub>8</sub> in tyramide ( <b>Ty</b> )
B <sub>β</sub>	53.3/3.43	C <sub>β</sub> /H <sub>β</sub> in phenylcoumarans ( <b>B</b> )
C <sub>β</sub>	53.5/3.05	C <sub>β</sub> /H <sub>β</sub> in β-β' resinols ( <b>C</b> )
MeO	55.3/3.72	C/H in aromatic methoxy group
A <sub>γ</sub>	59.7/3.23, 3.58	C <sub>γ</sub> /H <sub>γ</sub> in β-O-4' alkyl-aryl ethers ( <b>A</b> )
I <sub>γ</sub>	61.5/4.06	C <sub>γ</sub> /H <sub>γ</sub> in cinnamyl alcohol end-groups ( <b>I</b> )
B <sub>γ</sub>	62.6/3.70	C <sub>γ</sub> /H <sub>γ</sub> in phenylcoumarans ( <b>B</b> )
C <sub>γ</sub>	71.1/3.80, 4.17	C <sub>γ</sub> /H <sub>γ</sub> in β-β' resinols ( <b>B</b> )
A <sub>α</sub>	71.3/4.79	C <sub>α</sub> /H <sub>α</sub> in β-O-4' alkyl-aryl ethers ( <b>A</b> )
A <sub>βG</sub>	83.9/4.27	C <sub>β</sub> /H <sub>β</sub> in β-O-4' alkyl-aryl ethers ( <b>A</b> ) linked to a G unit
C <sub>α</sub>	84.9/4.67	C <sub>α</sub> /H <sub>α</sub> in β-β' resinols ( <b>C</b> )
A <sub>βS</sub>	83.6/4.28	C <sub>β</sub> /H <sub>β</sub> in β-O-4' alkyl-aryl ethers ( <b>A</b> ) linked to a S unit
B <sub>α</sub>	86.9/5.45	C <sub>α</sub> /H <sub>α</sub> in phenylcoumarans ( <b>B</b> )
S <sub>2,6</sub>	104.0/6.68	C <sub>2</sub> /H <sub>2</sub> and C <sub>6</sub> /H <sub>6</sub> in syringyl units ( <b>S</b> )
S' <sub>2,6</sub>	106.3/7.29	C <sub>2</sub> /H <sub>2</sub> and C <sub>6</sub> /H <sub>6</sub> in C <sub>α</sub> -oxidized syringyl units ( <b>S'</b> )
G <sub>2</sub>	111.1/6.97	C <sub>2</sub> /H <sub>2</sub> in guaiacyl units ( <b>G</b> )
Ty <sub>3,5</sub>	114.8/6.64	C <sub>3</sub> /H <sub>3</sub> and C <sub>5</sub> /H <sub>5</sub> in tyramine ( <b>Ty</b> )
G <sub>5/6</sub>	114.9/6.79	C <sub>5</sub> /H <sub>5</sub> and C <sub>6</sub> /H <sub>6</sub> in guaiacyl units ( <b>G</b> )
G <sub>6</sub>	119.0/6.76	C <sub>6</sub> /H <sub>6</sub> in guaiacyl units ( <b>G</b> )
I <sub>β</sub>	128.2/6.21	C <sub>β</sub> /H <sub>β</sub> in cinnamyl alcohol end-groups ( <b>I</b> )
I <sub>α</sub>	128.6/6.43	C <sub>α</sub> /H <sub>α</sub> in cinnamyl alcohol end-groups ( <b>I</b> )
Ty <sub>2,6</sub>	129.3/6.92	C <sub>2</sub> /H <sub>2</sub> and C <sub>6</sub> /H <sub>6</sub> in tyramine ( <b>Ty</b> )
U <sub>F</sub>	129.4/5.31	-CH=CH- in unsaturated fatty acid structures ( <b>U<sub>F</sub></b> )
FAm <sub>7</sub>	138.6/7.31	C <sub>7</sub> /H <sub>7</sub> in feruloyl amides ( <b>FAm</b> )



### 3.2.2 FT-IR spectra shows enhanced phenol accumulation in root xylem vasculature of H7996 against *R. solanacearum*

Complementing NMR, the FT-IR method measures predominantly the vibrations of bonds within chemical functional groups, generating a spectrum that can be regarded as a biochemical or metabolic “fingerprint” of a sample. FT-IR has been used as an analytical tool in structural analysis of lignocellulose chemistry, providing reliable insights into modifications of cell-wall components caused during pathogen infection (Martín *et al.*, 2005; Del Rio *et al.*, 2007; Taoutaou *et al.*, 2012; Lahlali *et al.*, 2017). Dried transverse taproot cross-sections of H7996 and Marmande plants, water-treated or *R. solanacearum*-inoculated by soil soak and containing bacteria  $10^5$  CFU g<sup>-1</sup> taproot tissue were analyzed in area adjacent to the vasculature using a FT-IR spectrophotometer Jasco 4700 with ATR accessory on the range of 300-4000 cm<sup>-1</sup>. The FT-IR results revealed that the average spectrum of infected resistant H9776 tomato roots displayed higher absorbance peaks than the corresponding spectra from infected susceptible and mock-treated plants (Fig. 2). Vibration bands (Table 2) were assigned after comparison of our data with previous analyses allowing peak identification (Dorado *et al.*, 2001; Martín *et al.*, 2005; Lahlali *et al.*, 2017). Increased formation of phenolic and other compounds compatible with lignin and suberin structure were specifically observed in H7996 after infection. Besides phenolic compounds, the most characteristic spectral features visible on the spectrum were connected with the presence of functional chemical groups of aliphatic compounds, aliphatic esters, amides as well as polysaccharides.

Relative absorbance ratios of the most diagnostic peaks were calculated against a reference value (Fig 3). Absorbance ratios revealed high variability between samples, typical for complex samples such as the ones analyzed here. Still, these data confirm the NMR results and support the idea that specific suberization processes taking place after infection in H7996. The most noticeable change is the specific increase in phenolic compounds, as can be seen by the significantly higher phenolic –OH stretching ( $\approx 3300$  cm<sup>-1</sup>) and slight increase in –OH bending ( $\approx 1423$  cm<sup>-1</sup>) when comparing H7996 infected to its mock control (Fig. 3). In addition to that, both aliphatic –CH ( $\approx 2930$  cm<sup>-1</sup>) and –CH<sub>3</sub> stretching ( $\approx 2850$  cm<sup>-1</sup>) are also slightly higher for H7996 infected plants compared to the mock controls. Furthermore, slightly increased –NH bending can be

observed at  $\approx 1634 \text{ cm}^{-1}$  in H7996 infected plants, which could correspond to the feruloylamides detected by 2D-NMR (Fig. 1b). Together, the NMR and FTIR data reveal a specific metabolic signature in infected H7996 plants compatible with suberization.

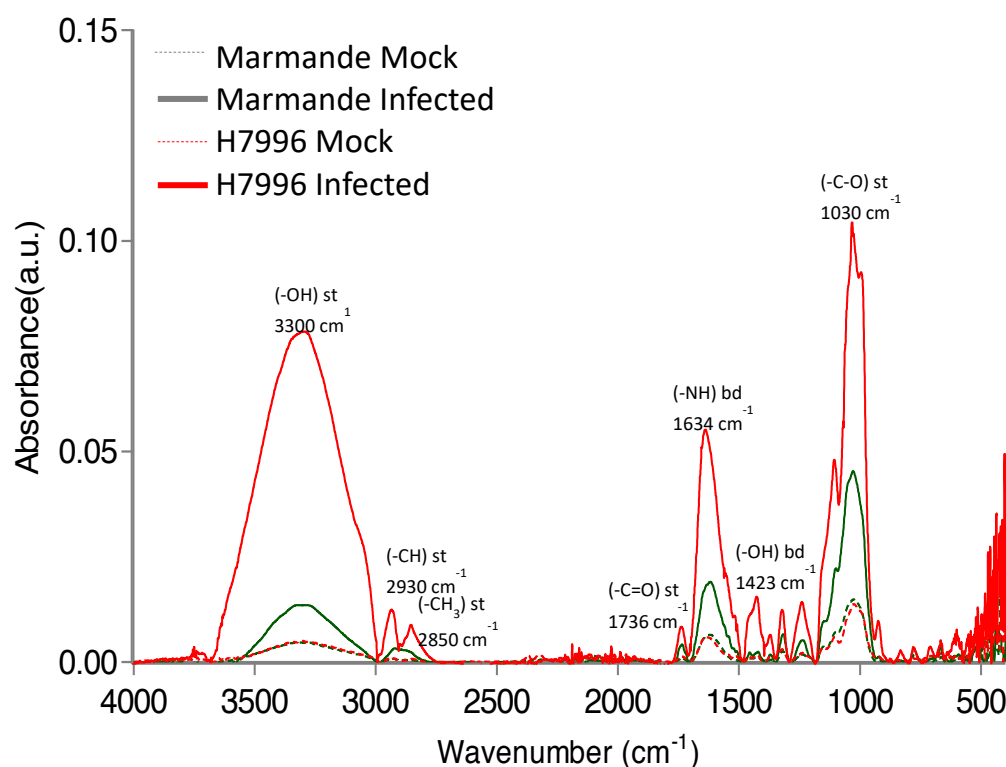


**Figure 2: FT-IR absorbance spectra showing functional groups of metabolites that accumulate in the xylem vasculature of tomato roots as defense response against *R. solanacearum*.** Average absorbance in the range of  $500\text{-}4000 \text{ cm}^{-1}$  is shown for both cultivars water-treated or infected by *R. solanacearum* with a bacterial load of  $10^5 \text{ CFU g}^{-1}$  taproot tissue. Based on the changes in peak values of infrared spectra post infection, the functional groups of the active components formed in response to the pathogen were analysed. Remarkable changes in infra-red spectra was observed after *R. solanacearum* infection in the xylem vasculature of tomato roots, indicating defense related metabolic reprogramming. Taproot cross-sections containing  $10^5 \text{ CFU g}^{-1}$  of *R. solanacearum* was lyophilized and used for analysis. FT-IR spectra of a representative experiment with  $n=3$ .

**Table 1: Primary FT-IR absorbance peaks of tomato taproot vasculature in tomato cultivar Marmande and H7996**

Wavenumber (cm <sup>-1</sup> )	Function group vibrations	Compounds
<b>3300</b>	-OH Stretching	Phenolics
<b>2930</b>	-CH Stretching	Alkynes from suberin (aliphatic -CH)
<b>2850</b>	-CH <sub>3</sub> Stretching	Alkanes from suberin (aliphatic -CH <sub>3</sub> )
<b>1736</b>	-C=O stretching	Carbonyl esters (from aliphatic suberin esters and pectin methyl esters)
<b>1634</b>	-N-H bending	Amides
<b>1423</b>	-O-H bending	Phenolics
<b>1030</b>	-C-O stretching	Cellulose

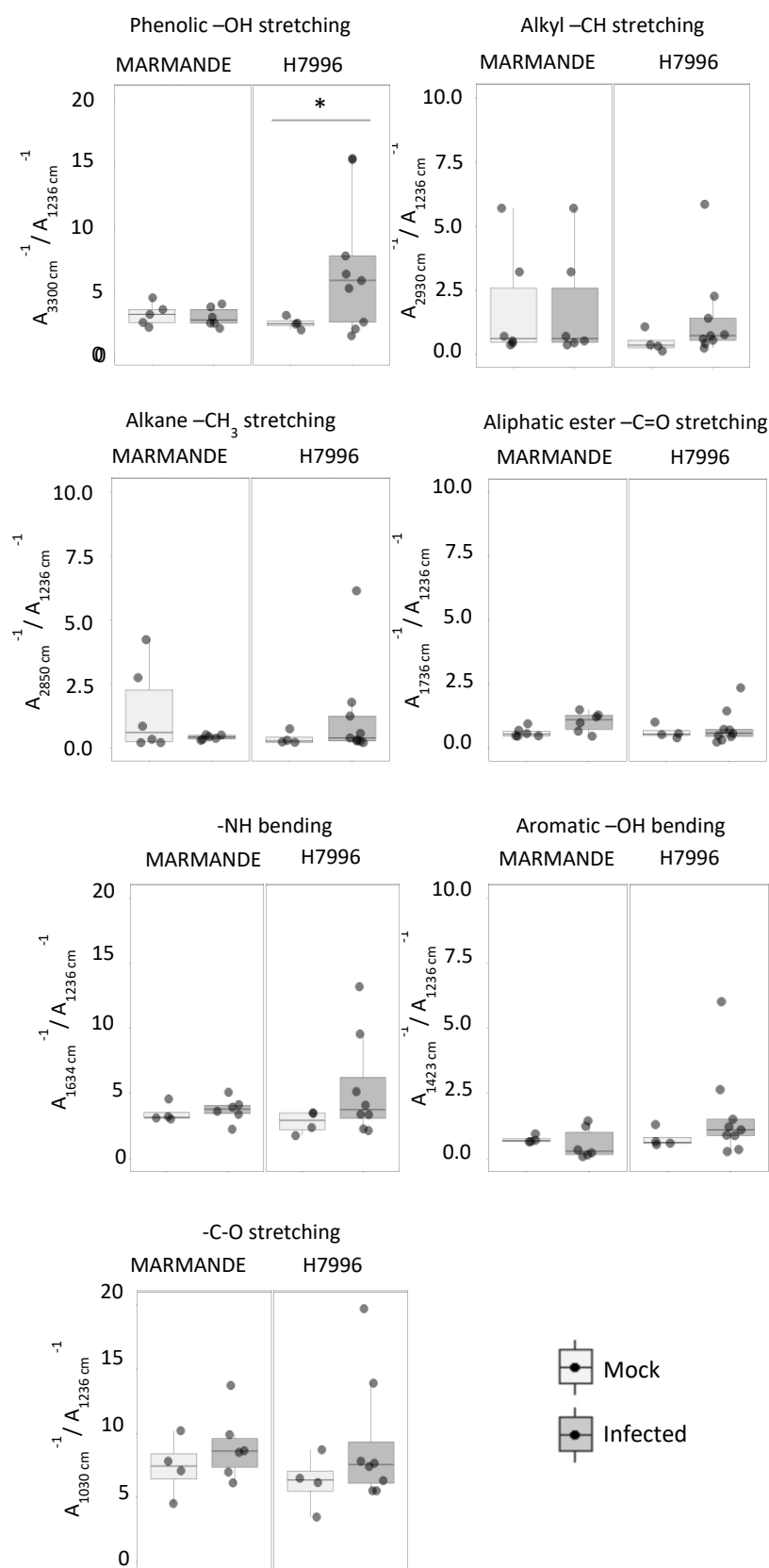


**Figure 3: Relative absorbance ratios of the most diagnostic peaks of the FT-IR spectra.** The relative absorbance ratios of the most prominent peaks in Fig. 2 were calculated corresponding to phenolic -OH stretching stretching ( $\approx 3300 \text{ cm}^{-1}$ ), alkyl -OH stretching ( $\approx 2930 \text{ cm}^{-1}$ ), alkane -CH<sub>3</sub> stretching ( $\approx 2850$

cm<sup>-1</sup>), aliphatic ester –C=O stretching ( $\approx 1736$  cm<sup>-1</sup>), –NH bending ( $\approx 1634$  cm<sup>-1</sup>), aromatic –OH bending ( $\approx 1423$  cm<sup>-1</sup>) and –C-O stretching ( $\approx 1030$  cm<sup>-1</sup>) by using the absorbance at 1236 cm<sup>-1</sup> as a reference. Susceptible Marmande and resistant H7996, 5-week-old tomato plants were inoculated through roots by soil-soak with 40 ml of *R. solanacearum* strain GMI1000 suspension per plant with a concentration of  $\sim 1 \times 10^7$  CFU/ml and incubated at 28°C. Taproots containing *R. solanacearum* at a level of  $10^5$  CFU g<sup>-1</sup> tissue were cross sectioned from H7996 and Marmande and lyophilized. For comparison taproot of mock plants from both cultivars of similar age was used. Asterisk (\*) indicate statistically significant differences ( $\alpha=0.05$ , Student's t-test). The assignments of main functional groups based on FT-IR spectra (Dorado *et al.*, 2001; Martín *et al.*, 2005; Lahlali *et al.*, 2017) of susceptible (S) and resistant (R) taproot samples. Wave numbers are the mean of vibrational range.

## CHAPTER III



## **4. Characterization of genes responsible for ferulo-suberin barrier formation in tomato root defense against *Ralstonia solanacearum***

### **4.1 Results & discussion**

#### **4.1.1 *R. solanacearum* infection activates expression of suberin biosynthesis genes in the root vasculature of resistant H7996**

Since a ferulate-suberin vascular reinforcement was observed to form in H7996 in response to *R. solanacearum* invasion, we surmised that genes related to suberin and the associated ferulate synthesis may be upregulated in response to infection in resistant tomato. To test this hypothesis, we analyzed expression of genes related to the ferulate and suberin biosynthetic pathway in samples obtained from taproot xylem vascular tissue, from *R. solanacearum*- or mock-treated resistant H7996 and susceptible Marmande plants. Since the phenylpropanoid and fatty acid biosynthesis pathways provide the necessary precursors for the suberin matrix (Lashbrooke *et al.*, 2016), we tested expression of genes in those two pathways by quantitative PCR (qPCR). Besides, we analyzed the changes in expression of suberin feruloyl transferase and hydroxycinnamic acid amide synthesis genes in response to *R. solanacearum* and their expression profile in silico.

##### **4.1.1.1 Phenylpropanoid and suberin fatty acid pathway**

Precursors of phenolic domain are derived from the phenylpropanoid pathway while the aliphatic domain is synthesized by suberin fatty acid pathway enzymes (Vishwanath *et al.*, 2015). Strikingly, expression of all genes analyzed from the suberin fatty acid biosynthetic pathway was significantly upregulated in H7996 infected plants compared to the mock controls (Fig.1, 16). Under basal conditions, expression of these genes in the vascular tissue was negligible and they were not upregulated by infection in Marmande plants (Fig. 1, 16). This indicates that upregulation of these genes is a very specific response of resistant H7996 plants that takes place in suberizing vasculature upon *R. solanacearum* infection. Genes of the suberin fatty acid biosynthesis pathway such as cytochrome P450 fatty acid  $\omega$ -hydroxylases (*SICY86A1*; Solyc06g076800 and *SICY86B1*; Solyc02g014730), fatty acyl-CoA reductase 3 (*SIFAR3*; Solyc02g014730), 3-ketoacyl-CoA synthase 1 (*SIKCS1*; Solyc10g009240), 3-ketoacyl-CoA synthase 2 (*SIKCS2/SIDAI5Y*; Solyc05g009280), glycerol-3-phosphate acyltransferase 5 (*SIGPAT5*; Solyc04g011600) were all highly up-regulated specifically in resistant H7996 upon

infection. In contrast, these genes were either unaffected or down-regulated by infection in Marmande plants. Further, these data are in agreement with the specific increase in fatty acid structures typical of suberin observed by NMR in infected H7996 (Chapter 2, Fig. 1).

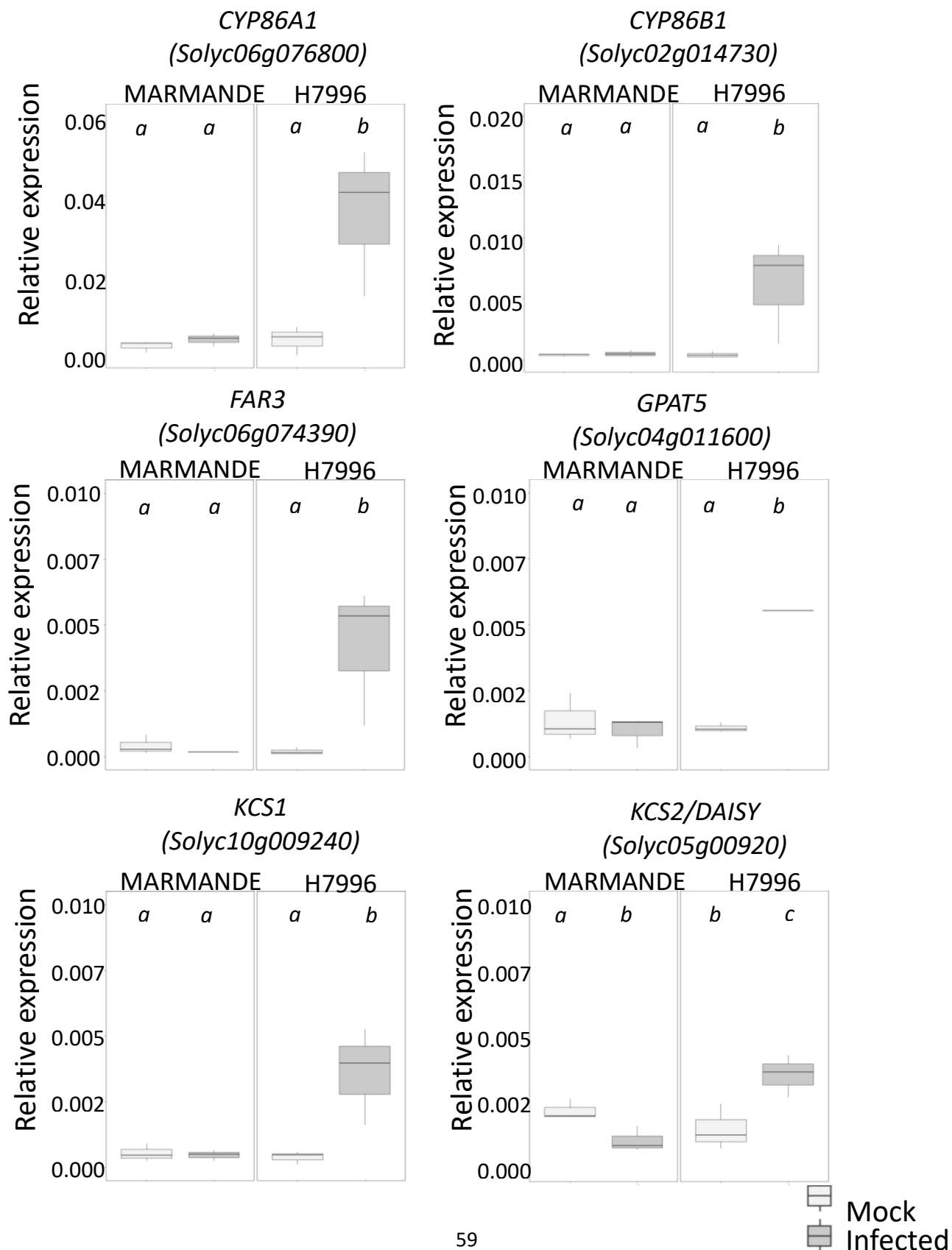


**Figure 1: Expression of suberin aliphatic genes in xylem vasculature of taproots upon infection of *R. solanacearum*.** Gene expression analyzed by qPCR of tomato putative orthologs of suberin fatty acid pathway genes in taproot xylem vasculature of resistant H7996 and susceptible Marmande plants water-treated or infected by *R. solanacearum*. The Elongation Factor 1 alpha (*eEF1  $\alpha$* ) gene was used as endogenous reference. H7996 and Marmande plants, with *R. solanacearum* inoculum of  $10^5$  CFU g<sup>-1</sup> in taproot, were selected and xylem vascular tissue, comprising of metaxylems and surrounding parenchyma cells was collected from taproots for RNA extraction and cDNA synthesis. Similarly, xylem tissue was collected from Marmande mock plants and H7996 mock plants. Three biological replicates (n=3) were used, and taproots of 6 plants were used in each replicate. Different letters indicate statistically significant differences ( $\alpha=0.05$ , Fisher's least significant difference test).

Genes in the phenylpropanoid pathway showed relatively high levels of expression under basal conditions in both Marmande and H7996 plants (Fig. 2, 16). This is not surprising, since this pathway provides precursors for both lignin and suberin, and the xylem vasculature is a lignified tissue. Infection with *R. solanacearum* did not result in major changes in expression of these genes (Fig. 2, 16) in the vasculature. In Marmande, *SIC3H* (coumarate 3-hydroxylase), *SIHCT* (hydroxycinnamoyl-CoA shikimate/quinic acid hydroxycinnamoyl transferase), *SICOMT* (Caffeic acid 3-O-methyltransferase), *SICCoAOMT1* and *SICCoAMT6* (caffeoyl CoA 3-O-methyltransferases) were slightly downregulated after infection (Fig. 2, 16). In H7996, *R. solanacearum* infection also resulted in a decrease of *SICOMT* expression, whereas *SIPAL1* (phenylalanine ammonia lyase), *SIHCT*, *SICCoAOMT1* and *SICCoAMT6* slightly increased (Fig. 2, 16).

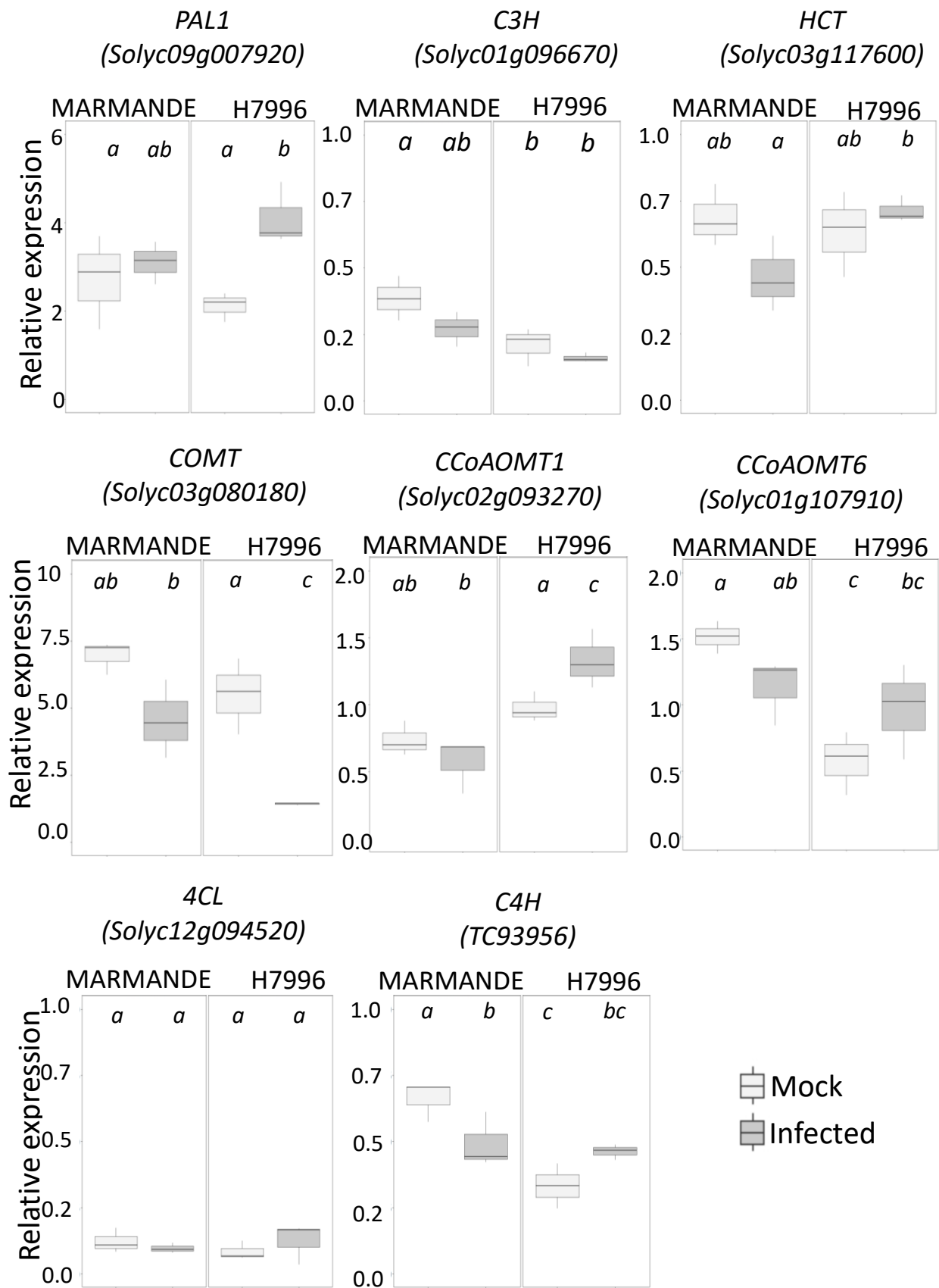


**Figure 2:** Expression of phenylpropanoid pathway genes in xylem vasculature of taproots upon invasion of *R. solanacearum*. Gene expression analyzed by qPCR of phenylpropanoid pathway genes in

taproot xylem vasculature of resistant H7996 and susceptible Marmande plants water-treated or infected by *R. solanacearum*. The Elongation Factor 1 alpha (*eEF1  $\alpha$* ) gene was used as endogenous reference. H7996 and Marmande plants, with *R. solanacearum* inoculum of  $10^5$  CFU g<sup>-1</sup> in taproot, were selected and xylem vascular tissue, comprising of metaxylems and surrounding parenchyma cells was collected from taproots for RNA extraction and cDNA synthesis. Similarly, xylem tissue was collected from Marmande mock plants and H7996 mock plants. Three biological replicates (n=3) were used, and taproots of 6 plants were used in each replicate. Different letters indicate statistically significant differences ( $\alpha=0.05$ , Fisher's least significant difference test).

#### 4.1.1.2 Suberin feruloyl esters synthesis pathway

Suberin feruloyl transferase (FHT) catalyzes the conjugation of feruloyl-CoA to aliphatic chains such as  $\omega$ -hydroxyacids and primary alcohols to form feruloyl esters (Molina *et al.*, 2009; Serra *et al.*, 2010b; Boher *et al.*, 2013). Hence, it acts as a linker of phenolic to aliphatic compounds to form suberin monomers. *FHT* gene encodes an acyltransferase of BAHD superfamily named after the first four biochemically characterized enzymes of the group, which are plant-specific enzymes that catalyze the transfer of coenzyme A-activated donors onto various acceptor molecules (Bontpart *et al.*, 2015). In Arabidopsis this gene is named as aliphatic suberin feruloyl transferase (*ASFT*) and hydroxycinnamoyl-CoA: $\omega$ -hydroxyacid O-hydroxycinnamoyltransferase (*HHT*) and has been functionally characterized and has been reported to be involved in the synthesis of aromatics of the suberin polymer. It specifically controls the accumulation of the ferulate constituent of suberin in roots and seeds, but has no effect on the content of p-coumarate or sinapate (Gou *et al.*, 2009; Molina *et al.*, 2009). Knocking out this gene causes elimination of the suberin-associated ester-linked ferulate leading to altered permeability and sensitivity of seeds and roots to salt stress (Gou *et al.*, 2009; Molina *et al.*, 2009). Like all BAHD acyltransferases, tomato FHT protein too have an HxxxD motif involved in catalysis and a DFGWG motif located at the C-terminal end which is presumed to have a structural function (Serra *et al.*, 2010b) (Fig. 3). Phylogenetic analysis shows that tomato FHT gene is very close in ancestry to potato FHT gene (Fig. 4)

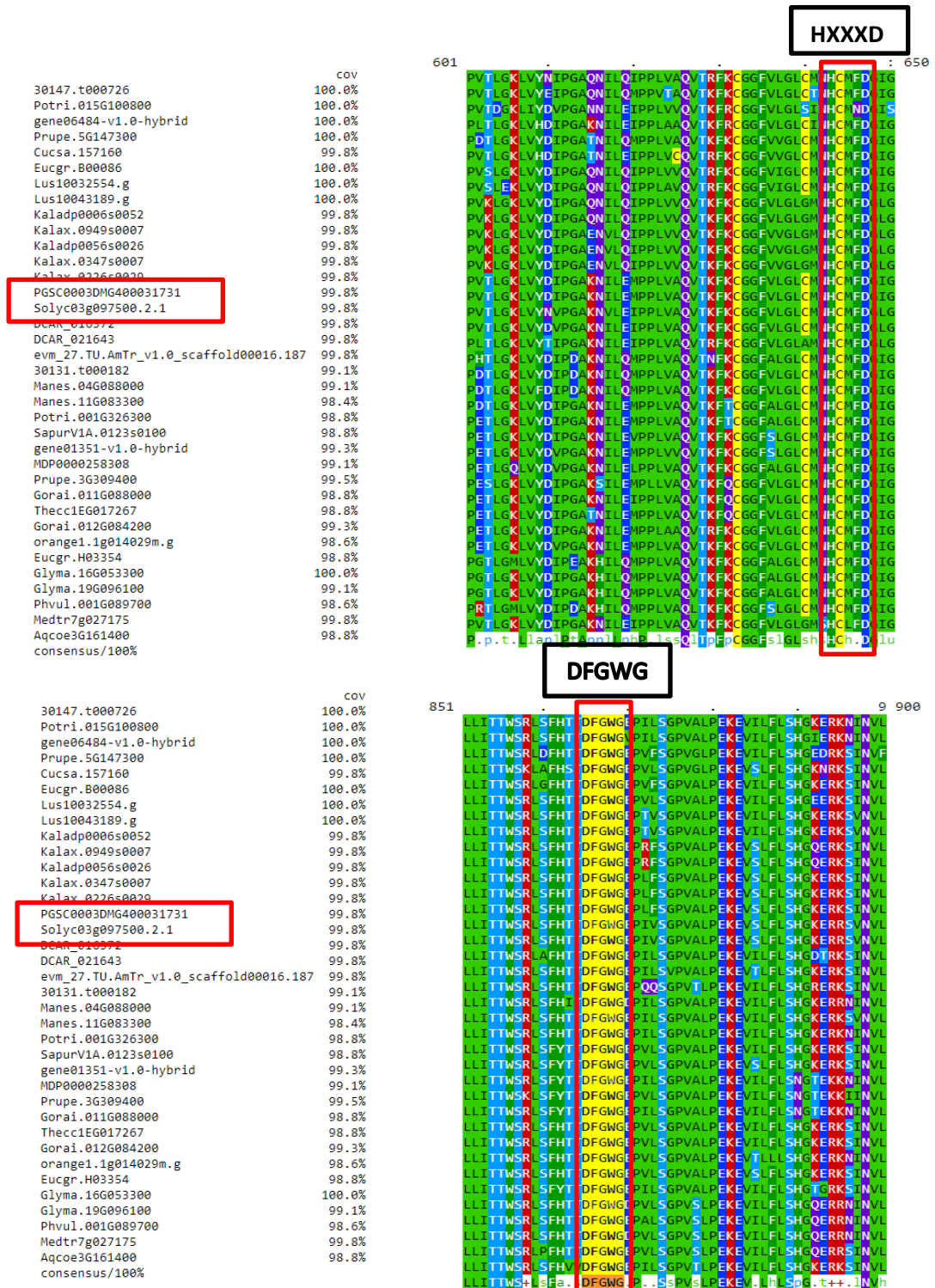


**Figure 3: Sequence alignment of feruloyl transferase (FHT) proteins in different plant species.** Protein homologs of tomato *FHT* gene (Solyc03g097500) were obtained from [www.phytozome.jgi.doe.gov](http://www.phytozome.jgi.doe.gov) and matches with more than 85 % similarity were used for amino acid sequence alignment in ClustalW and visualized by Mview using BAR (<http://bar.utoronto.ca/>) webpage. In agreement to the characteristics of BAHD acyltransferases, all FHT proteins of different plant species have conserved HxxxD motif involved in catalysis and DFGWG motif located at the C-terminal end which is presumed to have a structural function (Serra *et al.*, 2010b).



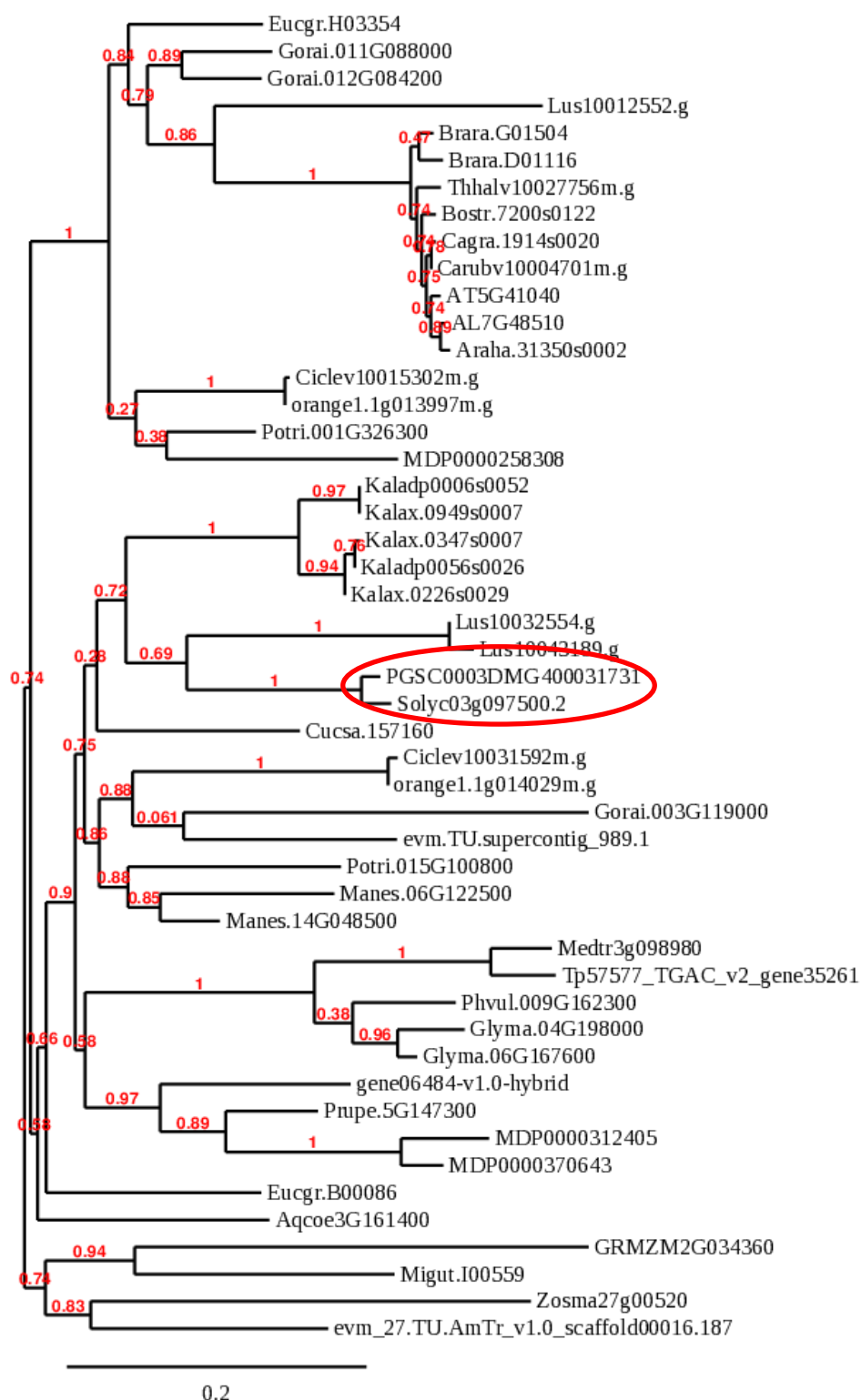


**Figure 4: Phylogeny of Feruloyl transferase (FHT) orthologues in different plant species.** Protein homologs of tomato *FHT* gene (Solyc03g097500) were obtained from [www.phytozome.jgi.doe.gov](http://www.phytozome.jgi.doe.gov) and matches with more than 80 % similarity were used for phylogenetic analysis using [www.phylogeny.fr](http://www.phylogeny.fr).

Here using the Botany array resource (BAR) gene expression (Toufighi *et al.*, 2005) analyzing tool (<http://bar.utoronto.ca/>) we present in a graphical form the tissue specific expression and cellular localization of *SIFHT* gene (Solyc03g097500) in tomato (Fig. 5).

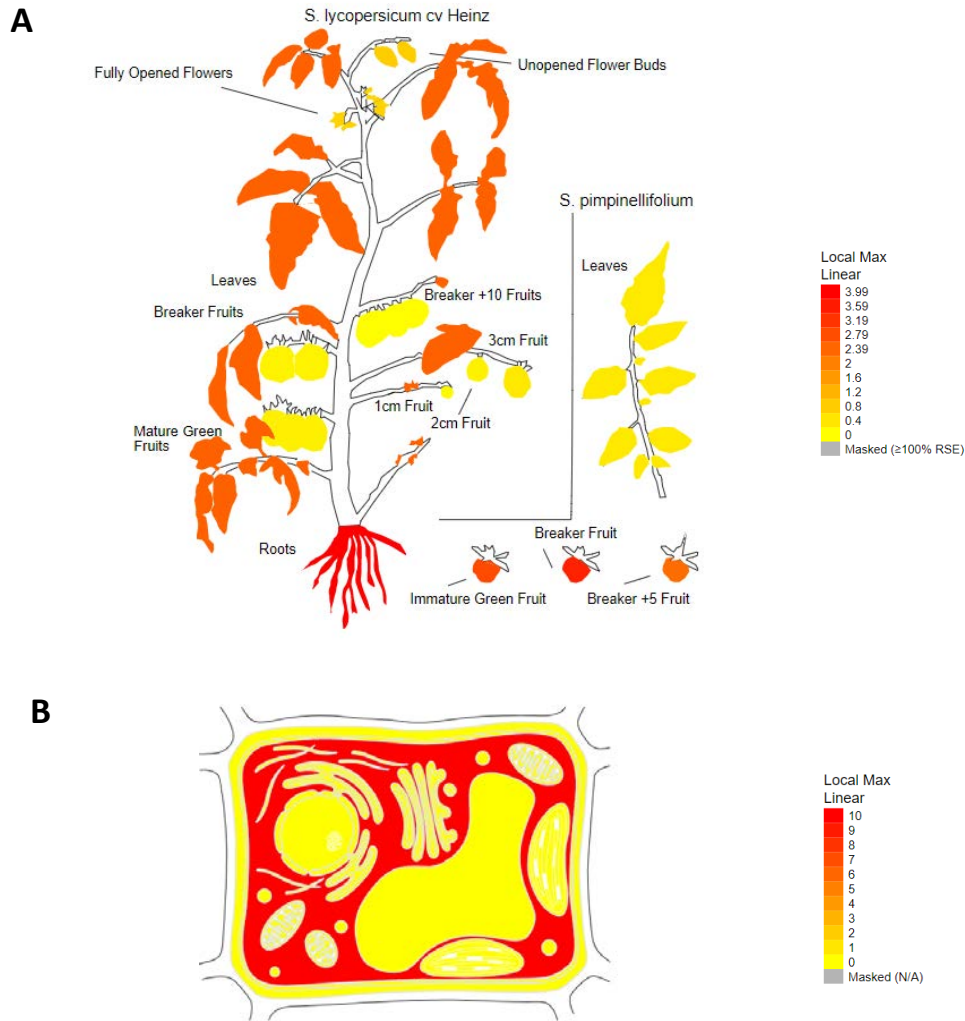


**Figure 5:** *SIFHT* is expressed in roots, fruits and leaves and the protein is predicted to be localized in the cytosol. (A) Expression level of *SIFHT* (Solyc03g097500) is shown in different tissues using BAR webpage with data from The Tomato Genome Consortium, 2012. (B) Sub-cellular localization of *SIFHT* protein was predicted to be cytosolic based on The Cell eFP Viewer tool of BAR (<http://bar.utoronto.ca/>) webpage.

Using the perturbations tool from the Gene search toolset in Genevestigator (<https://genevestigator.com/>) we searched for conditions where the tomato *FHT* gene is

specifically up- or down-regulated, and which minimally change in all other conditions. From the analysis based on curated data on tomato, induced expression of *FHT* could be observed in specific tissues during normal course of development, where suberin is known to deposit such as locules of green tomato fruit, placenta etc (Fig. 6). However, the expression of *FHT* gene was found to change minimally during stress responses, even though the polymer is known to be formed during several stress conditions such as salt injury. This can be justified by the fact that in most studies expression analysis were done in bulk tissues, whereas in our study a particular tissue was used where we expected suberin to accumulate. Moreover, *FHT* gene was found to be down regulated in nematode infection in susceptible tomato (Fig. 6).

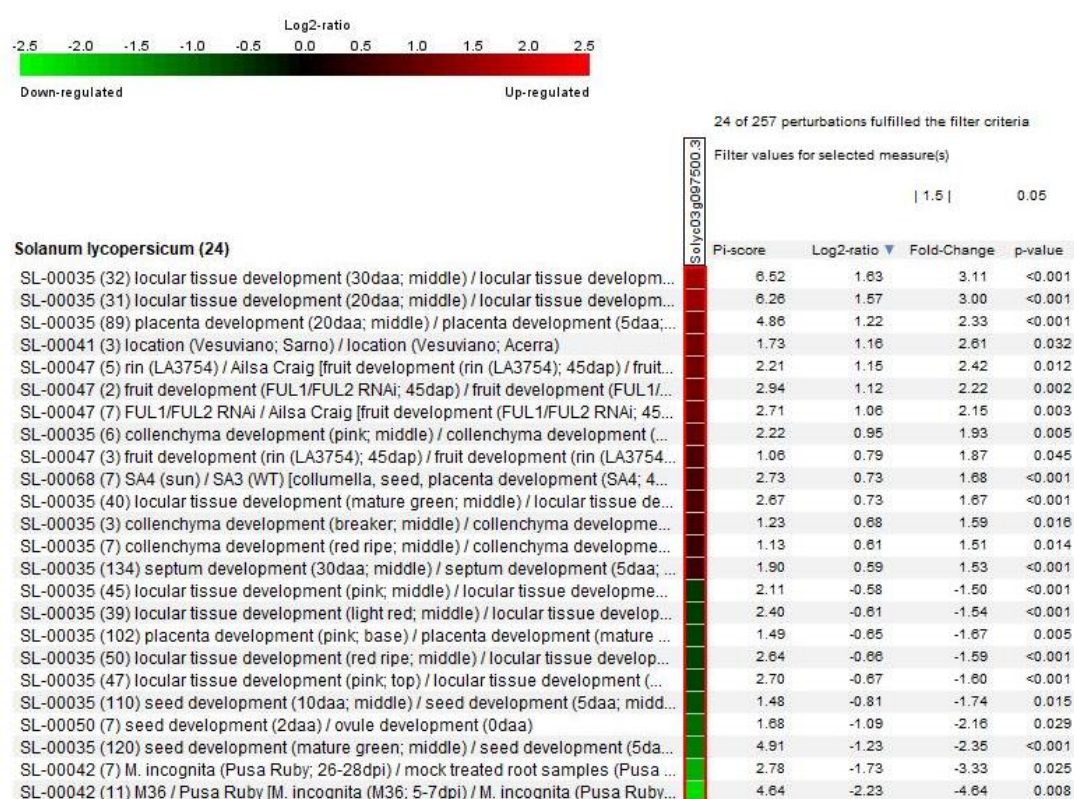


**Figure 6: Tomato *FHT* gene is upregulated in specific tissues know to deposit suberin.** The perturbations tool from GENE SEARCH toolset in GENEVESTIGATOR (<https://genevestigator.com/>) was used to find the conditions where *FHT* gene (Soly03g097500) is specifically upregulated or downregulated, which minimally change in all other conditions.

In potato, it is shown that transcriptional activation and protein accumulation of FHT takes place in specific tissues that undergo suberization such as the root boundary layers of the exodermis and the endodermis, along with the tuber periderm (Boher *et al.*, 2013). Likewise, transcriptomic studies show that *FHT* gene in different plant species is upregulated during suberization (Lashbrooke *et al.*, 2016; Cohen *et al.*, 2019). Hence, we next asked whether *R. solanacearum* infection has any influence on transcript level of *FHT* gene in root xylem vasculature. qPCR of samples obtained from taproot xylem vasculature showed that *FHT* gene is specifically upregulated in infected H7996 tomato, but not in infected Marmande (Fig. 7).

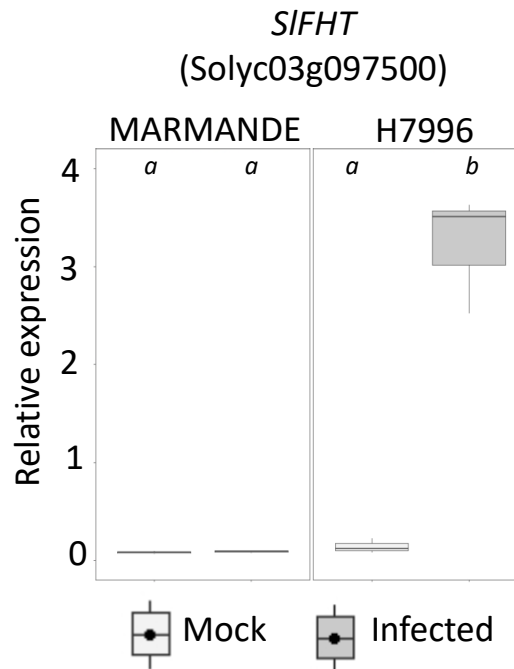


**Figure 7: Expression of tomato *FHT* gene in response to *Ralstonia solanacearum* infection.** Gene expression of the putative tomato *FHT* ortholog (*Solyc03g097500*) was analyzed by qPCR. Relative expression levels were calculated using the Elongation Factor 1 alpha (*eEF1 α*, *Solyc06g005060*) as the reference gene. H7996 and Marmande plants, containing a *R. solanacearum* inoculum of  $10^5$  CFU g<sup>-1</sup> in the taproot were selected. Xylem vascular tissue, comprising of metaxylems and surrounding parenchyma cells was collected from taproots for RNA extraction and cDNA synthesis. Similarly, xylem tissue was collected from Marmande mock plants and H7996 mock plants. Three biological replicates (n=3) were used, and taproots of 6 plants were used in each replicate. Different letters indicate statistically significant differences ( $\alpha=0.05$ , Fisher's least significant difference test).

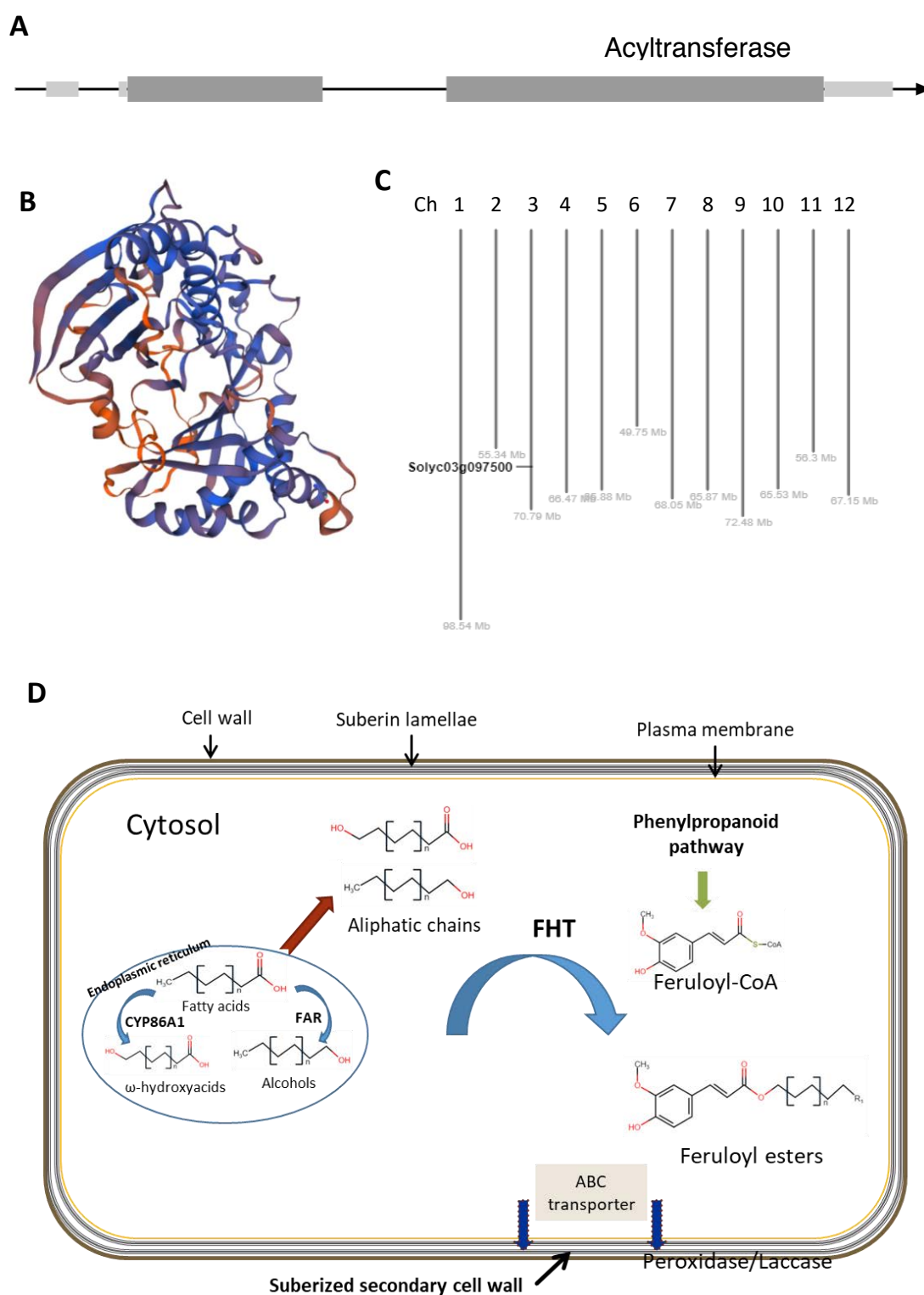


**Figure 8: Structure and function of suberin feruloyl transferase.** (A) FHT encodes an acyltransferase. (B) Protein crystal structure of SIFHT (Solyc03g097500) was built using SWISS-MODEL (<https://swissmodel.expasy.org/>) based on crystal structure of *Coleus blumei* Hydroxycinnamoyl-CoA:shikimate hydroxycinnamoyltransferase (HCT) (Levsh *et al.*, 2016). (C) FHT gene is located in

chromosome 3. (D) FHT catalyzes the conjugation of feruloyl-CoA to aliphatic chains such as  $\omega$ -hydroxyacids and primary alcohols to form feruloyl esters.

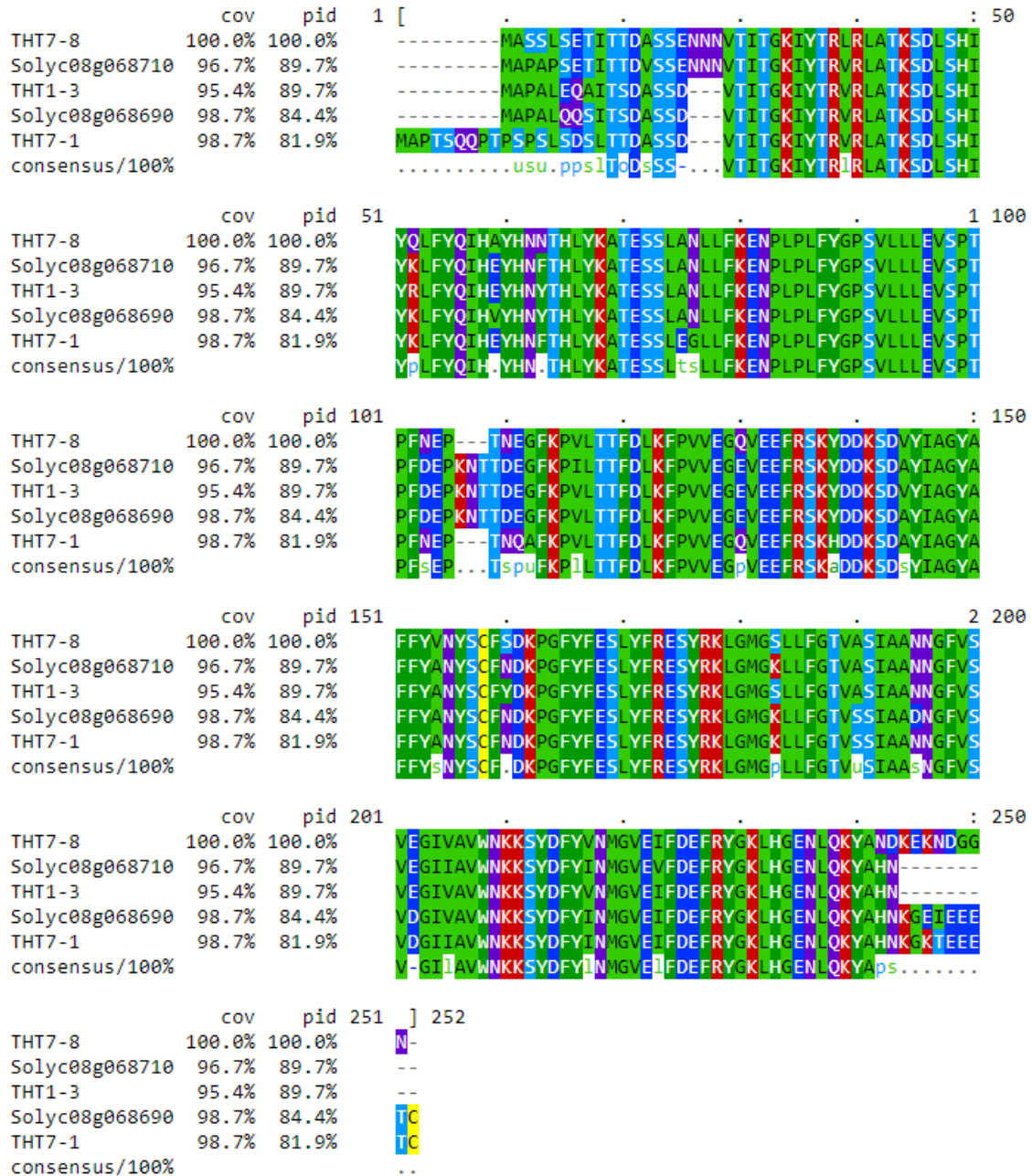
#### 4.1.1.3 Hydroxycinnamic acid amides synthesis pathway

Existing models of suberin describe it to be a heteropolymer composed of a poly-phenolic domain and a poly-aliphatic domain (Bernards *et al.*, 1995; Lashbrooke *et al.*, 2016; Woolfson *et al.*, 2018; Cohen *et al.*, 2019). Also, some studies describe the poly-phenolic domain to be lignin-like (Serra *et al.*, 2010a). However, the exact structure and composition of the suberin-associated poly-phenolic is elusive. This phenolic domain is reported in several studies to be enriched in ferulic acid (Bernards & Lewis, 1992; Bernards *et al.*, 1995; Graça, 2010, 2015; Cohen *et al.*, 2020). Depolymerization assays of suberin polymer by ester breaking showed that along with aliphatic monomers, soluble phenolics such as hydroxycinnamic ferulic acid is present in comparatively higher quantities along with hydroxycinnamic acid amides (HCAA), such as tyramine derivatives (Bernards *et al.*, 1995; Graça, 2010, 2015). Ferulic acid amides such as feruloyltyramine, and feruloyloctopamine, were found ether linked in the insoluble poly-aromatics domain (Negrel *et al.*, 1996). In wound healing potato scab lesions feruloyl amides, feruloyloctopamine, feruloyltyramine, a cross-linked feruloyltyramine dimer were isolated from suberin (King & Calhoun, 2005). Our HSQC 2D-NMR studies also showed signals corresponding to feruloyl tyramine specifically in the roots of resistant H7996. However, the role of HCAA accumulation on the polymer formation is an open question. Accumulation of such soluble aminated phenolics may act as a chemical barrier, initially acting as phytolaexin, but could also act as physical barrier if cross-linked to the lignin-like poly-aromatic domain of suberin.

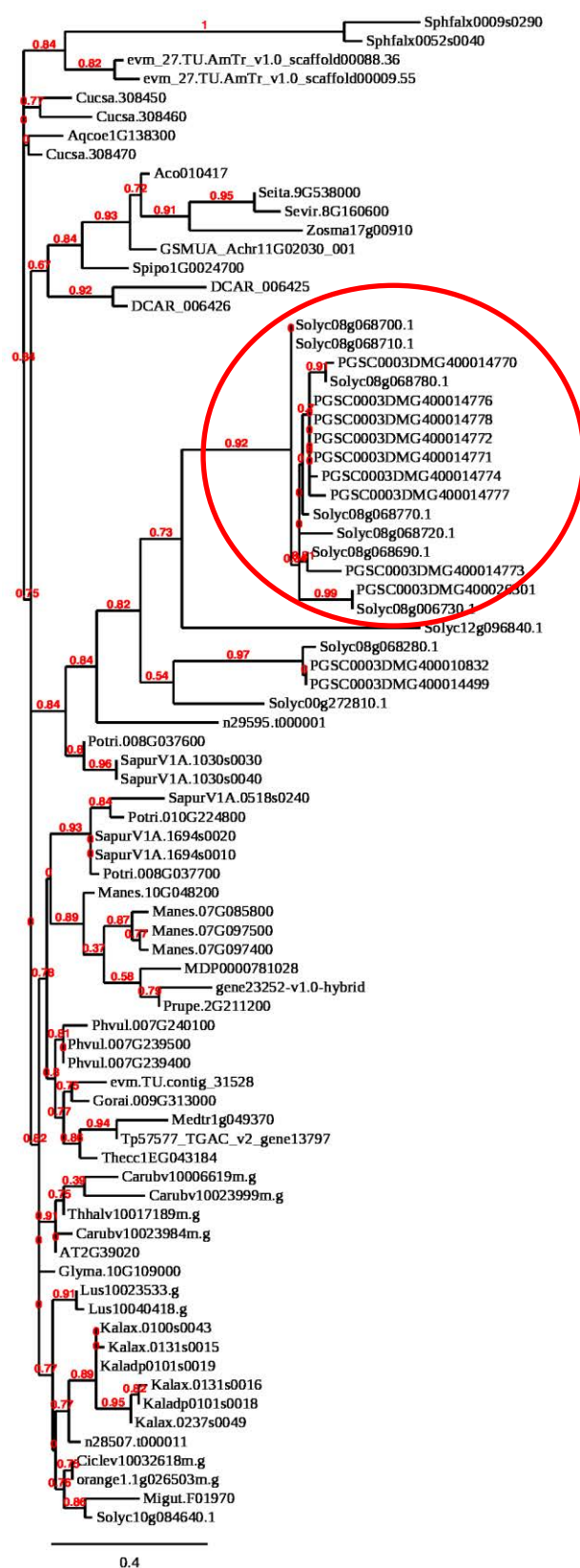
Tyramine hydroxycinnamoyl transferase or tyramine N-feruloyltransferase (THT) is the key regulatory enzyme responsible for the synthesis of HCAA (Hagel & Facchini, 2005). THT catalyzes the condensation of amines with hydroxycinnamoyl-CoA thioesters (Negrel *et al.*, 1995). For instance, THT conjugates tyramine, derived from the decarboxylation of tyrosine (tyrosine decarboxylase; TyDC), with feruloyl-CoA, to yield feruloyltyramine (Fig. 15D) (Woolfson, 2018; Woolfson *et al.*, 2018). In potato, the *THT* gene family members have been categorized as a phenolic suberin biosynthetic genes in



some studies (Woolfson, 2018; Woolfson *et al.*, 2018) . In tomato, *THT* is encoded by a multigene family comprising of at least six putative homologs. Tomato *THT* genes are very close in ancestry to potato *THT* genes (Figure 10).



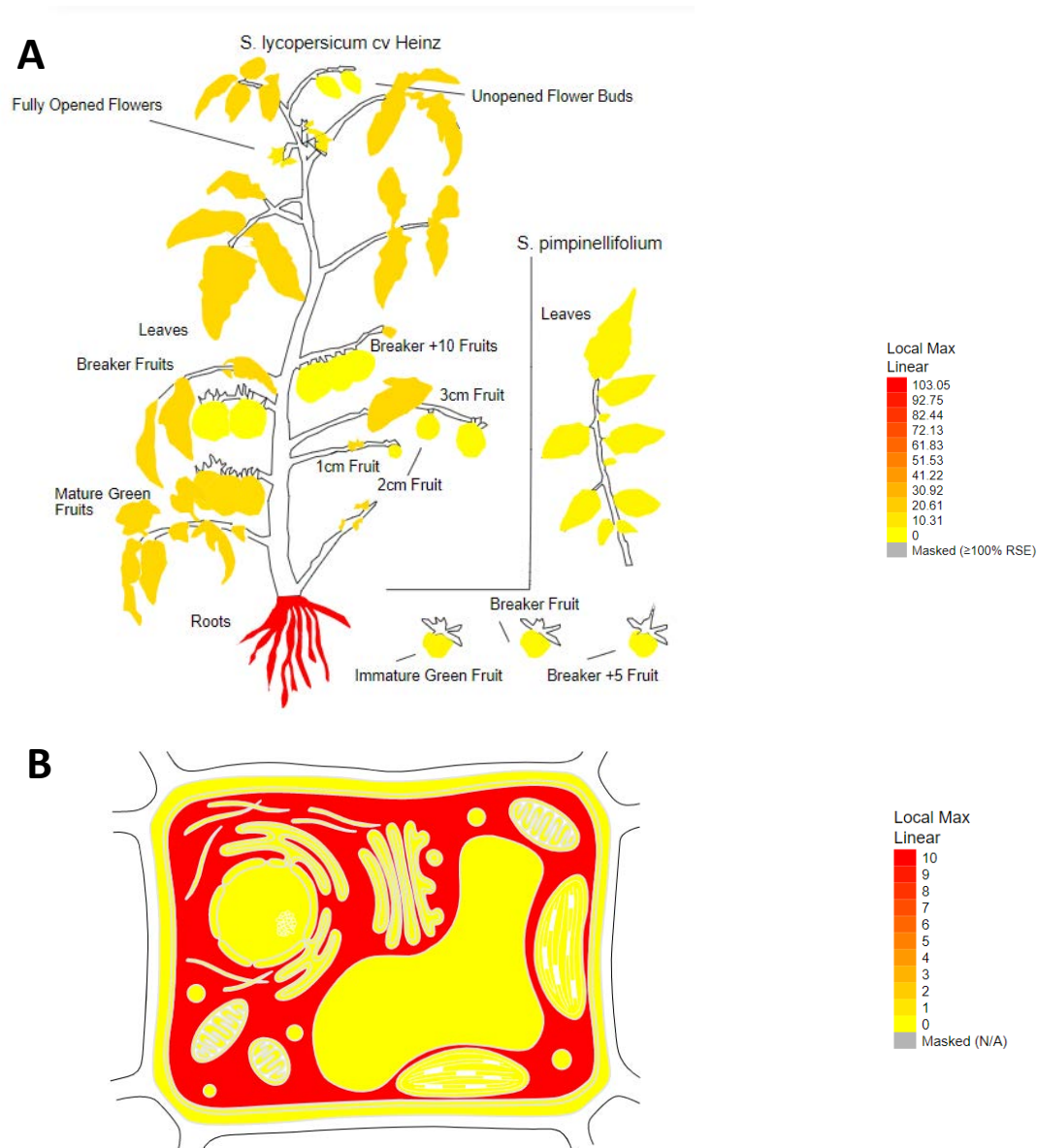
**Figure 9: Sequence alignment of THT proteins of tomato.** Amino acid sequences of tomato *THT* gene family members were aligned in ClustalW and visualized by Mview using BAR (<http://bar.utoronto.ca/>) webpage.



**Figure 10: Phylogeny of tyramine hydroxycinnamoyl transferase (THT) orthologues in different plant species.** Protein homologs of tomato *THT 1-3* gene (Solyc08g068730) was obtained from

phytozome.jgi.doe.gov and matches with more than 60 % similarity was used for phylogenetic analysis using webpage [www.phylogeny.fr](http://www.phylogeny.fr).

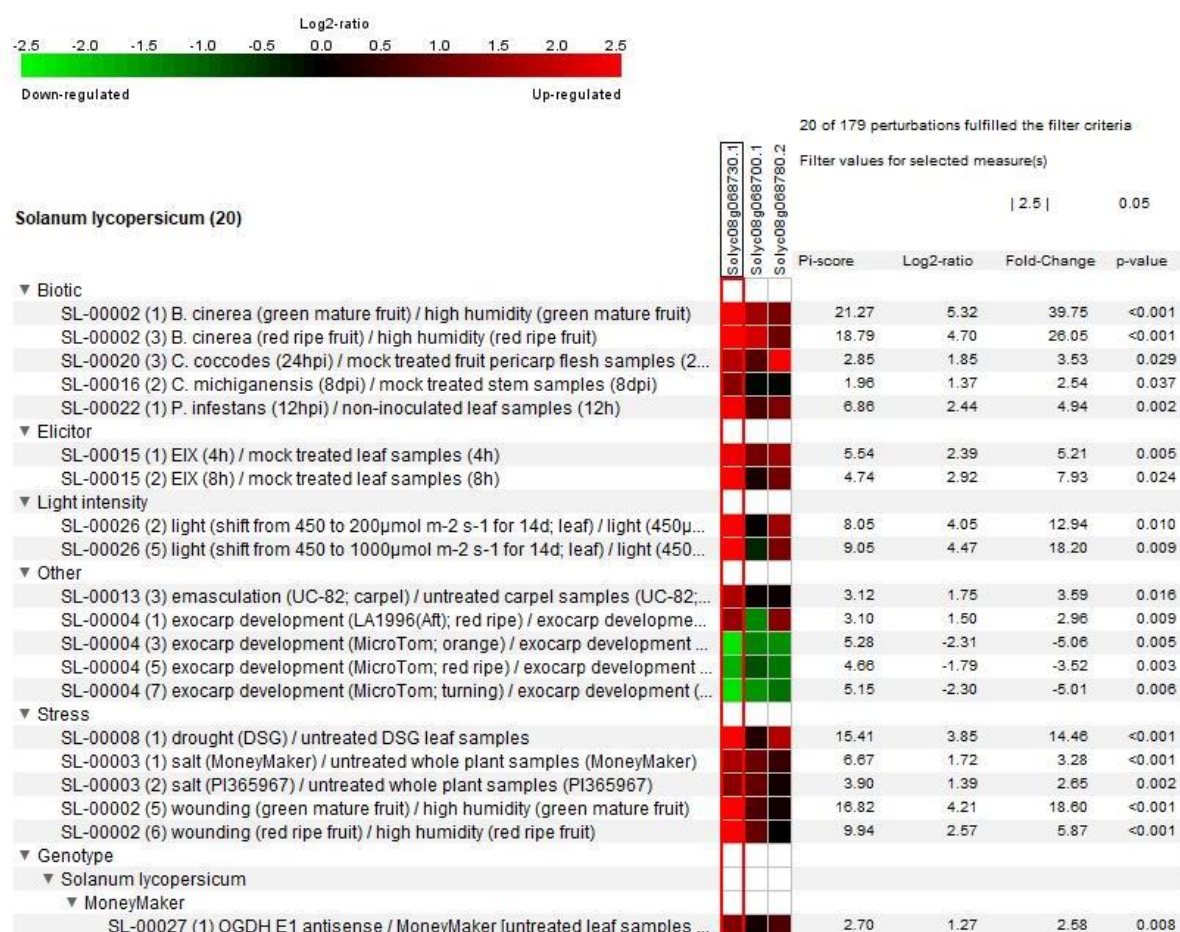
Here using BAR gene expression analyzing tool we present in a graphical form the tissue specific expression and cellular localization of a representative *THT* gene family member *SITH1-3* (Soly08g068730) in tomato (Fig. 11).



**Figure 11: *SITH1-3* is highly expressed in roots and the protein is predicted to localize in cytosol.** (A) Expression level of a representative THT gene *SITH1-3* (Soly08g068730) is shown in different tissues using BAR webpage with data from The Tomato Genome Consortium, 2012. (B) Sub-cellular localization of





*SITH1-3* protein was predicted to be cytosolic based on The Cell eFP Viewer tool of BAR (<http://bar.utoronto.ca/>) webpage.

Using Genevestigator we scanned the entire transcriptomic data available in its repository for tomato and analyzed the expression pattern of THT genes. Using perturbations tool we found that THT genes, namely, *SITH1-3* (*Solyc08g068730*), *SITH1-7-1* (*Solyc08g068700*) and *SITH1-7-8* (*Solyc08g068780*) are induced during pathogen attack, elicitor treatment, drought stress, salt stress and wounding, indicating their role in generalized defense and stress response of plants (Fig. 12).



**Figure 12: THT genes are upregulated during pathogen attack, elicitor treatment, salt stress and wounding.** The perturbations tool from Gene search toolset in Genevestigator was used to find the conditions where THT genes namely, *SITH1-3* (*Solyc08g068730*), *SITH1-7-1* (*Solyc08g068700*) and *SITH1-7-8* (*Solyc08g068780*) are specifically upregulated or downregulated, which minimally change in all other conditions.

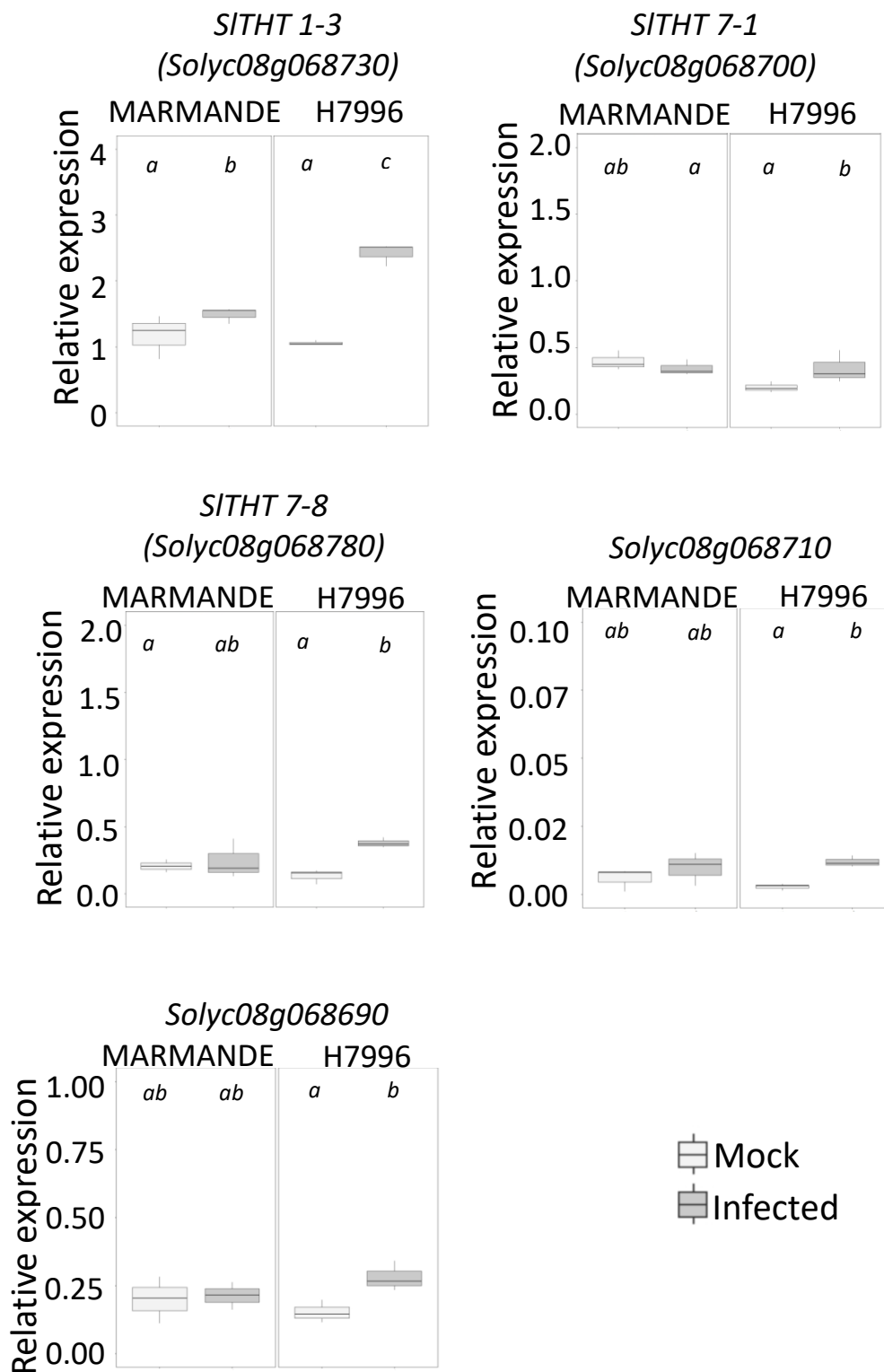
We also analyzed THT gene expression in a transcriptomic study done in tomato against *R. solanacearum* (Ishihara *et al.*, 2012). In this particular study, THT genes were upregulated at 1 dpi specifically in resistant cultivar LS-89, but not in susceptible cultivar Ponderosa (Fig 13).

	Fold Change	
	Susceptible Ponderosa	Resistant LS-89
THT 1-3	 -1.6	 5
THT7-1	 -1	 3.8

**Figure 13: Transcriptome of tomato *R. solanacearum* interaction showed *THT* genes are upregulated specifically in resistant tomato.** Expression of *SITHT 1-3* (*Solyc08g068730*) and *SITHT 7-1* (*Solyc08g068700*) genes in a transcriptome of tomato *R. solanacearum* interaction done in affymerix tomato genome array platform (Ishihara *et al.*, 2012).

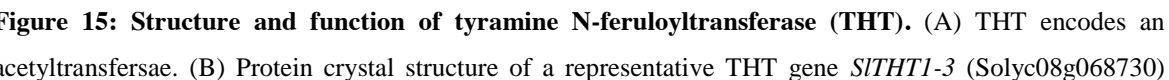
In our tomato root- *R. solanacearum* interaction, qPCR analysis showed that all *SITHTs* analyzed were induced by infection in the vascular tissue of H7996 (Fig. 14 and 16), albeit to lower levels than *FHT* (Fig. 7 and 16). *SITHT1-3* showed the strongest upregulation among *SITHTs* in H7996 after infection, although a slight upregulation could also be observed in Marmande (Fig. 14 and 16).

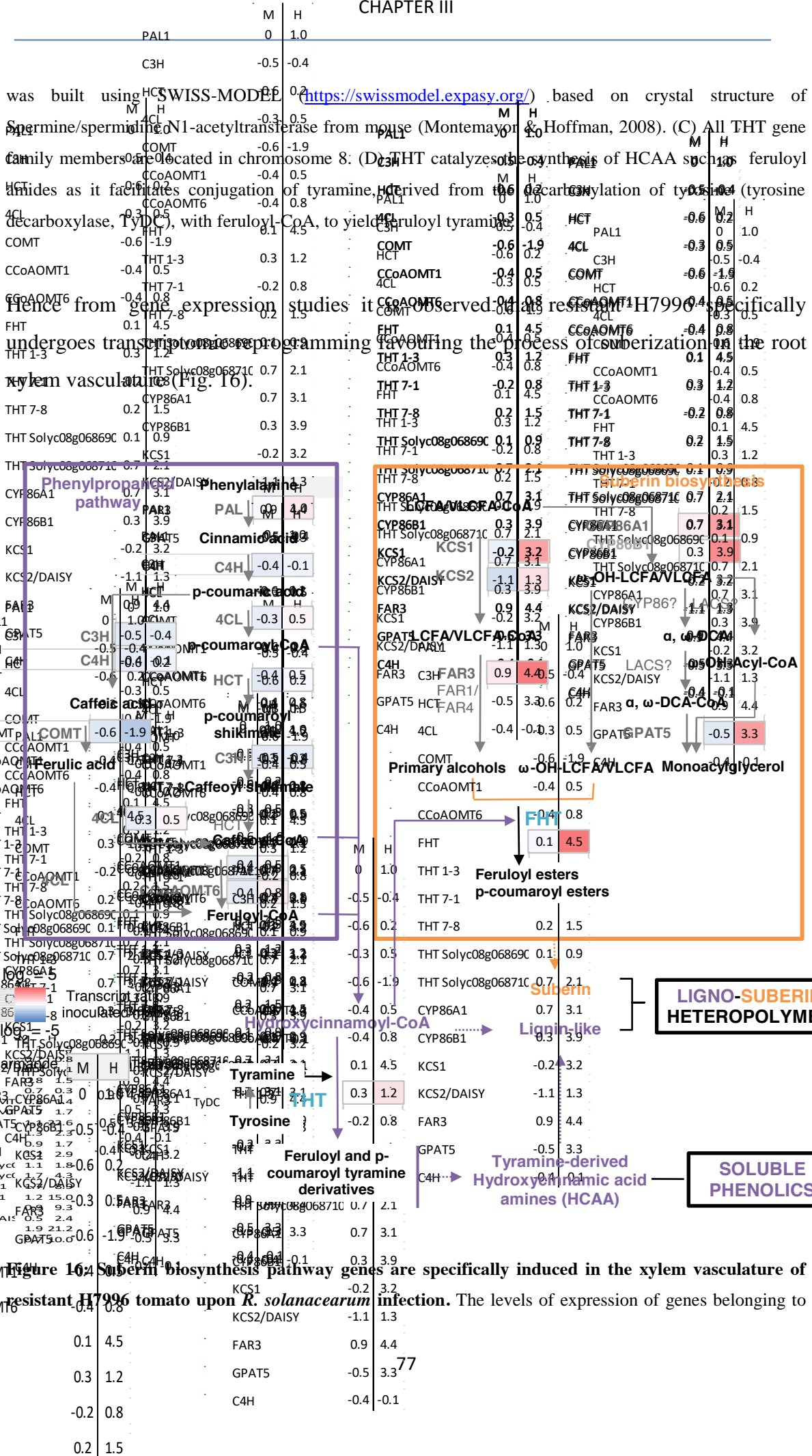




**Figure 14: Expression of the tomato *THT* gene family members in response to *R. solanacearum* infection.** Gene expression of the tomato *THT* gene family members were analyzed by qPCR. The







different steps of the suberin pathway were analyzed by qPCR of taproot vascular tissue in infected or mock-treated H7996 or Marmande tomato plants. Plants containing an *R. solanacearum* inoculum of  $10^5$  CFU g<sup>-1</sup> were selected and taproot xylem vascular tissue, comprising of metaxylems and surrounding parenchyma cells was collected for RNA extraction and cDNA synthesis. In parallel, xylem tissue was collected from mock plants. Heatmaps show log<sub>2</sub> fold change values of infected vs. mock Marmande (left) and Hawaii (right). The tomato gene encoding for the alpha-subunit of the translation elongation factor 1 (*SlEF1  $\alpha$* ) was used as endogenous reference. Three biological replicates (n=3) were used, and taproots of 6 plants were used in each replicate. The scheme represents the phenylpropanoid and fatty acid biosynthesis pathways providing precursors for the phenolic and aliphatic domains of suberin, respectively. The most abundant phenylpropanoid product in suberin is feruloyl-CoA. Downstream it is conjugated to aliphatics by the action of feruloyl transferase (FHT) to yield suberin monomers. Infected H7996 plants show a specific upregulation of genes belonging to the fatty acid biosynthesis pathway and FHT. Further, HCAA ferulic acid amides namely feruloyltyramine, and feruloyloctopamine are found co-solubilized from suberin matrix and were found ether linked in the insoluble polyaromatics. Tyramine hydroxycinnamoyl transferase (THT) is the key regulatory enzyme responsible for the synthesis of HCAA acting as non-structural phenolic and may also be incorporated into suberin aromatic domain. Abbreviations: PAL: Phenylalanine ammonia-lyase; C4H: Cinnamate-4-hydroxylase; C3H: Coumarate 3-hydroxylase; 4CL: 4-Coumarate-CoA ligase; HCT: Hydroxycinnamoyl-CoA shikimate/quinate hydroxycinnamoyl transferase; COMT: Caffeic acid 3-O-methyltransferase; CCoAOMT: Caffeoyl CoA 3-O-methyltransferase; CYP86A1 and CYP86B1: cytochrome P450 fatty acid  $\omega$ -hydroxylases; KCS1/2: 3-ketoacyl-CoA synthase; FAR 1/3/4: Fatty acyl-CoA reductase; GPAT5: glycerol-3-phosphate acyltransferase 5; THT: Tyramine hydroxycinnamoyl transferase; TyDC: Tyrosine decarboxylase; FHT: feruloyl transferase

#### 4.1.1.4 Induction of *Pro<sub>SIFHT</sub>::GUS* in xylem vascular tissue of resistant H7996 after infection of *R. solanacearum*

*SIFHT* (Soly03g097500) was found to be up-regulated specifically in resistant H7996 (Fig. 7). We hypothesized that *SIFHT* could be good marker to study spatiotemporally the *R. solanacearum*-induced suberization in xylem vascular tissue. Hence, we created *Pro<sub>SIFHT</sub>::GUS* lines in resistant H7996 in order to elucidate the participation of *SIFHT* in *R. solanacearum*-induced vascular coating. We could observe the induction of *Pro<sub>SIFHT</sub>::GUS* in xylem vascular tissue after infection of *R. solanacearum* (Fig 17). At 20 dpi this induction of *Pro<sub>SIFHT</sub>::GUS* was observed to expand, encompassing large areas of xylem vascular tissue (Fig 17). In water-treated plants induction of *Pro<sub>SIFHT</sub>::GUS* could not be observed in the xylem vasculature, but a faint induction could be observed in exodermis.

### *H7996 Pro<sub>SIFHT</sub>::GUS*

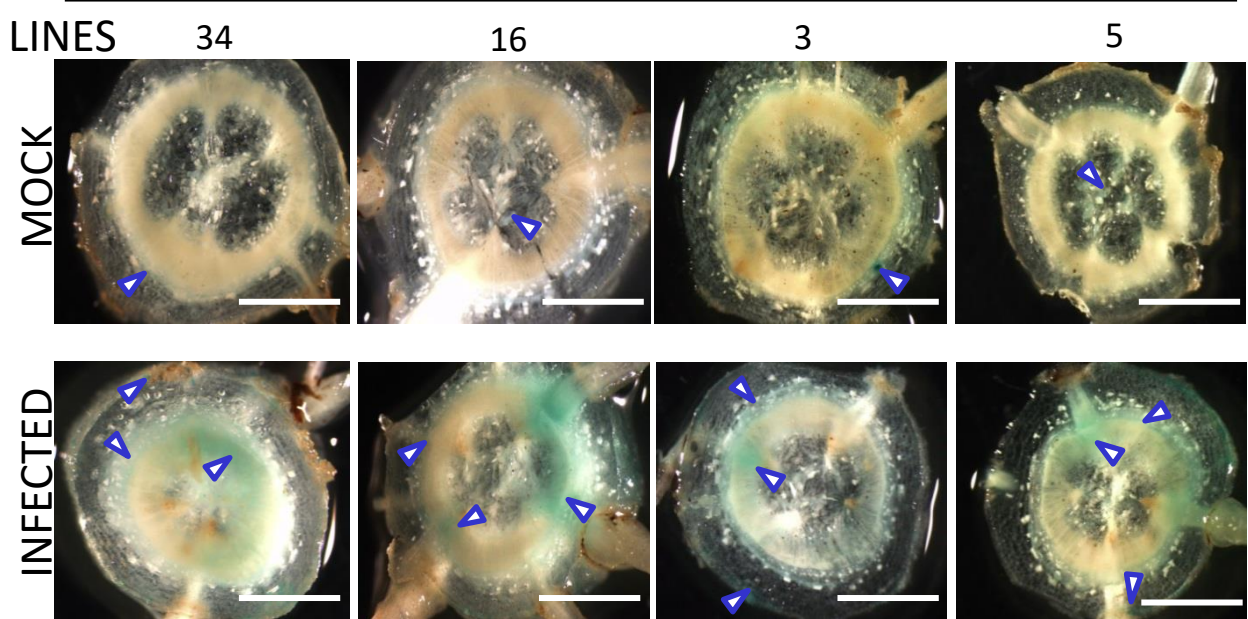


**Figure 17: Induction of *Pro<sub>SIFHT</sub>::GUS* covering large areas of taproot xylem vasculature of resistant H7996 at 20 DPI.** *Pro<sub>SIFHT</sub>::GUS* transgenic H7996 tomato plants of 5 weeks were inoculated through roots, by soil-soak with 40 ml of suspension per plant of *R. solanacearum* with a concentration of  $\sim 1 \times 10^7$  CFU ml<sup>-1</sup> and grown at 28°C. In water treated plants induction of *Pro<sub>SIFHT</sub>::GUS* could not be observed in xylem vasculature, but a faint induction could be observed in exodermis. In infected plants strong induction of *Pro<sub>SIFHT</sub>::GUS* could be observed in xylem vascular tissue at 20 DPI covering large areas of xylem vasculature. Scale bar = 2 mm.

Further, in agreement to its critical role in suberization, we could clearly observe the induction of *Pro<sub>SIFHT</sub>::GUS* in tissues known to accumulate suberin. Root epidermal cells are well known to deposit suberin (Watanabe *et al.*, 2013). We could observe strong induction of *Pro<sub>SIFHT</sub>::GUS* in the root epidermis of young seedlings (Fig 18A). Further, we could observe strong induction of *Pro<sub>SIFHT</sub>::GUS* in lateral root primordia, indicating a hardening process by suberin deposition in the cells of the developing lateral root cap, before emergence (Fig 18B). These tissues also accumulated ferulate, as observed by alkali UV microscopic technique described previously (Fig. 18C and D).



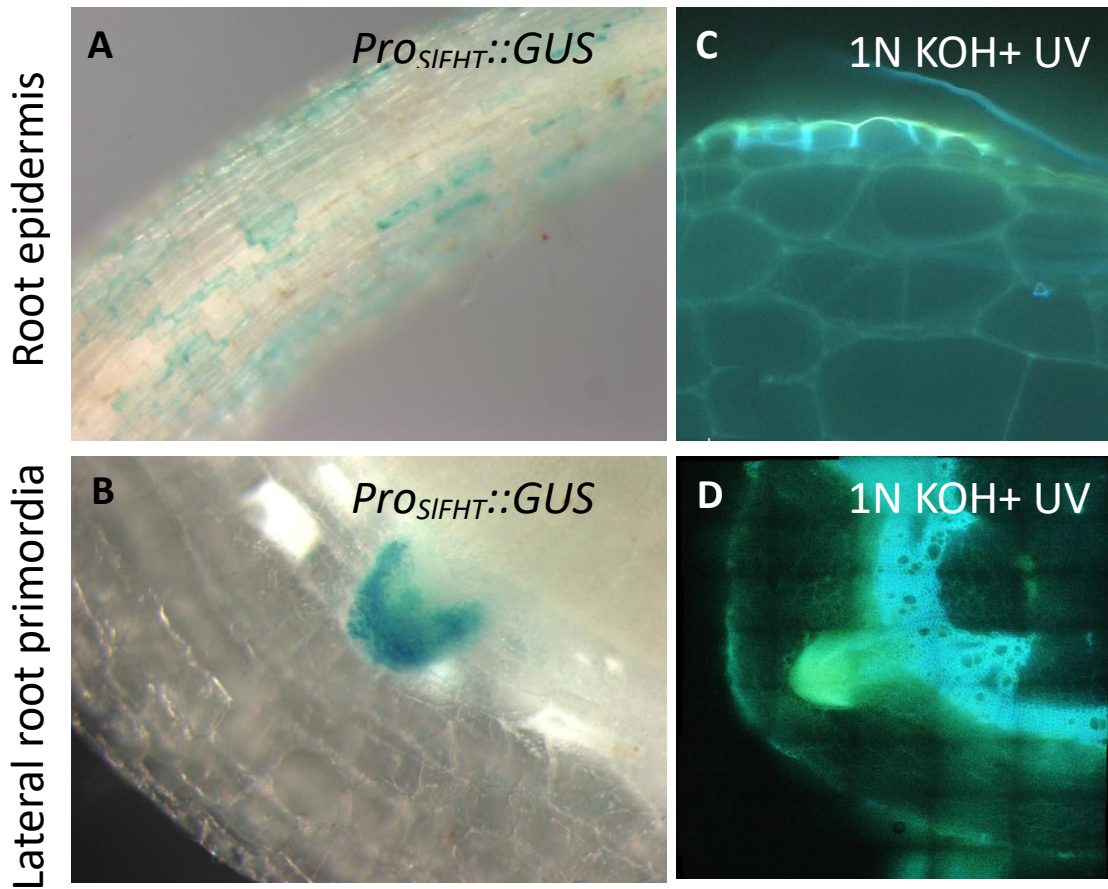


**Figure 18: Induction of *ProSIFHT::GUS* in tissues undergoing suberization.** Strong induction of *ProSIFHT::GUS* was observed in the (A) root epidermis of young seedlings and (B) in the emerging lateral root primordia. Correspondingly, ferulate signal was observed in (C) root epidermis of young seedlings and (D) lateral root primordia, as observed by alkali UV microscopic technique.

Since suberin deposition is known to occur as part of the wound healing response (Boher *et al.*, 2013; Graça, 2015), we analysed induction of *ProSIFHT::GUS* upon injury. At 48 hours post pin-prick injury on leaves, a strong induction of *ProSIFHT::GUS* could be observed surrounding the injured region (Fig 19 A, B). Also, when water imbalance leads to fruit cracks in tomato, plants have mechanism to seal this crack to prevent rotting. We could observe specific induction of *ProSIFHT::GUS* in the sealing region of the cracks, indicating suberization in this particular wound healing response (Fig 19 C, D).

### H7996 *Pro<sub>SIFHT</sub>::GUS*

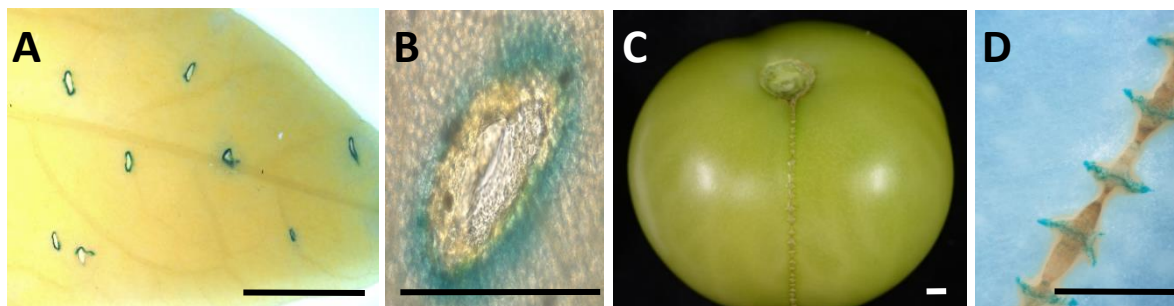


**Figure 19:** *Pro<sub>SIFHT</sub>::GUS* is induced in leaves and fruits of tomato during wound healing. (A) *Pro<sub>SIFHT</sub>::GUS* expression 48 hours after pin-prick injury on the leaves. (B) Magnified image from (A). (C) Induction of *Pro<sub>SIFHT</sub>::GUS* was observed in fruit cracks undergoing wound healing. (D) Magnified view of the crack showing clear GUS signal. Scale bar = 500 µm

#### 4.2 Overexpression of *SIFHT* in susceptible tomato caused slightly delay in disease progression and colonization

Considering the accumulation of suberin ferulates at early stages of *R. solanacearum* colonization in resistant H7996, we next tested whether overexpression of the acyltransferase *SIFHT* –important for the formation of suberin monomers- in susceptible tomato increased resistance against *R. solanacearum*. Previous studies have reported that overexpression of *Populus trichocarpa FHT* gene in Arabidopsis resulted in increased tolerance to salt stress (Cheng *et al.*, 2013). Hence, we undertook a variety of *R. solanacearum* infection assays in a transgenic tomato lines stably expressing *35S::SIFHT* on a susceptible tomato background.

We obtained 4 transgenic lines stably overexpressing *SIFHT* on a susceptible Marmande background. Accumulation of FHT-HA protein in Marmande expressing *35S::SIFHT-HA* was analyzed by immunoblot using HA antisera (Fig. 20).



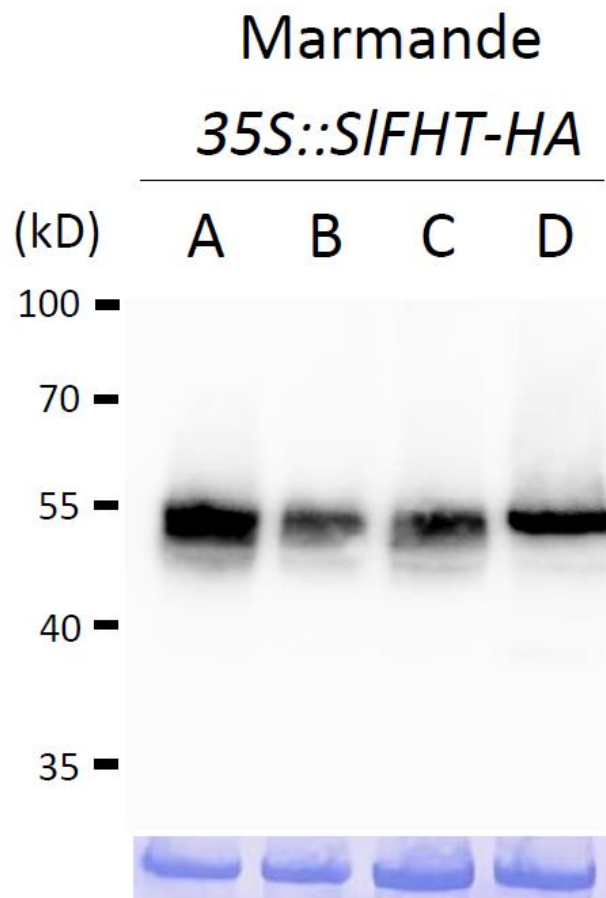


**Figure 20: Analysis of tomato lines expressing *35S::SIFHT-HA* in Marmande tomato.** Immunoblot using anti-HA antibody showing FHT protein levels of independent transgenic lines stably overexpressing SIFHT on a susceptible Marmande background (*35S::SIFHT-HA*). Data from 4 independent lines are shown (A, B, C, D). SIFHT-HA predicted protein size: 49 kDa.

These lines were used to perform pathogenicity assays to monitor the effect of *SIFHT* overexpression on symptom progression over time. *SIFHT* overexpression lines showed a slight delay in disease progression (Fig. 21A) and moderately milder symptoms (Fig. 21A). The taproot and hypocotyl of *SIFHT* overexpressors displayed a slight reduction in bacterial loads after soil-soak inoculation in comparison to Wt tomato (Fig. 21B). No significant restriction of *R. solanacearum* colonization was observed in the stem after petiole inoculation (Fig. 22). Growth of *R. solanacearum* GMI1000 in planta was also monitored in leaves of *35S::FHT* transgenic lines compared with Wt Marmande tomato lines over time, but no significant differences were observed (Fig. 23). The limited restriction shown by *SIFHT* overexpression lines could be due to the fact that in susceptible tomato varieties, despite overexpressing *FHT*, the level of expression of the genes in the fatty acid biosynthesis pathway is not sufficient to provide the aliphatic suberin precursors necessary to build up suberin (Fig. 16). In resistant varieties such as H7996 the increase in *FHT* expression is accompanied by an increase of expression of the genes from the fatty acid biosynthesis pathway, therefore providing the necessary precursors to create a suberization zone around infected vessels.

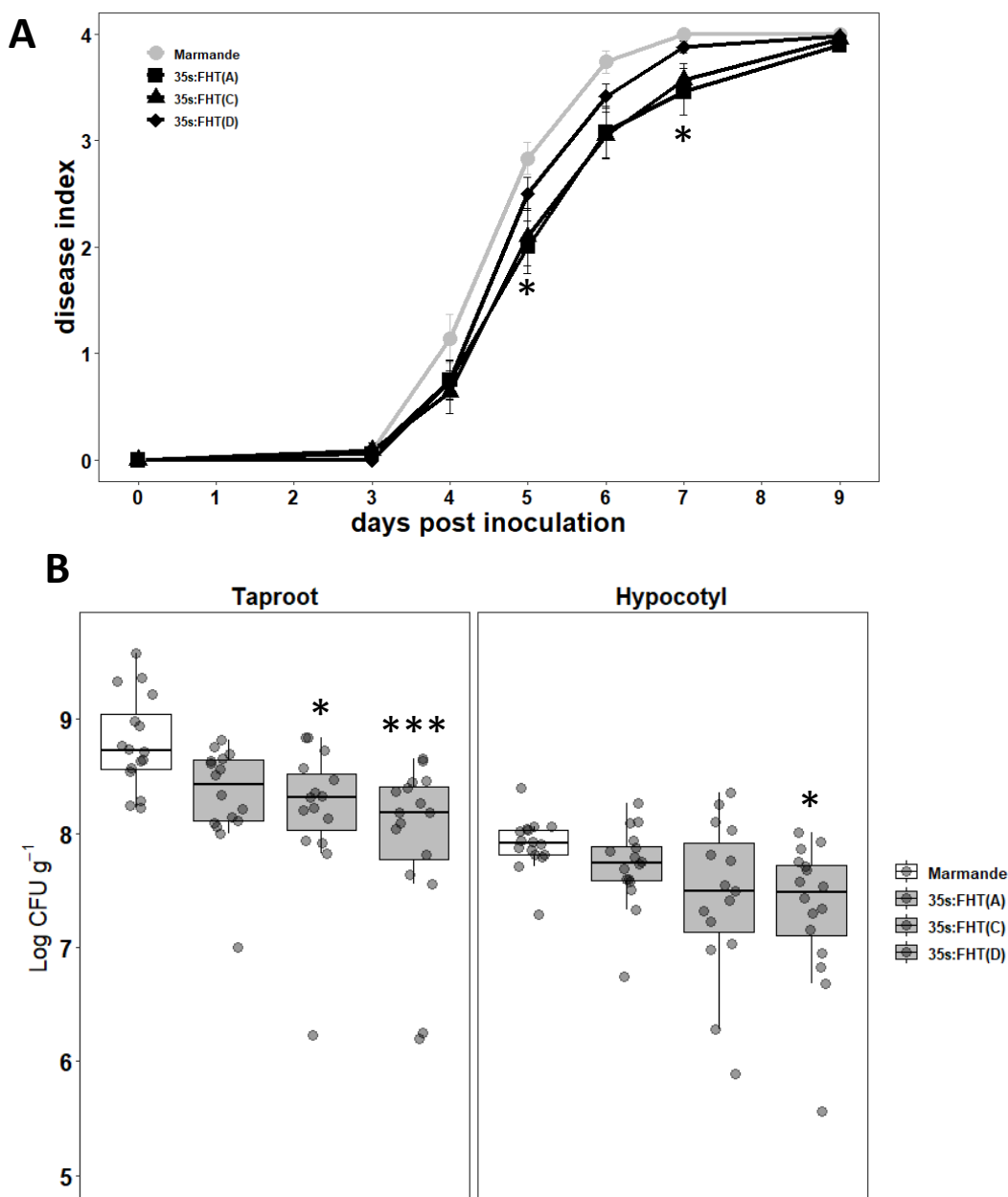


**Figure 21: Overexpression of *SIFHT* in susceptible tomato slightly restricts colonization by *R. solanacearum*.** (A, B) A pathogenicity assay was performed comparing Wt and 3 independent *35S::FHT-HA* Marmande tomato lines (A, C and D) after infection with *R. solanacearum* lux reporter strain of GMI1000. Five-week-old plants were soil-soak inoculated with  $\sim 1 \times 10^7$  CFU/ml or mock and grown at 28°C. (A) Wilting progress was monitored by rating plants daily on a 0 to 4 disease index scale where 0 = healthy and 4 = 100% wilted. Plotted values correspond to means  $\pm$  standard error of 24 independent plants ( $n=24$ ) from a representative experiment out of a total of 3. Asterisks indicate statistically significant differences between Wt and each of the *35S::FHT-HA* analyzed using a paired Student's t-test (\*  $p < 0.05$ ). (B) *R. solanacearum* colonization was analyzed in the taproot and hypocotyl tissue. The level of in planta colonization by *R. solanacearum* was calculated as colony forming units per gram of fresh taproot or hypocotyl tissue (CFU g<sup>-1</sup>) at 9 dpi. Data presented are of a representative experiment with  $n=15$  plants for each condition each

cultivar out of a total of 3 experiments. Box-and-whisker plots show data from a single representative experiment out of 3 (n =15). Asterisks indicate statistically significant differences between wild type and *35S::FHT-HA* tomato lines in a paired Student's t-test (\* corresponds to a p-value of  $p < 0.05$  and \*\*\* to  $p < 0.001$ ).

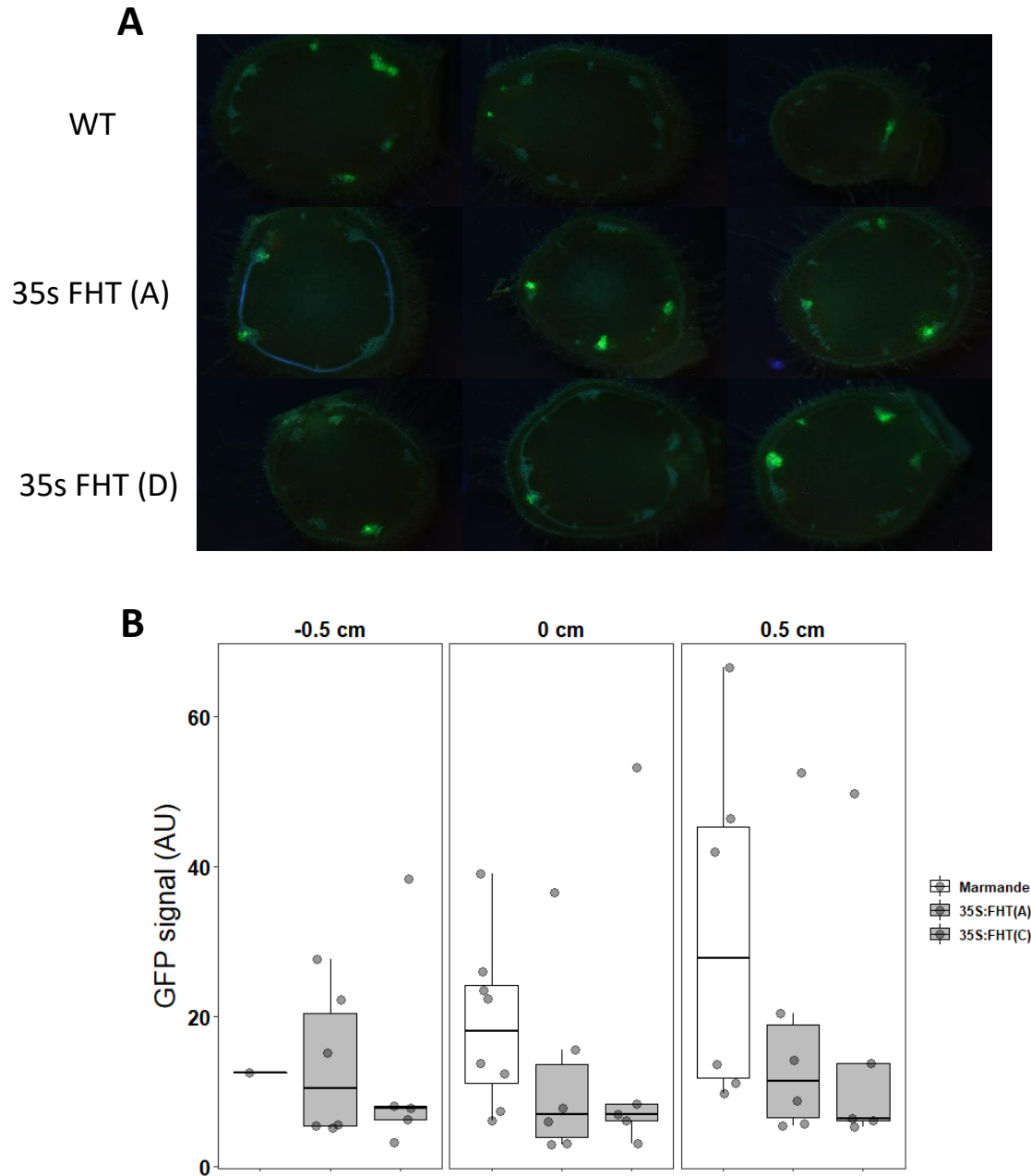


**Figure 22: Overexpression lines of *SIFHT-HA* in Marmande tomato showed no restricted to *R. solanacearum* colonization when petiole inoculated into stem (A) Transverse cross-sections of Wt and transgenic *35S::FHT-HA* tomato lines were imaged under a confocal microscope 6 dpi after infection with a *R. solanacearum* GFP reporter strain. *R. solanacearum* GMI1000 at a concentration of  $10^5$  CFU ml<sup>-1</sup> was injected directly into the xylem vasculature of the first internode through the petiole. Representative images**

of *R. solanacearum* colonization progress at the point of inoculation are shown. **(B)** Mean green fluorescence of the GFP signal emitted from *R. solanacearum* at cross-sections obtained as described in (a) at the point of inoculation (0), below the point of inoculation (-0.5 cm) and above the point of inoculation (+0.5 cm) was measured using ImageJ. Data from a representative experiment out of a total of 3, with  $n=5$  plants per condition. No significant differences were observed between Wt and the *FHT* overexpressing lines.

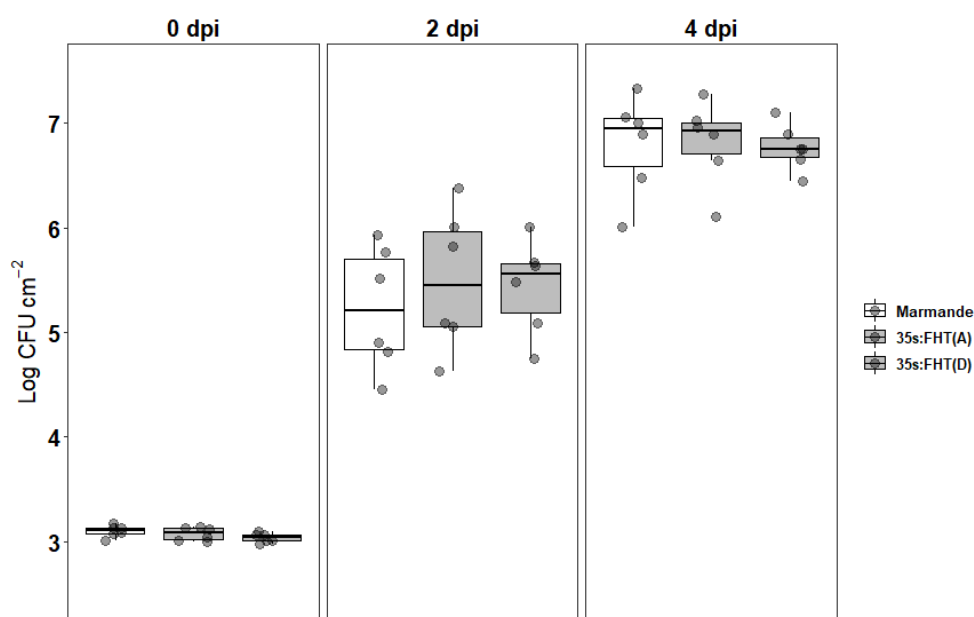


**Figure 23: Growth of *R. solanacearum* GMI1000 in planta was monitored in leaves of 35S::*FHT* transgenic lines compared with Wt Marmande tomato lines over time.** The bacterium was vacuum infiltrated into the leaves at a concentration of  $\sim 1 \times 10^5$  CFU/ml and growth was recorded at 0, 2 and 4 dpi. Box-and-whisker plots show data of 6 independent plants ( $n=6$ ) from a representative experiment out of 3. No significant differences were observed between Wt and the *FHT* overexpressing lines.

### 4.3 Overexpression of *THT* in a susceptible tomato cultivar confers resistance to *R. solanacearum*

HCAA are soluble phenolics which accumulate during several stress response including pathogen attack and may act as a phytoalexin (Campos *et al.*, 2014). HCAA such as feruloyl tyramine has been associated with the suberin poly-aromatic domain (Bernards *et al.*, 1995; Negrel *et al.*, 1996). Accumulation of such soluble aminated phenolics may act as a chemical barrier initially acting as phytoalexin but could also act as physical barrier if cross-linked to the lignin-like poly-aromatic domain of suberin. *THT* gene family members encode for acetyltransferases which regulate HCAA synthesis. Our data show that *THT* gene is induced by *R. solanacearum* infection. Also, 2D-NMR showed specific accumulation of feruloyl amides in lignin and suberin wall fraction of resistant H7996 roots. Hence, we undertook a variety of *R. solanacearum* infection assays in a transgenic tomato line stably expressing 35S::*SlTHT1-3* on a susceptible tomato background.

Tomato overexpressing *SlTHT1-3* was readily available on a susceptible Moneymaker background (Campos *et al.*, 2014). *R. solanacearum* disease progression in Moneymaker tomato was similar to Marmande, causing severe wilting (Fig. 24A, B and Chapter 1 Fig. 2A). Overexpression of *SlTHT1-3* resulted in an increase of resistance against *R. solanacearum*, with disease progressing remarkably slower in this line compared to Wt (Fig. 24A, B). Importantly, bacterial loads were significantly lower in the taproot and hypocotyl of the *SlTHT1-3* overexpressor after soil inoculation in comparison to Wt tomato (Fig. 24C). Also, leaf *in planta* multiplication assay after vacuum infiltration of *R. solanacearum* showed severe restriction in multiplication of *R. solanacearum* in 35S::*SlTHT1-3* overexpression line, compared to Wt Moneymaker tomato (Fig 24D).



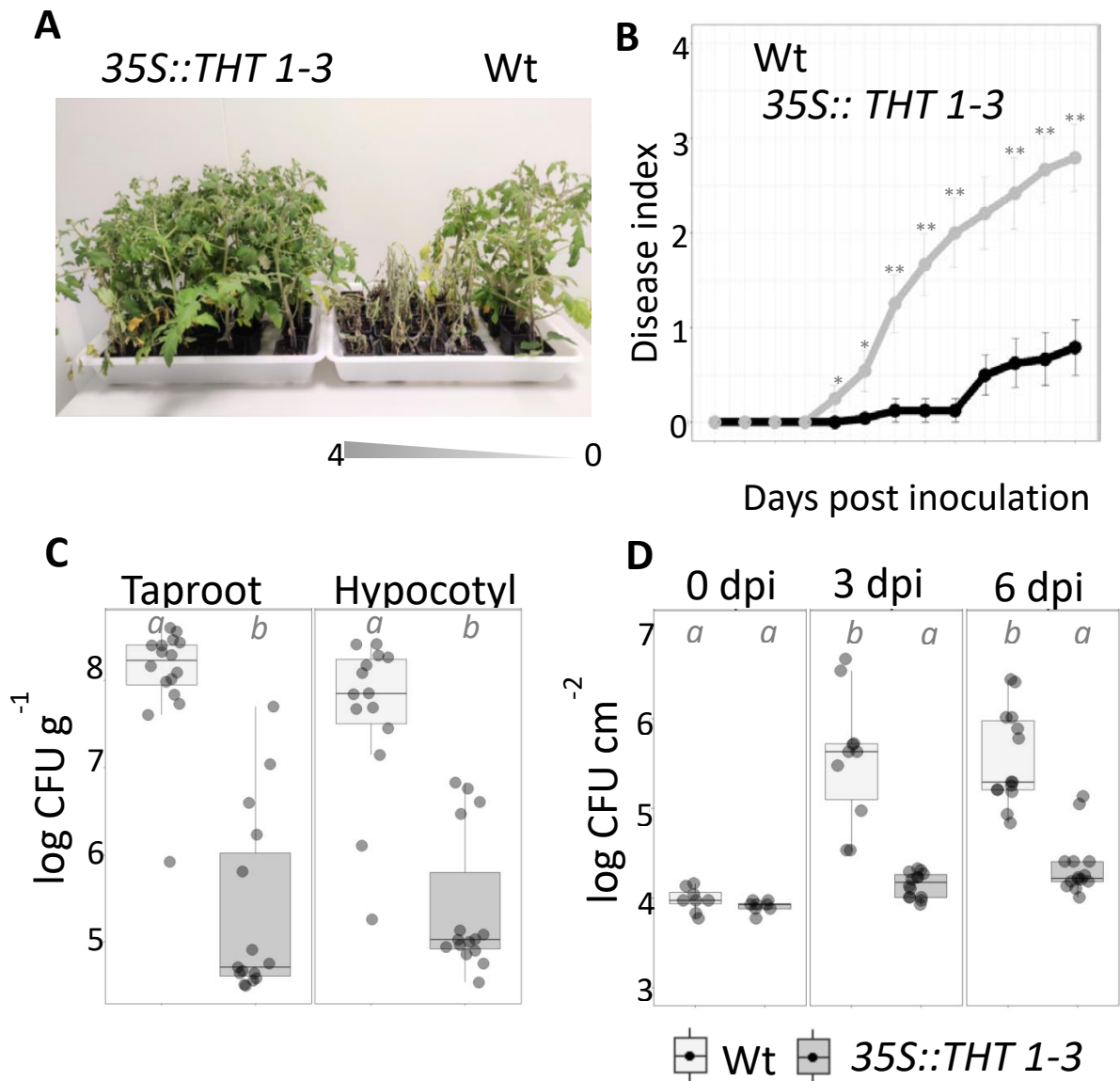


**Figure 24: Overexpression of *THT1-3* in susceptible tomato confers resistance to *R. solanacearum*.** (A, B) A pathogenicity assay was performed comparing Wt and *35S::THT1-3* tomato lines (MoneyMaker background) after infection with *R. solanacearum* lux reporter strain of GMI1000. Five-week-old plants were soil-soak inoculated with  $\sim 1 \times 10^7$  CFU/ml and grown at 28°C. (A) Pictures were taken 12 days post-infection. Wt plants were arranged according to the degree of symptom severity (from 4 to 0). (B) Wilting progress was monitored by rating plants daily on a 0 to 4 disease index scale where 0 = healthy and 4 = 100% wilted. Plotted values correspond to means  $\pm$  standard error of 24 independent plants (n=24) from a representative experiment out of a total of 3. Asterisks indicate statistically significant differences between Wt and *35S::THT1-3* using a paired Student's t-test (\*  $p < 0.05$ , \*\*  $p < 0.01$  and \*\*\*  $p < 0.001$ ). (C) Transgenic *35S::THT1-3* tomato significantly restricted *R. solanacearum* colonization in both the taproot and hypocotyl compared to Wt. Five-week-old tomato plants were root-inoculated with a *R. solanacearum* GMI1000 luciferase reporter strain at a concentration of  $\sim 1 \times 10^7$  CFU/ml or water mock. The level of in planta colonization by *R. solanacearum* was calculated as colony forming units per gram of fresh taproot or

hypocotyl tissue (CFU·g<sup>-1</sup>) at 12dpi. Box-and-whisker plots show data from a single representative experiment out of 3 (n =14 to 16). **(D)** Growth of *R. solanacearum* GMI1000 in planta was monitored in leaves of *35S::THT1-3* transgenics compared with Wt Moneymaker tomato lines over time. The bacterium was vacuum infiltrated into the leaves at a concentration of  $\sim 1 \times 10^5$  CFU/ml and growth was recorded at 0, 3 and 6 dpi. Box-and-whisker plots show data of 6 to 8 independent plants (n=6-8) from a representative experiment out of 3. Asterisk indicates statistically significant difference between WT and overexpression line in a paired Student's t-test (\* corresponds to p-value of  $p < 0.05$ ).

Similarly, petiole inoculation also showed severe bacterial growth restriction in the stem of the *THT1-3* overexpressing line (Fig. 25). We monitored the colonization patterns of a *R. solanacearum* GFP reporter strain after petiole inoculation of the *SlTHT1-3* overexpressing line compared to Wt (Planas-Marquès *et al.*, 2019) (Fig. 25). Colonization progress was tracked at 6 dpi in transverse stem cross-sections made at the point of inoculation as well as cross-sections made at 0.5, -1, -2 and -3 cm both upwards and downwards of the inoculation point. Bacteria spread unrestrictedly in susceptible wild type plants (Fig. 25A), whereas they stayed confined near the inoculation point in the *35s::SlTHT1-3* line (Fig. 25A). Quantification of the GFP signal showed that the bacterial inoculum was drastically reduced in *SlTHT1-3* overexpressing plants in comparison to Wt (Fig. 25B).

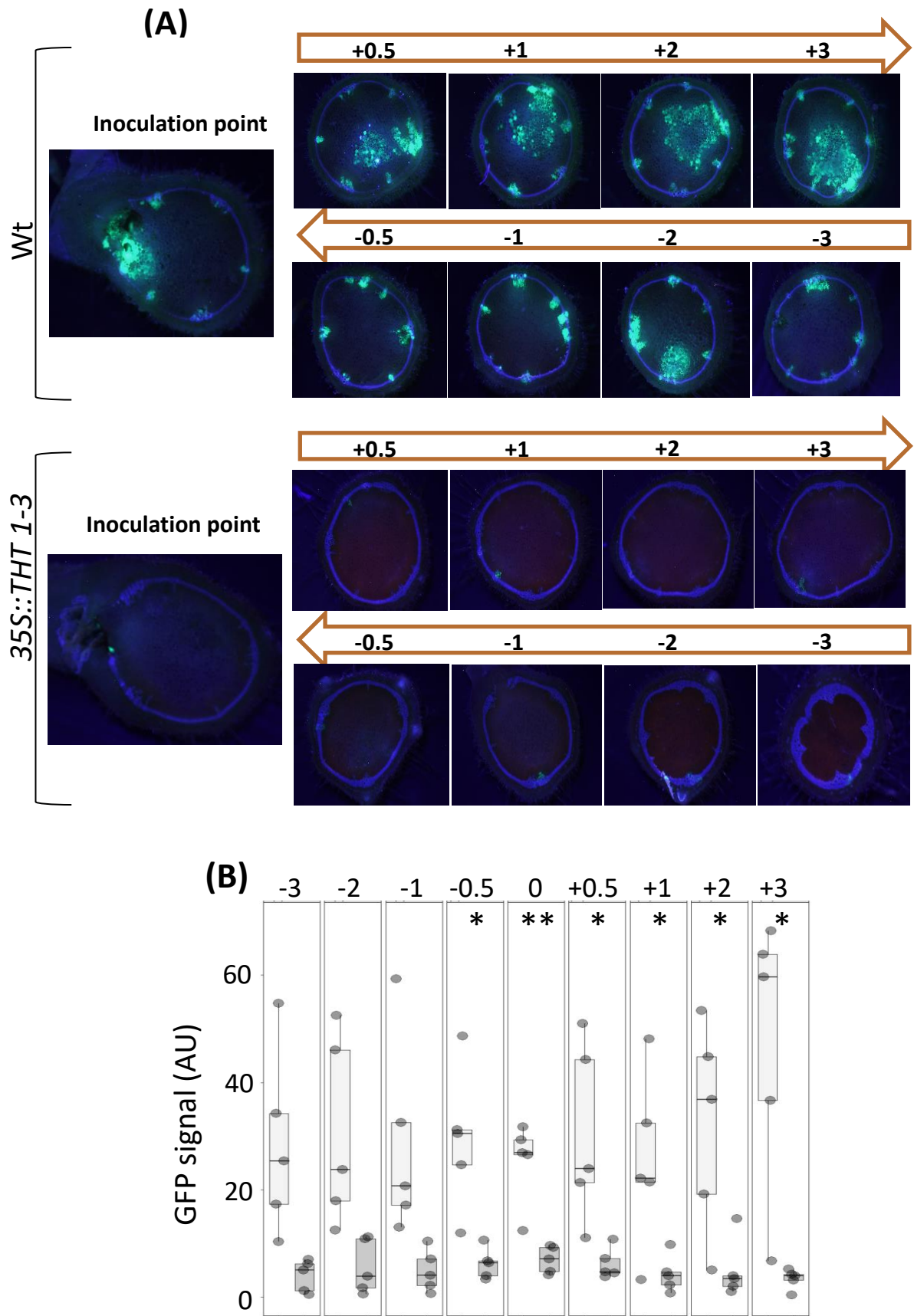


**Figure 25: Overexpression of *SITH1-3* in tomato results in restricted colonization by *R. solanacearum*.**

(A) Transverse cross-sections of Wt and transgenic 35S::THT1-3 tomato lines were imaged under UV

stereoscopic microscope 6 dpi after infection with a *R. solanacearum* GFP reporter strain. *R. solanacearum* was directly injected into the xylem vasculature of the first internode thorough the petiole at a concentration of  $10^5$  CFU ml<sup>-1</sup>. Colonization progress was analyzed at the point of inoculation, at higher (+0.5, +1, +2 and +3 cm) and lower -0.5, -1, -2 and -3 cm) sections. Images from a representative experiment out of 3 with  $n=5$  plants each. Scale bar = 2 mm. (B) Mean green fluorescence of the GFP signal emitted from *R. solanacearum* at cross-sections obtained as described in (A) at the point of inoculation (0), below the point of inoculation (-0.5, -1, -2 and -3 cm) and above the point of inoculation (+0.5, +1, +2 and +3 cm) was measured using ImageJ. Data from a representative experiment out of a total of 3, with  $n=5$  plants per condition. Asterisks indicate statistically significant differences between wild type and *35S::THT1-3* tomato plants in a paired Student's t-test (\* corresponds to a p-value of  $p < 0.05$ , \*\* to  $p < 0.01$  and \*\*\* to  $p < 0.001$ ). Scale bar = 2 mm.

However, this genetic intervention leading to resistance may be mainly because of accumulation of HCAA acting as chemical barrier, since in overexpression line wall reinforcement with phenolics and ferulates was not detectable in microscopic studies (Fig. 26).

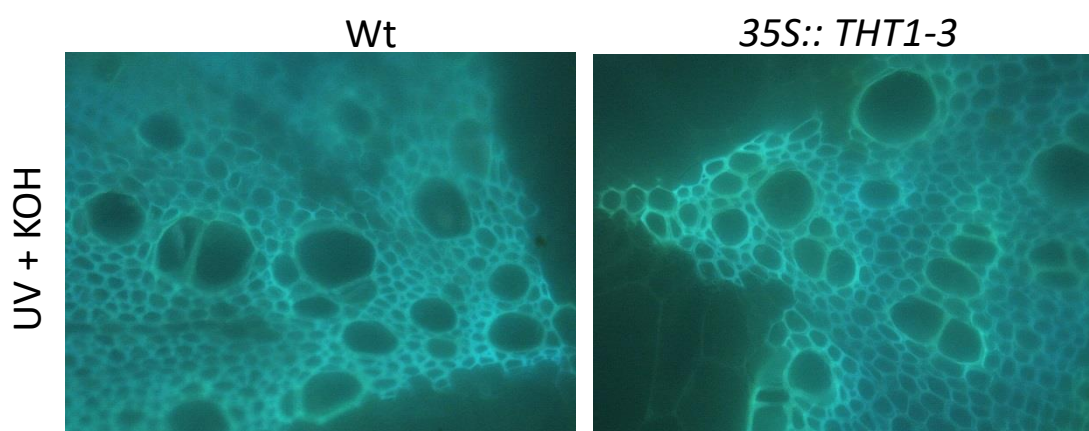


**Figure 26: *35S::THT1-3* line did not show enhanced ferulate or phenolic deposition in walls compared to WT.** Taproot cross-sections containing  $10^5$  CFU g<sup>-1</sup> of *R. solanacearum* in WT and *35S::THT1-3* line were treated with 1N KOH alkali (pH above 10) and observed under UV to detect green ferulate depositions or auto-fluorescence from phenolics .

## **DISCUSSION**

## 5. Discussion

### 5.1 Thesis overview

In this thesis we attempted to shed light on the defense responses in the roots against the soil borne vascular pathogen *R. solanacearum*. The bacterium invades through plant roots and advances inter- or intracellularly through the root cortex to reach the xylem, where it proliferates and spreads systemically to aerial plant parts. However, plants have evolved mechanisms in the roots to sense invading pathogens and mount a defense response against these aggressors (French *et al.*, 2018). During pathogen progression through the root cortex and into the vasculature and also horizontal colonization within the vasculature, the cell wall stands as the first barrier of defense against *R. solanacearum* (Lowe-Power *et al.*, 2018). *R. solanacearum* induced reinforcements in secondary cell wall of vascular tissue act as a potent barrier against colonization of the bacterium (Ferreira *et al.*, 2017). Timely formation of these physico-chemical vascular barriers upon pathogen perception can lead to confinement of the vascular pathogen at the infected vessel, avoiding the spread of wilt pathogens (Robb *et al.*, 2008; Zaini *et al.*, 2018; Planas-Marquès *et al.*, 2019). The integrity of the cell wall is maintained by a complex set of sensors located at the plasma membrane that controls changes in the wall's physico-chemical properties (Bacete *et al.*, 2018). In case of leaf pathogens cell wall reinforcements are a well-known response of pathogen-triggered immunity (PTI) and effector-triggered immunity (ETI) (Lee *et al.*, 2019). PTI is known to be activated on recognition of conserved pathogen-associated molecular patterns (PAMPs) by host pattern recognition receptors (PRRs), whereas ETI is activated by recognition of pathogen-secreted effectors via intracellular nucleotide-binding leucine-rich repeat proteins (NLRs) (Jones & Dangl, 2006). Besides, cell wall reinforcements occurs on recognition of endogenous elicitors called danger associated molecular patterns (DAMPs) such as host cell wall fragments viz. oligogalacturonides formed due to action of pathogen enzymes, leading to PTI (Boller & Felix, 2009; Luna *et al.*, 2011; Gupta *et al.*, 2013; Malinovsky *et al.*, 2014). Recent study shows that root defense responses are different from aerial parts in the sense that, it is relatively insensitive to most conserved molecular patterns, which may prevent mounting defense responses against commensal organisms in an environment such as the soil, full of microbes. Underlying this phenomenon, it has been recently shown that root PTI is only activated upon local tissue damage (Zhou *et al.*, 2020). Hence, a localized cell death upregulates



PRR expression in the neighboring cells, leading to restricted responsiveness to conserved molecular patterns of root invaders (Zhou *et al.*, 2020). Besides, root endodermis and casparian strip have precise signalling mechanisms to sense the integrity of this diffusion barrier, which controls the uptake of water and molecules from the soil into the water-conducting tissues, and prevents the entry of pathogens and other harmful substances. Casparian strip possesses a barrier surveillance pathway comprised of the receptor-like cytoplasmic kinase and leucine rich repeat-receptor-like kinase which interact with peptides expressed in the stele, leading to barrier formation (Alassimone *et al.*, 2016; Fujita *et al.*, 2020). This spatial separation of receptor and ligand constitutes a surveillance system where interaction stops after effective sealing by the strip, but any breach in the barrier leads to re-interaction and further strengthening of walls with lignin and suberin (Doblas *et al.*, 2017). Recent studies also show that the endodermis acts as a regulatory hub coordinating microbiota assembly and homeostatic mechanisms. Regulatory network controlling the endodermal root diffusion barriers influences the composition of the plant microbiota. Also, the composition of plant microbiome influences the development of endodermal diffusion barriers, especially suberin deposition, with consequences for the plant's ionome and abiotic stress tolerance (Salas-González *et al.*, 2021).

Inducible structural barriers formed at and around the root vasculature upon colonization constitute one of the most important defense components against *R. solanacearum* (Ishihara *et al.*, 2012). Plants have evolved effective structural defense mechanisms which include reinforcement of secondary cell walls to prevent vessel colonization or movement between vessels once vascular colonization has occurred. These root defenses against *R. solanacearum* have been identified in tomato resistant germplasms, which are used as rootstocks for grafting commercially important varieties (Caldwell *et al.*, 2017). However, the interaction and the type of barriers formed are not well understood. Hence, in this thesis we attempted to characterize these vascular reinforcements, in order to deploy these traits of interest for crop resistance.

The findings of this study underscore the formation suberin and the associated phenolics as a key defense response in root xylem vasculature of resistant tomato H7996 against *R.*

*solanacearum*. Several key results support this view including: (i) histological studies showing deposition of phenolic deposits in walls of vessels and the surrounding parenchyma cells of resistant H7996 after infection, but not in susceptible Marmande. These phenolic deposits at walls of vessel and surrounding parenchyma cells bind to Sudan IV but not to Phlorogucinol HCl indicating the presence of suberin in such deposits; (ii) intense accumulation of ferulates specifically at the xylem vasculature of resistant tomato H7996 upon *R. solanacearum* infection, which is one of the hallmarks of suberizing tissues; (iii) 2D NMR showing enrichment in poly-aliphatic structures characteristic of suberin, specifically in resistant H7996 root after *R. solanacearum* infection; (iv) upregulation of genes of suberin pathway in root xylem vasculature, specifically in resistant H7996.

## **5.2 *R. solanacearum* triggers a phenolic wall reinforcement at root xylem vasculature of resistant H7996**

Root xylem vasculature is one of the first sites of multiplication of *R. solanacearum* inside the host (Vasse *et al.*, 1995; Álvarez *et al.*, 2010; Digonnet *et al.*, 2012). Colonization of the xylem vasculature is critical as in this particular tissue the pathogen multiplies and moves vertically to the stem with xylem fluid. Also, the pathogen moves horizontally from colonized vessel to healthy vessel and surrounding parenchyma cells and apoplast (Nakaho *et al.*, 2000). To facilitate this process *R. solanacearum* secretes an array of cell wall degrading enzymes (Liu *et al.*, 2005; Pérez-Donoso *et al.*, 2010; Lowe-Power *et al.*, 2018). However, cell wall also acts as a dynamic barrier in resistant plants, acting as first line of defense against pathogens (Underwood, 2012). Quantitatively resistant tomato cultivars have been known to deposit electron dense compounds in pit membranes and vessel walls as defense response to *R. solanacearum* (Nakaho *et al.*, 2000; Kim *et al.*, 2016). In our study, resistant H7996 was observed to react aggressively to *R. solanacearum* infection by reinforcing the walls of vessels and the surrounding parenchyma cells with phenolic deposits. This vascular coating with wall bound phenolic compounds may restrict horizontal spread of the bacterium and H7996 recognize and induce such response at early stage of bacterial colonization (starting at  $\sim 10^5$  CFU g<sup>-1</sup> taproot tissue) and before the plant showing any visible wilting symptom (Chapter 1 Fig. 4, 6). These phenolic reinforcements in xylem vasculature may act as a shield against pathogen-derived

metabolites such as toxins and enzymes, and make water and nutrients inaccessible for pathogens, thereby impeding their growth (Araujo *et al.*, 2014).

In comparison to resistant H7996, susceptible Marmande is either not able to induce such vascular coating or induce a very weak and late response during infection of *R. solanacearum*, making its vascular walls prone to disruption by the pathogen's cell wall degrading enzymes. In absence of any reinforcements, the bacterium multiplies and colonizes abundantly moving out from vessel lumen into surrounding parenchyma cells and apoplastic spaces. At late stages of colonization, xylem vasculature of Marmande was observed to be highly degraded which was evident from reduced lignin staining (Chapter 1 Fig. 5). It is not known whether *R. solanacearum* can directly target lignin by enzymatic degradation. However, lignin polymer is deposited in spaces between cellulose, hemicellulose and pectin. *R. solanacearum* has several cell-wall-modifying proteins such as cellulases, expansin and pectinases which possibly disintegrate the cell wall matrix (Liu *et al.*, 2005; Pérez-Donoso *et al.*, 2010; Lowe-Power *et al.*, 2018; Kang *et al.*, 2019). Interestingly, 2D-NMR showed significant differences in the polymerization state of lignin between resistant and susceptible tomato cultivars after infection. Infected H7996 roots showed higher branching and cross-linking of lignin polymer compared to susceptible Marmande, thereby reducing the accessibility of the pathogen's hydrolytic enzymes.

### **5.3 A suberization zone at xylem vasculature acts as a physico-chemical barrier against *R. solanacearum* colonization**

Some models of suberin describe it to be heteropolymer comprising of a poly-phenolic and poly-aliphatic domain (Bernards, 2002; Lashbrooke *et al.*, 2016; Cohen *et al.*, 2020). However, some studies describe the poly-phenolic domain to be lignin-like (Serra *et al.*, 2010a). But, the exact structure and composition of the suberin-associated poly-phenolic domain is elusive. This phenolic domain is reported in several studies to be enriched in ferulic acid (Bernards & Lewis, 1992; Bernards *et al.*, 1995; Graça, 2010, 2015; Cohen *et al.*, 2020). The polymer is deposited in walls of specialized tissues such as epidermis, endodermis, seed coat and potato tuber periderm. Besides, it is deposited *de novo* upon stress responses such as wounding, salt injury and pathogen attack (Dixon & Paiva, 1995). A classical model for suberin studies has been the potato tuber periderm where suberin is

deposited under normal course of maturation as well as in response to wounding (Serra *et al.*, 2010b; Boher *et al.*, 2013). Recently, with the advent of genetic tools in *Arabidopsis* a number of studies on suberin deposition at the endodermis/ casparian strip have been carried out in this model species (Molina *et al.*, 2009; Cohen *et al.*, 2020; Salas-González *et al.*, 2021). However, when it comes to suberin deposition as defense response to pathogens, our knowledge on the mechanism is extremely limited. Suberin acts as potent barrier against pathogens as in addition to providing strength to the cell wall it may also act as an antimicrobial barrier (Vishwanath *et al.*, 2013). Recent study shows that microbiota inhabiting the roots influence suberin deposition at the endodermis (Salas-González *et al.*, 2021).

Our data provide evidences of suberin to be a major component of vascular coating of resistant H7996 and highlight some important facets of vascular suberization as a defense response to *R. solanacearum*. The strong UV auto-florescence emitted from xylem vessel walls and the surrounding parenchyma cells observed in resistant H7996 against *R. solanacearum* could not be quenched by Phloroquinol HCl, suggesting suberin deposits in observed vascular coatings (Chapter 1, Fig. 6) (Pouzoulet *et al.*, 2013). Further, the walls of vessel and surrounding parenchyma cells bind with Sudan IV suggesting the presence of the aliphatic domain of suberin (Chapter 1, Fig. 10). In the periphery of the aliphatic binding layers of xylem vessels and parenchyma cells we could observe cells with intense accumulation of phenolics as wall reinforcements, where Sudan IV does not bind. These peripheral phenolic reinforcements were identified as ferulates, through a microscopic technique used in monocots and conifers to study cell wall phenolics. Ferulic acid ester-linked to cell wall polysaccharides occur constitutively in the primary cell walls of many families of monocotyledons and conifers (Carnachan & Harris, 2000; Harris & Trethewey, 2010). These wall bound ferulates can be detected by emission of blue fluorescence with UV excitation at neutral pH that characteristically changes to a stronger green emission under conditions of high pH such as in the presence of alkali (Carnachan & Harris, 2000; Harris & Trethewey, 2010; Donaldson & Williams, 2018). The UV autofluorescence from the phenolic deposits at xylem vasculature of resistant H7996 showed a strong blue green colour conversion upon alkali treatment, indicating the deposition of ferulates as defense response to *R. solanacearum* (Chapter 1, Fig. 9).

## DISCUSSION

---

Interestingly, ferulates are a major component of suberin poly-phenolic domain (Negrel *et al.*, 1995; Graça, 2010; Cohen *et al.*, 2020). From the studies done in wound healing potato tubers it is known that in suberizing tissues, poly-phenolic domain comprising mainly ferulates are the first to accumulate (Bernards & Lewis, 1992; Negrel *et al.*, 1995). Feruloyl amides as well as esters are the compounds which accumulate at early stage of suberization and later other aliphatic compounds of suberin are deposited to form the mature suberin matrix (Bernards & Lewis, 1992; Negrel *et al.*, 1995; Serra *et al.*, 2010b). The early accumulation of ferulate is a critical aspect for the coupling of the aromatic and aliphatic suberin domains, considering that ferulates are able to form covalent bonds with cell wall polysaccharides and polyphenolics while leaving the aliphatic chain ready for esterification (Boher *et al.*, 2013). In support of this view, a recent study shows that transient overexpression in *Nicotiana benthamiana* leaves of an Arabidopsis MYB transcription factor SUBERMAN controlling endodermal suberization in roots, resulted in 668-fold increase of ferulates in the leaves in addition to formation of suberin lamella and upregulation of suberin pathway genes (Cohen *et al.*, 2020).

Based on the above observations, we propose a suberization model of resistant H7996 vasculature against *R. solanacearum* (Fig. 1). The pathogen on reaching the xylem vessel of resistant H7996, multiplies and tries to invade the surrounding healthy vessels and parenchyma cells by degradation of pit membranes and walls. However, this damage in colonized vessel by *R. solanacearum* in resistant H7996, leads to suberization of walls of vessel, and parenchyma cells present in the immediate vicinity of colonized vessels. While the walls of peripheral parenchyma cells, vessels and tracheids undergo feruloylation, a stage preceding suberization, where ferulate derivatives such as amides and esters as well as other hydroxycinnamates are deposited to form polyphenolic domain of suberin. Suberized and feruloylated layers of parenchyma cells, vessels and tracheids together form a “zone of suberization” creating a strong physico-chemical barrier to limit *R. solanacearum* spread from colonized xylem vessel lumen.

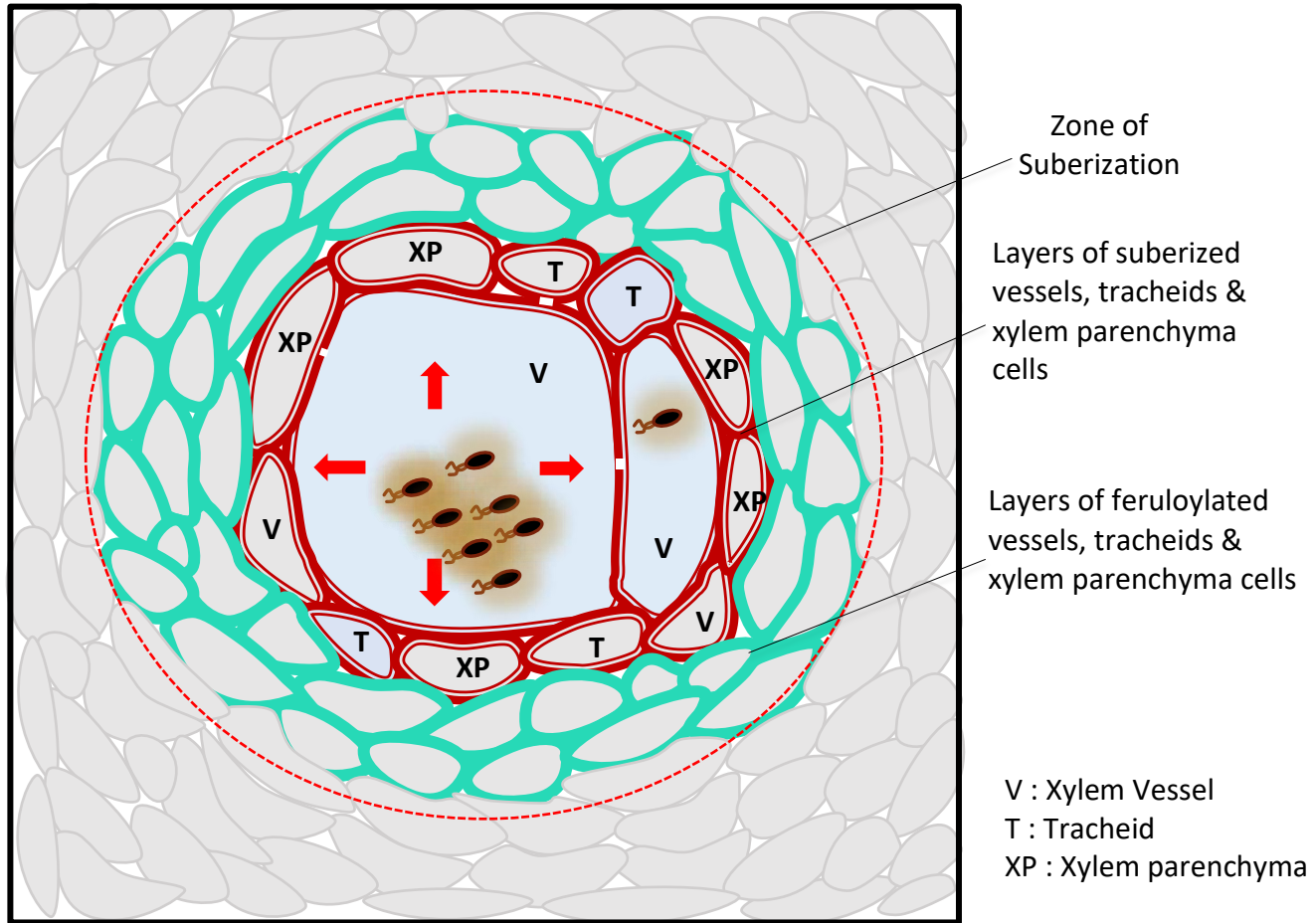


**Figure 1: Schematic representation of the vascular suberization process potentially taking place in infected vessels of resistant H7996 tomato upon *R. solanacearum* infection.** Colonization of the vasculature by *R. solanacearum* in resistant tomato plants induces a suberization-like process in the walls of the infected vessel and of the adjacent tracheids and parenchyma cells (red). In parallel, cell walls of peripheral parenchyma cells, vessels and tracheids undergo feruloylation, a stage preceding suberization, whereby ferulate derivatives such as amides and esters are deposited to form the polyphenolic domain of suberin (green). Suberized and feruloylated layers of parenchyma cells, vessels and tracheids together form a “zone of suberization” (red dashed line) creating a physico-chemical barrier to limit *R. solanacearum* spread from the colonized xylem vessel lumen.



ETI and PTI are two layers of immunity which operate synergistically, converging on several downstream responses including the cell death, oxidative burst, activation of kinase signaling cascades, expression of defense-related genes, accumulation of physico-chemical barriers and wall reinforcements (Thomma *et al.*, 2011; Ngou *et al.*, 2021; Yuan *et al.*, 2021). Although the molecular triggers for pathogen-induced suberization is unknown, it is likely that suberin deposition in resistant H7996 vasculature could be an outcome of pathogen recognition event. In *Arabidopsis* leaves, strong lignin deposition is known as a downstream response of ETI caused by an avirulent strain of *Pseudomonas. syringae* pv. *tomato*. It was shown that infection with either virulent or avirulent strains of the pathogen induced localized lignification at the site of pathogen attack. However, lignin deposition was more conspicuous upon avirulent pathogen recognition, leading to confinement of the pathogen, and restricting hypersensitive response cell death to the infection site. In contrast, virulent strains could overcome induced lignification, as the deposition in this case was milder, leading to unrestricted disease progression (Lee *et al.*, 2019). Further, vascular hypersensitive response in xylem parenchyma and pith cells surrounding xylem vessels have been reported in quantitative resistant tomato against *R. solanacearum* (Nakaho *et al.*, 2017). Such recognition may be facilitated in root vasculature by localized cell damage by *R. solanacearum*. Recent studies show roots to require a localized cell damage component to mount a PRR expression in the neighboring cells, leading to restricted responsiveness to root invaders, while co-existing with the millions of commensal microbes in the rhizosphere (Zhou *et al.*, 2020).

### **5.4 *R. solanacearum* infection induces a metabolic and genetic reprogramming towards vascular suberization in resistant H7996**

Tissues undergoing suberization, has to go through a complex genetic and metabolic reprogramming involving a network of metabolic pathways, in order to produce the precursors of the polymer and subsequently their polymerization into the matrix (Lashbrooke *et al.*, 2016). Precursors of phenolic domain come from the phenylpropanoid pathway while the aliphatic domain is synthesized by suberin fatty acid pathway enzymes (Vishwanath *et al.*, 2015). Aliphatic domain comprise of a glycerol-based fatty acid-derived polyester comprised primarily of  $\omega$ -hydroxyacids,  $\alpha$ ,  $\omega$ -dicarboxylic acids, fatty alcohols (Höfer *et al.*, 2008). The most abundant component of suberin aromatic domain is

feruloyl-CoA (Graça, 2010; Cohen *et al.*, 2020). After being synthesized through phenylpropanoid pathway, feruloyl-CoA acts as a substrate of acyltransferase feruloyl transferase (FHT) which catalyzes the conjugation of feruloyl-CoA to aliphatic chains such as  $\omega$ -hydroxyacids and primary alcohols to form feruloyl esters (Molina *et al.*, 2009; Serra *et al.*, 2010b; Boher *et al.*, 2013).

2D-NMR showed strong accumulation of suberin compatible metabolites specifically in roots of resistant H7996, upon infection of *R. solanacearum* (Chapter 2, Fig.1). As a defense response, resistant H7996 showed strong enrichment in poly-aliphatic structures characteristic of suberins. Also, olefinic cross-signal of unsaturated fatty acid structures was obtained, which is typical of suberin. Interestingly, correlation signals compatible with feruloylamides and with tyramide-related structures were obtained specifically in roots of resistant H7996 upon infection of *R. solanacearum*. In contrast the roots of susceptible Marmande did not display notable variations between mock-treated and infected plants in the signals corresponding to suberin. Further, FTIR showed significantly high induction of phenolics in the xylem vasculature of resistant H7996. Hence, these results corroborated the findings obtained in histopathological assays.

We further analyzed whether these metabolic changes that take place in xylem vasculature of resistant H7996 as defense response to *R. solanacearum*, correlate with the gene expression of suberin pathway genes. Quantitative PCR of samples obtained from taproot xylem vasculature showed up-regulation of tomato putative orthologs of suberin fatty acid pathway genes namely, cytochrome P450 fatty acid  $\omega$ -hydroxylases (*SlCYP86A1*; Solyc06g076800 and *SlCYP86B1*; Solyc02g014730), fatty acyl-CoA reductase 3 (*SlFAR3*; Solyc02g014730), 3-ketoacyl-CoA synthase 1 (*SlKCS1*; Solyc10g009240), 3-ketoacyl-CoA synthase 2 (*SlKCS2/SIDAI5Y*; Solyc05g009280), glycerol-3-phosphate acyltransferase 5 (*SlGPAT5*; Solyc04g011600), specifically in resistant H7996. These genes are responsible for synthesis of the aliphatic precursors of suberin lamella. Also, expression of *SlFHT* (*Solyc03g097500*) was found to be up-regulated specifically in resistant H7996, which links feruloyl-CoA with aliphatics (Chapter 3, Fig. 16). Further, assays with *ProSlFHT::GUS* H7996 transgenic lines showed that only in *R. solanacearum*

infected plants, the induction of the promoter could be observed in xylem vasculature, but not in mock plants. Besides, induction of the promoter could be observed in the tissues known to deposit suberin such as epidermis, endodermis and in tissues wounded mechanically. The transcripts of phenylpropanoid pathway genes were found in abundance in both cultivars under basal state, as xylem vasculature is a well lignified tissue. But, most of them show a slight up-regulation upon infection in resistant H7996, but down-regulation in Marmande. Transcriptome of suberizing tissues of several species such as tomato (Lashbrooke *et al.*, 2016), melon (Cohen *et al.*, 2019) and apple (Legay *et al.*, 2015; Lashbrooke *et al.*, 2016) showed massive up-regulation of most suberin fatty acid biosynthesis pathway genes as well as some phenylpropanoid pathway genes. Further, in agreement with the 2D NMR signals showing accumulation of feruloyl amides in resistant H7996 after infection, the gene *S1THT1-3* (*Solyc08g068730*) responsible for their synthesis of HCAA is significantly up-regulated in infected H7996 plants.

### **5.5 *FHT* overexpression in susceptible tomato had a minor effect on *R. solanacearum* colonization**

Considering the accumulation of suberin ferulate at early stage of *R. solanacearum* colonization in resistant H7996, we sought to understand the implications of overexpression of *FHT* gene in susceptible tomato cultivars, on defense against *R. solanacearum*. Previous studies have reported that overexpression of *Populus trichocarpa FHT* gene in Arabidopsis resulted in increased tolerance to salt stress (Cheng *et al.*, 2013). Hence, we undertook a variety of *R. solanacearum* infection assays in a transgenic tomato lines stably expressing *35S::SlFHT* on a susceptible tomato background. Interestingly, *FHT* overexpression did not have a large effect on the responses of susceptible tomato against *R. solanacearum*. *SlFHT* overexpressing lines showed only a slight delay in wilting symptoms together with a slight decrease of bacterial loads in the plant. This result may be due to the fact that in Marmande the low levels of aliphatic precursors constitute a bottleneck for suberin biosynthesis. In resistant H7996 tomato, *FHT* was highly induced at and around the vasculature upon *R. solanacearum* expression, but it was accompanied by a strong upregulation in fatty acid biosynthesis genes, which provide the aliphatic precursors to the *FHT* enzyme in order to form suberin. In Marmande *FHT* overexpressing plants,

increasing the levels of the enzyme may not have a strong impact due to a lack of aliphatic precursors, which prevent an increase of suberin formation.

### **5.6 *THT 1-3* overexpression in susceptible tomato background offers high degree of colonization restriction to *R. solanacearum***

HCAA are soluble phenolics which accumulate during several stress response including pathogen attack (Campos *et al.*, 2014). Also, HCAA such as feruloyl tyramine has been associated with the suberin poly-aromatic domain (Bernards *et al.*, 1995; Negrel *et al.*, 1996). Accumulation of such soluble aminated phenolics may act as a chemical barrier initially acting as phytoalexin but could also act as physical barrier if cross-linked to the lignin-like poly-aromatic domain of suberin. THT gene family members encode for acetyltransferases which regulate HCAA synthesis. Our data show that THT gene is induced by *R. solanacearum* infection. Also, 2D-NMR showed specific accumulation of feruloyl amides in lignin and suberin wall fraction of resistant H7996 roots. Hence, we undertook *R. solanacearum* infection assays in a *35s::SITHT 1-3* overexpression line in susceptible Moneymaker tomato background. *35s::SITHT 1-3* plants showed elevated amounts of HCAA such as feruloyl tyramine upon infection of *P. syringae* pv. *tomato* (Campos *et al.*, 2014). Soil drench inoculation of *R. solanacearum* resulted in drastically reduced wilting of *35s::SITHT 1-3* overexpression plants, in comparison to Moneymaker wild type plants. Further, the bacterial load in taproot and hypocotyl of *35s::SITHT 1-3* plants was significantly lower than the wild type plants, indicating restricted colonization of *R. solanacearum* in *35s::SITHT 1-3* overexpression plants. Leaf *in planta* multiplication also showed severe limitation of *R. solanacearum* multiplication in *35s::SITHT 1-3* plants. Further, live imaging of GFP fluorescent reporter strain of *R. solanacearum* inoculated through the petiole, showed high degree of colonization restriction in *35s::SITHT 1-3* plants, whereas the wild type plants showed abundant multiplication. However, this genetic intervention leading to resistance may be mainly because of accumulation of HCAA acting as chemical barrier, as in overexpression line a wall reinforcement with phenolics and ferulates was not observed in microscopic studies. In fact, feruloyl tyramine is known to exhibit antimicrobial activity against plant pathogens (Fattorusso *et al.*, 1999; Novo *et al.*, 2017).

## **CONCLUSIONS**

### 6. Conclusions

From the main goals of this work, we extract the following conclusions:

1. Xylem vascular tissue of resistant H7996 mounts a defense response to *R. solanacearum* leading to reinforcement of the walls of xylem vascular tissue with cell wall bound phenolic materials formed *de novo* upon infection, which severely impairs the movement of the bacterium from colonized vessel to the surrounding vessels and parenchyma cells.
2. Specific deposition of ferulates in the vessel walls and surrounding parenchyma cells and tracheids could be observed in H7996 after *R. solanacearum* infection which could act as a physico-chemical barrier against the bacterium, either by preventing the enzymatic degradation of the cell wall, by directly inhibiting the growth of pathogen, or both. This barrier would also prevent the spread of the bacterium from the colonized vessel.
3. Ferulates constitute a crucial component of the suberin polyphenolic domain, potentially acting as nucleating site for suberin matrix polymerization. Colonization of the vasculature by *R. solanacearum* in resistant tomato plants induces a suberization-like process in the walls of the infected vessel and of the adjacent tracheids and parenchyma cells. In parallel, cell walls of peripheral parenchyma cells, vessels and tracheids undergo feruloylation, a stage preceding suberization, whereby ferulate derivatives such as amides and esters are deposited to form the lignin-like polyphenolic domain of suberin. Suberized and feruloylated layers of parenchyma cells, vessels and tracheids together may form a “zone of suberization” potentially creating a physico-chemical barrier to limit *R. solanacearum* spread from colonized xylem vessel lumen.
4. Abundant tyloses could be observed in taproot of resistant H7996 vasculature. In resistant tomato these structures may play a role in restricting the vertical movement of the bacterium within the vessels. Enhanced deposition of calcium on the plasma membrane of tyloses and vessel walls was observed by SEM-



## CONCLUSIONS

---

- EDX and may have a role in defense against *R. solanacearum* in resistant H7996.
5. Spectroscopic studies showed strong accumulation of suberin-compatible metabolites specifically in roots of resistant H7996 upon infection with *R. solanacearum*. 2D-NMR showed strong enrichment in structures characteristic of suberins. Further, FTIR showed significantly high induction of phenolics in the xylem vasculature of resistant H7996.
  6. Significant differences in the polymerization state of lignin were observed between resistant and susceptible tomato cultivars after infection. Infected H7996 roots showed higher branching and cross-linking of lignin polymer compared to susceptible Marmande, thereby reducing the accessibility of the pathogen's hydrolytic enzymes.
  7. Specific enhancement in the expression of genes involved in the suberin biosynthetic pathway was observed in and around the vasculature of infected H7996.
  8. *ProSIFHT::GUS* lines in resistant H7996 served as a tool to study suberization spatiotemporally. In agreement to its critical role played by *SIFHT* in suberization process, we could observe the induction of *ProSIFHT::GUS* in tissues known to accumulate suberin such as root epidermis, exodermis and tissues undergoing wound healing. Further, induction of *ProSIFHT::GUS* was observed in taproot xylem vasculature upon *R. solanacearum* infection.
  9. Overexpression of the acyltransferase *SIFHT* –important for the formation of suberin monomers- in susceptible tomato caused a slight to non-significant delay in *R. solanacearum* colonization. Probably in susceptible tomato absence of aliphatic substrates required for conjugation with feruloyl-CoA may be a limiting factor.
  10. Overexpression of the acetyltransferase *SITHT1-3*- important for synthesis of HCAA- in susceptible tomato resulted in significantly high resistance induction against *R. solanacearum*. However, this resistance could be predominantly

## CONCLUSIONS

---

because of HCAA acting as phytoalexins against *R. solanacearum* and may not be due to reinforcements in the cell wall, as changes in wall phenolics were not detectable through microscopy.

## **MATERIALS & METHODS**

## 7. Materials & methods

### 7.1 Plant materials and growth conditions

In this study the tomato (*Solanum lycopersicum*) varieties Marmande and the quantitatively resistant public open-pollinated breeding line Hawaii 7996 were used. Seeds were germinated and plants were grown in pots containing soil (Substrate 2, Klasmann- Deilmann GmbH) mixed with perlite and vermiculite (30:1:1) in controlled growth chambers at 60% humidity and 12 h day/night with light intensity of 120–150  $\mu\text{mol}\cdot\text{m}^{-2}\cdot\text{s}^{-1}$ . Temperature was set at 28°C when using LED lighting and at 27°C when using fluorescent lighting.

### 7.2 *R. solanacearum* strains and growth conditions

All assays in tomato were performed using *R. solanacearum* GMI1000 strain (Phylotype I, race 1 biovar 3). Luminescent and fluorescent reporter strains of *R. solanacearum* GMI1000 were used in the study containing constructs *PpsbA::LuxCDABE* and *PpsbA::GFPuv*, respectively (Cruz *et al.*, 2014; Planas-Marquès *et al.*, 2019). *R. solanacearum* GMI1000 exopolysaccharide mutant strain was obtained from Caitilyn Allen, Department of Plant Pathology, University of Wisconsin-Madison (Milling *et al.*, 2011).

### 7.3 Bacterial inoculation in plants

Four- to five-week-old tomato plants were inoculated through roots with *R. solanacearum* using the soil drenching method as described in Planas-Marquès *et al.*, (2019). For this, roots were wounded by making four holes in the corners of the pot with a 1 ml pipette tip and inoculated with a  $1 \times 10^7$  CFU  $\text{ml}^{-1}$  ( $\text{OD}_{600} = 0.01$ ) suspension of bacteria (Planas-Marquès *et al.*, 2019). Inoculated plants were kept in a growth chamber at 28°C. The relative light units per second ( $\text{RLU}\cdot\text{s}^{-1}$ ) readings were converted to CFU  $\text{g}^{-1}$  taproot tissue as described in Planas-Marquès *et al.*, (2019). For tomato leaf infiltration, plants were vacuum-infiltrated by submerging the whole aerial part in a  $\sim 10^5$  CFU  $\text{ml}^{-1}$  ( $\text{OD}_{600} = 0.0001$ ) *R. solanacearum* suspension as described in Planas-Marquès *et al.*, (2018). For inoculation directly onto the stem vasculature, 10  $\mu\text{l}$  (5  $\mu\text{l}$  at a time) of  $10^5$  CFU  $\text{ml}^{-1}$  ( $\text{OD}_{600} = 0.0001$ ) *R. solanacearum* suspension was placed at the

node of the petiole and pin-inoculated using a sterile 0.3×13 mm needle (30G×½", BD Microlance, Becton Dickinson).

#### **7.4 *R. solanacearum* pathogenicity assays and quantification of bacterial growth in planta**

Infected plants were scored for wilting symptoms using a scale from 0 to 4: 0=healthy plant with no wilt, 1=25%, 2=50%, 3=75%, and 4=100% of the canopy wilted as described by Milling *et al.*, (2011) and Planas-Marquès *et al.*, (2019). For bacterial colonization assays by imaging using GFP reporter strain, transverse stem cross-sections were made at the taproot, using a sterile razor blade. The sections were photographed using an Olympus SZX16 stereomicroscope with a UV fluorescent lamp (BP330-385 BA420 filter) and equipped with a DP71 camera system (Olympus) (Planas-Marquès *et al.*, 2019). Quantification of mean green fluorescence from xylem vascular ring and pith parenchyma was done using ImageJ software (Planas-Marquès *et al.*, 2019). In experiments with the expolysaccharide mutant and Wt CFU g<sup>-1</sup> taproot tissue were calculated after dilution plating of samples and CFU counting 24 hours later (French *et al.*, 2018). For leaf *in planta* multiplication assays, 3 leaf discs of 0.8 cm<sup>2</sup> size were homogenized in 200 µl of sterile distilled water. CFU cm<sup>-2</sup> leaf tissue were calculated after dilution plating of samples with appropriate selection antibiotics and CFU counting 24 hours later.

#### **7.5 Histological methods**

Taproots of *R. solanacearum*-soil drench inoculated or water-treated plants were used for obtaining thin transverse cross-sections with a sterile razor blade. Inoculated plants were either sectioned at 9 dpi or when bacterial colonization level reached 10<sup>5</sup> CFU g<sup>-1</sup> taproot tissue, as indicated in the figure legend. Sections were kept in 70 % ethanol at room temperature for 5-7 days and examined using fluorescence microscopy using a Leica DM6B-Z microscope under UV illumination (340-380 nm excitation and 410-450 nm barrier filters). Autofluorescence emitted from phenolic deposits was recorded using a Leica-DFC9000GT-VSC07341 camera.

Sections were also stained with a Phloroglucinol-HCl solution (100 mg phloroglucinol in 8 ml of ethanol 95% and 8 ml of hydrochloric acid 37 %) for the detection of lignin

and observed under bright field (Pomar *et al.*, 2004). Photographs were taken in bright field using Leica DM6B-Z microscope with Leica MC190-HD-0518131623 digital camera. Since Phloroglucinol binds with lignin and quenches the autofluorescence emitted from it (Martín *et al.*, 2005), the cross-sections were then observed under UV microscopy (Leica DM6B-Z microscope with Leica-DFC9000GT-VSC07341 camera) to detect autofluorescence in the vasculature, which would correspond to non-lignin phenolic sources such as suberin (Pouzoulet *et al.*, 2013).

Auto-fluorescence from ferulates bound to the cell wall show a pH-dependent blue to green color conversion (Carnachan and Harris, 2000; Harris and Trethewey, 2010; Donaldson and Williams, 2018). Ferulates in the xylem vascular tissue were visualized by mounting cross-sections in 70 % ethanol (neutral pH) and illuminating them with UV with excitation bandpass filter in the range 340-380 nm to observe blue auto-fluorescence. These same sections were subsequently mounted in 1N KOH (pH above 10) to observe green auto-fluorescence from ferulates.

To visualize suberin aliphatics, sections were treated with 5 % Sudan IV, dissolved in 70 % ethanol and illuminated with UV light with excitation bandpass filter in the range 340-380 nm to produce the typical reddish-brown coloration. For both ferulates and suberin, the HC PL APO or HC PL FLUOTAR objectives of the Leica DM6B-Z microscope were used and images were captured using a Leica MC190-HD-0518131623 digital camera.

To visualize tyloses taproot cross-sections were stained in 1% toluidine blue solution, washed with water and observed in bright field with Leica DM6 microscope (Cao *et al.*, 2020).

Quantification of mean fluorescence in the green, blue, and red channels was done using ImageJ software. The UV auto-fluorescence signal was measured using the LAS X Leica software.



**Table 1: Details of microscope specifications used in histological studies**

Equipment	Camera	UV excitation
Leica DM6	Leica-DFC9000GT-VSC07341	340-380 nm
Leica DM6	MC190-HD-0518131623	340-380 nm
SZX16 stereomicroscope	DP71 camera system (Olympus)	330-385 nm
Leica DM6	Leica-DFC9000GT-VSC07341	340-380 nm
Leica DM6	MC190-HD-0518131623	340-380 nm
SZX16 stereomicroscope	DP71 camera system (Olympus)	330-385

## 7.6 SEM-EDX

Lyophilized thin taproot sections were coated with carbon and placed in grids and then analysis was done in Magellan 400L Field Emission Scanning Electron Microscope attached with X-Max Ultim Extreme Energy Dispersive X-Ray (EDX) (Oxford Instruments).

## 7.7 FT-IR

Dried taproot cross-sections of H7996 and Marmande plants, water-treated or *R. solanacearum*-inoculated by soil soak and containing bacteria  $10^5$  CFU g<sup>-1</sup> taproot tissue were analyzed using a FT-IR spectrophotometer Jasco 4700 with ATR accessory on the range of 300-4000 cm<sup>-1</sup>. The area analyzed was adjacent to the vasculature. All spectra were smoothened to minimize noise and baseline corrected, and the peak due to atmospheric CO<sub>2</sub> at 2300 cm<sup>-1</sup> was eliminated for clarity using OriginPro software. Relative absorbance ratios of peaks of significant importance were calculated by using the absorbance at 1236 cm<sup>-1</sup> as a reference.

## 7.8 2D-NMR

The samples of a pool of 15 tomato plant tap roots, water treated or having a bacterial load of  $10^5$  CFU.g-1 was obtained as lyophilized powder (300mg) and were milled and extracted sequentially with water (3 x 30 mL), 80% ethanol (3 x 30 mL), and with

acetone (2 x 40 mL), by sonicating in an ultrasonic bath during 30 min each time, centrifuging (9000 rpm, 25 min) and eliminating the supernatant. Then, lignin/suberin fraction was enzymatically isolated by hydrolyzing the carbohydrates fraction with Cellulysin (Calbiochem), as previously described (Rico *et al.* 2014). Approximately 20 mg of enzymatic lignin/suberin (ELS) preparation was dissolved in 0.6 mL of DMSO-d<sub>6</sub>. Heteronuclear single quantum coherence (HSQC) spectra were acquired on a Bruker AVANCE III 500 MHz spectrometer equipped with a 5 mm TCI cryoprobe, using the experimental conditions previously described (Rico *et al.*, 2015). HSQC cross-signals were assigned and quantified as described in (Rencoret *et al.*, 2018). In the aromatic region, the correlation signals of G2 and S2,6 were used to estimate the content of the respective G- and S-lignin units. The C $\alpha$ /H $\alpha$  signals of the  $\beta$ -O-4' ethers (A $\alpha$ ), phenylcoumarans (B $\alpha$ ), and resinols (C $\alpha$ ) in the linkages region were used to estimate their relative abundances, whereas the C $\gamma$ /H $\gamma$  signal was used in the case of cinnamyl alcohol end-units (I $\gamma$ ).

The HSQC experiment was performed using an adiabatic pulse sequence (Bruker standard pulse program 'hsqcetgpsisp.2'), which enabled a semi-quantitative analysis of the different <sup>13</sup>C-<sup>1</sup>H correlation signals. 2D-HSQC spectra were acquired from 10 to 0 ppm in F2 (<sup>1</sup>H) using 1000 data points for an acquisition time (AQ) of 100 ms, an interscan delay (D1) of 1 s, and from 200 to 10 ppm in F1 (<sup>13</sup>C) using 256 increments of 32 scan, for a total acquisition time of 2 h 34 min. The 1JCH used was 145 Hz. Processing used typical matched Gaussian apodization in <sup>1</sup>H (LB=-0.1 and GB=0.001) and a squared cosine bell in <sup>13</sup>C (LB=0.3 and GB=0.1). The central residual DMSO peak ( $\delta$ C/ $\delta$ H 39.5/2.49) was used as an internal reference. HSQC cross-signals were assigned by literature comparison (Del Río *et al.*, 2018; Rencoret *et al.*, 2018) and are detailed in Table 1. A semi-quantitative analysis of the volume integrals of the HSQC correlation peaks was performed using Bruker's Topspin 3.5 processing software. In the aromatic/unsaturated region, the correlation signals of G2 and S2,6 were used to estimate the content of the respective G- and S-lignin units (as the signal S2,6 involves two proton-carbon pairs, its volume integral was halved). The C $\alpha$ /H $\alpha$  correlation signals of the  $\beta$ -O-4' alkyl aryl ethers (A $\alpha$ ), phenylcoumarans (B $\alpha$ ), and resinols (C $\alpha$ ) in the aliphatic-oxygenated region of the spectra were used to estimate their relative abundances (as per 100 aromatic units), whereas the C $\gamma$ /H $\gamma$  correlation signal of the cinnamyl alcohol end-units (I $\gamma$ ) was used to estimate its relative abundance (as per 100

aromatic units); as signal  $I_\gamma$  involves two proton-carbon pairs, its volume integrals was also halved.

## 7.9 DNA constructs

The *ProFHT::GUS* construct was generated using the Gateway system (Invitrogen). A fragment consisting of 1713 bp upstream of the initial ATG codon (*Solyc03g097500*) was amplified from genomic DNA of H7996 tomato with the forward primer (ProFHTF1) and the reverse primer (ProFHTR1) containing the *attB* flanking sequences. This sequence was cloned into the Gateway entry vector pDONR 207 by a BP reaction and then transferred into the Gateway destination vector pGWB3 by LR reaction. For generation *35S::FHT-HA* construct the *FHT* (*Solyc03g097500*) coding sequence was amplified from tomato H7996 cDNA using the forward primer (part7FHTF1), having a flanking *SmaI* restriction enzyme digestion site at 5' end and reverse primer (part7FHTHAR1), including the sequence of hemagglutinin (HA) epitope tag and a *BamHI* restriction enzyme digestion site at the 5' end. The amplified product was cloned into the pJET1.2/blunt cloning vector using CloneJet PCR cloning kit (ThermoFisher) and then digested by *SmaI* and *BamHI*. The digested products were purified using NZYGelpure (Nzytech) followed by ligation into the pART7 and later to pART27 vector (Gleave, 1992).

## 7.10 Stable transformation of tomato

*ProFHT::GUS* and *35S::FHT-HA* were transformed into H7996 and Marmande respectively. For this, constructs were transformed into *Agrobacterium tumefaciens* strain C58C1. *A. tumefaciens* was used for co-culture with tomato cotyledons. Explant preparation, selection, and regeneration followed the methods described by (Mazier *et al.*, 2011). Transformants were selected on kanamycin-containing MS medium, and propagated into subsequent generations. Expression of GUS was analyzed as described below and accumulation of FHT-HA protein was assayed by immunoblot using Sigma-Aldrich anti-HA-HRP antibody at a dilution of 1:5000.

### 7.11 RNA extraction, cDNA synthesis and quantitative RT-PCR analysis

Tomato H7996 and Marmande plants were water-treated or inoculated with *R. solanacearum* by soil soak. Plants with a taproot inoculum of  $10^5$  CFU g<sup>-1</sup> were selected for RNA extraction. With a sharp razor blade, taproot sections of ~ 0.5 mm thickness were obtained and the xylem vascular tissues (vascular bundles and surrounding parenchyma cells) were collected and kept in liquid nitrogen. Each sample comprised taproot xylem tissues of 6 plants. RNA was extracted using the Maxwell RSC Plant RNA Kit (Promega) according to the manufacturer's recommendations. Extracted RNA was treated with RNase-free DNase provided in the kit. cDNA was synthesized from 2 µg RNA using High Capacity cDNA Reverse Transcription Kit (Applied Biosystems, USA). For each reaction 2.5 µl of cDNA (1:20 dilution), 1 µl forward and reverse primer mix (10 µM/µl), 5 µl SYBR Green PCR master mix (Roche) was used and analyzed using the LightCycler 480 System (Roche). The amplification program was performed as follows: 10 min at 95°C, followed by 45 cycles of 95°C for 10 sec, 60°C for 30 sec and 72°C for 30 sec. The Elongation Factor 1 alpha housekeeping gene (*eEF1 α*, *Solyc06g005060*) was used as a reference. All reactions were run in triplicate for each biological replicates. Melting curves and relative quantification of target genes were determined using the software LightCycler V1.5 (Roche). The level of expression relative to the reference gene was calculated using the formula  $2^{-\Delta CT}$ , where  $\Delta CT = (CT \text{ RNA target} - CT \text{ reference RNA})$ .

### 7.12 Detection of FHT promoter activity

Plant tissues or root sections were immersed in an ice-chilled 90% (v/v) acetone bath and incubated for 20 min on ice, after which they were rinsed with water. Tissues were vacuum-infiltrated for 20 min with a solution containing 1 mM 5-bromo-4-chloro-3-indolyl-beta-D-glucuronic acid (X-Gluc), 50 mM sodium phosphate buffer (pH 7), 1 mM potassium ferrocyanide, 1 mM potassium ferricyanide and 0.05% (v/v) Triton X-100. Samples were then incubated at 37°C for a maximum of 48 h. Stained tissues were washed 2–3 times with phosphate-buffered saline (PBS) and then cleared with 70% (v/v) ethanol and stored in 70% (v/v) ethanol. Images were obtained using an Olympus SZX16 stereomicroscope equipped with a DP71 camera system.

### 7.13 Statistical analysis

Statistical analyses were performed using Statgraphics software. All statistical tests are indicated in the respective figure legend.

### 7.14 Primers used in this study

Gene name	Primer 1	Primer 2
FHT Solyc03g097500 Cloning	ProFHTF1 ACAAGTTTGTACAAAAAAGCAGGCTAA ACAACAAAATAAGATTGCAC	ProFHTR1 ACCACTTTGTACAAGAAAGCTGGGTTTTCTCA AAATTAATAAATCCTG
FHT Solyc03g097500 Cloning	part7FHTF1 GGCCCGGGATGGAGAATGGTAAACACA GTGTTGC	part7FHTHAR1 GGGGATCCTTAAGCGTAGTCTGGGACGTCGT ATGGGTAGATCTCCATAAGTTCCTC
FHT Solyc03g097500 RT-qPCR	GGTGGCTCAGGTGACAAAGT	CCTCTCGCAATTCACCCCA
THT1-3 Solyc08g068730 RT-qPCR	CCCCTTTGTACGAACCTAAA	TTTGGATCGGAATTCCTCAA
EF Solyc06g005060 RT-qPCR	CCACCTCGAGATCCTAATGG	ACCCTCACGTATGCTTCCAG
PAL1 Solyc09g007920 RT-qPCR	TACGTGTTTGCCTATGCTGATG	CGGCCTTTAATTCGTCCTC
COMT Solyc03g080180 RT-qPCR	GGTGGTGGAACAGGGGCTACT	TAAACAATGCTCATCGCTCCAATC
CCoAOMT1 Solyc02g093270 RT-qPCR	GAGAGCCTGAAGCCATGAAAGAGC	GAGCCATGGCAGTAGCAAGCAGAG
CCoAOMT6 Solyc01g107910 RT-qPCR	ATTTTCGAGAGGGCCTGCTTTAC	ATCCGATCACACCACCAACTTTCA
HCT Solyc03g117600 RT-qPCR	CCCTCCTCCGTGCTCGTGA	CCCGGGTTAGTTGAAGATTGACA
C3H Solyc01g096670 RT-qPCR	CTGCAATGCGTGGCCAAGGAAGC	TCGCGAGCAACAGCCCAGACATT
4CL Solyc12g094520 RT-qPCR	CGA GCA TGG AAG GGA AAA TTG	TCA GAG TCT AGA GTG GAA GCA G
C4H TC93956 RT-qPCR	CTAGCTAACAACCCCGCCCA	AACTCCTCCTGCCAACACCG
THT 7-8 Solyc08g068780 RT-qPCR	GGAAACTGATAAGGAGAAGGTGG	GTTTGCACGGCGTATGGAG
THT HOMOLOG Solyc08g068710 RT-qPCR	AGTTTAGGTATGGCAAATTGCATGG	AAGAAAACACACAGTAGCTAACAGC
THT HOMOLOG Solyc08g068690 RT-qPCR	TCAGTCGATGGAATAGTAGCAGTT	TCCTCAATTTCCCCCTTGTTATG
CYP86A1 Solyc06g076800 RT-qPCR	GGTCTACTGGTGTATCCGCA	CCTTTAGGATAGTTATCGAACCTGG

## MATERIALS & METHODS

KCS1 Solyc10g009240 RT-qPCR	GTCGTAGGGGTGTCCTAGC	GTCATGAAAAACCTGAATTGCTCAG
GPAT5 Solyc04g011600 RT-qPCR	CCCTAGGCCAATGTATGAGGTAAC	GTTGCTGCCAAAATCCTCTGG
DAISY/KCS2 Solyc05g009280 RT-qPCR	TCCGAGTTCATCCCAAGTCG	AACAGTATGGCTGCACCTCC
FAR3 Solyc06g074390 RT-qPCR	TGGTGCTACTGGATTCTTGC	TGCCACAGCCTCATTGTTGA
THT 7-1 Solyc08g068700 RT-qPCR	GCTTGAACGCTTGGTTAGTGG	AGTCCTCCTTAGAGGGCTTGC
CY986B1 Solyc02g014730 RT-qPCR	TCCGTTGATTTTCAAGCCAGC	TCGTCTCAACAACCTCTTTGTG



## **REFERENCES**

- Agrelli D, Amalfitano C, Conte P, Mugnai L. 2009.** Chemical and spectroscopic characteristics of the wood of *Vitis vinifera* cv. Sangiovese affected by esca disease. *Journal of Agricultural and Food Chemistry* **57**: 11469–11475.
- Alassimone J, Fujita S, Doblas VG, Van Dop M, Barberon M, Kalmbach L, Vermeer JEM, Rojas-Murcia N, Santuari L, Hardtke CS, et al. 2016.** Polarly localized kinase SGN1 is required for casparian strip integrity and positioning. *Nature Plants* **2**: 16113 |.
- Alonso-Simón A, García-Angulo P, Mélida H, Encina A, Álvarez JM, Acebes JL. 2011.** The use of FTIR spectroscopy to monitor modifications in plant cell wall architecture caused by cellulose biosynthesis inhibitors. *Plant Signaling and Behavior* **6**: 1104–1110.
- Álvarez B, Biosca EG, López MM. 2010.** On the life of *Ralstonia solanacearum*, a destructive bacterial plant pathogen. In: Méndez-Vilas A, ed. Technology and education topics in applied microbiology and microbial biotechnology. Badajoz: Formatex, 267–279.
- Aoun M, Rioux D, Simard M, Bernier L. 2009.** Fungal colonization and host defense reactions in *Ulmus americana* callus cultures inoculated with *Ophiostoma novo-ulmi*. *Phytopathology* **99**: 642–650.
- Araujo L, Bispo WMS, Cacique IS, Moreira WR, Rodrigues FA. 2014.** Resistance in mango against infection by *Ceratocystis fimbriata*. *Phytopathology* **104**: 820–833.
- Baayen RP, Elgersma DM. 1985.** Colonization and histopathology of susceptible and resistant carnation cultivars infected with *Fusarium oxysporum* f. sp. *dianthi*. *Netherlands Journal of Plant Pathology* **91**: 119–135.
- Bacete L, Mélida H, Miedes E, Molina A. 2018.** Plant cell wall-mediated immunity: cell wall changes trigger disease resistance responses. *Plant Journal* **93**: 614–636.
- Bae C, Han SW, Song YR, Kim BY, Lee HJ, Lee JM, Yeam I, Heu S, Oh CS. 2015.** Infection processes of xylem-colonizing pathogenic bacteria: possible explanations for the scarcity of qualitative disease resistance genes against them in crops. *Theoretical and Applied Genetics* **128**: 1219–1229.
- Beckman CH, Roberts EM. 1995.** On the nature and genetic basis for resistance and tolerance to fungal wilt diseases of plants. *Advances in Botanical Research* **21**: 35–77.
- Benhamou N. 1995.** Ultrastructural and cytochemical aspects of the response of eggplant parenchyma cells in direct contact with *Verticillium*-infected xylem vessels. *Physiological and Molecular Plant Pathology* **46**: 321–338.
- Bernards MA. 2002.** Demystifying suberin. *Canadian Journal of Botany* **80**: 227–240.
- Bernards MA, Lewis NG. 1992.** Alkyl ferulates in wound healing potato tubers. *Phytochemistry* **31**: 3409–3412.
- Bernards MA, Lewis NG. 1998.** The macromolecular aromatic domain in suberized tissue: a changing paradigm. *Phytochemistry* **47**: 915–933.
- Bernards M, Lopez M, Zajicek J, Lewis N. 1995.** Hydroxycinnamic acid-derived polymers constitute the polyaromatic domain of suberin. *The Journal of Biological*

*Chemistry* **270**: 7382–7386.

**Biggs A. 1984.** Intracellular suberin: Occurrence and detection in tree bark. *IAWA Bulletin* **5**: 243–248.

**Boher P, Serra O, Soler M, Molinas M, Figueras M. 2013.** The potato suberin feruloyl transferase FHT which accumulates in the phellogen is induced by wounding and regulated by abscisic and salicylic acids. *Journal of Experimental Botany* **64**: 3225–3236.

**Boller T, Felix G. 2009.** A Renaissance of Elicitors: Perception of Microbe-Associated Molecular Patterns and Danger Signals by Pattern-Recognition Receptors. *Annual Review of Plant Biology* **60**: 379–406.

**Bontpart T, Cheynier V, Ageorges A, Terrier N. 2015.** BAHD or SCPL acyltransferase? What a dilemma for acylation in the world of plant phenolic compounds. *New Phytologist* **208**: 695–707.

**Caldwell D, Kim B, Iyer-Pascuzzi AS. 2017.** *Ralstonia solanacearum* differentially colonizes roots of resistant and susceptible tomato plants. *Phytopathology* **107**: 528–536.

**Campos L, Lisón P, López-Gresa MP, Rodrigo I, Zacarés L, Conejero V, Bellés JM. 2014.** Transgenic tomato plants overexpressing tyramine N -hydroxycinnamoyltransferase exhibit elevated hydroxycinnamic acid amide levels and enhanced resistance to *Pseudomonas syringae*. *Molecular Plant-Microbe Interactions* **27**: 1159–1169.

**Cao P, Ployet R, Nguyen C, Dupas A, Ladouce N, Martinez Y, Pettenati J, Marque C, Mounet F, Teulier C. 2020.** Wood architecture and composition are deeply remodeled in frost sensitive Eucalyptus overexpressing CBF / DREB1 transcription factors. *International Journal of Molecular Sciences* **21**: 3019.

**Carnachan SM, Harris PJ. 2000.** Ferulic acid is bound to the primary cell walls of all gymnosperm families. *Biochemical Systematics and Ecology* **28**: 865–879.

**Cháves-Gómez JL, Becerra-Mutis LM, Chávez-Arias CC, Restrepo-Díaz H, Gómez-Caro S. 2020.** Screening of different *Physalis* genotypes as potential rootstocks or parents against vascular wilt using physiological markers. *Frontiers in Plant Science* **11**: 806.

**Cheng AX, Gou JY, Yu XH, Yang H, Fang X, Chen XY, Liu CJ. 2013.** Characterization and ectopic expression of a populus hydroxyacid hydroxycinnamoyltransferase. *Molecular Plant* **6**: 1889–1903.

**Cohen H, Dong Y, Szymanski J, Lashbrooke J, Meir S, Almekias-Siegl E, Zeisler-Diehl VV, Schreiber L, Aharoni A. 2019.** A multilevel study of melon fruit reticulation provides insight into skin ligno-suberization hallmarks. *Plant Physiology* **179**: 1486–1501.

**Cohen H, Fedruk V, Wang C, Wu S, Aharoni A. 2020.** SUBERMAN regulates developmental suberization of the Arabidopsis root endodermis. *The Plant Journal* **102**: 431–447.

**Cruz APZ, Ferreira V, Pianzola MJ, Siri MI, Coll NS, Valls M. 2014.** A novel, sensitive method to evaluate potato germplasm for bacterial wilt resistance using a luminescent *Ralstonia solanacearum* reporter strain. *Molecular Plant-Microbe Interactions* **27**: 277–285.

- Daayf F, Nicole M, Boher B, Pando A, Geiger JP. 1997. Early vascular defense reactions of cotton roots infected with a defoliating mutant strain of *Verticillium dahliae*. *European Journal of Plant Pathology* **103**: 125–136.
- Digonnet C, Martinez Y, Denancé N, Chasseray M, Dabos P, Ranocha P, Marco Y, Jauneau A, Goffner D. 2012. Deciphering the route of *Ralstonia solanacearum* colonization in *Arabidopsis thaliana* roots during a compatible interaction: Focus at the plant cell wall. *Planta* **236**: 1419–1431.
- Dixon RA, Paiva NL. 1995. Stress induced phenylpropanoid metabolism. *The Plant Cell* **7**: 1085–1097.
- Doblas V, Geldner N, Barberon M. 2017. The endodermis , a tightly controlled barrier for nutrients. *Current Opinion in Plant Biology* **39**: 136–143.
- van der Does HC, Constantin ME, Houterman PM, Takken FLW, Cornelissen BJC, Haring MA, van den Burg HA, Rep M. 2019. *Fusarium oxysporum* colonizes the stem of resistant tomato plants, the extent varying with the R-gene present. *European Journal of Plant Pathology* **154**: 55–65.
- Donaldson L, Williams N. 2018. Imaging and spectroscopy of natural fluorophores in pine needles. *Plants* **7**: 10.
- Dorado J, Almendros G, Field JA, Sierra-alvarez R. 2001. Infrared spectroscopy analysis of hemp (*Cannabis sativa*) after selective delignification by *Bjerkandera* sp. at different nitrogen levels. *Enzyme and Microbial Technology* **28**: 550–559.
- Falter C, Ellinger D, Von Hulsén B, Heim R, Voigt CA. 2015. Simple preparation of plant epidermal tissue for laser microdissection and downstream quantitative proteome and carbohydrate analysis. *Frontiers in Plant Science* **6**: 194.
- Fattorusso E, Lanzotti V, Taglialatela-Scafati O. 1999. Antifungal N-feruloyl amides from roots of two allium species. *Plant Biosystems* **133**: 199–203.
- Ferreira V, Pianzola MJ, Vilaró FL, Galván GA, Tondo ML, Rodriguez M V., Orellano EG, Valls M, Siri MI. 2017. Interspecific potato breeding lines display differential colonization patterns and induced defense responses after *Ralstonia solanacearum* infection. *Frontiers in Plant Science* **8**: 1424.
- Franke R, Fry SC, Kauss H. 1998. Low-molecular-weight precursors for defense-related cell wall hydroxycinnamoyl esters in elicited parsley suspension cultures. *Plant Cell Reports* **17**: 379–383.
- French E, Kim B-S, Rivera-Zuluaga K, Iyer-Pascuzzi AS. 2018. Whole root transcriptomic analysis suggests a role for auxin pathways in resistance to *Ralstonia solanacearum* in tomato. *Molecular Plant-Microbe Interactions* **31**: 432–444.
- Fujita S, De Bellis D, Edel KH, Köster P, Andersen TG, Schmid-Siegert E, Dénervaud Tendon V, Pfister A, Marhavý P, Ursache R, *et al.* 2020. SCHENGEN receptor module drives localized ROS production and lignification in plant roots. *The EMBO Journal* **39**: e103894.
- Gleave AP. 1992. A versatile binary vector system with a T-DNA organisational structure

conductive to efficient integration of cloned DNA into the plant genome. *Plant Molecular Biology* **20**: 1203–1207.

**Gou J-Y, Yu X-H, Liu C-J. 2009.** A hydroxycinnamoyltransferase responsible for synthesizing suberin aromatics in Arabidopsis. *Proceedings of the National Academy of Sciences* **106**: 18855–18860.

**Graça J. 2010.** Hydroxycinnamates in suberin formation. *Phytochemistry Reviews* **9**: 85–91.

**Graça J. 2015.** Suberin: The biopolyester at the frontier of plants. *Frontiers in Chemistry* **3**: 62.

**Grimault V, Anais G, Prior P. 1994a.** Distribution of *Pseudomonas solanacearum* in the stem tissues of tomato plants with different levels of resistance to bacterial wilt. *Plant Pathology* **43**: 663–668.

**Grimault V, Gélie B, Lemattre M, Prior P, Schmit J. 1994b.** Comparative histology of resistant and susceptible tomato cultivars infected by *Pseudomonas solanacearum*. *Physiological and Molecular Plant Pathology* **44**: 105–123.

**Gupta S, Bhar A, Chatterjee M, Das S. 2013.** *Fusarium oxysporum* f.sp. *ciceri* Race 1 induced redox state alterations are coupled to downstream defense signaling in root tissues of chickpea (*Cicer arietinum* L.). *PLoS ONE* **8(9)**: e73163.

**Hagel JM, Facchini PJ. 2005.** Elevated tyrosine decarboxylase and tyramine hydroxycinnamoyltransferase levels increase wound-induced tyramine-derived hydroxycinnamic acid amide accumulation in transgenic tobacco leaves. *Planta* **221**: 904–914.

**Harris PJ, Trethewey JAK. 2010.** The distribution of ester-linked ferulic acid in the cell walls of angiosperms. *Phytochemistry Reviews* **9**: 19–33.

**He M, Ding N. 2020.** Plant unsaturated fatty acids: multiple roles in stress response. *Frontiers in Plant Science* **11**: 562785.

**Höfer R, Briesen I, Beck M, Pinot F, Schreiber L, Franke R. 2008.** The Arabidopsis cytochrome P450 CYP86A1 encodes a fatty acid  $\omega$ -hydroxylase involved in suberin monomer biosynthesis. *Journal of Experimental Botany* **59**: 2347–2360.

**Hutson RA, Smith IM. 1980.** Phytoalexins and tyloses in tomato cultivars infected with *Fusarium oxysporum* f.sp. *lycopersici* or *Verticillium albo-atrum*. *Physiological Plant Pathology* **17**: 245–257.

**Iiyama K, Lam TBT, Stone B. 2020.** Covalent cross-links in the cell wall. *Plant Physiology* **104**: 315–320.

**Ishihara T, Mitsuhara I, Takahashi H, Nakaho K. 2012.** Transcriptome analysis of quantitative resistance-specific response upon *Ralstonia solanacearum* infection in tomato. *PLoS ONE* **7(10)**: e46763.

**Jones JDG, Dangl JL. 2006.** The plant immune system. *Nature* **444**: 323–329.

- Kang X, Kirui A, Dickwella Widanage MC, Mentink-Vigier F, Cosgrove DJ, Wang T. 2019.** Lignin-polysaccharide interactions in plant secondary cell walls revealed by solid-state NMR. *Nature Communications* **10**: 347.
- Kashyap A, Planas-marquès M, Valls M. 2021.** Blocking intruders : inducible physico-chemical barriers against plant vascular wilt pathogens. *Journal of Experimental Botany* **72**: 184–198.
- Kim SG, Hur OS, Ro NY, Ko HC, Rhee JH, Sung JS, Ryu KY, Lee SY, Baek HJ. 2016.** Evaluation of resistance to *Ralstonia solanacearum* in tomato genetic resources at seedling stage. *Plant Pathology Journal* **32**: 58–64.
- Kim B, Hwang IS, Lee HJ, Lee JM, Seo E, Choi D, Oh CS. 2018.** Identification of a molecular marker tightly linked to bacterial wilt resistance in tomato by genome-wide SNP analysis. *Theoretical and Applied Genetics* **131**: 1017–1030.
- Kim H, Ralph J. 2014.** A gel-state 2D-NMR method for plant cell wall profiling and analysis: A model study with the amorphous cellulose and xylan from ball-milled cotton linters. *RSC Advances* **4**: 7549–7560.
- King RR, Calhoun LA. 2005.** Characterization of cross-linked hydroxycinnamic acid amides isolated from potato common scab lesions. *Phytochemistry* **66**: 2468–2473.
- Lahlali R, Song T, Chu M, Yu F, Kumar S, Karunakaran C, Peng G. 2017.** Evaluating changes in cell-wall components associated with clubroot resistance using fourier transform infrared spectroscopy and RT-PCR. *International Journal of Molecular Sciences* **18**: 2058.
- Lashbrooke J, Cohen H, Levy-Samocha D, Tzfadia O, Panizel I, Zeisler V, Massalha H, Stern A, Trainotti L, Schreiber L, et al. 2016.** MYB107 and MYB9 homologs regulate suberin deposition in Angiosperms. *The Plant Cell* **28**: 2097–2116.
- Lee M, Jeon HS, Kim SH, Chung JH, Roppolo D, Lee H, Cho HJ, Tobimatsu Y, Ralph J, Park OK. 2019.** Lignin-based barrier restricts pathogens to the infection site and confers resistance in plants. *EMBO Journal* **38**: e101948.
- Legay S, Guerriero G, Deleruelle A, Lateur M, Evers D, André CM, Hausman JF. 2015.** Apple russetting as seen through the RNA-seq lens: strong alterations in the exocarp cell wall. *Plant Molecular Biology* **88**: 21–40.
- Leśniewska J, Öhman D, Krzesłowska M, Kushwah S, Barciszewska-Pacak M, Kleczkowski LA, Sundberg B, Moritz T, Mellerowicz EJ. 2017.** Defense responses in aspen with altered pectin methylesterase activity reveal the hormonal inducers of tyloses. *Plant Physiology* **173**: 1409–1419.
- Levsh O, Chiang YC, Tung CF, Noel JP, Wang Y, Weng JK. 2016.** Dynamic conformational states dictate selectivity toward the native substrate in a substrate-permissive acyltransferase. *Biochemistry* **55**: 6314–6326.
- Liu H, Zhang S, Schell MA, Denny TP. 2005.** Pyramiding unmarked deletions in *Ralstonia solanacearum* shows that secreted proteins in addition to plant cell-wall-degrading enzymes contribute to virulence. *Molecular Plant-Microbe Interactions* **18**: 1296–1305.



- Lourenço A, Rencoret J, Chemetova C, Gominho J. 2016.** Lignin composition and structure differs between xylem, phloem and pith in *Quercus suber* L. *Frontiers in Plant Science* **7**:1612.
- Lowe-Power TM, Khokhani D, Allen C. 2018.** How *Ralstonia solanacearum* exploits and thrives in the flowing plant xylem environment. *Trends in Microbiology* **26**: 929–942.
- Luna E, Pastor V, Robert J, Flors V, Mauch-Mani B, Ton J. 2011.** Callose deposition: A multifaceted plant defense response. *Molecular Plant-Microbe Interactions* **24**: 183–193.
- Malinovsky FG, Fangel JU, Willats WGT. 2014.** The role of the cell wall in plant immunity. *Frontiers in Plant Science* **5**: 178.
- Mangin B, Thoquet P, Olivier J, Grimsley NH. 1999.** Temporal and multiple quantitative trait loci analyses of resistance to bacterial wilt in tomato permit the resolution of linked loci. *Genetics* **151**: 1165–1172.
- Mansfield SD, Kim H, Lu F, Ralph J. 2012.** Whole plant cell wall characterization using solution-state 2D NMR. *Nature Protocols* **7**: 1579–1589.
- Marques A, Rencoret J, Gutierrez A, Del Rio J, Pereira H. 2016.** Ferulates and lignin structural composition in cork. *Holzforschung* **70**: 275–289.
- Martín JA, Solla A, Coimbra MA, Gil L. 2005.** Metabolic distinction of *Ulmus minor* xylem tissues after inoculation with *Ophiostoma novo-ulmi*. *Phytochemistry* **66**: 2458–2467.
- Mazier M, Flamain F, Nicolai M, Sarnette V, Caranta C. 2011.** Knock-down of both eIF4E1 and eIF4E2 genes confers broad-spectrum resistance against potyviruses in tomato. *PLoS ONE* **6**(12): e29595.
- Milling A, Babujee L, Allen C. 2011.** *Ralstonia solanacearum* extracellular polysaccharide is a specific elicitor of defense responses in wilt-resistant tomato plants. *PLoS ONE* **6**: e15853.
- Molina I, Li-Beisson Y, Beisson F, Ohlrogge JB, Pollard M. 2009.** Identification of an Arabidopsis Feruloyl-Coenzyme A transferase required for suberin synthesis. *Plant Physiology* **151**: 1317–1328.
- Montemayor EJ, Hoffman DW. 2008.** The crystal structure of spermidine/spermine N1-acetyltransferase in complex with spermine provides insights into substrate binding and catalysis. *Biochemistry* **47**: 9145–9153.
- Nakaho K, Hibino H, Miyagawa H. 2000.** Possible mechanisms limiting movement of *Ralstonia solanacearum* in resistant tomato tissues. *Journal of Phytopathology* **148**: 181–190.
- Nakaho K, Inoue H, Takayama T, Miyagawa H. 2004.** Distribution and multiplication of *Ralstonia solanacearum* in tomato plants with resistance derived from different origins. *Journal of General Plant Pathology* **70**:115–119.
- Nakaho K, Seo S, Ookawa K, Inoue Y, Ando S, Kanayama Y, Miyashita S, Takahashi**

- H. 2017.** Involvement of a vascular hypersensitive response in quantitative resistance to *Ralstonia solanacearum* on tomato rootstock cultivar LS-89. *Plant Pathology* **66**: 150–158.
- Negrel J, Lotfy S, Javelle F. 1995.** Modulation of the activity of two hydroxycinnamoyl transferases in wound-healing potato tuber discs in response to pectinase or abscisic acid. *Journal of Plant Physiology* **146**: 318–322.
- Negrel J, Pollet B, Lapierre C. 1996.** Ether-linked ferulic acid amides in natural and wound periderms of potato tuber. *Phytochemistry* **43**: 1195–1199.
- Ngou BPM, Ahn HK, Ding P, Jones JDG. 2021.** Mutual potentiation of plant immunity by cell-surface and intracellular receptors. *Nature* **592**: 110–115.
- Novo M, Silvar C, Merino F, Martínez-Cortés T, Lu F, Ralph J, Pomar F. 2017.** Deciphering the role of the phenylpropanoid metabolism in the tolerance of *Capsicum annuum* L. to *Verticillium dahliae* Kleb. *Plant Science* **258**: 12–20.
- Peeters N, Guidot A, Vailleau F, Valls M. 2013.** *Ralstonia solanacearum*, a widespread bacterial plant pathogen in the post-genomic era. *Molecular Plant Pathology* **14**: 651–662.
- Pérez-Donoso AG, Sun Q, Caroline Roper M, Carl Greve L, Kirkpatrick B, Labavitch JM. 2010.** Cell wall-degrading enzymes enlarge the pore size of intervessel pit membranes in healthy and *Xylella fastidiosa*-infected grapevines. *Plant Physiology* **152**: 1748–1759.
- Planas-Marquès M, Kressin JP, Kashyap A, Panthee DR, Louws FJ, Coll NS, Valls M. 2019.** Four bottlenecks restrict colonization and invasion by the pathogen *Ralstonia solanacearum* in resistant tomato. *Journal of Experimental Botany* **71**: 2157–2171.
- Pomar F, Novo M, Bernal MA, Merino F, Barceló AR, Barceló AR. 2004.** Changes in stem lignins ( monomer composition and crosslinking ) and peroxidase are related with the maintenance of leaf photosynthetic integrity during *Verticillium* wilt in *Capsicum annuum*. *New Phytologist* **163**: 111–123.
- Potter C, Harwood T, Knight J, Tomlinson I. 2011.** Learning from history, predicting the future: The UK Dutch elm disease outbreak in relation to contemporary tree disease threats. *Philosophical Transactions of the Royal Society B: Biological Sciences* **366**: 1966–1974.
- Pouzoulet J, Jacques A, Besson X, Dayde J, Mailhac N. 2013.** Histopathological study of response of *Vitis vinifera* cv. Cabernet Sauvignon to bark and wood injury with and without inoculation by *Phaeomoniella chlamydospora*. *Phytopathologia Mediterranea* **52**: 313–323.
- Prakash A, Darren Grice I, Vinay Kumar KS, Sadashiva MP, Shankar HN, Umesha S. 2017.** Extracellular polysaccharide from *Ralstonia solanacearum*; a strong inducer of eggplant defense against bacterial wilt. *Biological Control* **110**: 107–116.
- Rencoret J, Gutierrez A, Nieto L, Jime J, Faulds CB, Kim H, Ralph J. 2011.** Lignin composition and structure in young versus adult *Eucalyptus globulus* plants. *Plant Physiology* **155**: 667–682.
- Rencoret J, Kim H, Evaristo AB, Gutiérrez A, Ralph J, Del Río JC. 2018.** Variability

in lignin composition and structure in cell walls of different parts of Macaúba (*Acrocomia aculeata*) palm fruit. *Journal of Agricultural and Food Chemistry* **66**: 138–153.

**Rico A, Rencoret J, del Río JC, Martínez AT, Gutiérrez A. 2015.** In-Depth 2D NMR study of lignin modification during pretreatment of Eucalyptus Wood with laccase and mediators. *Bioenergy Research* **8**: 211–230.

**Del Río J, Marques G, Rencoret J, Martinez A, Gutierrez A. 2007.** Occurrence of naturally acetylated lignin units. *Journal of Agricultural and Food Chemistry* **55**: 5461–5468.

**Del Río JC, Rencoret J, Gutiérrez A, Kim H, Ralph J. 2018.** Structural characterization of lignin from Maize (*Zea mays* L.) Fibers: Evidence for Diferuloylputrescine incorporated into the lignin polymer in Maize Kernels. *Journal of Agricultural and Food Chemistry* **66**: 4402–4413.

**Rioux D, Blais M, Nadeau-Thibodeau N, Lagacé M, Des Rochers P, Klimaszewska K, Bernier L. 2018.** First extensive microscopic study of butternut defense mechanisms following inoculation with the canker pathogen *Ophiognomonia clavignenti-juglandacearum* reveals compartmentalization of tissue damage. *Phytopathology* **108**: 1237–1252.

**Rioux D, Nicole M, Simard M, Ouellette GB. 1998.** Immunocytochemical evidence that secretion of pectin occurs during gel (gum) and tylosis formation in trees. *Phytopathology* **88**: 494–505.

**Robb J, Lee S-W, Mohan R, Kolattukudy PE. 2008.** Chemical characterization of stress-induced vascular coating in tomato. *Plant Physiology* **97**: 528–536.

**Rudd JJ, Franklin-tong VE. 2001.** Unravelling response-specificity in Ca<sup>2+</sup> signalling pathways in plant cells. *New Phytologist* **151**: 7–33.

**Sakthivel K, Gautam RK, Kumar K, Dam Roy S, Kumar A, Devendrakumar C, Vibhuti M, Neelam S, Vinatzer BA. 2016.** Diversity of *Ralstonia solanacearum* strains on the Andaman Islands in India. *Plant Disease* **100**: 732–738.

**Salas-González I, Reyt G, Flis P, Custódio V, Gopaulchan D, Bakhoun N, Dew TP, Suresh K, Franke RB, Dangl JL, et al. 2021.** Coordination between microbiota and root endodermis supports plant mineral nutrient homeostasis. *Science* **371**: eabd0695.

**Scortichini M. 2020.** The multi-millennial olive agroecosystem of salento (Apulia, Italy) threatened by *Xylella fastidiosa* subsp. Pauca: A working possibility of restoration. *Sustainability (Switzerland)* **12**: 6700.

**Serra O, Figueras M, Franke R, Prat S, Molinas M. 2010a.** Unraveling ferulate role in suberin and periderm biology by reverse genetics. *Plant Signaling and Behavior* **5**: 953–958.

**Serra O, Hohn C, Franke R, Prat S, Molinas M, Figueras M. 2010b.** A feruloyl transferase involved in the biosynthesis of suberin and suberin-associated wax is required for maturation and sealing properties of potato periderm. *Plant Journal* **62**: 277–290.

**Serrano M, Coluccia F, Torres M, L'Haridon F, Métraux JP. 2014.** The cuticle and

- plant defense to pathogens. *Frontiers in Plant Science* **5**: 274.
- Street PFS, Robb J, Ellis BE. 1986.** Secretion of vascular coating components by xylem parenchyma cells of tomatoes infected with *Verticillium albo-atrum*. *Protoplasma* **132**: 1–11.
- Sun Q, Sun Y, Walker MA, Labavitch JM. 2013.** Vascular occlusions in grapevines with Pierce’s disease make disease symptom development worse. *Plant Physiology* **161**: 1529–1541.
- Taoutaou A, Socaciu C, Pamfil D, Fetea F, Balazs E, Botez C. 2012.** New markers for potato late blight resistance and susceptibility using FTIR spectroscopy. *Notulae Botanicae Horti Agrobotanici* **40**: 150–154.
- The Tomato Genome Consortium. 2012.** The tomato genome sequence provides insights into fleshy fruit evolution. *Nature*. **485**: 635– 641.
- Thomma BPHJ, Nürnberger T, Joosten MHAJ. 2011.** Of PAMPs and effectors: The blurred PTI-ETI dichotomy. *Plant Cell* **23**: 4–15.
- Thoquet P, Olivier J, Sperisen C, Rogowsky P, Laterrot H, Grimsley N. 1996.** Quantitative trait loci determining resistance to bacterial wilt in tomato cultivar Hawaii7996. *Molecular Plant-Microbe Interactions* **9**: 826–836.
- Toufighi K, Brady SM, Austin R, Ly E, Provart NJ. 2005.** The botany array resource: e-Northerns, expression angling, and promoter analyses. *Plant Journal* **43**: 153–163.
- Underwood W. 2012.** The plant cell wall: A dynamic barrier against pathogen invasion. *Frontiers in Plant Science* **3**: 85.
- VanderMolen GE, Beckman CH, Rodehorst E. 1987.** The ultrastructure of tylose formation in resistant banana following inoculation with *Fusarium oxysporum* f.sp. *cubense*. *Physiological and Molecular Plant Pathology* **31**: 185–200.
- Vasse J, Frey P, Trigalet A. 1995.** Microscopic studies of intercellular infection and protoxylem invasion of tomato roots by *Pseudomonas solanacearum*. *Molecular Plant-Microbe Interactions* **8**: 241–251.
- Vishwanath SJ, Delude C, Domergue F, Rowland O. 2015.** Suberin: biosynthesis, regulation, and polymer assembly of a protective extracellular barrier. *Plant Cell Reports* **34**: 573–586.
- Vishwanath SJ, Kosma DK, Pulsifer IP, Scandola S, Pascal S, Joubès J, Dittrich-Domergue F, Lessire R, Rowland O, Domergue F. 2013.** Suberin-associated fatty alcohols in Arabidopsis: distributions in roots and contributions to seed coat barrier properties. *Plant Physiology* **163**: 1118–1132.
- Wang JF, Ho FI, Truong HTH, Huang SM, Balatero CH, Dittapongpitch V, Hidayati N. 2013.** Identification of major QTLs associated with stable resistance of tomato cultivar ‘Hawaii 7996’ to *Ralstonia solanacearum*. *Euphytica* **190**: 241–252.
- Wang JF, Olivier J, Thoquet P, Mangin B, Sauviac L, Grimsley NH. 2000.** Resistance of tomato line Hawaii 7996 to *Ralstonia solanacearum* Pss4 in Taiwan is controlled

mainly by a major strain-specific locus. *Molecular Plant-Microbe Interactions* **13**: 6–13.

**Watanabe K, Nishiuchi S, Kulichikhin K, Nakazono M. 2013.** Does suberin accumulation in plant roots contribute to waterlogging tolerance? *Frontiers in Plant Science* **4**: 178.

**Woolfson KN. 2018.** Suberin biosynthesis and deposition in the wound- healing potato (*Solanum tuberosum* L.) tuber model. PhD thesis, The University of Western Ontario, London, Canada. <https://ir.lib.uwo.ca/cgi/viewcontent.cgi?article=8075&context=etd>. Accessed July 2020.

**Woolfson KN, Haggitt ML, Zhang Y, Kachura A, Bjelica A, Rey Rincon MA, Kaberi KM, Bernards MA. 2018.** Differential induction of polar and non-polar metabolism during wound-induced suberization in potato (*Solanum tuberosum* L.) tubers. *Plant Journal* **93**: 931–942.

**Yadeta KA, Thomma BPHJ. 2013.** The xylem as battleground for plant hosts and vascular wilt pathogens. *Frontiers in Plant Science* **4**: 97.

**Yuan M, Jiang Z, Bi G, Nomura K, Liu M, Wang Y, Cai B, Zhou JM, He SY, Xin XF. 2021.** Pattern-recognition receptors are required for NLR-mediated plant immunity. *Nature* **592**: 105–109.

**Zaini PA, Nascimento R, Gouran H, Cantu D, Chakraborty S, Phu M, Goulart LR, Dandekar AM. 2018.** Molecular profiling of pierce's disease outlines the response circuitry of *Vitis vinifera* to *Xylella fastidiosa* infection. *Frontiers in Plant Science* **9**: 771.

**Zhou F, Emonet A, Dénervaud Tendon V, Marhavy P, Wu D, Lahaye T, Geldner N. 2020.** Co-incidence of damage and microbial patterns controls localized immune responses in roots. *Cell* **180**: 440–453.

**ANNEX**



## **ANNEX I**



RESEARCH PAPER

# Four bottlenecks restrict colonization and invasion by the pathogen *Ralstonia solanacearum* in resistant tomato

Marc Planas-Marquès<sup>1,†</sup> , Jonathan P. Kressin<sup>2,3,†,‡</sup>, Anurag Kashyap<sup>1</sup>, Dilip R. Panthee<sup>3</sup>, Frank J. Louws<sup>2,4</sup>, Nuria S. Coll<sup>1,§,\*</sup> , and Marc Valls<sup>1,5,§,\*</sup>

<sup>1</sup> Centre for Research in Agricultural Genomics (CRAG), CSIC-IRTA-UAB-UB, Campus UAB, Bellaterra, 08193 Barcelona, Spain

<sup>2</sup> Department of Entomology and Plant Pathology, North Carolina State University, Raleigh, NC 27695, USA

<sup>3</sup> Department of Horticultural Science, North Carolina State University, Mountain Horticultural Crops Research and Extension Center, Mills River, NC 28759, USA

<sup>4</sup> Department of Horticultural Science, North Carolina State University, Raleigh, NC 27695, USA

<sup>5</sup> Department of Genetics, University of Barcelona, 08028 Barcelona, Spain

<sup>†</sup> Current address: Department of Breeding, Hortigenetics Research (S.E.Asia) Ltd, East-West Seed Co., Chiang Mai 50290, Thailand

<sup>‡</sup> MPM and JPK should be considered joint first authors.

<sup>§</sup> NSC and MV should be considered joint senior authors.

\* Correspondence: [nuria.sanchezcoll@cragenomica.es](mailto:nuria.sanchezcoll@cragenomica.es) or [marcvalls@ub.edu](mailto:marcvalls@ub.edu)

Received 4 September 2019; Editorial decision 11 December 2019; Accepted 20 December 2019

Editor: Peter Bozhkov, Swedish University of Agricultural Sciences, Sweden

## ABSTRACT

*Ralstonia solanacearum* is a bacterial vascular pathogen causing devastating bacterial wilt. In the field, resistance against this pathogen is quantitative and is available for breeders only in tomato and eggplant. To understand the basis of resistance to *R. solanacearum* in tomato, we investigated the spatio-temporal dynamics of bacterial colonization using non-invasive live monitoring techniques coupled to grafting of susceptible and resistant varieties. We found four ‘bottlenecks’ that limit the bacterium in resistant tomato: root colonization, vertical movement from roots to shoots, circular vascular bundle invasion, and radial apoplastic spread in the cortex. Radial invasion of cortical extracellular spaces occurred mostly at late disease stages but was observed throughout plant infection. This study shows that resistance is expressed in both root and shoot tissues, and highlights the importance of structural constraints to bacterial spread as a resistance mechanism. It also shows that *R. solanacearum* is not only a vascular pathogen but spreads out of the xylem, occupying the plant apoplast niche. Our work will help elucidate the complex genetic determinants of resistance, setting the foundations to decipher the molecular mechanisms that limit pathogen colonization, which may provide new precision tools to fight bacterial wilt in the field.

**Keywords:** Bacterial wilt, disease resistance, *Ralstonia solanacearum*, tomato, vascular pathogen, xylem.

## Introduction

Bacterial wilt caused by the *Ralstonia solanacearum* species complex is a disease of major economic importance, impacting the production of solanaceous crops, legumes, banana, ginger, and ornamentals (Hayward, 1994). *R. solanacearum* enters the roots

through wounds, colonizes the xylem tissue, moves up into the stem, and causes a rapid, permanent wilt through a combination of high bacterial density and mass production of extracellular polysaccharides (Hayward, 1991; Grimault and Prior,

1993; McGarvey *et al.*, 1999; Schell, 2000). *R. solanacearum* can move across the root following either an apoplastic pathway through the middle lamella or a pseudo-symplastic pathway via the xylem vessel lumens and axillary pits (Schell, 2000).

The management of bacterial wilt is challenging due to the aggressiveness of *R. solanacearum* and its broad geographical distribution, wide host range, and persistence in soil and water for long periods (Genin, 2010; Mansfield *et al.*, 2012). Strong quantitative resistance to bacterial wilt in tomato has been available for many decades, but has been successfully deployed only in small-fruited varieties (<200 g) and rootstocks for grafting, due to a seemingly unbreakable linkage between small fruit size and resistance (Scott *et al.*, 2005; Rivard and Louws, 2008). The Hawaii breeding line series, particularly Hawaii 7996, is the most effective source of resistance against various strains of *R. solanacearum* under different environmental conditions, and are widely used rootstocks for management of bacterial wilt (Grimault *et al.*, 1994a; Prior *et al.*, 1996; Wang *et al.*, 1998). The commercially successful hybrid Shield has been the most commonly planted rootstock for bacterial wilt resistance in North Carolina, USA, in recent years; in this location, this hybrid is highly resistant in fields with moderate disease pressure (Suchoff *et al.*, 2015) but shows an intermediate resistance under strong disease pressure (Kressin, 2018). Resistance in a mapping population derived from Hawaii 7996 (resistant) × West Virginia 700 (susceptible) has been reported to be mainly quantitative, involving two major quantitative trait loci (QTLs) located in chromosomes 12 and 6 (Bwr-12 and Bwr-6), accounting for 18–56% and 11–22% of the phenotypic variation, respectively (Wang *et al.*, 2013), and three minor loci (Bwr-3, Bwr-4, and Bwr-8). Some of these QTLs are strain- and/or environment-specific (Thoquet *et al.*, 1996a, b; Mangin *et al.*, 1999; Wang *et al.*, 2000; Carmeille *et al.*, 2006; Wang *et al.*, 2013).

Initial studies of *R. solanacearum* colonization in several resistant and susceptible tomato varieties reported that bacterial wilt resistance was associated with the capability of the plant to limit bacterial spread from the root collar to the midstem, and not with limited root invasion (Grimault and Prior, 1993; Nakaho, 1997a). However, when similar experiments were performed without wounding the roots, limited bacterial growth in Hawaii 7996 was observed in all tissues analyzed (taproot, hypocotyl, petiole and mid-stem; McGarvey *et al.*, 1999).

Studies analyzing plant colonization in grafted tomatoes showed that the bacterium was capable of crossing the graft junction into the susceptible scion. Hawaii 7996 rootstocks were the most efficient in limiting susceptible scion infection to 38% and wilting to only 10% in conditions where susceptible varieties were 100% infected and wilted (Nakaho *et al.*, 2004).

Microscopic studies of bacterial wilt in tomato described the presence of inducible physico-chemical barriers (tyloses, gums, and modifications to the primary cell wall) that seemed to limit bacterial spread in the resistant variety Caraïbo (Grimault *et al.*, 1994b). Light microscopic examination of upper hypocotyls revealed that bacterial masses were present only in the primary xylem tissues of resistant LS-89 plants (derived from the line Hawaii 7998), whereas bacteria were found in

both the primary and secondary xylem tissues of the susceptible line Ponderosa (Nakaho, 1997a). Thus, disease severity in *R. solanacearum*-infected tomato plants was proposed to correlate with the extent of bacterial invasion into the secondary xylem tissues (Nakaho, 1997a, b). This limitation of pathogen movement from the protoxylem or the primary xylem to other xylem tissues was most conspicuous in Hawaii 7996 (Nakaho *et al.*, 2004). Other studies reported that the cell walls were thicker in parenchyma and vessel cells of infected xylem tissues in resistant LS-89 than in susceptible Ponderosa or mock-inoculated plants (Nakaho *et al.*, 2000). Accumulations of electron-dense materials in vessels and parenchyma cells were also more apparent in LS-89, while Ponderosa showed necrosis in all parenchyma cells adjacent to vessels containing bacteria (Nakaho *et al.*, 2000). A recent microscopic study of the distribution of *R. solanacearum* in roots of Hawaii 7996 and the susceptible cultivar West Virginia 700 found that colonization of the root vascular cylinder was delayed and movement inside the vasculature was spatially restricted in Hawaii 7996 (Caldwell *et al.*, 2017). Together, these studies underscore the existence of a complex set of events that restrict bacterial colonization in space and time in resistant varieties of tomato. However, a systematic investigation of *R. solanacearum* invasion patterns at the whole-plant and tissue level is lacking.

Here, we applied luminescent and fluorescent bacteria for the characterization of resistance to bacterial wilt in tomato root, hypocotyl, and stem organs at the tissue level. We compared highly susceptible, moderately resistant, and highly resistant grafted tomato plants using a standard soil-based seedling grafting method and an *in vitro* grafting method. We propose an integrative model for bacterial wilt in resistant tomato lines that highlights the importance of four different ‘bottle-necks’ that limit bacterial colonization: (i) invasion of the root; (ii) vertical movement upwards to the stem; (iii) circular passage from vessel to vessel; and (iv) escape from the xylem and radial spread into the pith/cortex tissues.

## Materials and methods

### *Plant and bacterial materials and growth conditions*

The tomato (*Solanum lycopersicum*) lines used in this study were the highly susceptible commercial variety Marmande (Leroy Merlin), the moderately resistant commercial hybrid rootstock Shield (Rijk Zwaan), and the highly resistant public open-pollinated breeding line Hawaii 7996.

For *in vitro* experiments, tomato seeds were surface sterilized in 35% bleach and 0.02% Triton-X 100 for 10 minutes and then rinsed with sterile distilled water five times before sowing them on semi-solid medium [Murashige and Skoog (MS) with agar] in square culture plates (Sudelab S.L.). Plates were placed standing upright in a walk-in tissue culture growth chamber set at 22 °C under long-day light conditions.

For pot experiments, plants were grown on soil (Substrate 2, Klasmann-Deilmann GmbH) mixed with perlite and vermiculite (30:1:1) in a growth chamber: either a FITOCLIMA 1200 (Aralab) set at 27 °C, with LED lighting, or a SCLAB S.L. set at 25 °C, with fluorescence lighting. In both cases, conditions were set at 60% humidity and 12 h day/night with light intensity of 120–150  $\mu\text{mol}\cdot\text{m}^{-2}\cdot\text{s}^{-1}$ .

All assays were performed using *R. solanacearum* GMI1000 strain. The constructs PpsbA::LuxCDABE and PpsbA::GFPuv generated by Cruz *et al.* (2014) were naturally transformed into *R. solanacearum* GMI1000 to generate the luminescent and fluorescent reporter strains,

respectively. *R. solanacearum* was grown as previously described (Planas-Marquès *et al.*, 2018).

### Plant grafting

For *in vitro* grafting, seeds were sown on to sterile filter paper placed on MS-containing plates. Eight days after germination (7 for Marmande to obtain equivalent stem diameters), the cotyledons were removed and the plants were cut at a perpendicular angle 1–2 cm below the cotyledons using sterile tools. For double-grafted plants, two cuts were made 2–3 cm apart. Rootstocks and scions were transferred to fresh plates without filter paper and matched with the corresponding reciprocal tissues without any stabilizing device. Plates were kept standing upright in the growth chamber. After 10 days, successfully healed plants were either pin-inoculated with the luminescent strain of *R. solanacearum* and monitored over time or transferred to soil-containing pots and grown as described for the pathogenicity assays after acclimation for 48 h in transparent boxes (Altuna 2594005, Stewart Garden) with the vented lids opened after 24 h.

For standard grafting, plants with stems 1.5–2 mm in diameter (9 days after sowing) were grafted 2 cm below the cotyledons using a 70° angle cut and 1.6 or 2 mm diameter grafting clips (Bato Plastics B.V.). Grafted plants were kept in misted acclimation boxes in growth chambers and acclimated to light (24 h darkness, 24 h at 10% light, 24 h at 50% light) and then to ambient humidity (by opening the vents 4 days after grafting and partly opening the lid for 48 h before removing it).

### Plant inoculation and pathogenicity assays

For *in vitro* assays, 10-day-old plantlets or plantlets 10 days after grafting were pin-inoculated 1 cm below the root collar using a sterile 0.3×13 mm needle (30G×½", BD Microlance, Becton Dickinson) submerged in a 10<sup>6</sup> colony-forming units (CFU)·ml<sup>-1</sup> (OD<sub>600</sub>=0.001) *R. solanacearum* suspension. Plates were kept in a growth chamber (25 °C day, 22 °C night), and wilting symptoms were recorded and bacterial invasion visualized as described below.

For soil-drenching inoculations, plants were grown until they reached the 7–9 true leaf stage (4–5 weeks after sowing, and 5–6 weeks for grafted plants). Inoculations were performed by pouring 40 ml of a 10<sup>7</sup> CFU·ml<sup>-1</sup> (OD<sub>600</sub>=0.01) bacterial suspension on every pot after making four holes in the soil with a disposable 1 ml pipette tip. Infected plants were kept in a growth chamber set at 27 °C and scored for wilting symptoms using a scale from 0 to 4: 0=healthy plant with no wilt, 1=25%, 2=50%, 3=75%, and 4=100% of the canopy wilted. To assess shoot colonization, 4–5-week-old plants were pin-inoculated with 10 µl of a 10<sup>6</sup> CFU·ml<sup>-1</sup> suspension (Ishihara *et al.*, 2012) when indicated (see Supplementary Fig. S9 at JXB online).

### Assessment of bacterial invasion

Invasion of tomato tissues by *R. solanacearum* was assessed using the luminescent and fluorescent strains. For *in vitro* assays, pin-inoculated plants were photographed using a live imaging system (ChemiDoc Touch Imaging System, Bio-Rad) as previously described by Cruz *et al.* (2014), using a 5-minute exposure time with 3×3 sensitivity. Images were processed using Image Lab software (Bio-Rad). Inoculated soil-grown plants were uprooted and the roots were surface sterilized in water with ~5–10% bleach for at least 1 minute followed by a wash in water. Plants inoculated with the luminescent strain were sliced from the apex to the roots using a sterile razor blade. Transverse sections 1 mm thick and the two halves of longitudinal slices 1–2 cm in length were placed flat on a square plate with a misted lid and visualized using a live imaging system as described above. For each location, a 0.5 cm section was excised and incubated for at least 30 minutes in a sterile 2 ml tube with 200 µl of sterile distilled water. Luminescence was measured with a luminometer (FB 12, Berthold Detection Systems). The relative light units per second (RLU·s<sup>-1</sup>) were related to CFU·g<sup>-1</sup> tissue after dilution plating of samples and CFU counting 24 h later.

Plants inoculated with the fluorescent strain were dissected as described above and photographed using binocular microscopy with a UV

fluorescent lamp (BP330–385 BA420 filter) and a SZX16 stereomicroscope equipped with a DP71 camera system (Olympus). Quantification of mean fluorescence in the green, blue, and red channels was achieved using ImageJ software.

### Statistical analysis

Statistical analyses were performed using Statgraphics software. All statistical tests are indicated in the respective figure legends.

## Results

### *The first 'bottleneck' in R. solanacearum colonization: the root-to-shoot boundary*

Limited shoot colonization by *R. solanacearum* in resistant tomatoes has been proposed to be due to reduced spread of the bacterium from the root to the stem (Grimault and Prior, 1993; Nakaho, 1997a) and/or limited root invasion in resistant varieties (McGarvey *et al.*, 1999; Caldwell *et al.*, 2017). To clearly define the location within the plant at which resistance was acting, we made use of a constitutively luminescent *R. solanacearum* that we had previously generated (Cruz *et al.*, 2014) to follow bacterial colonization in resistant and susceptible tomato plants in a non-disruptive manner. For this, we established a miniaturized *in vitro* tomato–*R. solanacearum* infection system. Tomato seedlings were grown on semi-solid medium and pin-inoculated in the roots with the luminescent strain. This forced inoculation ensured the infection of all plants to enable the study of bacterial spread in the plant tissues. Disease symptoms were recorded as the percentage of wilted plants (Fig. 1A) and plants were photographed using a live imaging system over time. This non-destructive assay mimicked the disease symptomatology observed in field or greenhouse conditions under strong disease pressure, as indicated by the reduced wilting of the resistant line Hawaii 7996 (H7996) compared with the susceptible line Marmande (Fig. 1A). While all tomato roots in both lines were colonized 3 days post-inoculation (dpi), shoot colonization was clearly delayed and reduced in H7996 compared with Marmande (Fig. 1B). A representative photograph of the assay at 4 dpi, when the susceptible plants start to wilt, is presented in Fig. 1C. This image shows that, besides the difference in shoot colonization in the two varieties, a colonization 'bottleneck' exists in resistant plants at the root collar. In addition, luminescence intensity was lower in the roots of H7996 (Fig. 1C), indicating lower bacterial loads compared with Marmande.

### *Resistant rootstocks reduce plant invasion and limit bacterial multiplication in the roots of grafted plants*

To analyze the contribution of the roots to resistance in further detail, we grafted rootstocks and scions of Marmande and H7996. Grafts were made at the upper hypocotyl and at the root collar, and bacterial colonization and disease progression were evaluated using the luminescent *R. solanacearum* strain after pin-inoculation of the roots (Fig. 2). Resistant H7996 rootstocks hampered bacterial



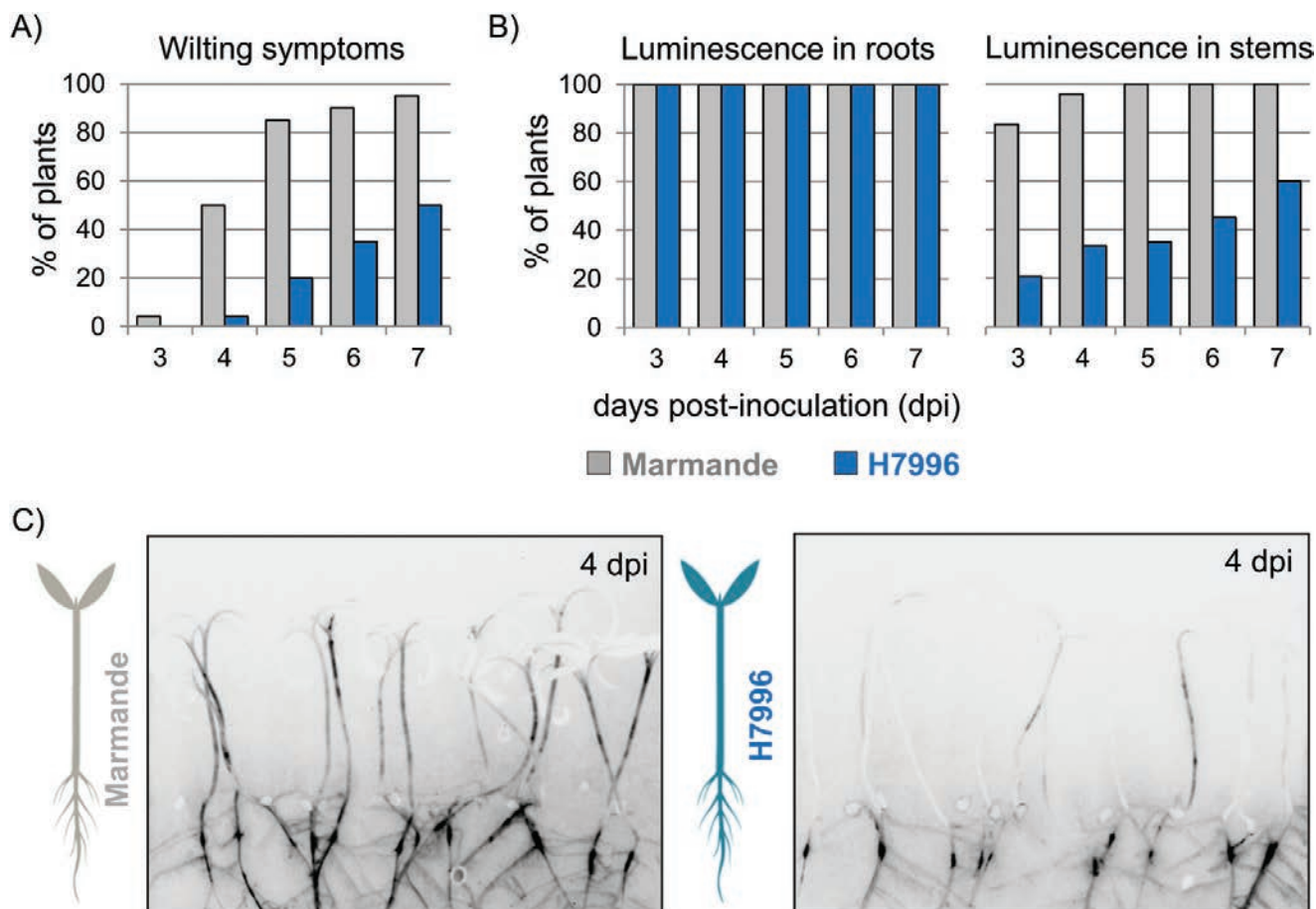


**Fig. 1.** Evaluation of *R. solanacearum* colonization in *in vitro*-grown resistant and susceptible tomato plants. Tomato seedlings of the susceptible variety Marmande and the resistant variety Hawaii 7996 (H7996) were pin-inoculated in the roots with a luminescent *R. solanacearum* strain, and bacterial colonization and wilting symptoms were evaluated over time. (A) Percentage of plants showing wilting symptoms. (B) Percentage of plants colonized in the roots and stems based on the luminescence signal emitted by the reporter strain. (C) Representative photographs showing infected seedlings at 4 days post-inoculation (dpi). The outline of the plants is due to background light from photosynthetic tissues, while luminescence is shown as darker areas. Saturation was never reached. The experiment was repeated three times with similar colonization kinetics;  $n=20$  plants per variety. (This figure is available in colour at JXB online.)

colonization of Marmande scions, while Marmande roots did not prevent colonization of H7996 scions (Fig. 2A). The presence of a resistant root system was sufficient to cause a reduction in shoot colonization, as stem luminescence was comparable in grafted plants with or without a resistant lower stem (Fig. 2B).

To strengthen these observations, we investigated root colonization by *R. solanacearum* in fully developed plants inoculated by soil drenching with the luminescent *R. solanacearum* strain. The tomato variety Shield, which is moderately resistant to bacterial wilt, was introduced in these experiments for comparison with the susceptible Marmande and highly resistant H7996 varieties. We imaged whole roots of plants of each variety obtained at 6 dpi (see Supplementary Fig. S1 at JXB online), when plants were already showing wilting symptoms (Supplementary Fig. S2). Roots of Marmande displayed strong luminescence intensity, while roots of Shield or H7996 displayed weak luminescence (Supplementary Fig. S1A). This phenomenon was consistent regardless of the intensity of the signal in the stem or the level of wilting, and correlated with our previous results obtained using the miniaturized *in vitro* system (Fig. 1).

To quantify the reduced root colonization with *R. solanacearum* in resistant varieties, we measured bacterial loads in the taproot at 3 dpi, when susceptible plants started to show symptoms. Bacterial concentrations were calculated from luminescence units (RLU) measured from taproots with a luminometer, based on the extremely high correlation ( $r^2=0.96$ ,  $P<0.0001$ ) between the luminescence emitted by the tissue samples and the bacterial CFU (Supplementary Fig. S3). This experiment revealed that the resistant rootstocks Shield and H7996 had a significantly lower mean bacterial density at the root compared with the susceptible variety Marmande, which exhibited bacterial concentrations two orders of magnitude higher (Supplementary Fig. S1B).

#### *The second 'bottleneck': resistant shoots restrict vertical movement of bacteria along the xylem*

Next, we investigated *R. solanacearum* shoot colonization in soil-inoculated fully developed Marmande, Shield, and H7996 plants. Intact 4–5-week-old plants grown in pots could not be imaged for luminescence because of size limitations and reduced sensitivity resulting from the stem

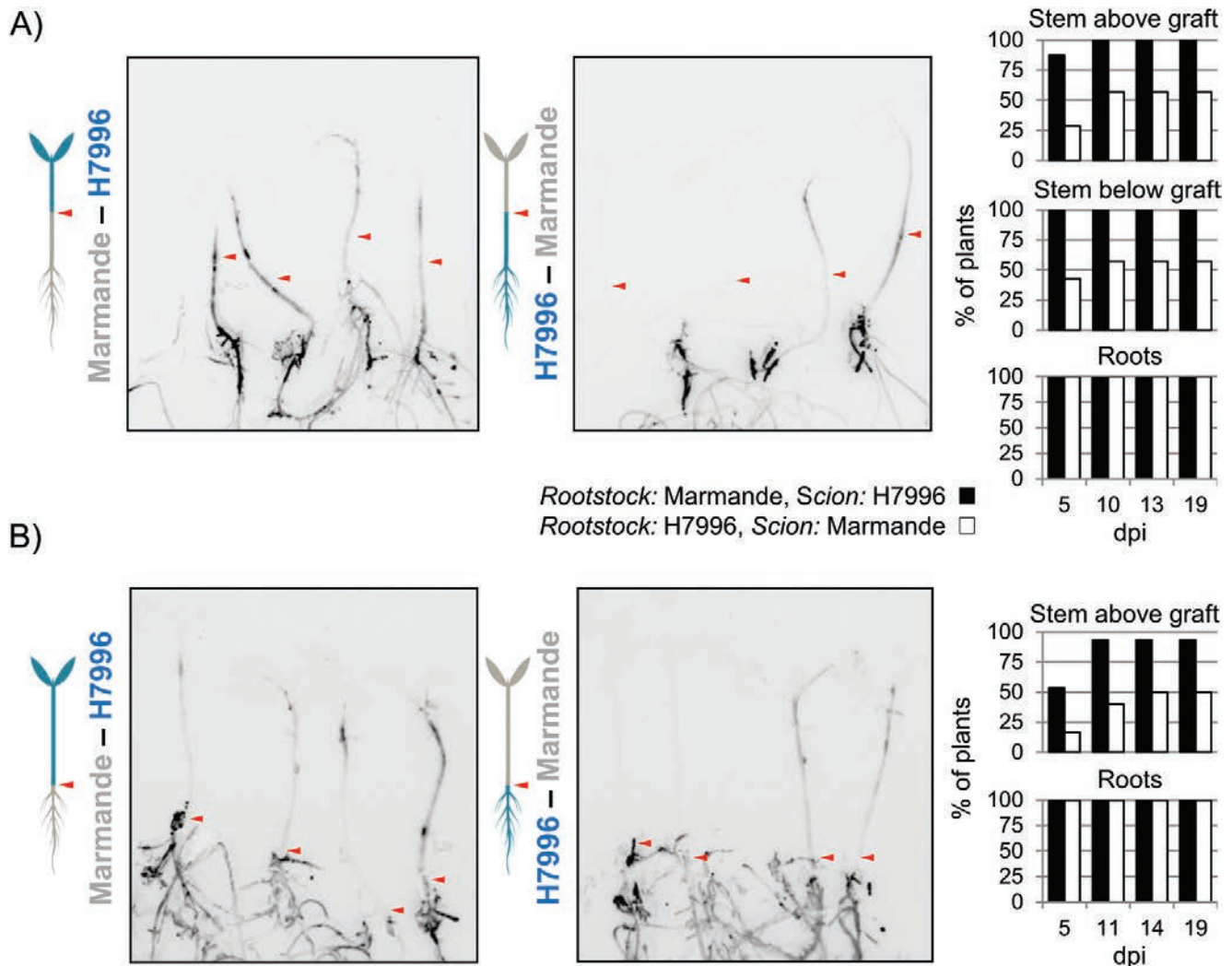


**Fig. 2.** Bacterial shoot colonization in Marmande and Hawaii 7996 (H7996) grafted plants. Seedlings of Marmande and H7996 were grafted at the mid-stem (A) or the root collar (B) and then pin-inoculated in the roots with the luminescent *R. solanacearum* strain. A representative photograph of reciprocally grafted plants is shown for each graft type at 10 dpi. The percentages of plants colonized in the roots and the tissues immediately below and above the graft are shown on the right. Arrowheads indicate the grafting junction. Both experiments were repeated at least three times, with similar colonization kinetics. In (A),  $n=7-8$  plants per grafting combination; in (B),  $n=12-15$  plants per grafting combination. (This figure is available in colour at JXB online.)

thickness. Therefore, we obtained 1–2 cm stem sections up to the third internode from plants 6 dpi, when wilting symptoms could be observed (Supplementary Fig. S2). In order to track the movement of luminescent bacteria throughout the stem, slices were taken from the top and bottom of each section and the remaining stem was divided longitudinally into two pieces. Representative photographs of all sections from a plant of each variety are presented in Fig. 3. In all cases, the luminescence matched the location of xylem bundles, indicating that bacteria were mostly confined to the xylem at this stage of infection. As expected, bacterial colonization in the shoot was much more apparent in Marmande, as indicated by the intense luminescence observed, compared with the resistant varieties, in which luminescence was in most cases detected only at a higher exposure setting (Fig. 3A Supplementary Fig. S4). In addition, the number of luminescent bundles decreased occasionally with height in the resistant varieties, whereas it remained constant in the susceptible Marmande plants. In summary, resistant tomato lines

display a lower number of colonized xylem fiber bundles and some limited bacterial vertical movement along the vessels, compared with susceptible plants (Fig. 3).

To avoid between-plant variation in colonization and directly compare the behavior of susceptible and resistant tissues when confronted with equivalent bacterial loads, we characterized *R. solanacearum* distribution in reciprocally grafted plants. We used adult plants inoculated by soil drenching and monitored the vertical movement of the luminescent bacterial strain in the hypocotyl region (where grafting was performed) at 6 dpi (Fig. 3B). Colonized vessels and luminescence were almost undetectable in self-grafted resistant H7996 (Fig. 3B), similar to what was observed in non-grafted plants (Fig. 3A). Self-grafting of the Marmande variety demonstrated that grafting *per se* did not restrict vertical movement (Fig. 3B). Colonization was hampered in H7996 scions grafted on to Marmande rootstocks, and was higher in Marmande scions than in the H7996 rootstocks grafted on to them (Fig. 3B). These results demonstrated that at comparable



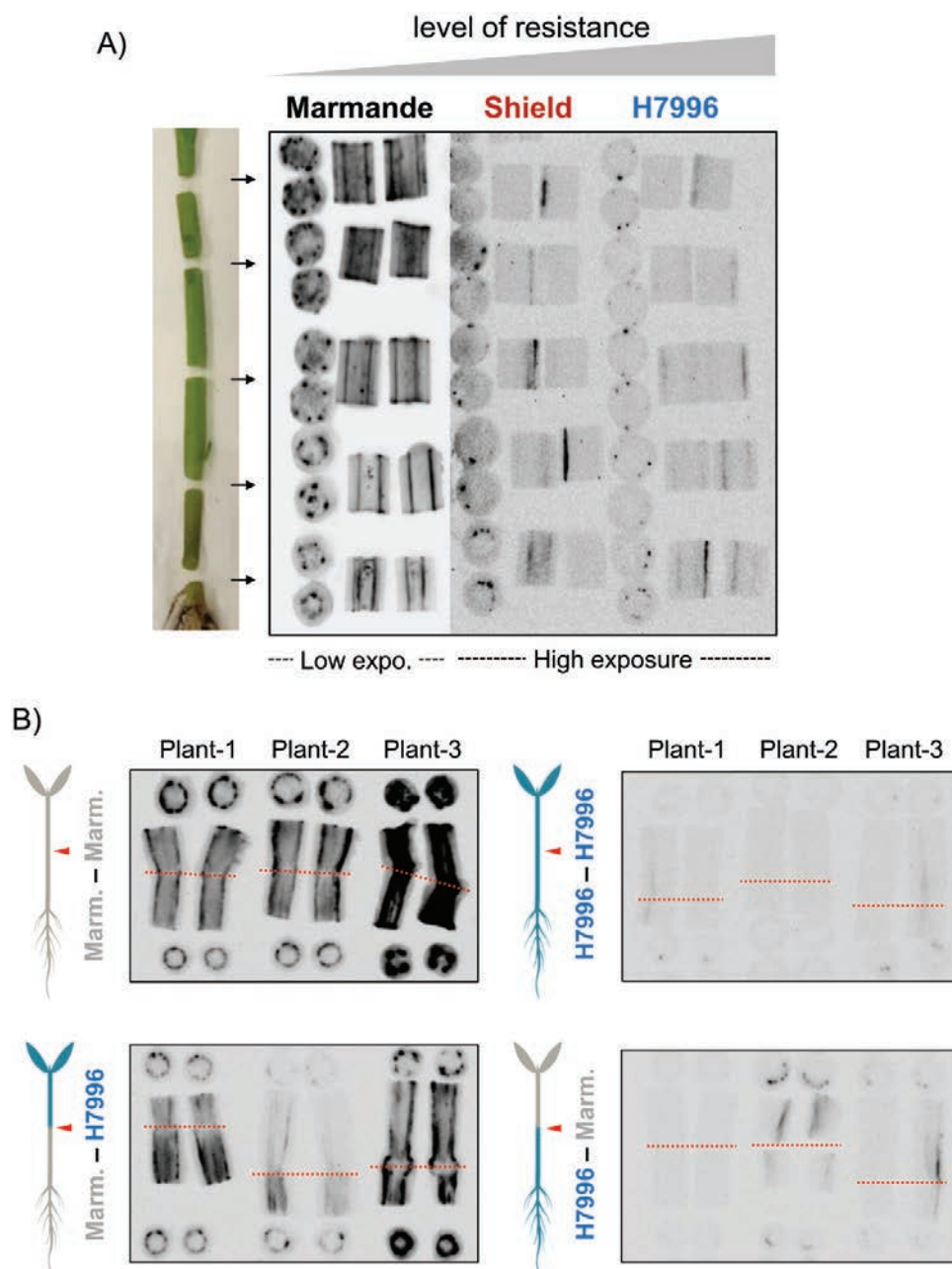


**Fig. 3.** Vertical movement of *R. solanacearum* in tomato shoots. Tomato plants (4–6 weeks old) of (A) the susceptible variety Marmande, the moderately resistant variety Shield, and the highly resistant variety H7996, and (B) reciprocally grafted Marmande and H7996 plants grown in pots were soil inoculated with luminescent *R. solanacearum*. Shoot sections were obtained at 6 dpi and photographed in a live imager. In (A), photographs show each bisected fragment and its top and bottom slices. Sections were obtained at the base of the hypocotyl, the distal hypocotyl (immediately below the cotyledons), and internodes 1, 2, and 3. In Image Lab software (Bio-Rad) the following 'High'/'Low'/'Gamma' values were used for low and high exposure settings, respectively: 10000/60/1 and 1300/60/2. In (B), sections were obtained above and below the graft junction. Arrowheads and dotted lines indicate the position of the graft junction. (This figure is available in colour at JXB online.)

bacterial concentrations, vertical colonization is inhibited and overall bacterial density is strongly reduced along the xylem of H7996 compared with Marmande. Similar results were observed in Marmande–Shield grafting combinations (Supplementary Fig. S5).

A decrease in vertical colonization could be explained by a timing artefact: if luminescence photographs were taken too soon for the bacteria to grow in the resistant scion, this would give a false impression of hampered invasion. To rule

out this possibility, we exchanged a fragment of hypocotyl between Marmande and H7996 plants in a double-grafting approach (Supplementary Fig. S6). Grafted plants contained a 2 cm fragment of the hypocotyl from one of the varieties in-between the basal and distal hypocotyl regions of the other variety (Supplementary Fig. S6A, B). The double-grafted plants were grown on soil to the 7–9 true leaf stage and were infected with the luminescent *R. solanacearum* strain (Fig. S6C–G). As expected, plants that contained the roots and

basal hypocotyl from Marmande wilted to a similar extent to plants with Marmande rootstocks (Supplementary Figs S2, S6D, E). We observed and quantified bacterial movement along the xylem in the two combinations of double-grafted plants using luminescence (Fig. 4). Marmande rootstocks were heavily colonized by *R. solanacearum*, and bacterial density decreased as soon as the pathogen crossed the first grafting junction and encountered H7996 tissue. When *R. solanacearum* moved upwards into susceptible tissue for the second time, it again multiplied to high concentrations (Fig. 4). The opposite result was observed in the reciprocal grafting: colonization with *R. solanacearum* was hampered in H7996 rootstocks, especially at 10 dpi (Supplementary Fig. S6F, G), increased in Marmande hypocotyls, and decreased when the bacteria crossed the second grafting junction and encountered H7996 tissue again (Fig. 4). Altogether, these results demonstrate the ability of H7996 to restrict vertical

movement of *R. solanacearum* along the xylem in a root-independent manner.

#### *Plant wilting is determined by a bacterial density threshold in the hypocotyl*

To trace the vertical movement of bacteria in the plant in a quantitative manner, we measured bacterial loads from the taproot to the third internode in at least 30 plants per grafting combination, sampled at different times (3–10 dpi), which showed a range of wilting symptoms. The results in Fig. 5 clearly show that, regardless of the degree of susceptibility, asymptomatic tomato plants contained bacterial concentrations generally lower than  $10^7$  CFU g<sup>-1</sup> tissue and wilted plants always showed bacterial counts above this threshold in the taproot and basal hypocotyl, although they may have had lower numbers of bacteria in the shoot above the cotyledons. Additionally, the hypocotyl

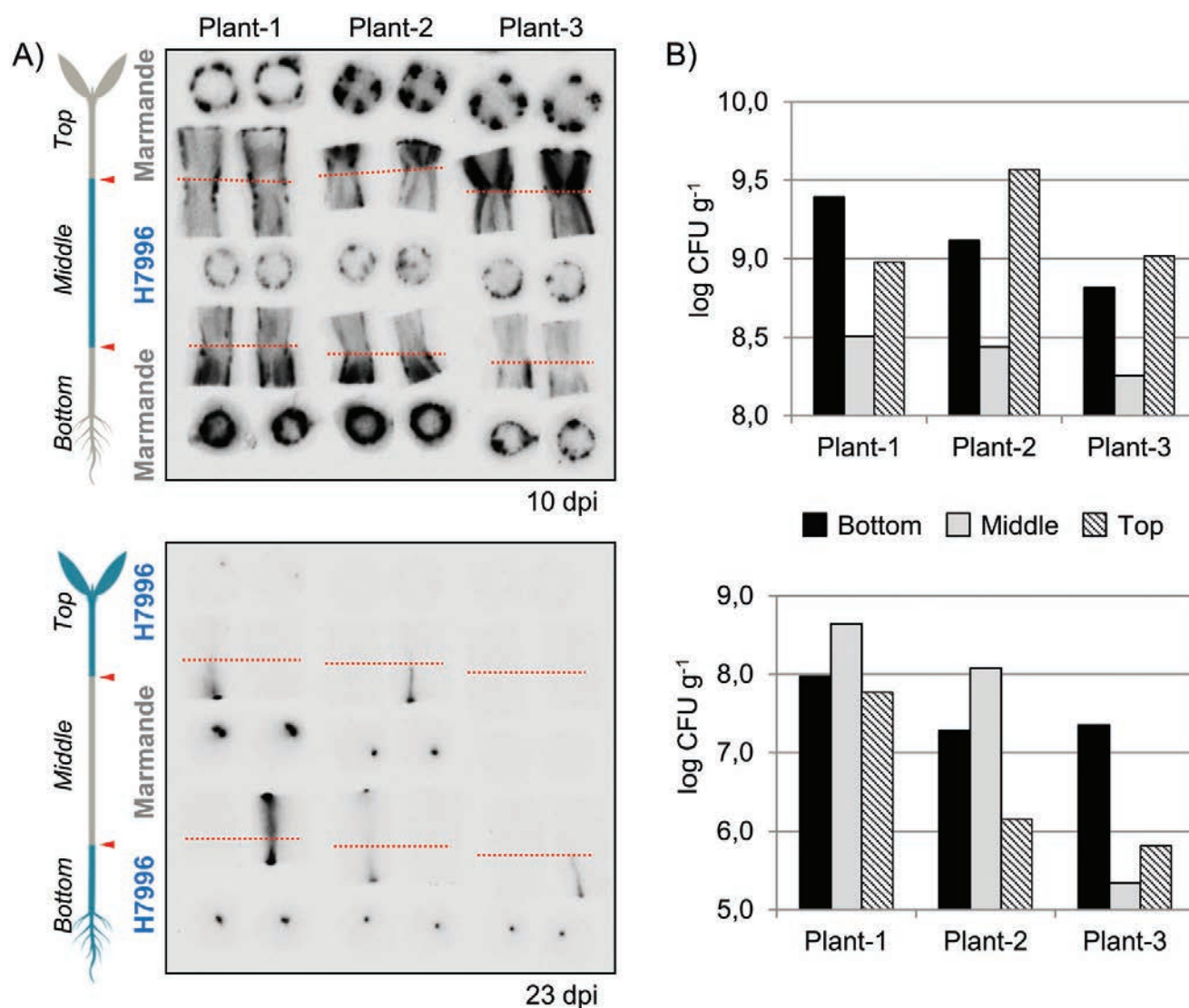


**Fig. 4.** Bacterial shoot colonization in Marmande and H7996 double-grafted plants. Seedlings of Marmande and H7996 were double-grafted in the middle of the stem, transferred to pots, and grown for 3–4 weeks. They were then inoculated with the luminescent *R. solanacearum* strain by soil drenching. (A) Shoot sections from the hypocotyl were obtained at 10 dpi (upper panel) or 23 dpi (lower panel) and photographed in a live imager. 'Bottom' and 'Top' refer to the basal and distal hypocotyl locations, respectively; 'Middle' refers to the region between the two graft junctions. Graft junctions are indicated by arrowheads and dotted lines. (B) Bacterial loads in the shoots of the plants shown in (A) were calculated from the luminescence and are expressed as log CFU g<sup>-1</sup> tissue. (This figure is available in colour at JXB online.)

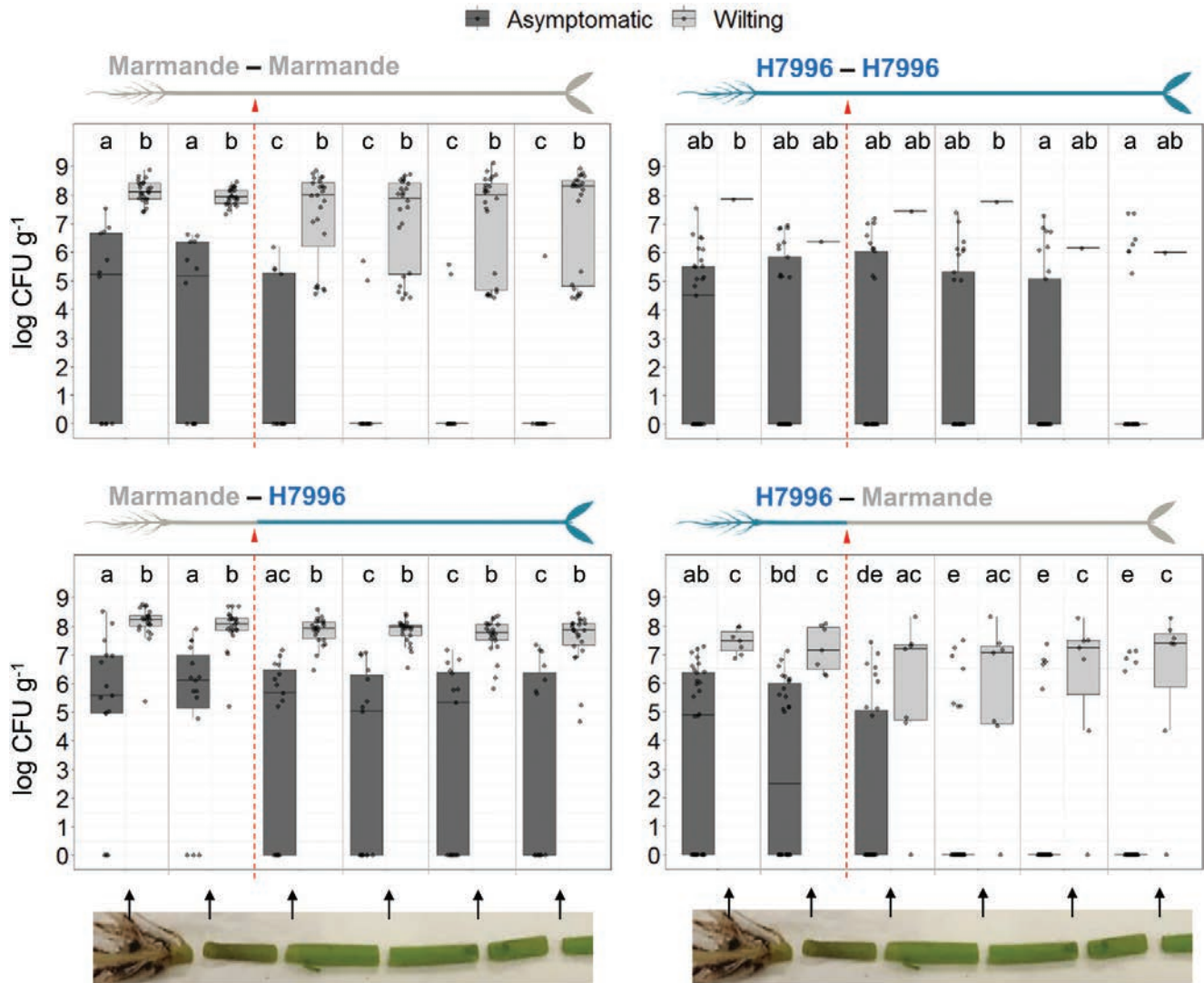


**Fig. 5.** Density of colonization of *R. solanacearum* assessed over the height of grafted tomato plants. Bacterial concentrations at different heights in the tissues of wilting (light grey) and asymptomatic (dark grey) grafted plants are shown. Luminescence was measured with a luminometer in 0.5 cm sections from at least 30 inoculated plants per grafting combination. Bacterial counts were calculated from the luminescence and are expressed as log CFU g<sup>-1</sup> tissue. Each dot represents one plant. Only one self-grafted H7996 plant wilted, hence the lack of a boxplot. Values between 0 and 4 lie below the threshold for luminescence detection (see [Supplementary Fig. S3](#)) and are considered as 0 here. From left to right, sections correspond to: taproot, basal hypocotyl, distal hypocotyl, and internodes 1, 2, and 3. The dashed line and arrowhead indicate the location of the graft junction. Different letters above each boxplot indicate statistically significant differences ( $\alpha=0.05$ , Fisher's least significant difference test). In each boxplot, the whiskers extend vertically from the hinges (the upper and lower bounds of the box) to the largest (upper whisker) or smallest (lower whisker) value no further than  $1.5 \times$  the interquartile range (the distance between the first and third quartiles) from the hinge. Dots beyond the ends of the whiskers are outliers. The horizontal band inside each box indicates the median. (This figure is available in colour at *JXB* online.)

seemed to act as an additional vertical threshold in susceptible plants, since asymptomatic Marmande plants were often colonized below the hypocotyl but the plants always wilted when the bacteria moved above the hypocotyl (Fig. 5). In contrast, when H7996 scions were grafted on to Marmande rootstocks—a situation in which the barrier in the roots of the resistant variety is absent—the tissues of the resistant variety were able to cope with high bacterial concentrations in the shoot and the plants remained asymptomatic (Fig. 5). Similar results were observed using the Shield variety (Supplementary Fig. S7).

#### *The third and fourth 'bottlenecks': resistant shoots restrict circular and radial movement of bacteria*

In order to examine the patterns of colonization within the stems at the tissue level, we inoculated 4-week-old Marmande,

H7996, and Shield plants grown in pots with a *R. solanacearum* strain constitutively expressing GFPuv (Cruz *et al.* 2014) and observed slices of the shoots with a fluorescence stereomicroscope. Fig. 6A shows representative images of transverse hypocotyl sections of the three tomato varieties at 8 dpi. At this stage, the stem xylem tissue was arranged into four primary bundles and typically two to four smaller secondary bundles, connected by the interfascicular cambium formed by xylem parenchyma and some xylary fibers. The microscopic images indicate that *R. solanacearum* can move horizontally from vessel to vessel (circular movement) and from the vessels to the adjacent parenchyma tissues (radial movement). In the susceptible variety Marmande, fluorescent bacteria occupied almost the entire vascular ring and even extended radially to the apoplast of the pith and cortical tissues (Fig. 6A). In contrast, in the resistant variety H7996 bacteria were confined to a few single



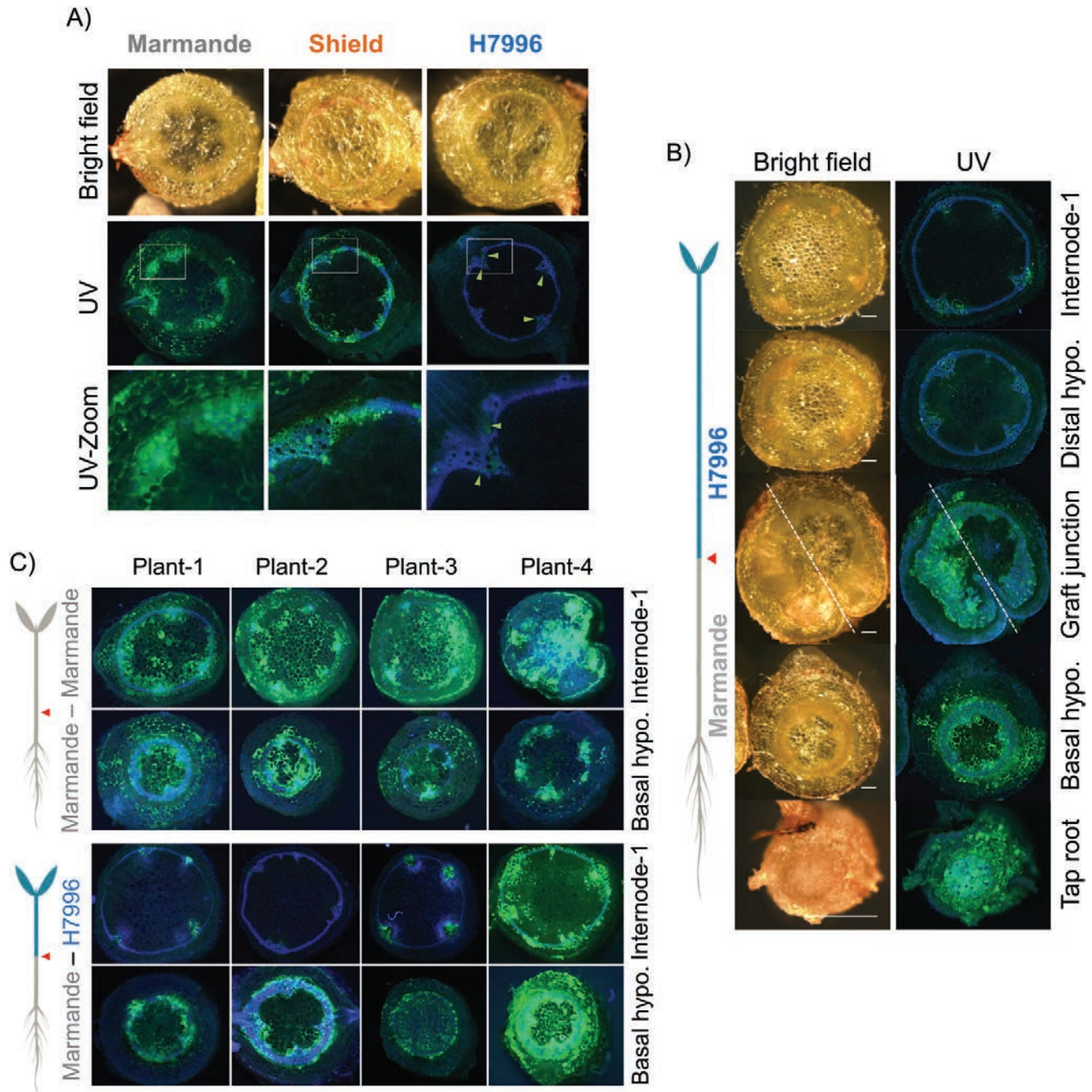


**Fig. 6.** Distribution of a fluorescent *R. solanacearum* strain in susceptible and resistant tomato shoots. (A) Plants (4–5 weeks old) of the susceptible variety Marmande, the moderately resistant variety Shield, and the highly resistant variety H7996 grown in pots were inoculated with a fluorescent *R. solanacearum* strain by soil drenching. Basal hypocotyl stem sections were obtained and photographed with a fluorescence stereomicroscope under white light (upper panels) and UV light (middle and lower panels). The lower panels show a magnification of the areas indicated with rectangles in the middle panels. The sections were visualized through a UV light filter, highlighting the autofluorescence of lignin in blue and the fluorescence emitted by the bacteria in green. Green dots correspond to clumps of bacteria. Arrowheads indicate xylem vessels with limited colonization. (B) Plants consisting of H7996 scions grafted on to Marmande rootstocks were grown and inoculated with the fluorescent strain, and transverse sections taken at different heights below and above the graft junction were photographed with a fluorescence stereomicroscope. (C) Fluorescence photomicrographs of highly colonized and fully wilted Marmande and H7996 shoots from four plants at the basal hypocotyl and the first internode.

xylem vessels (Fig. 6A). The moderately resistant variety Shield showed an intermediate phenotype, with colonization more restricted to the vascular ring and limited radial spread to neighboring tissues (Fig. 6A).

The extremely limited vertical colonization of the xylem in H7996 hampered precise characterization of the circular and radial bacterial movements in the shoots. To overcome this limitation, we grafted H7996 scions on to Marmande

rootstocks, to enable high bacterial numbers to reach the resistant stem tissues (Figs 3B, 4, 5), and inoculated the grafted plants with the fluorescent *R. solanacearum* strain by soil drenching. Examination of shoot sections obtained at different shoot heights at 8 dpi revealed extensive vertical, circular, and radial colonization of the Marmande tissues below the graft (Fig. 6B, Supplementary Fig. S8). The section at the graft junction showed that the H7996 tissues immediately blocked the

spread of the bacterium both circularly through the xylem ring and radially to the pith and cortical tissues (Fig. 6B). These restrictions became more apparent in higher sections consisting exclusively of resistant tissue (Fig. 6B, Supplementary Fig. S8).

To better compare the behavior of *R. solanacearum* in resistant and susceptible tissues, we repeated this experiment using a larger number of plants, and observed shoot sections of resistant scions that showed the most pronounced wilting with the fluorescence stereomicroscope. Fig. 6C shows these H7996 shoot sections confronted with a high bacterial inoculum introduced from the susceptible rootstock, compared with Marmande shoot sections. Notably, radial movement of bacteria from the highly colonized xylem bundles was strongly restricted in the H7996 shoots, even when the xylem tissue was highly colonized (Fig. 6C right panel). This restriction was also observed when the fluorescent *R. solanacearum* strain was directly pin-inoculated into the shoots (Supplementary Fig. S9).

Finally, we performed a time-course invasion assay in which we quantified the amounts of bacteria that were moving outside the vascular ring over time (Fig. 7). We observed that *R. solanacearum* escaped from the vascular ring as early as 5 dpi and heavily colonized the pith and cortical tissues of Marmande by 9 dpi (Fig. 7). Moreover, the amount of bacteria outside the vascular tissues was directly correlated with the extent of vascular ring colonization (Fig. 7B). This contrasted with the ability of H7996 shoots to impede the escape of the pathogen from the vascular ring (Figs 6 and 7). These results indicate that the capacity of *R. solanacearum* to radially invade the pith and cortex tissues is dependent on the degree of susceptibility of the plant and that invasion occurs as a consequence of increased colonization.

## Discussion

In this work we propose a model that relates the spatio-temporal dynamics of *R. solanacearum* invasion and proliferation in tomato plants to disease development and shows how quantitative resistance affects these parameters (Fig. 8). Systematic analysis of the progression of bacterial colonization inside the plant reveals four clear limitations of growth in resistant tomato tissues that hamper disease progression: colonization of the root, invasion of the stem vascular bundle, vertical invasion up the vessels, and invasion of the pith/cortex. The basically binary outcome of death-by-permanent-wilting caused by *R. solanacearum* in tomato seems to require the bacterium to surmount each of these physio-anatomical plant barriers, which are quantitatively determined by host resistance. We will discuss each of these four important 'bottlenecks' that can determine either host resistance or successful colonization of the plant by the bacterium.

### Restriction of root colonization

We analyzed the interaction of *R. solanacearum* with tomato using two main variables: susceptible versus resistant varieties and soil drenching versus pin-inoculation. Soil-drenching inoculations clearly reproduced the progression of disease and

the resistance observed in controlled-environment studies with comparable conditions and plant ages for the different varieties investigated (Supplementary Fig. S2; Wang *et al.*, 1998; McGarvey, Denny and Schell, 1999; Nakaho *et al.* 2004; Rivard and Louws, 2008). Root pin-inoculation of plantlets grown *in vitro* showed similar results (Fig. 1A), but bacterial concentrations reached higher numbers in the tissues of pin-inoculated resistant varieties compared with soil-drenched plants of the same resistant varieties, while the susceptible variety was highly colonized by both methods of inoculation (Figs. 1 and 2, Supplementary Fig. S1). The differences in the inoculation methods imply that resistant varieties have the ability to restrict invasion of the root—a step that is overcome when pin-inoculation of the roots is used. Our findings are in agreement with the limited bacterial growth in the taproot of H7996 observed when roots were not wounded before inoculation (McGarvey *et al.*, 1999). Additionally, *in vitro*-grafted pin-inoculated plants displayed slightly delayed colonization compared with non-grafted plants (3 dpi in Fig. 1A versus 5 dpi in Fig. 2). This difference might be linked to the developmental stage. Since older plants (in this case the grafted ones) are more developed, their cell walls might be reinforced, thus partly hindering *R. solanacearum* invasion. Finally, the pin-inoculated resistant plants that are highly colonized likely mimic the situation encountered in nature when environmental conditions are highly favorable to the pathogen. Indeed, it has been shown that even the most highly resistant varieties that are available cannot completely prevent root and stem colonization by *R. solanacearum* in greenhouse conditions (Nakaho, 1997a, b; Nakaho *et al.*, 2004).

### Restriction of vertical movement up the stem

The fact that *R. solanacearum* can colonize the stems of many resistant tomato plants when soil-drenching is used as the method of inoculation indicates that additional mechanisms of resistance must be in place in the aerial tissues to prevent wilting. Previous studies have demonstrated that bacterial counts in the stems of resistant tomato plants were always lower than those in susceptible varieties and that this was due to a limitation of pathogen movement from the primary xylem to other xylem tissues (Nakaho *et al.*, 2004). In this work, we have analyzed the vertical dimension of bacterial spread and demonstrated that resistant tissues limit movement up the xylem vessels (Fig. 3). Double-grafting experiments, in which a small portion of resistant stem was introduced into an otherwise susceptible adult plant or *vice versa*, ruled out any effect of grafting *per se* on bacterial movement inside the xylem and suggested that resistance to bacterial wilt could be due to non-diffusible xylem structures/compounds originating from the stem, as has been described for other bacterial vascular diseases (Chatterjee *et al.*, 2008).

The nature of the plant components or structures hindering root-to-shoot vertical bacterial movement is still unknown, although reports have described the presence of tyloses (evaginations of the adjacent parenchyma cells into the xylem lumen) and gums that seemed to limit bacterial spread in the xylem of bacterial wilt-resistant Caraïbo tomato plants (Grimault *et al.*, 1994b). Obstruction of xylem vessels with gums and tyloses



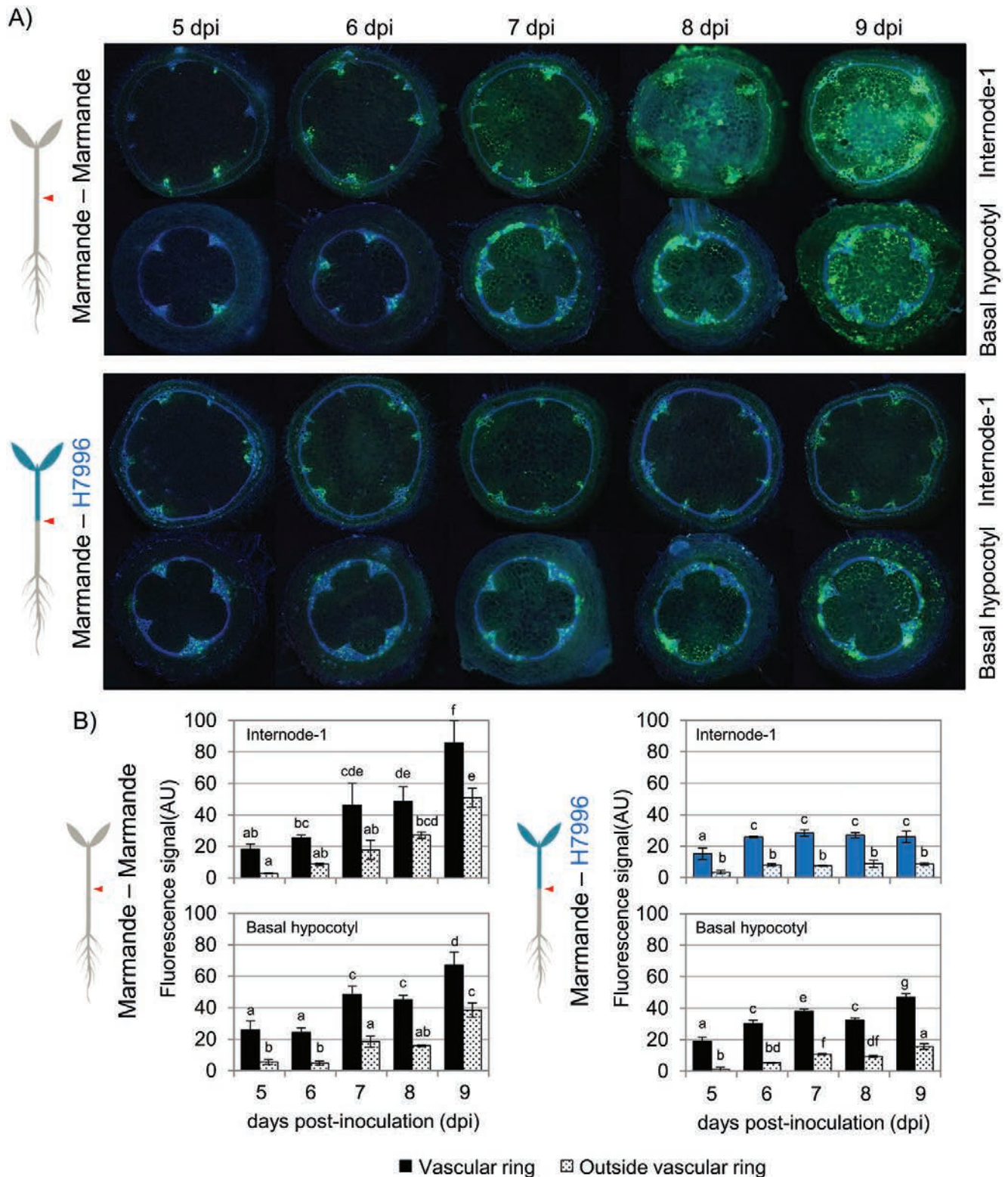


**Fig. 7.** Time course of invasion of the fluorescent *R. solanacearum* strain in grafted tomato shoots. (A) Fluorescence photomicrographs of self-grafted Marmande and plants consisting of H7996 scions grafted on to Marmande rootstocks inoculated with the fluorescent *R. solanacearum* strain. Sections were taken at the basal hypocotyl and the first internode. The sections were visualized through a UV light filter, highlighting the autofluorescence of lignin in blue and the fluorescence emitted by the bacteria in green. (B) Quantification of fluorescence signal (AU, arbitrary units) within and outside the vascular ring in the basal hypocotyl and the first internode of plants from each stage of the infection shown in (A). Three biological replicates ( $n=3$ ) were used. Data presented are means  $\pm$  SE. Different letters above the bars indicate statistically significant differences ( $\alpha=0.05$ , Fisher's least significant difference test).

is a common plant response to restrict systemic infection by vascular pathogens (VanderMolen *et al.*, 1987; Grimault *et al.*, 1994; Cl  rivel *et al.*, 2000; Sun *et al.*, 2013). For instance,

vascular gelation is considered an essential part of *Fusarium* wilt resistance in carnation (Baayen and Elgersma, 1985). Tyloses have been similarly proposed to restrict pathogen movement



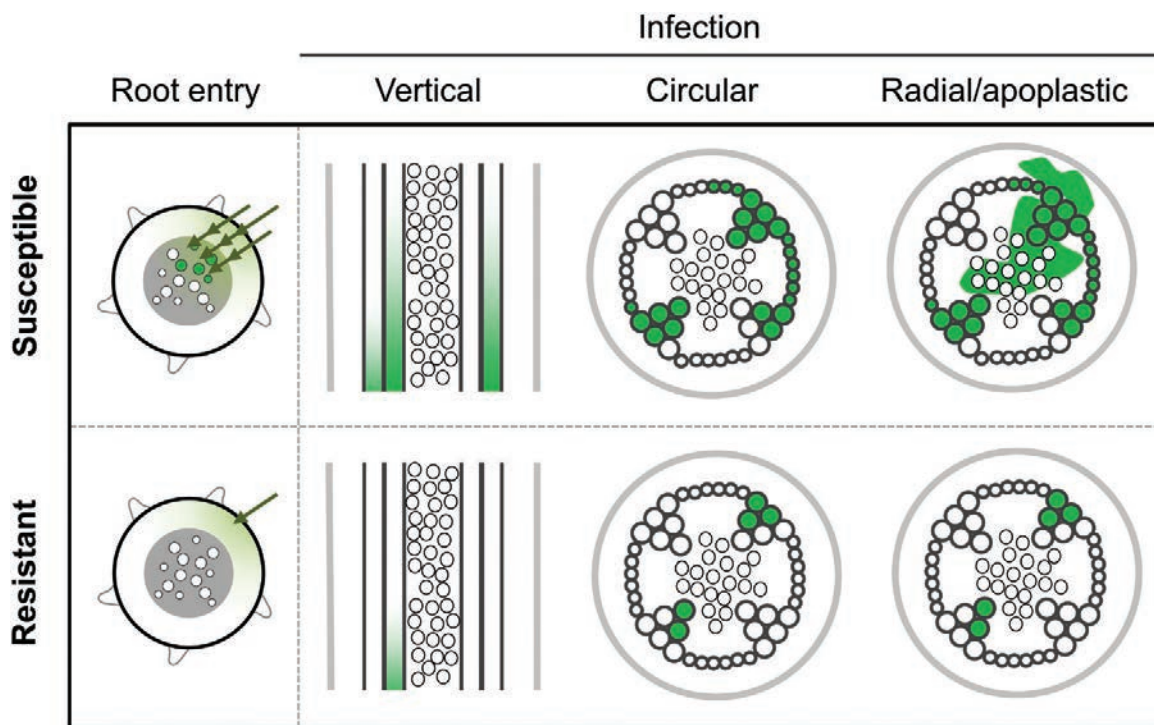


**Fig. 8.** Model of the tomato-*R. solanacearum* pathosystem in susceptible and resistant germplasm. Schematic representation of the colonization movements of *R. solanacearum* (shown in green) in susceptible and resistant tomato tissues.

in tomato cultivars resistant to the vascular pathogens *Fusarium oxysporum*, *Verticillium albo-atrum*, and *R. solanacearum* (Hutson and Smith, 1980; VanderMolen et al., 1987; Grimault et al., 1994b). Although Grimault et al. (1994b) correlated the presence of tyloses in Caraïbo to the limitation of *R. solanacearum* spread, in another resistant cultivar (LS-89) the formation of these structures was neither induced by the pathogen nor seemed to affect bacterial colonization (Nakaho, 1997a). Similarly, tyloses formed in grapevines in response to *Xylella fastidiosa* infection were found to be more abundant in susceptible cultivars and did not affect the vertical movement of the pathogen (Sun et al., 2013). These observations suggest that the role of tyloses in vascular pathogen restriction may be cultivar- or species-specific and/or depend on the lignification status of the plant host. The results presented here and our recent finding that *R. solanacearum*-tolerant potato lines also induced the development of tyloses upon infection (Ferreira et al., 2017) seem to indicate that these structures are important components of bacterial wilt resistance in solanaceous plants.

#### Restriction of vascular bundle invasion and the bacterial density threshold

Restriction of *R. solanacearum* colonization in the stems of H7996 is also achieved by limiting the horizontal movement of the pathogen from vessel to vessel (referred to hereafter as circular movement). Confinement of *R. solanacearum* to primary xylem vessels has been observed in the stems and roots of different resistant tomato cultivars compared with susceptible ones (Nakaho, 1997a; Nakaho et al., 2004; Caldwell et al., 2017). A similar correlation between *R. solanacearum* movement between stem vessels, bacterial growth, and the level of

susceptibility has been observed in potato (Cruz et al., 2014; Ferreira et al., 2017). Similarly, *X. fastidiosa* has been shown to invade 10 times fewer stem vessels and exhibit lower population densities in resistant grapevine cultivars (Chatterjee et al., 2008). These results indicate that limitation of circular movement in the xylem ring is a conserved mechanism for resistance against vascular bacterial pathogens. Restriction of *R. solanacearum* to the primary xylem vessels could explain why resistant tomato plants often remain asymptomatic. If a blockage occurs in the primary xylem, which is largely non-functional after the secondary xylem has been produced (Esau, 1977), flow conduction could occur undisturbed through the uninfected secondary xylem.

In susceptible plants, *R. solanacearum* can move horizontally through the xylem ring by directly degrading the cell walls of primary xylem vessels or pit membranes in the secondary xylem vessels (Wallis and Truter, 1978; Grimault et al., 1994b; Vasse et al., 1995; Nakaho et al., 2000). To counter such circular movement, plants have evolved structural defenses that are induced upon attack by vascular pathogens, involving the deposition of various coating materials to reinforce the walls of xylem vessels, pit membranes, and surrounding parenchyma cells. Vascular coatings are thicker in resistant tomato cultivars infected with *R. solanacearum*, and this may be the cause of the observed limitation of bacterial movement between xylem tissues (Nakaho et al., 2000, 2004). The detailed description of the process we present here will be crucial to decipher the genetic determinants and the composition of these vascular coatings, which remain unknown.

Restriction of circular movement in the stem is a very efficient confinement strategy, since it is still acting when high loads of bacteria are forced into the stem through root

inoculations using H7996 scions grafted on to Marmande rootstocks (Fig. 6). However, there seems to be an upper limit of bacterial inoculum above which this restriction is no longer effective (see plant 4 in the lower panel of Fig. 6C). This finding is in agreement with previous reports showing that delivery of a high *R. solanacearum* inoculum ( $10^9$  CFU  $\text{ml}^{-1}$ ) directly into tomato stems overcomes resistance (Nakaho, 1997b). This idea relates to the concept of a density threshold in the interaction between tomato and *R. solanacearum*. Earlier observations established the onset of bacterial wilt symptoms at a bacterial density in the stem of between  $10^6$  and  $10^8$  CFU  $\text{g}^{-1}$  fresh tissue (Grimault and Prior, 1994; Nakaho, 1997a; Huang and Allen, 2000; Nakaho *et al.*, 2004). We have characterized this threshold systematically by assessing bacterial densities throughout the plant in large populations of grafted tomato plants with varying resistance. We conclude that, in both resistant and susceptible varieties, symptoms invariably appear when bacterial populations in the hypocotyl exceed a threshold of  $10^7$  CFU  $\text{g}^{-1}$  tissue (Fig. 5, Supplementary Fig. S7). Plating dilutions of homogenized tissues to establish bacterial counts is labor intensive, but we show that light emission from tissues inoculated with a luminescent strain is a useful alternative measure of bacterial counts (correlation coefficient  $r^2=0.96$ ). Since bacterial density and distribution are predictive of the degree of disease resistance, we have started to use luminescent strains to screen potato germplasm for resistance to bacterial wilt as a way of aiding the breeding process (Cruz *et al.*, 2014; Ferreira *et al.*, 2017).

#### *Restriction of radial movement out of the xylem into the pith and cortex*

Our work has also revealed a fourth limitation restricting bacterial spread in the tissues of resistant tomato varieties: restriction of radial movement of *R. solanacearum* out of the xylem into the adjacent parenchyma cells in the pith and cortex (Figs 6 and 7). These metabolically active cells are in close contact with the xylem vessels through the pits and are thought to be pivotal for the induction of plant defenses against pathogens within the xylem, although very little is known about the mechanisms regulating this response.

Earlier studies detected widespread *R. solanacearum* colonization of stem parenchyma cells in susceptible tomato varieties at late stages of infection, when plants showed extensive wilting (Nakaho, 1997a; Nakaho *et al.*, 2000). These cells appeared to be filled with bacteria and displayed necrosis and signs of degeneration. In contrast, in resistant tomato varieties, necrotic parenchyma cells containing bacteria were observed only occasionally (Nakaho *et al.*, 2000). Our data confirm these observations and additionally show that parenchyma cell invasion starts at early times in susceptible plants (5 dpi in our experimental setup) and spreads massively through the pith at later time points (8–9 dpi, Fig. 7A). In contrast, colonization remains limited to xylem vessels in resistant tomato (Fig. 6).

As was the case for the circular bacterial movements described above, radial restriction of movement out of the xylem in resistant varieties could be partially overridden by grafting to susceptible rootstocks that enabled high bacterial densities

to access resistant tissues, as can be seen in some of the images in Fig. 6C. This observation is in agreement with a previous report showing that when high bacterial inocula ( $10^9$  CFU  $\text{ml}^{-1}$ ) were used, *R. solanacearum* could also be detected in the parenchyma cells of resistant tomato (Nakaho, 1997b). Thus, restriction of radial bacterial movement is no longer effective when the bacterial density exceeds a certain threshold.

Structural changes in cell walls and pit membranes in response to *R. solanacearum* infection are more conspicuous in resistant tomato (Nakaho *et al.*, 2000). Thus, bacteria may be prevented from escaping the xylem in resistant tomato by a combination of inducible structural defense mechanisms that may appear later and/or with less intensity in susceptible lines, rendering them ineffective to restrict colonization. Interestingly, slightly decreased invasion was also observed in the susceptible hypocotyls of the Marmande–H7996 grafting combination (Fig. 7). This finding could be explained by a cross-talk between the scion and rootstock. This interaction could trigger the expression of putative defense-related genes or genes that reinforce plant cell wall structures in the susceptible rootstock. Alternatively, defense-related or structure-remodeling proteins might be secreted by the resistant scion and reinforce nearby tissues (in this case the susceptible hypocotyl). These two explanations seem plausible given the existing vascular connectivity between the grafted tissues. Indeed, transcriptional reprogramming occurs even in rootstocks and scions of the tomato/potato heterografting system (Zhang *et al.*, 2019). Additionally, peroxidases and other cell wall remodeling enzymes, such as glycosyl hydrolases, are secreted into the xylem by the resistant line H7996 upon *R. solanacearum* infection (M. Planas-Marquès, F. Kaschani, M. Kaiser, R. A. L. van der Hoorn, M. Valls, N. Sánchez-Coll, unpublished results). Hence, increased lignification and cell wall reinforcement could also take place in neighboring susceptible tissues in grafted plants.

#### *An integrated model for tomato resistance to bacterial wilt*

As we have discussed, in the past three decades, various laboratories have aimed to understand how resistant tomato varieties restrict *R. solanacearum* colonization and remain asymptomatic despite having relatively high bacterial loads. The fact that the defenses are not limited to a particular plant site, as the bacterium has to traverse different tissues to reach the xylem, has complicated this work. A question that arises is whether the xylem is the final destination of *R. solanacearum*.

Here, we have defined the barriers encountered by *R. solanacearum* as it progresses from the soil into the xylem and have found that, after systematic spread through the xylem, the final destination of the bacterium may be extensive invasion of the stem apoplast. It has already been suggested that vascular bacteria use plant cell wall degradation products as carbon and energy sources (Chatterjee *et al.*, 2008; Genin and Denny, 2012). It is tempting to speculate that *R. solanacearum* has evolved not only to colonize the xylem but also to escape from it to obtain richer sources of nutrition from metabolically active parenchyma cells, facilitating the death and decay of

infected plants and thus allowing the pathogen to spread in the soil and move into the next host.

In conclusion, here we clearly define four ‘bottlenecks’ to bacterial colonization in tomato and demonstrate that the degree of resistance of a given variety correlates with its capacity to restrict bacterial movement at these locations. The ability to restrict bacterial movement at all four anatomical points makes H7996 the most resistant tomato line, consistent with the polygenic nature of its resistance (Wang *et al.*, 2013), which has made introgression breeding extremely difficult (Scott *et al.*, 2005; Hanson *et al.*, 2016). We believe that this integrative study will serve as a first step towards the characterization of the genetic and molecular determinants that govern resistance at each stage of *R. solanacearum* invasion.

## Supplementary data

Supplementary data are available at *JXB* online.

Fig. S1. Measurement of bacterial root colonization in tomato plants.

Fig. S2. Symptom development over time in grafted tomato plants.

Fig. S3. Correlation between luminescence and bacterial counts.

Fig. S4. *R. solanacearum* vertical movement in tomato shoots as seen by different intensities of exposure.

Fig. S5. *R. solanacearum* vertical movement in the shoots of Marmande and Shield grafted plants.

Fig. S6. Disease evolution over time in double-grafted plants.

Fig. S7. *R. solanacearum* bacterial density assessed over the height of grafted tomato plants.

Fig. S8. Circular and radial invasion of *R. solanacearum* in susceptible and resistant tomato shoots.

Fig. S9. Invasion of *R. solanacearum* in susceptible and resistant pin-inoculated tomato shoots.

## Acknowledgements

This work was funded by projects AGL2016-78002-R to NSC and MV, and RyC 2014-16158 to NSC (Spanish Ministry of Economy and Competitiveness). JPK was supported partially by the National Institute of Food and Agriculture of the United States Department of Agriculture grant nos 2011-51181-30963 and 2016-51181-25404 to FJL and DRP, and a Monsanto Graduate Fellowship award through North Carolina State University. AK was supported by a Netaji Subhas international fellowship from the Indian Council of Agricultural Research. The authors acknowledge financial support from the Severo Ochoa Program for Centers of Excellence in R&D (SEV-2015-0533) and the CERCA Program from the Catalan Government (Generalitat de Catalunya).

## Author contributions

MPM, JPK, DRP, FJL, NSC and MV designed the research; MPM, JPK, and AK performed the research; MPM, JPK, AK, NSC, and MV analyzed data; MPM, JPK, DRP, FJL, NSC, and MV interpreted data; MPM, JPK, NSC, and MV wrote the manuscript.

## References

- Baayen RP, Elgersma DM. 1985. Colonization and histopathology of susceptible and resistant carnation cultivars infected with *Fusarium oxysporum* f. sp. *dianthi*. *Netherlands Journal of Plant Pathology* **91**, 119–135.
- Caldwell D, Kim BS, Iyer-Pascuzzi AS. 2017. *Ralstonia solanacearum* differentially colonizes roots of resistant and susceptible tomato plants. *Phytopathology* **107**, 528–536.
- Carmeille A, Caranta C, Dintinger J, Prior P, Luisetti J, Besse P. 2006. Identification of QTLs for *Ralstonia solanacearum* race 3-phylo type II resistance in tomato. *Theoretical and Applied Genetics* **113**, 110–121.
- Chatterjee S, Newman KL, Lindow SE. 2008. Cell-to-cell signaling in *Xylella fastidiosa* suppresses movement and xylem vessel colonization in grape. *Molecular Plant-Microbe Interactions* **21**, 1309–1315.
- Clérivet A, Déon V, Alami I, Lopez F, Geiger J-P, Nicole M. 2000. Tyloses and gels associated with cellulose accumulation in vessels are responses of plane tree seedlings (*Platanus × acerifolia*) to the vascular fungus *Ceratocystis fimbriata* f. sp. *platani*. *Trees* **15**, 25–31.
- Cruz AP, Ferreira V, Pianzola MJ, Siri MI, Coll NS, Valls M. 2014. A novel, sensitive method to evaluate potato germplasm for bacterial wilt resistance using a luminescent *Ralstonia solanacearum* reporter strain. *Molecular Plant-Microbe Interactions* **27**, 277–285.
- Esau K. 1977. *Anatomy of seed plants*. New York: Wiley.
- Ferreira V, Pianzola MJ, Vilaró FL, Galván GA, Tondo ML, Rodríguez MV, Orellano EG, Valls M, Siri MI. 2017. Interspecific potato breeding lines display differential colonization patterns and induced defense responses after *Ralstonia solanacearum* infection. *Frontiers in Plant Science* **8**, 1–14.
- Genin S. 2010. Molecular traits controlling host range and adaptation to plants in *Ralstonia solanacearum*. *New Phytologist* **187**, 920–928.
- Genin S, Denny TP. 2012. Pathogenomics of the *Ralstonia solanacearum* species complex. *Annual Review of Phytopathology* **50**, 67–89.
- Grimault V, Anais G, Prior P. 1994a. Distribution of *Pseudomonas solanacearum* in the stem tissues of tomato plants with different levels of resistance to bacterial wilt. *Plant Pathology* **43**, 663–668.
- Grimault V, Gélle B, Lemattre M, Prior P, Schmit J. 1994b. Comparative histology of resistant and susceptible tomato cultivars infected by *Pseudomonas solanacearum*. *Physiological and Molecular Plant Pathology* **44**, 105–123.
- Grimault V, Prior P. 1993. Bacterial wilt resistance in tomato associated with tolerance of vascular tissues to *Pseudomonas solanacearum*. *Plant Pathology* **42**, 589–594.
- Grimault V, Prior P. 1994. Grafting tomato cultivars resistant or susceptible to bacterial wilt - analysis of resistance mechanisms. *Journal of Phytopathology* **141**, 330–334.
- Hanson P, Lu SF, Wang JF, *et al.* 2016. Conventional and molecular marker-assisted selection and pyramiding of genes for multiple disease resistance in tomato. *Scientia Horticulturae* **201**, 346–354.
- Hayward AC. 1991. Biology and epidemiology of bacterial wilt caused by *Pseudomonas solanacearum*. *Annual Review of Phytopathology* **29**, 65–87.
- Hayward AC. 1994. The hosts of *Pseudomonas solanacearum*. In: Hayward AC, Hartman GL, eds. *Bacterial wilt: the disease and its causative agent, Pseudomonas solanacearum*. Wallingford: CAB International, 9–24.
- Huang Q, Allen C. 2000. Polygalacturonases are required for rapid colonization and full virulence of *Ralstonia solanacearum* on tomato plants. *Physiological and Molecular Plant Pathology* **57**, 77–83.
- Hutson RA, Smith IM. 1980. Phytoalexins and tyloses in tomato cultivars infected with *Fusarium oxysporum* f.sp. *lycopersici* or *Verticillium albo-atrum*. *Physiological Plant Pathology* **17**, 245–257.
- Ishihara T, Mitsuhashi I, Takahashi H, Nakaho K. 2012. Transcriptome analysis of quantitative resistance-specific response upon *Ralstonia solanacearum* infection in tomato. *PLoS One* **7**, e46763.
- Kressin JP. 2018. Resistance dynamics of tomato and the *Ralstonia solanacearum* species complex: assessing resistance mechanisms and methods for practical evaluation in breeding and pathology programs within a diverse set of rootstock and founder germplasm. PhD thesis, North Carolina State University, Raleigh, USA. <https://repository.lib.ncsu.edu/bitstream/handle/1840.20/35399/etd.pdf?sequence=1&isAllowed=y>



- Mangin B, Thoquet P, Olivier J, Grimsley NH.** 1999. Temporal and multiple quantitative trait loci analyses of resistance to bacterial wilt in tomato permit the resolution of linked loci. *Genetics* **151**, 1165–1172.
- Mansfield J, Genin S, Magori S, et al.** 2012. Top 10 plant pathogenic bacteria in molecular plant pathology. *Molecular Plant Pathology* **13**, 614–629.
- McGarvey JA, Denny TP, Schell MA.** 1999. Spatial-temporal and quantitative analysis of growth and EPS I production by *Ralstonia solanacearum* in resistant and susceptible tomato cultivars. *Phytopathology* **89**, 1233–1239.
- Nakaho K.** 1997a. Distribution and multiplication of *Ralstonia solanacearum* (synonym *Pseudomonas solanacearum*) in tomato plants of resistant rootstock cultivar LS-89 and susceptible Ponderosa. *Annals of the Phytopathological Society of Japan* **63**, 83–88.
- Nakaho K.** 1997b. Distribution and multiplication of *Ralstonia solanacearum* in stem-inoculated tomato rootstock cultivar LS-89 resistant to bacterial wilt. *Annals of the Phytopathological Society of Japan* **63**, 341–344.
- Nakaho K, Hibino H, Miyagawa H.** 2000. Possible mechanisms limiting movement of *Ralstonia solanacearum* in resistant tomato tissues. *Journal of Phytopathology* **148**, 181–190.
- Nakaho K, Inoue H, Takayama T, Miyagawa H.** 2004. Distribution and multiplication of *Ralstonia solanacearum* in tomato plants with resistance derived from different origins. *Journal of General Plant Pathology* **70**, 115–119.
- Planas-Marquès M, Bernardo-Faura M, Paulus J, Kaschani F, Kaiser M, Valls M, van der Hoorn RAL, Coll NS.** 2018. Protease activities triggered by *Ralstonia solanacearum* infection in susceptible and tolerant tomato lines. *Molecular & Cellular Proteomics* **17**, 1112–1125.
- Prior P, Bart S, Leclercq S, Darrasse A, Anais G.** 1996. Resistance to bacterial wilt in tomato as discerned by spread of *Pseudomonas (Burholderia) solanacearum* in the stem tissues. *Plant Pathology* **45**, 720–726.
- Rivard CL, Louws FJ.** 2008. Grafting to manage soilborne diseases in heirloom tomato production. *HortScience* **43**, 2104–2111.
- Schell MA.** 2000. Control of virulence and pathogenicity genes of *Ralstonia solanacearum* by an elaborate sensory network. *Annual Review of Phytopathology* **38**, 263–292.
- Scott JW, Wang JF, Hanson PM.** 2005. Breeding tomatoes for resistance to bacterial wilt, a global view. *Acta Horticulturae* **695**, 161–172.
- Suchoff D, Gunter C, Schultheis J, Louws FJ.** 2015. On-farm grafted tomato trial to manage bacterial wilt. *Acta Horticulturae* **1086**, 119–128.
- Sun Q, Sun Y, Walker MA, Labavitch JM.** 2013. Vascular occlusions in grapevines with Pierce's disease make disease symptom development worse. *Plant Physiology* **161**, 1529–1541.
- Thoquet P, Olivier J, Sperisen C, Rogowsky P, Laterrot H, Grimsley N.** 1996a. Quantitative trait loci determining resistance to bacterial wilt in tomato cultivar Hawaii7996. *Molecular Plant-Microbe Interactions* **9**, 826–836.
- Thoquet P, Olivier J, Sperisen C, Rogowsky P, Prior P, Anais G, Mangin B, Bazin B, Nazer R, Grimsley N.** 1996b. Polygenic resistance of tomato plants to bacterial wilt in the French West Indies. *Molecular Plant-Microbe Interactions* **9**, 837–842.
- VanderMolen GE, Beckman CH, Rodehorst E.** 1987. The ultrastructure of tylose formation in resistant banana following inoculation with *Fusarium oxysporum* f.sp. *cubense*. *Physiological and Molecular Plant Pathology* **31**, 185–200.
- Vasse J, Frey P, Trigalet A.** 1995. Microscopic studies of intercellular infection and protoxylem invasion of tomato roots by *Pseudomonas solanacearum*. *Molecular Plant-Microbe Interactions* **8**, 241–251.
- Wallis FM, Truter SJ.** 1978. Histopathology of tomato plants infected with *Pseudomonas solanacearum*, with emphasis on ultrastructure. *Physiological Plant Pathology* **13**, 307–310.
- Wang JF, Hanson P, Barnes J.** 1998. Worldwide evaluation of an international set of resistance sources to bacterial wilt in tomato. In: Prior P, Allen C, Elphinstone J, eds. *Bacterial wilt disease: molecular and ecological aspects*. Berlin: Springer, 269–275.
- Wang JF, Ho FI, Truong HTH, Huang SM, Balatero CH, Dittapongpitch V, Hidayati N.** 2013. Identification of major QTLs associated with stable resistance of tomato cultivar 'Hawaii 7996' to *Ralstonia solanacearum*. *Euphytica* **190**, 241–252.
- Wang JF, Olivier J, Thoquet P, Mangin B, Sauviac L, Grimsley NH.** 2000. Resistance of tomato line Hawaii7996 to *Ralstonia solanacearum* Pss4 in Taiwan is controlled mainly by a major strain-specific locus. *Molecular Plant-Microbe Interactions* **13**, 6–13.
- Zhang G, Mao Z, Wang Q, Song J, Nie X, Wang T, Zhang H, Guo H.** 2019. Comprehensive transcriptome profiling and phenotyping of rootstock and scion in a tomato/potato heterografting system. *Physiologia Plantarum* **166**, 833–847.

## **ANNEX II**

## **A primary cell wall cellulose-dependent defense mechanism against vascular pathogens revealed by time-resolved dual-transcriptomics**

Alexandra Menna<sup>1\*</sup>, Susanne Dora<sup>1\*</sup>, Gloria Sancho-Andrés<sup>1\*</sup>, Anurag Kashyap<sup>2</sup>, Debora Gasperini<sup>3</sup>, Martijn Rep<sup>4</sup>, Nuria Sánchez-Coll<sup>2</sup>, Clara Sánchez-Rodríguez<sup>1</sup> †

### **Affiliations**

<sup>1</sup>Department of Biology, ETH Zürich, 8092 Zürich, Switzerland

<sup>2</sup>Centre for Research in Agricultural Genomics (CRAG), CSIC-IRTA-UAB-UB, 08193 Barcelona, Spain

<sup>3</sup>Department of Molecular Signal Processing, Leibniz Institute of Plant Biochemistry, 06120 Halle (Saale), Germany

<sup>4</sup>Department of Phytopathology, University of Amsterdam, Amsterdam, The Netherlands

\* Equal contribution

† Corresponding author: [clara\\_sanchez@ethz.ch](mailto:clara_sanchez@ethz.ch)



## Abstract

### Background

Cell walls (CWs) are protein-rich polysaccharide matrices essential for plant growth and environmental adaptation. The CW constitutes the first physical barrier as well as a primary source of sugars for plant microbes, such as the vascular pathogen *Fusarium oxysporum* (Fo). Fo colonizes roots, advancing through the plant primary CWs towards the vasculature, where it grows causing devastation in many crops. The pathogenicity of Fo and other vascular microbes relies on their capacity to reach and colonize the xylem. However, little is known about the root-microbe interaction before the pathogen reaches the vasculature and the role of the plant CW during this process.

### Results

Using the pathosystem Arabidopsis-Fo5176, we show dynamic transcriptional changes in both fungus and root during their interaction. One of the earliest plant responses to Fo5176 was the downregulation of primary CW synthesis genes. We observed enhanced resistance to Fo5176 in Arabidopsis mutants impaired in primary CW cellulose synthesis. Previous studies showed an induction of ectopic lignification, accumulation of defence-related phytohormones, and dwarfism in primary CW cellulose synthesis deficient plants, potentially explaining their resistance to Fo5176. We confirmed that Arabidopsis roots deposit lignin in response to Fo5176 infection but we show that lignin-deficient mutants were as susceptible as wildtype plants to Fo5176. Genetic impairment of jasmonic acid biosynthesis and signaling did not alter Arabidopsis response to Fo5176, whereas impairment of ethylene signaling did increase vasculature colonization by Fo5176. This ethylene signaling interruption attenuated the observed resistance while maintaining the dwarfism observed in primary CW cellulose-deficient mutants.

### Conclusions

Our study provides significant insights on the dynamic root-vascular pathogen interaction at the transcriptome level and the vital role of primary CW cellulose during defence response to these pathogens. These findings represent an essential resource for the generation of plant resistance to Fo that can be transferred to other vascular pathosystems.

### Keywords

Arabidopsis, *Fusarium oxysporum*, *Ralstonia solanacearum*, plant-pathogen interaction, dual-time course transcriptomics, cellulose, ethylene, defence response

## Introduction

All living organisms must adapt to their environment to survive and reproduce in their habitats. This is particularly challenging for sessile organisms like plants, which rely on remarkable plasticity to adjust to different and simultaneous external cues. In addition, plant cells are immobile, so each of them is fully equipped with sophisticated molecular artillery to perceive and respond to incoming stresses [1]. The plant cell wall (CW), a rigid yet dynamic polysaccharide-protein matrix, is an essential player in plant responses to external stimuli. The CW acts as the first physical barrier to outside invaders or stresses and as a source of signals to trigger downstream responses upon perception of incoming danger [2]. Moreover, plant adaptation to the environment relies on accurate developmental changes that depend on the precise remodeling of the CWs [1, 3]. Therefore, plant CW alteration directly influences growth and stress response pathways. This is especially relevant during plant response to microbes who mainly live in the apoplast, like the root vascular pathogen *Fusarium oxysporum* (Fo).

Fo is a soil-borne root-infecting hemibiotrophic fungal pathogen, responsible for the devastation of many economically-important crop species such as banana, tomato, cotton, and cabbage [4]. Fo attaches to the outer epidermal root cell layer to find wounds or weak points to penetrate these outer cell layers [4, 5]. Hyphae then advance towards the xylem, where fungal proliferation blocks water and nutrient uptake, causing wilting and eventually plant death. Because of these dramatic symptoms, most studies characterize Fo infections within aerial plant tissues, while the essential root-colonization stage remains poorly understood due to the difficulty of studying this plant organ. Moreover, this infection phase before Fo reaches the xylem is described as asymptomatic based on the absence of aerial infection symptoms, despite the fact that roots begin to exhibit evidence of response to stress at this stage [4]. Various phytohormones, including salicylic acid (SA), jasmonic acid (JA), and ethylene (ET), among others, have been implicated in plant response to various Fo strains [6–8]. Fo is genetically diverse, with different strains grouped based on narrow host ranges [4, 9]. Despite our knowledge of Fo host specificity, details of the infection strategies and plant defence mechanisms are still unclear for many Fo-plant pathosystems. Fo5176 infects the model plant *Arabidopsis thaliana*, constituting an ideal pathosystem to study root colonization of vascular pathogens [10, 11]. Some studies have used this pathosystem to provide relevant information regarding root-mediated and plant tissue-specific defence responses to Fo. Novel plant players were identified to confer resistance to Fo5176, including reactive oxygen species (ROS) production [12], as well as enhanced auxin and abscisic acid

signaling [13]. The conclusions from these studies reflect plant responses during the biotrophic colonization phase (1 and 2 days after treatment (dpt) with the spores in [12, 13]), or when Fo is potentially transitioning from a biotrophic to a necrotrophic lifestyle (6 dpt in [13]). Therefore, a deeper understanding of the Fo infection progression inside the root at a higher temporal and spatial resolution is necessary. In this path towards the root vasculature, Fo passes through plant CWs. Therefore, as other microbes, Fo modifies and degrades the plant CW polysaccharides during host colonization [14]. As of yet, many aspects of this essential plant CW degradation and modification processes remain largely unknown.

Plant root cells, with the exception of the xylem and the differentiated endodermis cells, have only primary CWs. Cellulose is one of the most abundant polymers in primary CWs, and provides the majority of the load-bearing strength of the plant CW [15, 16]. Cellulose is synthesized as glucan chains at the plasma membrane by cellulose-synthase (CESA) complexes, which extrude these chains into the apoplast guided by cortical microtubules [17, 18]. Mutations in the primary CW CESA subunits, like *prc1-1* impaired in CESA6, lead to significant reduction in cellulose content that results in abnormal cell elongation and dwarfism [19, 20]. Similar phenotypes are observed in plants compromised in the activity of the apoplastic chitinase-like 1 (CTL1), the glycosylphosphatidylinositol (GPI)-linked COBRA (COB), and the PM-bound endo-1,4- $\beta$ -glucanase KORRIGAN (KOR), also required for primary CW-cellulose synthesis [19, 21–23]. The biological response to genetic or chemically-induced primary CW-cellulose deficiency includes ectopic lignification, upregulation of stress-related genes, and accumulation of the phytohormones JA, ET and SA [24]. These transcriptional and cellular changes have been associated with increased resistance to pathogens of primary CW cellulose-deficient mutants, as lignin deposition restricts pathogen infection [25] and JA, ET and SA are well-known players in plant defence [7, 26, 27]. However, evidence connecting primary CW cellulose mutants with biotic stress response has only been described for the *cesa3/cev1* mutant, impaired in the primary CW CESA subunit CESA3 [28, 29]. The constitutive activation of JA/ET signaling pathways in the *cesa3/cev1* mutant, typically associated with primary CW cellulose-deficiency, was demonstrated to contribute to its enhanced resistance to three leaf-biotrophic pathogens [30]. Deeper connections linking primary CW perturbations, fluxes in hormonal regulation, and pathogen defence remain to be fully clarified. Moreover, an abundance of studies characterized defence mechanisms activated in response to leaf-infecting pathogens, while the role of hormones during root-infecting pathogen invasion is largely under-studied [31]. Besides, the complex interaction between Fo and its host indicates a communication at the

root primary CWs precisely fine-tuned at a high temporal and spatial resolution, which remains largely unknown.

To investigate the Fo-host interaction prior to xylem colonization, we performed a time course dual transcriptome study on Fo5176-infected *Arabidopsis* roots at the different colonization stages that we classified by confocal microscopy. Our data uncovered a fast and relevant role of primary CW cellulose modulation in plant response to Fo. We hypothesized that primary CW cellulose-deficiencies would directly impact Fo5176 infection either by facilitating fungal colonization due to the weakened CWs, or by restricting fungal proliferation due to increased physical (lignin) and/or chemical (hormones) defences. By further elucidating ways through which primary CW-cellulose mutants mitigate vascular pathogen invasion, we shed light on the inextricably-linked connections between primary CWs, phytohormone-signaling, and defence response activation.

## Results

### ***Arabidopsis* root and Fo5176 transcriptomics reveal temporal adaptations during their interaction**

To study the Fo5176 infection progression at the microscopic level we imaged the roots of hydroponically- and plate-grown *Arabidopsis* plants exposed to the fluorescently labelled strain Fo5176 pGPD::GFP [32] over a period of 6 days (Figure 1A). Microconidia germination and attachment to the root were observed at 1 dpt. Fungal hyphae entered the roots at 2 dpt, mainly at emerging lateral roots, colonizing the apoplastic space of the epidermis layer. At 3 dpt the hyphae were visible in the cortex both inter- and intracellularly. At 4 dpt the first fungal vascular penetrations were observed in some plants and all roots had at least one vascular penetration event at 6 dpt.

We then explored the temporal transcriptional changes in both Fo5176 and *Arabidopsis* roots at the identified colonization stages (Figure 1A). For each time point, mock-treated roots were included and four biological replicates were generated. All samples were collected at the middle of the day to reduce the influence of the circadian clock in the results. As an additional reference, we included Fo5176-treated roots for 30 minutes, when no microconidia germination was observed (0dpt), and Fo5176 was grown exponentially *in vitro*. By Illumina sequencing of 3'mRNA libraries, we obtained more than 234 billion reads from all samples, which were mapped to the *Arabidopsis* TAIR10 gene models [33] and the Fo5176 genome [10] (Supplementary Table 2). These data have been deposited in the NCBI Gene Expression

Omnibus [34]. For the early time points of 0 dpt and 1 dpt, reads mapping to the fungal genome were heavily underrepresented (0.07% and 0.35%, respectively, of total reads; Supplementary Table 2). The fungal reads steadily increased from 2 dpt on, reaching 50% at 3 dpt (Figure 1B). The number of fungal mapped reads correlated with the increased fungal biomass quantified during root colonization (Figures 1B and C). Only those genes represented with more than 3 counts per million (CPM) across all samples and conditions (almost 58% of the *Arabidopsis* genes and 46% of Fo5176; Supplementary Table 2) were considered to be actively expressed and included in further analysis.

To determine overall changes in the host and the pathogen transcriptomes over time, a multi-dimensional scaling (MDS) analysis was performed. Following this approach, 5 samples from the plant mapped reads that do not cluster with the rest of the samples from the same time point were identified: 0 dpt mock, 1 dpt Fo, 3 dpt Fo, 4 dpt Fo and 6 dpt Fo (Supplementary Figure 1). After the removal of these 5 samples, we continued with the analysis of at least 3 independent biological replicates for each investigated time point under control and infection condition (Figure 1D). Fo5176 mapped reads from 0 and 1 dpt were excluded from the analysis due to the insufficient amount of reads obtained for those time points. In both organisms, the infected samples formed clusters distinct from control-treated samples starting at 2 dpt, and the largest difference between infected clusters was observed between 2 dpt and 3 dpt (Figure 1D and 1E). These results suggest different behavior of plant and pathogen transcript profiles when the fungus reaches the root cortex (2 to 3 dpt; Figure 1A). Moreover, Fo5176 transcriptomes at 4 and 6 dpt were very similar, coinciding with the fungal entrance in the vasculature. This indicates that the fungal gene expression pattern changes along with continued growth towards the vasculature and accumulation of fungal biomass in the root. We continued the transcriptomic study by comparing gene expression at all time points; i.e. 0 - 6 dpt for *Arabidopsis* and 2 - 6 dpt for Fo5176 (Figures 1F and 1G). These analyses revealed a total of 7053 plant genes and 2902 fungal genes being differentially expressed (DEGs) at least at one time point (adj. p-value < 0.05,  $\log_2FC > |1|$ ; Figures 1F and 1G, Tables 1 and 2, respectively). The majority of these DEGs were downregulated in the host and upregulated in Fo5176 (Figure 1F and 1G). To validate the expression data, for each organism we randomly picked six genes expressed at different expression levels and performed RT-qPCR using *de novo* generated RNA samples (Supplementary Figure 2).

## ANNEX

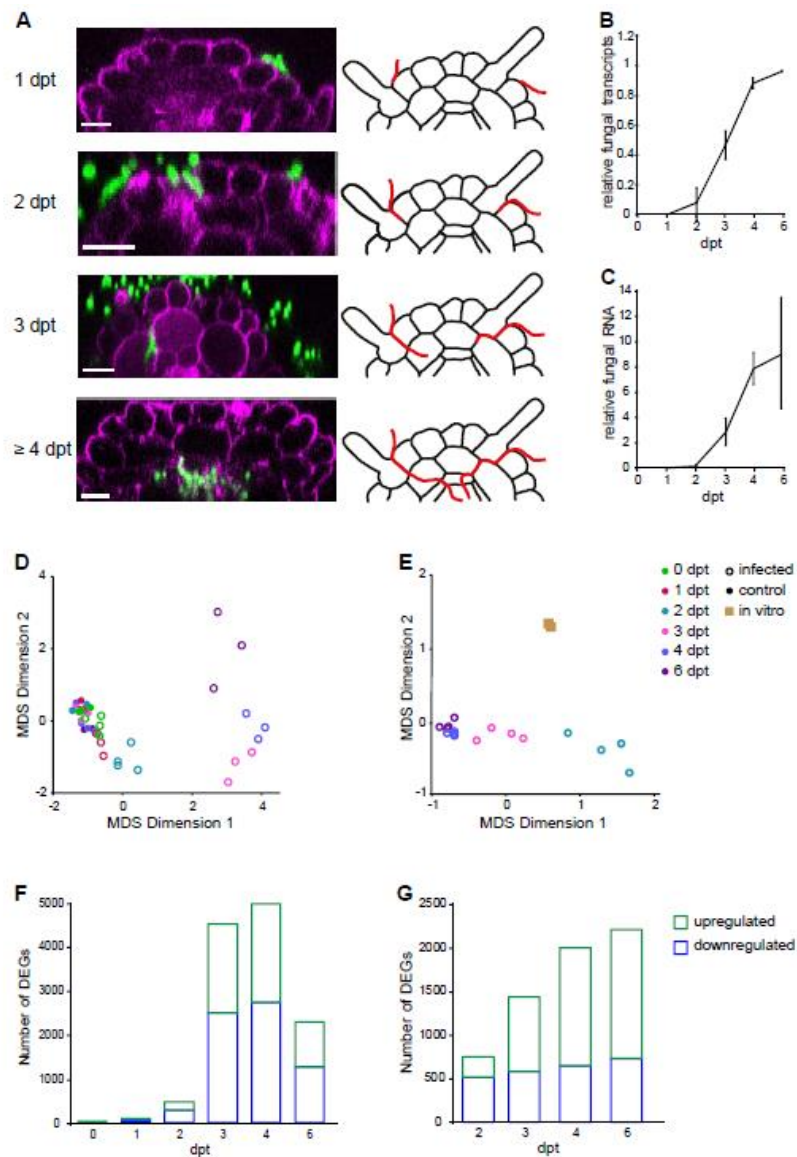


**Figure 1. Fo5176 infection of Arabidopsis roots leads to temporal dynamic changes in the plant and the fungal transcriptomes.** (A) Microscopic analysis of root infection by Fo5176 over 4 days after microconidia treatment (dpt). Left panels: Representative confocal images of Fo5176 (green) colonizing the different cell layers of Arabidopsis roots (magenta). Scale bars: 20µm. Right panels: Schematic view of cross sections of Fo5176 (red) infected roots illustrating the confocal images in the left panels. Each image represents a minimum of 9 hydroponically-infected and 4 plate-infected roots/dpt. (B) Percentage of transcripts based on the RNA-seq analysis mapped to the fungal reference genome at all investigated time points using a splice aware sequence aligner (STAR). Values represent the mean  $\pm$  standard error of four biological replicates. (C) Fo5176 biomass determination over time based on RNA and determined by RT-qPCR using a fungus-specific primer (Fo5176  $\beta$ -Tub) relative to an Arabidopsis reference gene (At GAPDH). Values represent the mean  $\pm$  standard error of four biological replicates. (D) and (E) Multidimensional scaling analysis (MDS) of transcriptional profiles of

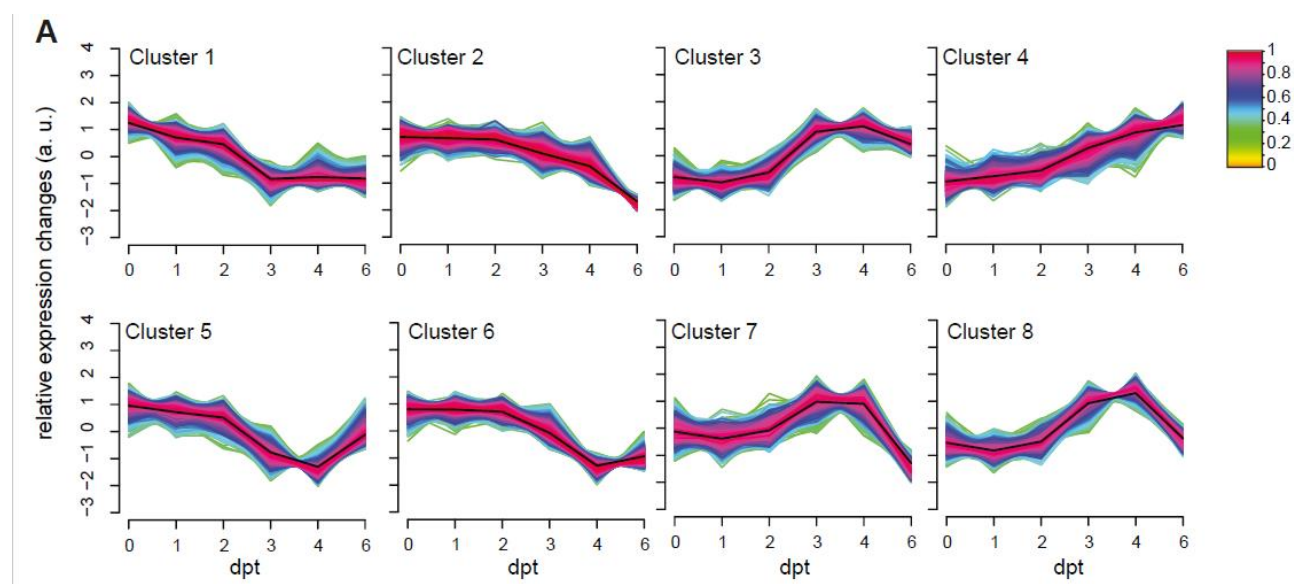


Arabidopsis (D) and Fo5176 (E). (F) and (G) Number of differentially expressed genes (DEGs) up- (green) or downregulated (blue) at each root colonization stage (0-6dpt) in Arabidopsis (F) and Fo5176 (G).

DEGs were further analyzed for their expression pattern over time by fuzzy c-means clustering [35]. This soft clustering approach was selected to enable the sorting of genes to centroids depending on the similarity of their expression profile over time and their membership to the cluster. Based on the membership threshold, a gene can be present in more than one cluster. The fungal DEGs grouped in 5 expression clusters showing different temporal gene expression patterns (Table 1 and Supplementary Figure 3A): increase (Cluster 1 and 2), increase-decrease (Cluster 3 and 4), or decrease (Cluster 5). 5 fungal DEGs were excluded from clustering, as they do not show any expression *in planta* (g14801, g5058, g8821, g8822, g8995). We observe that the gene expression profiles of different clusters peak at different days, suggesting that the genes contained in these clusters serve a function during that specific stage of the infection. We aimed to further identify the transcriptomic profile of fungal metabolism involved in plant cell wall modification. Due to limited Gene Ontology (GO)-annotations available for Fo5176, we focused our analyses on the plant CW-related genes within these clusters. We further separated glycosyl hydrolases that might act directly on cell wall moieties from other cell wall related functions (Table 1). The majority of the genes encoding for cell wall related genes clustered together in Cluster 3 (Supplementary Figure 3B), whose expression progressively increases until 4dpt, when the fungus reaches the vasculature.

Fuzzy clustering of the gene expression profiles for the Arabidopsis DEGs identified 8 expression clusters showing different temporal gene expression patterns (Figure 2A): decrease (Cluster 1 and 2), increase (Cluster 3 and 4), decrease-increase (Cluster 5 and 6), or increase-decrease (Cluster 7 and 8). To obtain a picture of the biological processes associated with root response to Fo5176, each cluster was subjected to a GO term enrichment analysis (Table 2) [36]. This analysis revealed that downregulated genes are enriched in biological processes related to cell wall synthesis and remodeling: plant-type cell wall biogenesis (GO:0009832), plant-type cell wall organization (GO:0009664), plant-type secondary cell wall biogenesis (GO:0009834), and cell wall polysaccharide metabolic process (GO:0010383). Among others, we detected downregulation of seven out of the ten cellulose synthase genes (CESAs): CESA1, CESA2, CESA3, CESA4, CESA5, CESA7 and CESA8 [37]; other cellulose synthesis genes: CTL1 and CTL2 [21], and more than 20

arabinogalactan proteins (AGPs) [38]. Cluster 1 was particularly enriched in these GO categories (Figure 2B and Table 2). Conversely, upregulated genes from 3 dpt showed overall enrichment in biological processes associated with defence (Table 2): plant-type hypersensitive response (GO:0009626), camalexin metabolic process (GO:0052317), innate immune response (GO:0045087), defence response to fungus (GO:0050832), JA, ET and SA responses (GO:0009753, GO:0009723, GO:0009751), and JA-mediated signaling (GO:2000022, GO:0009867). Among them, we found chitinase family proteins associated with the CAZY-family GH19 (Table 2), potentially needed for defence against fungal pathogens; several plant defensins [39]; genes reported to be involved in plant immune responses: WRKY33 [40], PR4 [41], PEPR1 [42]; peroxidases (PRX33, PRX34; [43] and hormone-related genes like JAZs and ERFs transcription factors [44–46]. Many of these genes clustered together in Cluster 3 (Figure 2B, Table 2). Taken together, these results suggest that infected *Arabidopsis* roots undergo major transcriptional reprogramming leading to overall repression of growth followed by activation of stress and defence responses.



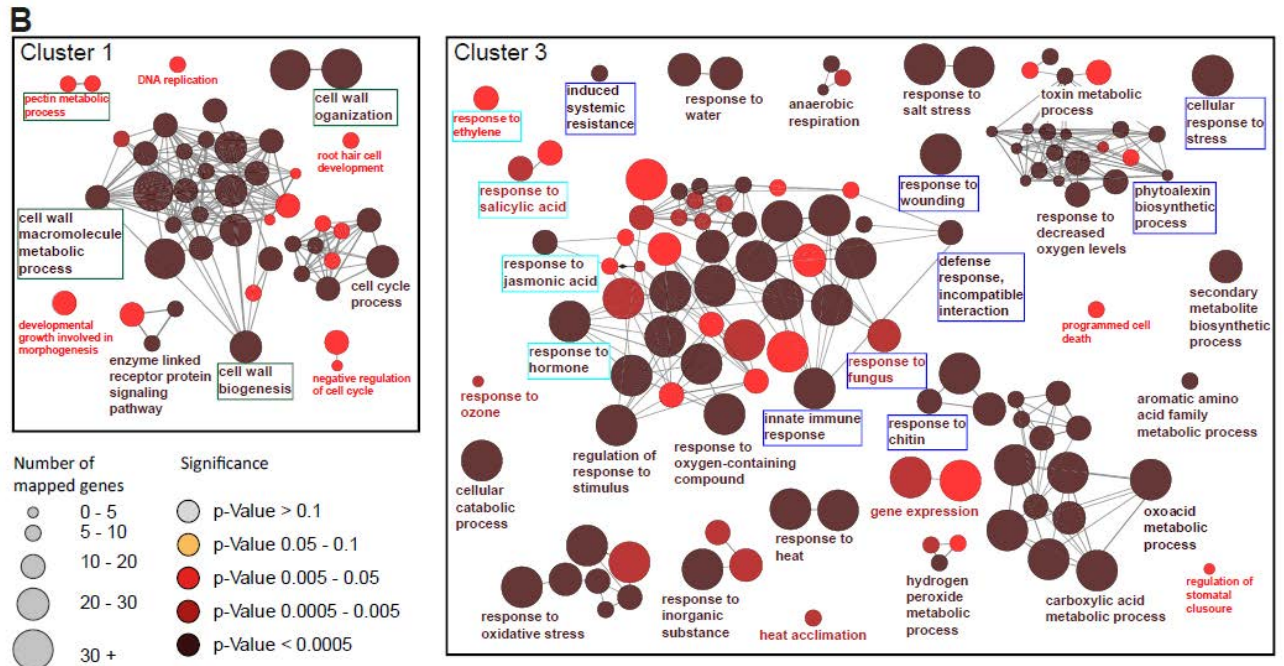


**Figure 2. Temporal dynamics of Arabidopsis DEGs during infection reveal a significant alteration of cell wall biology and hormonal process in response to Fo5176. (A) Clusters of Arabidopsis coexpressed DEGs during infection using fuzzy c-means clustering. (B) Biological Processes Enriched in Selected Clusters from (A) using GO enrichment analysis. Enriched GO-terms are depicted as circles, lines connecting the circles show relation between GO-terms. In each group of GO-terms, the most significant category is labelled with the GO-term description. The genes downregulated over time during Fo5176 root colonization (coexpressed in Cluster 3 in (A)) are enriched in plant cell wall biological processes (left panel, green). The Cluster 7 (right panel) represents general defence responses (dark blue) and responses to hormonal signalling (light blue).**

## **Down-regulation of primary cell wall cellulose synthesis results in enhanced Fo5176 resistance**

We observed significant downregulation of genes encoding for proteins involved in primary cell wall cellulose synthesis from 3 dpt on: CESAs, CTL1, COBRA, and KORRIGAN (Table 2). Plant roots are predominantly surrounded by cellulose-rich primary CWs. Therefore, we sought to determine the potential outcome of primary CW-cellulose synthesis reduction during plant response to Fo5176. With this aim, we characterized the infection phenotypes of the corresponding previously described primary CW cellulose-deficient mutants *ctl1-2*, *cobra-6*, *procuste1-1*, *cesa3-3*, and *kor1-4* [27]. All cellulose-deficient mutants tested displayed a significant reduction in vascular penetrations compared to their respective wildtype (WT) backgrounds – standard Col-0 for *ctl1-2*, *cobra-6*, *prc1-1* or Col-0 *JAZ10<sub>pro</sub>-GUS-Plus<sup>sec</sup>* (JGP) for *cesa3-3*, *kor1-4* (Figure 3A and B; Supplementary Tables 3A and B) [27, 47, 48]. No significant differences among the cellulose-deficient mutants themselves were observed (Figure 3A and B; Supplementary Tables 3A and B). To corroborate whether reduced vascular penetration events corresponded to reduced root colonization, we harvested surface-sterilized roots of Fo5176-infected plants and quantified fungal colonies originating from these roots. We observed a significantly reduced number of colonies growing from *ctl1-2*, *cobra-6*, and *prc1-1* plants compared to WT (Figure 3C). Similarly, we observed reduced colonies originating from *cesa3-3* plants compared to WT (Figure 3D).

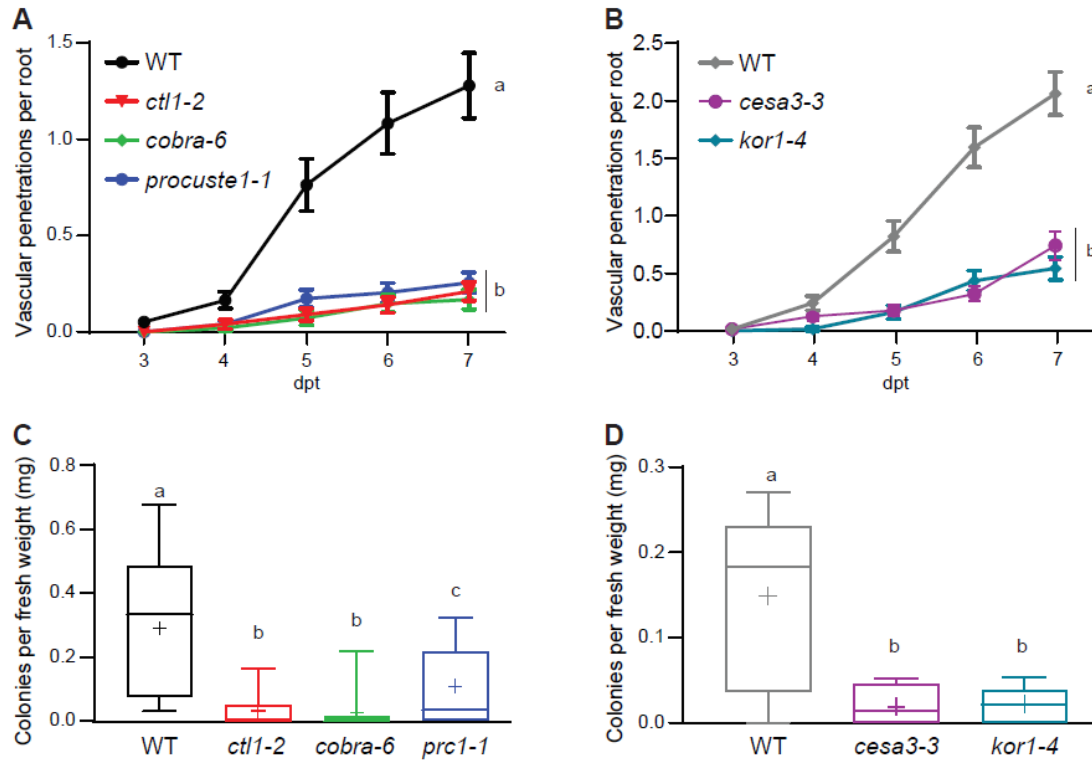


**Figure 3. Primary cell wall cellulose-deficient mutants exhibit enhanced resistance to Fo5176.** (A) and (B) Root vascular penetration of WT (Col-0 in (A) and Col-0 JGP in (B)) and primary cellulose deficient mutants at various days post-treatment (dpt) with Fo5176 pSIX1::GFP microconidia. Values represent the mean  $\pm$  standard error of at least 3 independent experiments, each one containing at least 12 seedlings. Statistical significance calculated via repeated measures two-way ANOVA with Tukey post-hoc test ( $p$ -value  $\leq 0.05$  (genotype),  $p$ -value  $\leq 0.05$  (time),  $p$ -value  $\leq 0.05$  (genotype x time)). Significant differences at the last time point shown (7 dpt) are indicated on the graph using letters; statistics of remaining time points summarized in Supplementary Tables 3A and B. (C) and (D) Quantification of Fo5176 pSIX1::GFP colonies after surface sterilization of infected roots at 7dpt. Box plots: centerlines show the medians; box limits indicate the 25<sup>th</sup> and 75<sup>th</sup> percentiles; whiskers extend to the minimum and maximum.  $N \geq 3$  independent experiments, each one containing at least 6 roots. Statistical significance was calculated via one-way ANOVA with a Tukey post-hoc test ( $p$ -value  $< 0.05$ ).

To investigate underlying biological contexts that may contribute to the observed resistance in primary CW cellulose-deficient mutants, we conducted a transcriptomic analysis of 14 days-old WT and *ctl1-2* roots. Differential gene expression analysis resulted in only 50 DEGs between the genotypes (adj.  $p$ -value  $< 0.05$ ,  $\log_2FC > |1|$ ; Table 3). Among them, we observed the up-regulation of biological processes related with plant defence which were also activated in roots during Fo5176 infection: various peroxidases and ET- and JA-related genes (Tables 1 and 3). Our transcriptomic data supports previously reported results of cellulose-deficient

mutants exhibiting up-regulation of defence response-related genes [49]. Taken together, these data suggest that plants impaired in primary CW cellulose synthesis could be “primed” for defence response activation, which we aimed to confirm.

### **Lignin deposition is a consequence of Fo5176 infection but is not essential for plant defence**

Plants exposed to microbes have been reported to increase lignin deposition in their CWs to reinforce this structural barrier [25]. Our time course transcriptome revealed a significant up-regulation of several early-stage lignin biosynthesis genes from 3 dpt on: *phenylalanine ammonia-lyase 1 and 2 (PAL1, 2)*, and *cinnamate-4-hydroxylase (C4H)* (Table 2). In addition, PRXs implicated in lignin cross-linking at the CW were also upregulated in our transcriptome data set (Table 2). Accordingly, we could detect an increase in lignin deposition in Fo5176-infected WT roots starting at 4 dpt (Figure 4A, upper panel). Therefore, the ectopic lignification associated with primary CW cellulose-deficiency in regions surrounding the plant vasculature could explain the resistance of these mutants to Fo5176 [24, 25, 50]. Indeed, *ctl1-2* roots exhibit increased deposition of lignin in response to Fo5176 already at 1 dpt (Figure 4A). To further understand the role of lignification during infection, we evaluated the response of lignin-deficient mutants to Fo5176. The mutants used – *4cl1-1* and *4cl1-2*, *c4h3-1*, and *ccoAomt1-5* – are impaired in various early stages in the lignin biosynthesis process and are all lignin-deficient (Figure 4B [51]). All the lignin-deficient mutants tested exhibited vascular penetration events similar to WT, except for *c4h3-1*, which exhibited significantly reduced vascular penetration events at 6 and 7 dpt (Figure 4C; Supplementary Table 3C). Our results indicate that Arabidopsis roots deposit lignin in their CWs in response to Fo5176 colonization, but lack of lignin synthesis does not impair plant defence against the fungus. Therefore, we conclude that ectopic lignin accumulation does not seem to account for the resistance observed in *ctl1-2* and other cellulose-deficient mutants.



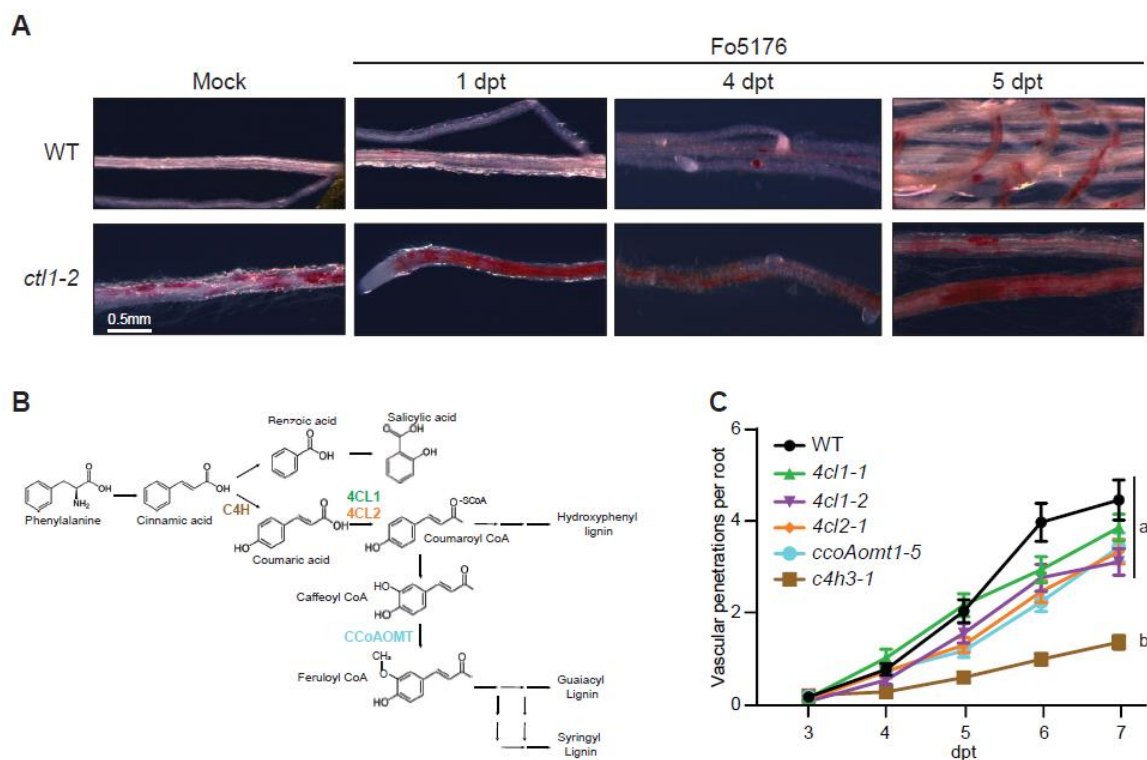


**Figure 4. Ectopic lignification in cellulose-deficient mutants does not contribute to Fo5176 resistance. (A)** Representative images of lignin staining of WT (Col-0) and *ctl1-2* mock and Fo5176-infected roots at 1, 4, and 5 days post-treatment (dpt) with Fo5176 pSIX1::GFP microconidia. A minimum of 10 plants per genotype from at least 3 independent experiments were observed per dpt with similar results. **(B)** Schematic representation of the lignin biosynthesis pathway with focus on the bifurcation between phenylpropanoids and salicylic acid synthesis pathways. Mutants of biosynthesis enzymes in coloured text are used in this study (see (C)). Figure adapted from [96]. **(C)** Root vascular penetration of WT (Col-0) and lignin-deficient mutants at various days post-treatment (dpt) with Fo5176 pSIX1::GFP microconidia. Values represent the mean  $\pm$  standard error of at least 3 independent experiments, each one containing at least 13 seedlings. Statistical significance calculated via repeated measures two-way ANOVA with Tukey post-hoc test ( $p$ -value  $\leq 0.05$  (genotype),  $p$ -value  $\leq 0.05$  (time),  $p$ -value  $\leq 0.05$  (genotype  $\times$  time)). Significant differences at the last time point shown (7 dpt) are indicated on the graph using letters; statistics of remaining time points summarized in Supplementary Table 3C.

## ET, but not JA signaling, induced by cellulose-deficiency contributes to Fo5176 resistance

Together with the described ectopic deposition of lignin, primary CW cellulose-deficient mutants have been reported to over-accumulate JA and ET compared to their WT counterparts [24, 50, 52]. Phytohormone-mediated signaling is absolutely imperative to proper defence response activation, and pre-existing enhanced accumulation of JA or ET

could provide an explanation for enhanced disease resistance in primary CW cellulose-deficient mutants [7, 24, 26, 53]. Our time-course transcriptomic data indicated an up-regulation of JA biosynthesis-related genes, including *ALLENE OXIDE CYCLASE (AOC) 1* and 2, over the course of infection (Table 1). These same genes were constitutively upregulated in *ctl1-2* compared to WT (Table 3). Therefore, we tested whether JA-deficiency would negatively impact the resistance observed in cellulose-deficient mutants. We observed that the JA-biosynthesis mutant *aos* [54] demonstrated similar vascular penetrations compared to its wildtype (WT), WT (Figure 5A; Supplementary Table 3D). We generated a *ctl1-2 aos* double mutant and observed that the *aos* mutation does not alter the resistance phenotype observed in *ctl1-2* (Figure 5A; Supplementary Table 3D). We then asked whether impairing JA-mediated signaling, but not biosynthesis, could explain the resistance observed in cellulose-deficient mutants. To this end, we made use of *coi1-34*, a null mutant of COI1 [55]. We observed that *coi1-34* mutants exhibit less vascular penetrations than WT, while those of the *ctl1-2 coi1-34* double mutant were not significantly different from *ctl1-2* at any time-point (Figure 5B; Supplementary Table 3E). Therefore, our data indicate that neither increased JA biosynthesis nor signaling explain the resistance phenotype associated with cellulose-deficiency.

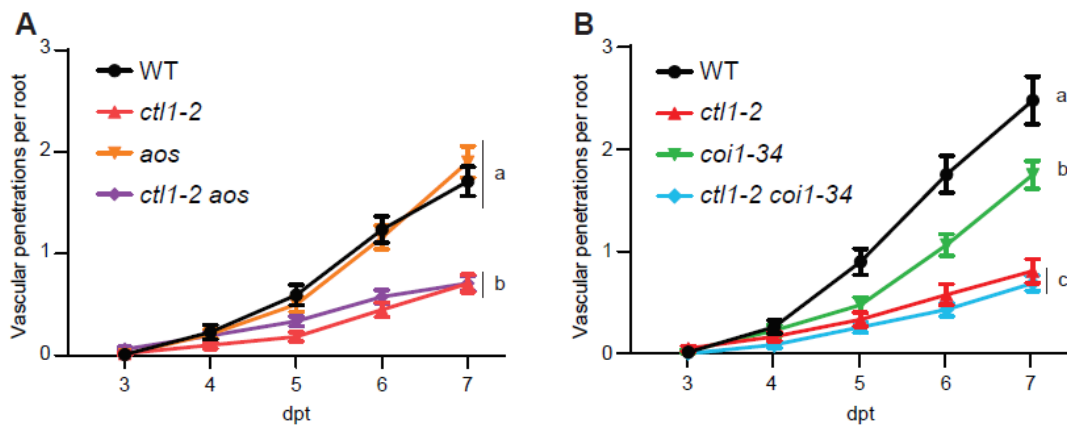


**Figure 5. JA-mediated response does not contribute to the Arabidopsis resistance to Fo5176.** (A) and (B) Root vascular penetration of JA biosynthesis (A) and signaling (B) mutants in WT (Col-0) and *ctl1-2* genetic backgrounds at various days post-treatment (dpt) with Fo5176 pSIX1::GFP microconidia. Values represent the mean  $\pm$  standard error of at least 3 independent experiments, each one containing at least 10 seedlings. Statistical significance calculated via repeated measures two-way ANOVA with Tukey post-hoc test ( $p$ -value  $\leq 0.05$  (genotype),  $p$ -value  $\leq 0.05$  (time),  $p$ -value  $\leq 0.05$  (genotype x time)). Significant differences at the last time

point shown (7 dpt) are indicated on the graph using letters; statistics of remaining time points summarized in Supplementary Tables 3D and E.

We then asked whether upregulated ET signaling contributed to the observed Fo5176 resistance in *ctl1-2*. Transcriptomics analyses revealed that several ET response related genes were upregulated during Fo5176 infection, and one of them, *ERF94/ORA59*, was also constitutively upregulated in *ctl1-2* (Tables 1 and 3). Based on these observed trends, we sought to understand the impact of impairing ET signaling in a cellulose-deficient background. To this end, we made use of the ET-signalling mutant *ein2-5* [56–58] and generated a *ctl1-2 ein2-5* double mutant. *ein2-5* displayed a significant increase in Fo5176 vascular penetrations compared to its WT and restored the *ctl1-2* resistance to WT levels, as the *ctl1-2 ein2-5* double mutant was as susceptible as WT to Fo5176 (Figure 6A; Supplementary Table 3F). Importantly, the *ctl1-2 ein2-5* does not suppress root growth stunting of *ctl1-2* plants (Figure 6B and C), demonstrating that shorter root length of primary CW cellulose-deficient mutants is not a contributing factor to their resistance to Fo5176. In addition, our results indicate that ET-mediated signaling plays a major role in Arabidopsis defence against Fo5176 root colonization and is a preeminent reason for the resistance to this fungus observed in *ctl1-2*.

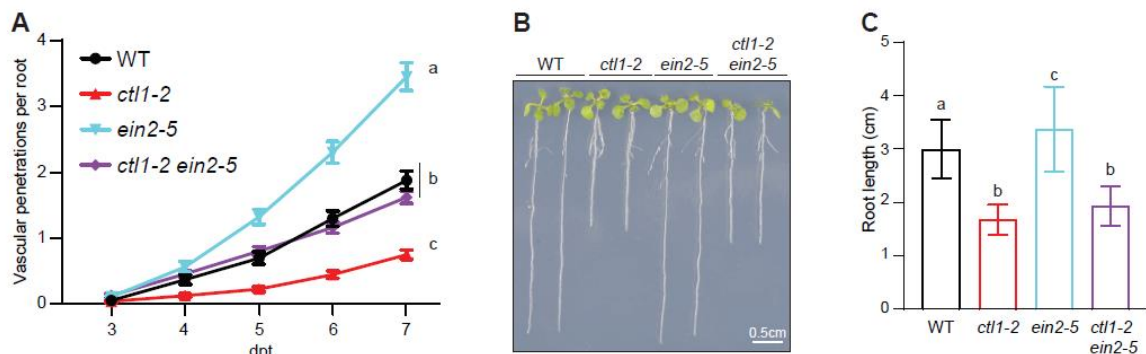


**Figure 6. Up-regulation of ET signaling contributes to the resistance of cellulose-deficient mutants during Fo5176 infection.** (A) Root vascular penetration of the ET signaling mutant *ein2-5* in WT (Col-0) and *ctl1-2* genetic backgrounds at various days post-treatment (dpt) with Fo5176 pSIX1::GFP microconidia. Values represent the mean  $\pm$  standard error of at least 3 independent experiments, each one containing at least 16 seedlings. Statistical significance calculated via repeated measures two-way ANOVA with Tukey post-hoc test ( $p$ -value  $\leq 0.05$  (genotype),  $p$ -value  $\leq 0.05$  (time),  $p$ -value  $\leq 0.05$  (genotype x time)). Significant differences at

the last time point shown (7 dpt) are indicated on the graph using letters; statistics of remaining time points summarized in Supplementary Table 3F. **(B)** Representative images of 8-day-old light-grown seedlings impaired in ET signaling in WT (Col-0) or *ctl1-2* background. **(C)** Quantification of root length of plants grown as depicted in (E). Bars represent the mean  $\pm$  standard deviation of  $N \geq 40$  plants averaged over three independent experiments. Statistical significance calculated via one-way ANOVA with Tukey post-hoc test ( $p$ -value  $< 0.05$ ). Significant differences indicated using letters.

### **Cellulose-deficiency contributes to enhanced resistance to the vascular bacterial pathogen *Ralstonia solanacearum***

Down-regulation of cell wall-related processes has also been observed in early infection stages of *Arabidopsis* colonization by the bacterial root vascular pathogen, *Ralstonia solanacearum* [59]. Consistent with observations during Fo5176 pathogenesis, the primary CW cellulose-deficient mutants *ctl1-2*, *cobra-6*, and *prc1-1* exhibited significantly increased resistance to *R. solanacearum*, as these mutants showed lower disease scores compared to WT (Figure 6A; Supplementary Table 4A). We sought to understand whether ET signaling also contributes to the resistance conferred by cellulose-deficiency during *R. solanacearum* infection. We observed that the *ein2-5* mutant is significantly more susceptible to *R. solanacearum* than *ctl1-2*, but is slightly more resistant than the WT (Figure 6B, Supplementary Table 4B). Furthermore, no significant difference was observed in the infection phenotypes of *ctl1-2* compared to *ctl1-2 ein2-5* double mutants (Figure 6B, Supplementary Table 4B). Our data indicate that the cellulose alterations in primary CWs contribute to broad disease resistance to root vascular pathogens, due to the role of ET signaling, specifically in resistance to Fo5176.

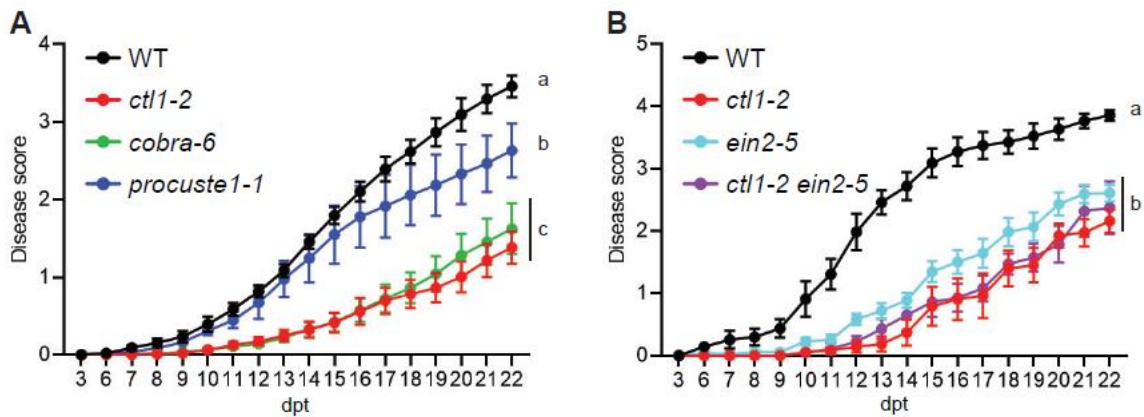


**Figure 6. Cellulose-deficient mutants exhibit enhanced resistance to the bacterial pathogen *Ralstonia solanacearum*.** (A) and (B) Disease scoring of cellulose-deficient mutants (A) and the ET signaling mutant *ein2-5* in WT (Col-0) and *ctl1-2* genetic backgrounds (B) at various days post-treatment (dpt) with the vascular bacteria *R. solanacearum*. Qualitative data represented as line plots represents the average of at least 3 independent experiments, each one including  $\geq 24$  plants per genotype. Based on plant symptoms on each day, an average disease score was calculated per time point represented in line graphs. The disease scoring index measured symptoms on a scale of 1 to 4 (0 = no wilting, 1 = 25% wilted leaves, 2 = 50%, 3 = 75%, and 4 = death) as described in the methods. Statistical significance based on absolute number of plants assigned to either the least ( $\leq 1$ ) or most ( $>3 \leq 4$ ) diseased category calculated via Fisher's exact contingency test indicated in Supplementary Tables 4A and B.

## Discussion

In this study, we provide detailed information about the intricate processes which govern root immune responses to Fo5176 using a multi-faceted approach. The intercellular infection strategy used by Fo to advance towards the root vasculature makes it an ideal candidate for understanding host-pathogen interactions in the apoplast with a focus on cellulose-rich plant primary CWs. Our dual transcriptomics approach, based on the characterization of Fo5176 root infection strategy via confocal microscopy, allowed us to provide spatial and temporal resolution of plant root and fungal genes involved in the Fo5176-Arabidopsis interaction. We observed significant and rapid down-regulation of CW-related genes during the early stages of fungal proliferation in the apoplast, particularly of those related with primary CW-cellulose biosynthesis. Due to the importance of this polysaccharide in plant root biology we focused on characterizing defence response in the corresponding cellulose-deficient mutants. Our experimental data allowed us to conclude that down-regulation of the primary CW-

cellulose synthesis machinery vastly reduces the capacity of Fo5176 to reach the root vasculature due to the up-regulation of ET-signaling in primary CW mutants.

### **Dual transcriptomics reveals an important role for cell wall-related genes during Fo defence**

The use of dual transcriptomics allows for the simultaneous study of microbe and host adaptation to the interaction at the gene expression level. Our time course analysis spans the Fo5176 infection process from microconidia adhesion and germination at the root surface to xylem colonization (Figure 1).

Our dataset showed that Fo5176 regulates its transcriptomic profile while it invades the root. Over time, an increasing amount of genes show upregulated expression compared to the fungal microconidia germinated *in vitro*. We identified more than 400 DEGs continuously up- or downregulated *in planta* compared to *in vitro* at every investigated time point (Table 1; Clusters 1, 2, and 5 in Supp Fig 3). These genes seem to be responsible for the fungal adaptation to the host and are not necessarily connected to changes in the fungal lifestyle in the different root layers. Most of the CW modifying genes co-expressed following a non-homogenous expression pattern through the root layers: they were upregulated until the first xylem colonization events (4dpt) and then their expression decayed (Table 1; Cluster 3 in Supp Fig 3). This significant activation of the fungal CW modification machinery in the cell root layers that precedes the vasculature concur with the need of the microbe to pass through the plant primary CWs. The fungal hyphae have to switch from a nutrient-rich growth in PDB to a nutrient-poor situation in plants. Using the CW modifying artillery, Fo could improve the availability of nutrient resources from plant CWs as well as restructure its own CW to enable root colonization.

The fungus remains undetected by the plant while it stays at the root surface (1dpt), reflected in no significant transcriptional reprogramming compared with mock treated plants. A clear host response to Fo5176 was exhibited at the early time point of 2pt, when the epidermal apoplast was invaded. The downregulation of primary CW-cellulose synthesis was one of the first responses of the plant to the pathogen, while we could not detect a strong activation of defence mechanisms at this time point ([60]; Figure 2B; Table 2). From 3dpt on, the expression of defence-related genes significantly increased, like the JA- and ET-responsive defensin PDF1.2 [61] and the NADPH oxidase RBOHD required for ROS production during



innate immunity [60] (Figure 2B; Table 2). This corresponds to the time point when the fungal hyphae reach the cortex layer (Fig. 1A) [31]. Our data suggest that the root is not significantly affected until the microbe reaches the cortex, in agreement with a recent work showing that the root epidermal cell layer responds to microbes only when a certain threshold of damage has been exceeded [62]. Time-course transcriptome analysis revealed that the mechanism by which roots respond to Fo5176 infection is an evolutionary process that transitioned from growth inhibition to active defence. Our data expand and precise the published studies about *Arabidopsis* root transcriptional reprogramming upon Fo5176 infection [12, 13] (Table 4).

### **Fo5176-resistance in cell wall cellulose-deficient mutants requires ET signaling**

We observed down-regulation of primary CW *CESA* genes at the early Fo5176 infection stages corresponding to hyphal penetration into the epidermal layers (Figure 1A). This response could be induced by the fungus to weaken host cell walls or could be a response from the plant to temporarily pause developmental growth to favor resource allocation towards defence response. Our work demonstrates that, despite their weakened cell walls, plants with reduced primary CW-cellulose are more resistant to root vascular pathogens. We initially observed that the primary CW-cellulose deficient mutants *ctl1-2*, *cobra-6*, and *prc1-1*, *cesa3-3* and *kor1-4* were all more resistant to Fo5176 in terms of reduced vascular penetration and fungal colony counting than their respective WT (Figure 3). To better understand the broad-spectrum effects of primary CW-cellulose-deficiency on defence response, disease phenotypes upon infection with the vascular bacterial pathogen *R. solanacearum* were also evaluated. This pathogen is the causative agent of bacterial wilt, and its infection strategy has been well-established to involve modification and degradation of the plant cell wall [49, 63]. Consistent with our observations of Fo5176 infection, a clear trend towards resistance was observed in *ctl1-2*, *cobra-6*, and *prc1-1* compared to WT (Figure 7A). Our results suggest that mutation of primary cell wall genes, including *CESAs*, also confers enhanced resistance to root vascular pathogens of different Kingdoms.

A connection between primary CW-cellulose-deficiency and biotic resistance has been hypothesized based, among others, on the ectopic deposition of lignin shown by the corresponding plant mutants [24]. Lignin has been shown to contribute to plant resistance to foliar bacteria [25], however deposition of lignin in roots during fungal infection has not been

demonstrated. Our data confirmed the reinforcement of the WT root CWs with lignin in response to Fo5176 infection (Figure 4A) as a consequence of the upregulation of lignin biosynthesis and deposition-related genes from 3 dpt on (Table 2). However, we observed that lignin-deficient mutants do not exhibit enhanced susceptibility to Fo5176 compared to WT (Figure 4C). Therefore, our data indicate that root lignification is a programmed response to Fo5176, but is not essential as a physical barrier to block fungal advance. In addition, *ctl1-2* mutants increased the amount of lignin in the roots in response to Fo5176 much earlier than the WT (1dpt vs 5dpt; Figure 4A). These observations indicate that WT plants need to activate resources in order to achieve this lignification only upon successful perception of the fungus, while the lignin deposition machinery of *ctl1-2* plants is readily activated upon Fo5176 detection. We observed increased expression of genes encoding for peroxidases, PRX37 and PRX52, in *ctl1-2* compared to WT, while the expression of lignin biosynthesis genes was not altered by *ctl1-2* mutation (Tables 3). Both PRX37 and PRX52, also upregulated in WT roots over the course of Fo5176 infection, are involved in lignin deposition [64, 65]. Thus, indicating that ectopic lignification in *ctl1-2* and its rapid over-lignification response to Fo5176 is likely influenced by the activity of PRXs and other late-stage lignin biosynthesis proteins.

Our data corroborated previous reports that connect modifications in primary cell wall cellulose with differential regulation of JA/ET-related genes in *ctl1-2* (Table 3) [24, 29, 66]. Moreover, evidence exists to support a connection between hormone regulation and defence response signaling pertaining to vascular pathogens, such as Fo5176, corroborated in this study by the up-regulation of hormone-related genes during infection (Table 2) [67–69]. It was previously demonstrated that *F. oxysporum* specifically hijacks non-defence response-related aspects of JA signaling mediated by COI1 to induce Arabidopsis infection [70]. This host manipulation led to an enhanced wilting resistance observed in the JA-signaling mutant *coil-34*, but not in the synthesis mutant *aos* [8, 70]. Accordingly, Arabidopsis *coil-34* exhibited reduced susceptibility to the soil-borne bacterial pathogen *R. solanacearum* [63, 70]. Importantly, the Arabidopsis *coil*-mediated resistance to Fo was only associated with late stages of the infection (approximately 21 dpt) but not with reduced fungal penetration and xylem colonization, as similar amounts of Fo were detected in the mutant and the wild-type [70]. Our data confirmed this result and further expanded it, as we showed that neither JA biosynthesis nor signaling influence the ability of Fo5176 to reach the xylem in primary cell wall cellulose-deficient mutants (Figure 5).

Based on the observations that ectopic lignification nor defects in JA signaling could fully explain the enhanced resistance observed in primary CW-cellulose-deficient mutants, we then investigated the role of ET signaling. It was previously suggested that ethylene response factor 1 (ERF1), a downstream component of the ET and JA pathways, acted as a positive defence response signal in the context of Fo infection using a spray infection method [46, 67]. Our data confirm previous studies showing that ET-dependent genes are activated as the primary response during pathogen response activation prior to JA-mediated signaling [71, 72]. We observed upregulation of genes encoding ET responsive transcription factors (*ERF1*, 62, 73, 94 and 113) during Fo5176 infection from 2 dpt on, while JA-responsive genes were significantly upregulated only at 3 dpt on, including various JAZs (Table 2). Additionally, ET-responsive transcription factor *ERF94* was constitutively expressed in *ctl1-2* plants compared to WT (Table 3). We observed that a blockage of ET signaling impaired plant defence against Fo5176 and is sufficient to disrupt *ctl1-2*-associated resistance phenotypes (Figure 6). An additional explanation for the general resistance of cellulose-deficient mutants to Fo5176 could simply be due to their shorter root length. As previously reported, all the primary CW cellulose-deficient mutants tested in this study display the classic primary CW cellulose-deficient mutant dwarfed root phenotype [19, 23, 73, 74]. It could be more difficult for the fungus to reach shorter roots or to find an area of weakness for penetration due to lack of available root space. Impairing ET-signaling did not alter the dwarfed root phenotype of *ctl1-2*, but restored the observed Fo5176 resistance (Figure 6). Thus, negating the possibility that root length is a contributing factor to the enhanced defence response observed in *ctl1-2*. Our data strongly support a role for ET-dependent but JA-independent root defence against Fo5176. We observed that impairing ET signaling in the context of primary CW-cellulose-deficiency eliminates the observed resistance phenotype to Fo5176. Interestingly, our data indicate that plant response to *R. solanacearum* is not ET signaling-dependent (Figure 6B). This observation indicates that primary CW-cellulose defects increase plant defence to various root vascular pathogens, but the molecular mechanisms underlying these resistant phenotypes are heavily dependent on the pathosystem. Our observations ultimately point to an important role for hormones, specifically ET, in enhanced disease resistance in primary CW-cellulose-deficient mutants.

## Conclusions

In this study we show how plant roots and their vascular pathogens tightly control their gene expression dynamics during their interaction. Our time-resolved dual transcriptomic approach represents a useful tool to identify root and fungal molecular players implicated in the infection process. Specifically, our findings reveal a critical role of rapid reduction of primary CW cellulose synthesis in plant defence against root vascular pathogens. Furthermore, we highlight a novel role for ET signaling as a molecular basis for resistance associated with primary CW cellulose-deficiency during Fo5176 infection, which is surprisingly JA-independent. In summary, we shed light on the complex interaction between hormone-mediated signaling, root CW composition, and defence response activation.

## Materials & Methods

### Arabidopsis growth conditions

Arabidopsis plants were grown under long-day conditions (16h light, 8h dark) with optimized light intensity ( $130\text{--}150 \mu\text{E m}^{-2} \text{s}^{-1}$ ) at  $20\text{--}22^\circ\text{C}$ , unless otherwise indicated. Seeds used for all *in vitro* experiments were either gas or liquid-sterilized and grown on  $\frac{1}{2}$  MS media (Duchefa; catalog number M0222.0025) supplemented with 1% (w/v) sucrose (when indicated) and 0.9% bacteriological grade agar (Difco; catalog number 214530). For hydroponic experiments, Arabidopsis seeds were germinated at  $24^\circ\text{C}$ , long day conditions, on 2 mm foam plugs suspended on 200 ml  $\frac{1}{2}$  MS + 1% sucrose media in 330ml pots at pH 5.7 adjusted by KOH. The media was exchanged 6 days after germination to  $\frac{1}{2}$  MS and seedlings were further grown.

Mutant genotypes were confirmed using primers previously reported or designed for this work (Supplementary Table 1): *ctl1-2* (SALK\_093049) [21, 73], *cobra-6* (SALK\_051906) [75], *procuste1-1* [19, 20], *kor1-4* [27], lignin-deficient mutants (*4cl1-1*, *4cl1-2*, *4cl2-1*, *ccoAomt1-5*, *c4h3-1*) [76], *aos* (*CYP74A*) [54], *coil-34* [47], *ein2-5* [57, 77]. The *cesa3-3* allele was identified as a negative regulator of JA signalling in a forward genetic EMS screen [47]. The mutant allele exhibited ectopic expression of the JA-responsive reporter *JAZ10p:GUSPlus* and increased *JAZ10* transcript levels in both shoots and roots. The causative GAT to AAT transition leading to a D378N mutation underlying the *cesa3-3* phenotype was identified via mapping-by-whole-genome-sequencing of bulk segregants as described [47], and confirmed by allelism tests with the characterized *cesa3* mutant allele *cev1* [28, 29].

### **Fungal constructs, growth, and infection assays**

To obtain the Fo5176 pGPD::GFP line, the previously reported pPK2-*hphgfp* construct containing a Hygromycin resistance-GFP fusion protein under the control of the constitutive *gpdA* promoter (pGPD) [78] was inserted into Fo5176 by *Agrobacterium* mediated transformation as described before [79].

Fo5176 growth and *in plate* infection assays were conducted as previously described [32, 80]. Briefly, sterilized *Arabidopsis* seeds were sown on sterilized Whatman paper strips (VWR International, catalog number 514-8013) placed on top of the media as described above. Plants were grown vertically in long-day conditions for 8 days and infected as previously reported. Vascular penetrations were counted using fluorescence stereomicroscopy and root length measurements were quantified via scanned images. Infection time-points are referred to as “days post-treatment” (dpt). Statistical analyses were conducted in GraphPad Prism 8 (version 8.4.3).

For hydroponic infections, the roots of 10-day-old seedlings were infected with 20µl of a solution containing  $10^7$  microconidia/ml Fo5176. All pots were incubated for 30 minutes at 100 rpm on a rotary shaker. The media of the infected plants was then replaced with fresh ½ MS media. The plants were further grown under the same conditions until the roots were harvested for RNA extraction or for imaging at 0, 1, 2, 3, 4, and 6 days post treatment.

For Fo5176 transcriptomics in the absence of a plant host,  $10^7$  microconidia/ml were germinated in ½ MS + 1% (w/v) sucrose overnight at 180rpm at 28°C in the dark. The germinated microconidia were harvested via two centrifugation steps at 4000 xg for 15 minutes at 10° C, washed twice with water, discarding supernatant in between washes. The pellet was frozen in liquid nitrogen (LN<sub>2</sub>) and subsequently freeze-dried. The lyophilized pellet was used for RNA extraction.

For colony quantification after Fo5176 infection, roots of infected plants were harvested at 7 dpt and weighed. Roots were surface sterilized for 1 minute in 80% ethanol (alcosuisse), followed by 1 minute in 0.25% sodium hypochlorite (Chemie Brunschwig AG), lastly followed by three 1 minute washes in sterile water. The water from the final wash was collected as a sterilization control. 4-10 sterile glass beads (2.85-3.45 mm diameter, Carl Roth GmbH + Co, Germany) were added to tubes and washed/sterilized root material was then ground in 1mL of sterile water using a GenoGrinder (Retsch MM301, Retsch GmbH + Co, Germany) for approximately 3 minutes at maximum speed. 100ul of the sterilization control and 1mL of ground root material were plated separately on ½ Potato Dextrose Broth

(BD Difco, catalog number: 0549-17-9) + 1% agar plates (BD Difco, catalog number: 214530) supplemented with 25ug/ml chloramphenicol (Sigma Aldrich, catalog number: C0378) and 55ug/ml hygromycin (Sigma Aldrich, catalog number: H9773). Plates were then sealed with parafilm and incubated at 28°C. Fungal colonies were quantified after 3 days of incubation. Colony quantifications were normalized to root fresh weight (mg).

### ***Ralstonia solanacearum* growth and infection assay**

*R. solanacearum* pathogenicity tests were carried out using the soil-drench method as previously described [81]. Briefly, Arabidopsis was grown for 4 to 5 weeks on Jiffy pots (Jiffy Group, Lorain, OH, U.S.A.) in a controlled chamber at 22°C, 60% humidity, and an 8-h light and 16-h dark photoperiod. 3 vertical holes were made in Jiffy pots, and the pots were immediately submerged for 30 minutes into a solution of overnight-grown *R. solanacearum* adjusted to OD<sub>600</sub> = 0.1 with distilled water (30mL of bacterial solution per plant). Inoculated plants were then transferred to trays containing a thin layer of soil drenched with the same *R. solanacearum* solution and were kept in a chamber at 27°C, 60% humidity, and 12 h of light and 12 h of dark. Plant wilting symptoms were recorded every day and were expressed according to a disease index scale. The disease index measured symptoms on a 1 to 4 scale (0 = no wilting, 1 = 25% wilted leaves, 2 = 50%, 3 = 75%, and 4 = death). Infection time-points associated with soil-drenching infection are referred to as “days post-inoculation” (dpi). Statistical analyses were conducted in GraphPad Prism 8 (version 8.4.3).

### **Confocal imaging**

Arabidopsis Col-0 seedlings were infected with the fluorescently labeled strain Fo5176 pGPD::GFP, placed on chambered cover glasses (Thermo Scientific™ Nunc™ Lab-Tek™) and covered with thin blocks of solid ½ MS medium. Images were taken with a Zeiss LSM 780 Axioobserver microscope, using the LD C-Apochromat 40x / 1.1 W Korr M27 objective and Immersol W (Zeiss) between lens and coverslip. GFP (fungus) was excited at 488 nm and emitted fluorescence was detected at 514 nm. RFP (Arabidopsis autofluorescence) was excited at 561 nm and emission was detected at 641 nm, being the Pinhole for both channels 36.28 um. Z-stacks of individual roots were obtained imaging every 1.91 um to obtain a transversal optical section (Zen Lite 2012).



## RNA extraction and sequencing

For the dual time course transcriptome analysis, roots from 2 pots were pooled for each condition and time point separately for RNA-extraction. Roots were harvested by manual removal from foam plugs and were dried gently using tissue paper. Roots were weighed and immediately frozen in liquid N<sub>2</sub>. The root samples were stored at -80° C until RNA was extracted. 4 replicates were harvested per time point for infected and control plants and 2 replicates for the *in vitro* grown microconidia.

For the RNA-Seq of *ctl1-2* and WT (Col-0) plants, roots from 14 days-old seedlings grown on plates as described above were harvested and immediately frozen in LN<sub>2</sub>. Three independent replicates were used for the transcriptome assay.

Root material or germinated microconidia were ground with mortar and pestle in LN<sub>2</sub>. 50 - 100 mg of ground material was used for RNA extraction using the RNeasy plant mini Kit (Qiagen). Extraction was performed according to the user manual provided by the supplier (RNeasy Mini Kit handbook, Fourth edition, June 2012, Qiagen). Extraction buffer RLC with 10 µl/ml β-mercaptoethanol freshly added was used to extract the RNA. An on-column DNA digestion (RNase-Free DNase Set, Qiagen) was performed. Before elution of the RNA the column was incubated 1 min with 30 µl RNase-free water to resolve the RNA. Concentration of the RNA was determined by Nanodrop (Thermo Fisher) and integrity of the RNA was examined by gel electrophoresis on a 1% agarose gel. For samples with low concentration, the RNA content was additionally measured by Qubit Fluorometer using the RNA BR assay kit (Qubit, Thermo Fisher).

3'mRNA-libraries were prepared using the 3'mRNA-Seq library Prep Kit (QuantSeq, Lexogen). The manual from the supplier was followed with the following modifications. At least 1 µg RNA was used as input. For first strand synthesis of cDNA the incubation time at step 4 was increased to 60 min. For library indexing and amplification 13-17 amplification cycles of the given PCR were used depending on the amount of input RNA. 17 µl of the purified library was transferred to a fresh tube. The finished libraries were stored at -20° C until quality control and pooling. The quality of the libraries was assessed with D1000 ScreenTape on Agilent 4200 Bioanalyzer at the Functional Genomic Center Zürich (FGCZ) with the included software from the manufacturer. Libraries were pooled equi-molecularly for sequencing.

Sequencing of the time course experiment was performed in an Illumina HiSeq2500 sequencer (single-end 125 bp) with a read depth of around 5 mio reads per sample. Samples

were divided in three charges and sequenced in different runs of the sequencer. Sequencing of the *ctl1-2* vs WT experiment was performed in an Illumina NovaSeq6000 sequencer (single-end 100 bp) with a read depth of around 8 mio reads per sample. Resulting reads were assigned to the samples based on their index-number by FGCZ. Raw reads separated by sample were obtained in FastQ-format from FGCZ.

### **Read mapping**

Read mapping and quantification was performed on SUSHI (FGCZ) [82]. The reads were trimmed (Trimmomatic, version 0.36) [83] and adapters were removed (Flexbar, version 3.0.3) [84]. Reads > 20bp were kept. Reads were mapped by STAR (version 2.6.1c) [85] against the *Arabidopsis thaliana* genome (TAIR10 [33]) and *Fusarium oxysporum* Fo5176 [10]. Uniquely mapped reads were counted by featureCounts [86], based on the R package Rsubread (version 1.32.1) [87].

### **Differential expression analysis and co-expression analysis of DEGs**

Differential expression analysis was conducted using the Bioconductor package edgeR (version 3.24.3) [88]. The raw read-counts were imported to EdgeR and counts were normalized using trimmed means of M-values (TMM) normalization [89]. Genes with  $\geq 3$  counts per million (CPM) were assigned as actively transcribed genes. Dispersion was estimated using the quantile - adjusted conditional maximum likelihood (qCLM) method. Differential expression was computed using glmTREAT, p-value was adjusted using Benjamini-Hochberg correction.

Significantly differentially expressed genes (DEGs) were considered those with aLog<sub>2</sub> fold-change > |1| and a FDR < 0.05 and were used for clustering expression profiles along the time points of the experiment (Mfuzz version 2.46.0, Bioconductor) [35].

### **Gene functional analysis**

Gene ontology (GO) term enrichment for Arabidopsis was performed in cluster-wise manner with ClueGO (version 2.5.7) [90] in Cytoscape (version 3.7.0) [91]. A list of Arabidopsis cell wall related genes was generated based on the data available on the Cell Wall Genomics database (<https://cellwall.genomics.purdue.edu/>, 24 March 2020). A list of Arabidopsis transcription factors, carbohydrate active enzymes, hormone-related genes and hormone biosynthetic genes was obtained from [92]. A list of Fo5176 carbohydrate active proteins was generated using the online service dbCAN2 with HMMER, DIAMOND and Hotpep tools.

Genes with a Carbohydrate Active enZYme (CAZY) -domain prediction by at least 2 tools were considered as CAZY-domain containing genes (<http://bcb.unl.edu/dbCAN2/>, 8 October 2020 [93]).

### **RT-qPCR validation of DEGs**

Control and infected samples of 4 additional biological replicates were used for validation of the DEGs. Root material was ground by mortar and pestle in LN<sub>2</sub>. 1 ml TRI Reagent for DNA, RNA and protein isolation (Sigma-Aldrich, Merck, Germany) was added and mixed thoroughly by hand. Tubes were incubated 5 min slowly shaking at room temperature and 0.2ml chloroform was added. Tubes were shaken manually for 15s, followed by 3 min incubation at room temperature. Samples were centrifuged at 4° C, 12000 xg, 15min; 400 µl of the supernatant was transferred to fresh tubes. 500µl isopropanol (4° C) was added, the tubes were inverted three times and incubated for 10 min on ice followed by 15 min centrifugation at 4°C, 15000 xg. Supernatant was removed and pellets were resuspended in 1 ml 75% ethanol (4° C), mixed by vortexing and centrifuged for 5 min at 4° C, 7500 xg. Supernatant was removed and samples were air-dried on ice for 10 min. Pellets were resuspended in 45 µl of RNase-free water. 5 µl of RNA was kept on ice to measure concentration and evaluate integrity as described above. Remaining 40 µl were frozen in LN<sub>2</sub> and kept at -80° C until cDNA-synthesis.

cDNA synthesis was performed using Maxima H Minus cDNA-synthesis-kit (Maxima H Minus First Strand cDNA Synthesis Kit, with dsDNase; Thermo-Fisher) according to the instructions of the supplier. 1 µg of RNA was used in each reaction as a template.

RT-qPCR was performed on a LightCycler 480 (Roche), using Fast SYBR Green Master Mix (ThermoFisher Scientific). 4 µl 1:16 diluted cDNA, 5 µl of SYBR Green Master Mix and 0.5 µl of each primer (Supp. Tab. 4) was prepared in a 384-well plate. The RT-qPCR-program was set as follows: initial denaturation for 3 min, 95°C; 50 cycles of denaturation at 95° C, 15 s, annealing at 60° C, 10 s, elongation at 72° C, 15 s; final elongation at 72° C, 30 s; melting curve of 0.11° C/s temperature increase from 42° C to 95° C; cooling down to 20° C, 30 s. Two control sets of primers were used for Arabidopsis GAPDH 3'-end and 5'-end [94]. The mean of the two reference transcripts were used for normalization of signal for the other genes tested. Fo5176 β-Tubulin (Fo5176.g4360) was used as a reference gene for *Fusarium oxysporum* gene expression. For the calculation of the expression the  $2^{-\Delta\Delta C_t}$  method was used

[95], and the fold changes in expression were represented as the ratio of the mean value of infected/ mean value of control Ct.

### **Lignin staining**

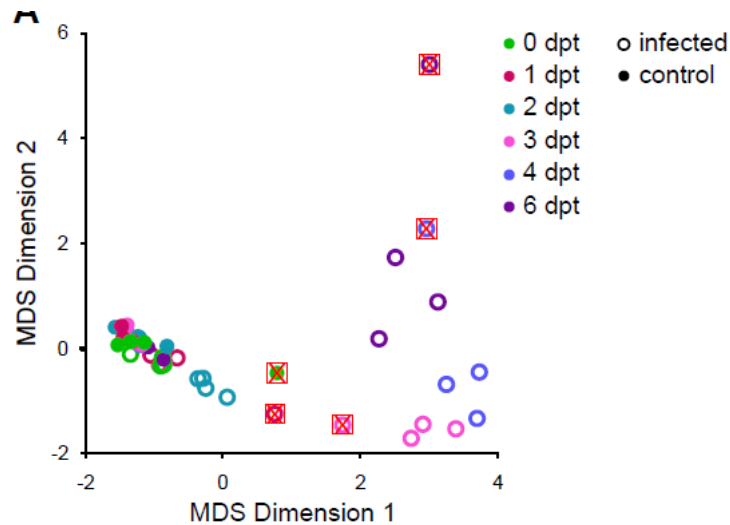
Plants infected as described above (“Fungal constructs, growth, and infection assays”) at the indicated time points were incubated for 10 minutes with soft agitation in phloroglucinol stain prepared as follows: 25mg phloroglucinol (Brunschwig, catalog number ACR24176-0250), 25mL 37% hydrochloric acid (Sigma Aldrich, catalog number 30721-1L), 25mL methanol. Phloroglucinol stain was removed using a plastic pipette and replaced with a 3:1 mixture of glycerol: water. Plants were placed on plates containing ½ MS media + 1% sucrose and immediately imaged using a stereomicroscope.

### **List of abbreviations**

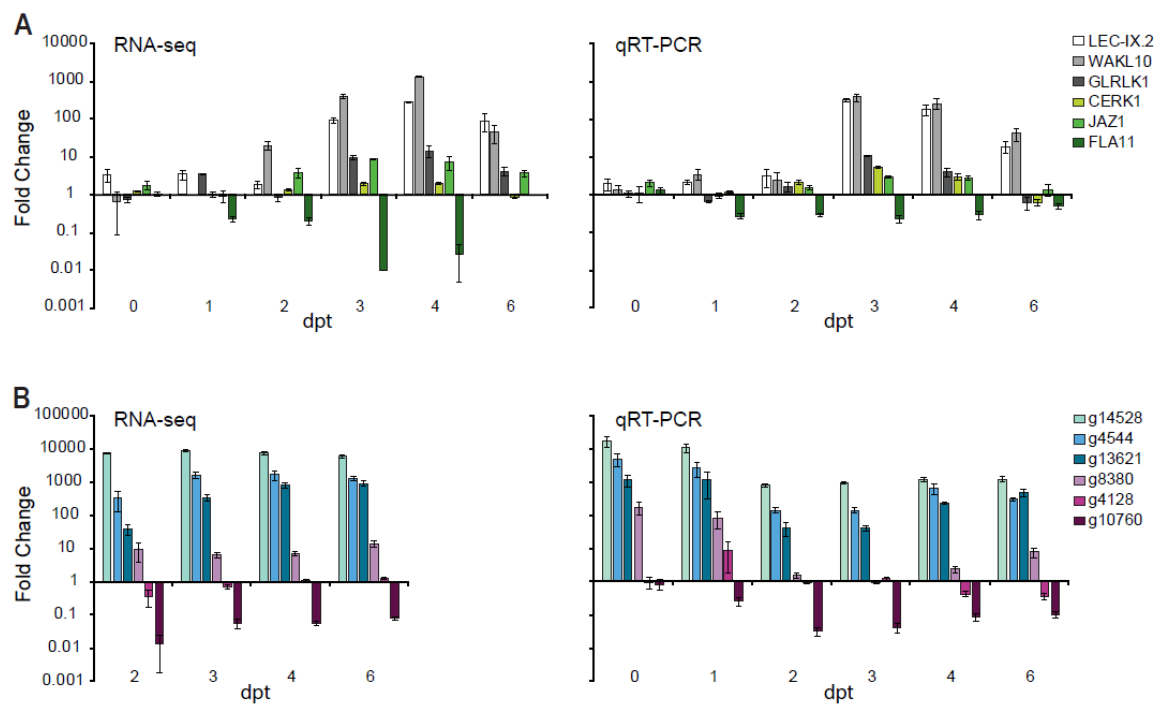
CW	Cell wall
Fo	<i>Fusarium oxysporum</i>
SA	Salicylic acid
JA	Jasmonic acid
ET	Ethylene
ROS	Reactive oxygen species
CESA	Cellulose synthase subunit
CTL1	CHITINASE-LIKE1
GPI	Glycophosphatidyl-inositol
COB	COBRA
KOR	KORRIGAN

**SUPPLEMENTARY  
MATERIAL**

## ANNEX



**Supplemental Figure 1. Complete MDS-Analysis of Arabidopsis transcriptional profiles.** Multidimensional scaling analysis (MDS) of transcriptional profiles of Arabidopsis. Samples clearly deviating from the rest of the samples at the same time point and condition (surrounded by a red square and crossed out) were not used for further analysis.

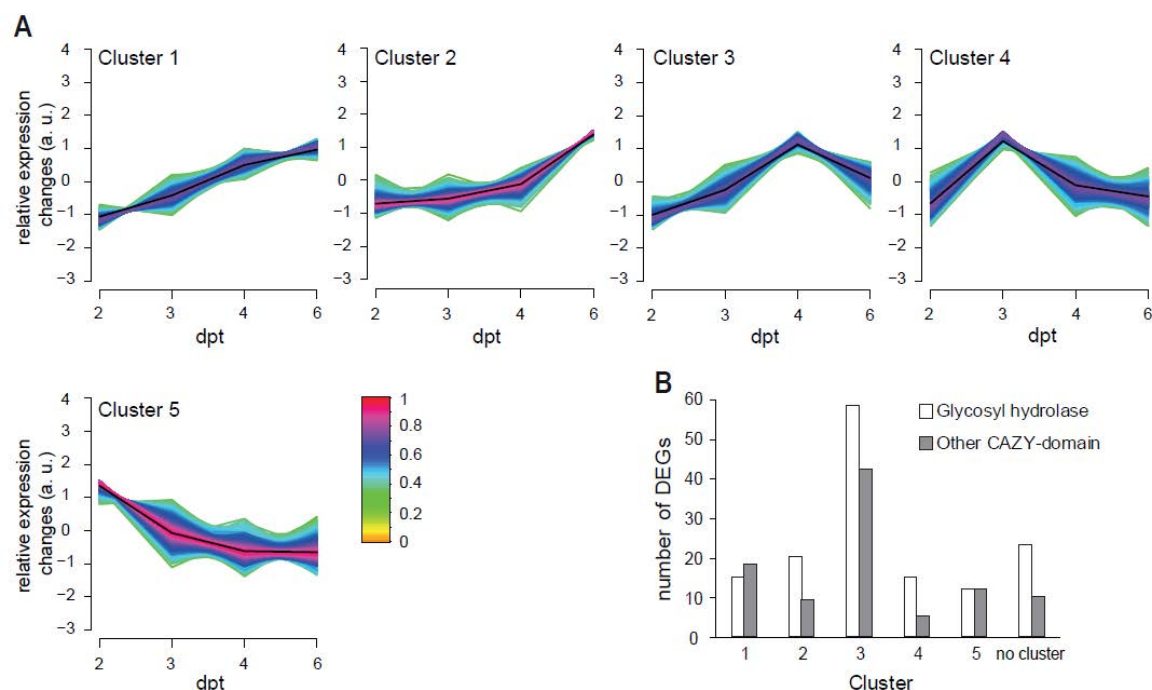


**Supplemental Figure 2. RNAseq validation by RT-qPCR.** (A) and (B) The expression of 6 randomly picked DEGs from Arabidopsis (A) or Fo5176 (B) expressed at different levels based on the RNA-sequencing (left



## ANNEX

panels) was confirmed by RT-qPCR (right panels) using *de novo* generated RNA samples. The RT-qPCR-based expression of each gene was determined relative to the corresponding reference gene; i.e. At GAPDH in (A) and Fo5176  $\beta$ -Tub in (B).



**Supplemental Figure 3. Temporal dynamics of Fo5176 DEGs during root infection reveal a significant alteration of proteins containing catalytic and carbohydrate-binding modules (CAZY).** (A) Clusters of Fo5176 coexpressed DEGs during infection using fuzzy c-means clustering. (B) Number of DEGs encoding proteins with carbohydrate active enzyme-domains (CAZY) and glycosyl hydrolases in the different clusters. DEGs with the entry “no cluster” were not associated to a cluster by the clustering algorithm.

### Tables

**Table 1. Fo5176 differentially expressed genes (DEGs) during Arabidopsis root infection over time.** Significant DEGs in Fo5176 during Arabidopsis root infection compared to *in vitro* germinated microconidia. Logarithmic fold-change (logFC) and corrected p-value (FDR) are presented in columns for each time point separately, gaps correspond to non-significant changes in gene expression at those time points. The genes are clustered based on their co-expression pattern (Supplementary Figure 2A). DEGs with the entry “no cluster” were not associated to a cluster by the clustering algorithm, DEGs with the entry “excluded” were not taken into account for clustering. All DEGs were further analysed for presence of carbohydrate active domains in their corresponding encoded protein sequences using the dbCAN2-meta server (<http://bcb.unl.edu/dbCAN2/>, 8 October 2020) and were highlighted in yellow (Supplementary Figure 2B). The genes were described based on

IPR and PFAM; IPR\_description: protein family classification by InterPro, PFAM: protein family classification by PFAM (both obtained from [10]).

**Table 2. Arabidopsis differentially expressed genes (DEGs) in response to Fo5176 infection over time. (Sheet 1)** Significant DEGs in Arabidopsis roots upon infection with Fo5176 at different time points after treatment (dpt) with Fo5176 microconidia compared to mock-treated roots. Logarithmic fold-change (logFC) and corrected p-value (FDR) are presented in columns for each time point separately, gaps correspond to non-significant changes in gene expression at those time points. The genes are clustered based on their co-expression (Figure 2A). DEGs with the entry “no cluster” were not associated to a cluster by the clustering algorithm. Genes encoding proteins containing a CAZY-domain or related with plant cell wall biology are highlighted in yellow and orange, respectively. **(Sheet 2)** GO-enrichment analysis of the clusters from (Sheet 1). GO-ID: Gene ontology identifier, GO-term: Gene ontology descriptive term, Bonferroni-corrected p-value, % of associated genes: percentage of genes in that GO-term that are present in the analysed cluster, No. of genes: absolute number of genes associated to the GO-term.

**Table 3. Differentially expressed genes in *ctl1-2* mutant compared to WT. (Sheet 1)** Significant DEGs in *ctl1-2* 14-days old roots compared to its WT (Col-0). Logarithmic fold-change (logFC) and corrected p-value (FDR) are presented. Genes encoding proteins containing a CAZY-domain, related with plant cell wall, or with hormone biology are highlighted in yellow, orange and green, respectively. **(Sheet 2)** GO-enrichment of all upregulated genes from (Sheet1) GO-ID: Gene ontology identifier, GO-term: Gene ontology descriptive term; % of associated genes: percentage of genes in that GO-term that are present in the analysed cluster; No. of genes: absolute number of genes associated to the GO-term.

**Table 4. Comparison of published Arabidopsis root-Fo5176 transcriptomic studies.** All published Arabidopsis root DEGs in response to Fo5176 (Chen et al. (2dpt) [12] and Lyons et al. (1dpt and 6dpt) [13]) were compared to the DEGs we obtained in our study. Genes highlighted in grey are identified as DEGs in our transcriptomic. Cell wall- and hormone-related DEGs reported in any of the previous studies and ours are highlighted in orange and green, respectively.

## Supplemental Tables

### Supplemental Table 1. Primers used in this study

Gene name	Primer 1	Primer 2
<i>cesa3-3_Hpy188I</i> (AT5G05170) <sup>a</sup>	TGTTTGCCTATACTGTTTC CCA	GTGCACGAGGCTCTATGCTA
<i>coi1-34</i> (AT2G39940) <sup>b</sup>	GGTTCTCTTTAGTCTTTAC	CAGACAACTATTTTCGTTACC

# ANNEX

<i>LEC-IX.2</i> ( <i>AT5G65600</i> ) <i>RT-qPCR</i>	CCTCGCTAAGGTTCTGCC AT	CAAACCCGGAAGCCGAAATG
<i>WAKL10</i> ( <i>AT1G79680</i> ) <i>RT-qPCR</i>	TCGTGCTAGCGGAGCTAA TC	TCCTTGCAATTTTTGCGGCT
<i>GLRLK1</i> ( <i>AT4G21390</i> ) <i>RT-qPCR</i>	CGCAGCCGAATCTTGAAC AC	GAATGCTTGCAGGCTTGGTA
<i>CERK1</i> ( <i>AT3G21630</i> ) <i>RT-qPCR</i>	GATTTCTGCGAAAGGTGC GG	CGGGTAACTATCACCGAGCC
<i>FLA11</i> ( <i>AT5G03170</i> ) <i>RT-qPCR</i>	CTGAGAAAGGCGGCTCTG TT	ATGGCTGCAACGGTAGTGAT
<i>JAZ1</i> ( <i>AT1G19180</i> ) <i>RT-qPCR</i>	TTCTGAGTTCGTCGGTAGC C	AGGCTTGCATGCCATTCCTA
<i>Fo5197.g14528</i> <i>RT-qPCR</i>	GCCATTTCCAACCACGCTT T	TCATGGGGATGACGGTCGTA
<i>Fo5176.g4544</i> <i>RT-qPCR</i>	GCTGGCACTTACACTCCCT T	TGCTCTCATCACAGGCGAAG
<i>Fo5176.g13621</i> <i>RT-qPCR</i>	CCCACCCCTCTTACTCTCC A	GTGCGAGATACACCGAGGAG
<i>Fo5176.g8380</i> <i>RT-qPCR</i>	AAGGCTATGGCCAAGTTC CC	CAAGTCCGACATGAGTCCCC
<i>Fo5176.g4128</i> <i>RT-qPCR</i>	CATGAGTTGCCGTTCTCGT G	CGCCGAGGTTGGTAACAGTA
<i>Fo5176.g10760</i> <i>RT-qPCR</i>	TCGACCGAGACTGTCTTT GC	CAGCCCTTGACGACATGTGA
<i>Fo5176.g4360</i> <i>RT-qPCR</i>	AACTCCGATGAGACCTTC TG	GACATGACAGCAGAAACGAG
<i>AT_GAPDH_3'</i> <i>RT-qPCR</i>	TTGGTGACAACAGGTCAA GCA	AAACTTGTCGCTCAATGCAATC
<i>AT_GAPDH_5'</i> <i>RT-qPCR</i>	TCTCGATCTCAATTTTCGCA AAA	CGAAACCGTTGATTCCGATTC

<sup>a</sup> Amplification products were digested with *Hpy188I*; cut products of 212, 58, 48bp were confirmed as WT, while cut products of 261 and 58bp were confirmed as *cesa3-3* mutants.

<sup>b</sup> These primers were used for gene-specific sequencing to confirm point-mutation

**Supplemental Table 2. Overview of read counts mapping to Arabidopsis and Fo5176. (Sheet 1)** Read mapping overview of sequencing libraries mapped to the Arabidopsis reference genome (TAIR10, [33]) or the Fo5176 reference genome [10]. **(Sheet 2)** Arabidopsis and Fo5176 mapped genes with  $\geq 3$  CPM (counts per million). Genes with  $<3$  CPM in all samples were excluded from differential gene expression analysis. **(Sheet 3)** Read mapping overview of sequencing libraries of *ctl1-2* and WT (Col-0) mapped to the Arabidopsis reference genome (TAIR10, [33]) and overview of genes detected with CPM  $\geq 3$  compared to all genes used for analysis.

**Supplemental Tables 3A-G. Statistical analysis of root vascular penetrations upon Fo5176 pSIX1::GFP infection.** Repeated measures two-way ANOVA with post-hoc Tukey test for multiple comparisons corresponding to root vascular penetration events (*p-value*  $< 0.05$  \*, 0.01 \*\*, 0.001 \*\*\*, 0.0001 \*\*\*\*). Days on which there were no statistically significant differences (*p-value*  $> 0.05$ ) are not included in the tables.

## References

1. Kesten C, Menna A, Sánchez-Rodríguez C. Regulation of cellulose synthesis in response to stress. *Curr Opin Plant Biol.* 2017;40:106–13. doi:10.1016/j.pbi.2017.08.010.
2. Rui Y, Dinneny JR. A wall with integrity: surveillance and maintenance of the plant cell wall under stress. *New Phytol.* 2020;225:1428–39. doi:10.1111/nph.16166.
3. Tenhaken R. Cell wall remodeling under abiotic stress. *Front Plant Sci.* 2015;5 January:1–9. doi:10.3389/fpls.2014.00771.
4. Michielse CB, Rep M. Pathogen profile update: *Fusarium oxysporum*. *Mol Plant Pathol.* 2009;10:311–24. doi:10.1111/j.1364-3703.2009.00538.x.
5. Gawehns F, Houterman PM, Ichou FA, Michielse CB, Hijdra M, Cornelissen BJC, et al. The *Fusarium oxysporum* Effector Six6 Contributes to Virulence and Suppresses I-2-Mediated Cell Death. *Mol Plant Microbe Interact.* 2014;27:336–48. doi:10.1094/MPMI-11-13-0330-R.
6. Liu L, Sonbol FM, Huot B, Gu Y, Withers J, Mwimba M, et al. Salicylic acid receptors activate jasmonic acid signalling through a non-canonical pathway to promote effector-triggered immunity. *Nat Commun.* 2016;7:1–10. doi:10.1038/ncomms13099.
7. Di X, Takken FLW, Tintor N. How Phytohormones Shape Interactions between Plants and the Soil-Borne Fungus *Fusarium oxysporum*. *Front Plant Sci.* 2016;7 February:1–9. doi:10.3389/fpls.2016.00170.
8. Di X, Gomila J, Takken FLW. Involvement of salicylic acid, ethylene and jasmonic acid signalling pathways in the susceptibility of tomato to *Fusarium oxysporum*. *Mol Plant Pathol.*

2017;1:1–12. doi:10.1111/mpp.12559.

9. Thatcher LF, Gardiner DM, Kazan K, Manners JM. A Highly Conserved Effector in *Fusarium oxysporum* Is Required for Full Virulence on *Arabidopsis*. *Mol Plant Microbe Interact*. 2012;25:180–90. doi:10.1094/MPMI-08-11-0212.

10. Fokkens L, Guo L, Dora S, Wang B, Ye K, Sánchez-Rodríguez C, et al. A Chromosome-Scale Genome Assembly for the *Fusarium oxysporum* Strain Fo5176 To Establish a Model *Arabidopsis*-Fungal Pathosystem. *G3*. 2020;10:3549–55. doi:10.1534/g3.120.401375.

11. Kesten C, Gámez-Arjona FM, Menna A, Scholl S, Dora S, Huerta AI, et al. Pathogen-induced pH changes regulate the growth-defense balance in plants. *EMBO J*. 2019;38. doi:10.15252/embj.2019101822.

12. Chen YC, Wong CL, Muzzi F, Vlaardingerbroek I, Kidd BN, Schenk PM. Root defense analysis against *Fusarium oxysporum* reveals new regulators to confer resistance. *Sci Rep*. 2014;4:5584. doi:10.1038/srep05584.

13. Lyons R, Stiller J, Powell J, Rusu A, Manners JM, Kazan K. *Fusarium oxysporum* triggers tissue-specific transcriptional reprogramming in *Arabidopsis thaliana*. *PLoS One*. 2015;10:1–23. doi:10.1371/journal.pone.0121902.

14. Jonkers W, Rep M. Mutation of CRE1 in *Fusarium oxysporum* reverts the pathogenicity defects of the FRP1 deletion mutant. *Mol Microbiol*. 2009;74:1100–13. doi:10.1111/j.1365-2958.2009.06922.x.

15. Cosgrove DJ. Growth of the plant cell wall. *Nat Rev Mol Cell Biol*. 2005;6:850–61. doi:10.1038/nrm1746.

16. Cosgrove DJ. Re-constructing our models of cellulose and primary cell wall assembly. *Curr Opin Plant Biol*. 2014;22:122–31. doi:10.1016/j.pbi.2014.11.001.

17. McFarlane HE, Döring A, Persson S. The Cell Biology of Cellulose Synthesis. *Annu Rev Plant Biol*. 2014;65:69–94. doi:10.1146/annurev-arplant-050213-040240.

18. Lampugnani ER, Khan GA, Somssich M, Persson S. Building a plant cell wall at a glance. *J Cell Sci*. 2018;131. doi:10.1242/jcs.207373.

19. Fagard M, Desnos T, Desprez T, Goubet F, Refregier G, Mouille G, et al. PROCUSTE1 encodes a cellulose synthase required for normal cell elongation specifically in roots and dark-grown hypocotyls of *Arabidopsis*. *Plant Cell*. 2000;12:2409–24. doi:10.1105/tpc.12.12.2409.

20. Desnos T, Orbović V, Bellini C, Kronenberger J, Caboche M, Traas J, et al. Procuste1 mutants identify two distinct genetic pathways controlling hypocotyl cell elongation, respectively in dark- and light-grown *Arabidopsis* seedlings. *Development*. 1996;122:683–93. <https://www.ncbi.nlm.nih.gov/pubmed/8625819>.

21. Sánchez-Rodríguez C, Bauer S, Hématy K, Saxe F, Ibáñez AB, Vodermaier V, et al. CHITINASE-LIKE1/POM-POM1 and Its Homolog CTL2 Are Glucan-Interacting Proteins Important for Cellulose Biosynthesis in *Arabidopsis*. *Plant Cell*. 2012;24:589–607. doi:10.1105/tpc.111.094672.

22. Schindelman G, Morikami A, Jung J, Baskin TI, Carpita NC, Derbyshire P, et al. COBRA encodes a putative GPI-anchored protein, which is polarly localized and necessary for oriented cell expansion in Arabidopsis. *Genes Dev.* 2001;15:1115–27. doi:10.1101/gad.879101.
23. Nicol F, His I, Jauneau A, Vernhettes S, Canut H, Höfte H. A plasma membrane-bound putative endo-1,4- $\beta$ -D-glucanase is required for normal wall assembly and cell elongation in Arabidopsis. *EMBO J.* 1998;17:5563–76. doi:10.1093/emboj/17.19.5563.
24. Cano-Delgado A, Penfield S, Smith C, Catley M, Bevan M. Reduced cellulose synthesis invokes lignification and defense responses in Arabidopsis thaliana. *Plant J.* 2003;34:351–62. doi:10.1046/j.1365-313X.2003.01729.x.
25. Lee M-H, Jeon HS, Kim SH, Chung JH, Roppolo D, Lee H-J, et al. Lignin-based barrier restricts pathogens to the infection site and confers resistance in plants. *EMBO J.* 2019;:1–17. doi:10.15252/embj.2019101948.
26. Bürger M, Chory J. Stressed Out About Hormones: How Plants Orchestrate Immunity. *Cell Host Microbe.* 2019;26:163–72. doi:10.1016/j.chom.2019.07.006.
27. Mielke S, Zimmer M, Meena MK, Dreos R, Stellmach H, Hause B, et al. Jasmonate biosynthesis arising from altered cell walls is prompted by turgor-driven mechanical compression. *Sci Adv.* 2021;7. doi:10.1126/sciadv.abf0356.
28. Ellis C, Turner JG. The Arabidopsis mutant cev1 has constitutively active jasmonate and ethylene signal pathways and enhanced resistance to pathogens. *Plant Cell.* 2001;13:1025–33. doi:10.1105/tpc.13.5.1025.
29. Ellis C, Karafyllidis I, Wasternack C, Turner JG. The Arabidopsis mutant cev1 links cell wall signaling to jasmonate and ethylene responses. *Plant Cell.* 2002;14:1557–66. doi:10.1105/tpc.002022.
30. Ellis C, Karafyllidis I, Turner JG. Constitutive activation of jasmonate signaling in an Arabidopsis mutant correlates with enhanced resistance to Erysiphe cichoracearum, Pseudomonas syringae, and Myzus persicae. *Mol Plant Microbe Interact.* 2002;15:1025–30. doi:10.1094/MPMI.2002.15.10.1025.
31. Chuberre C, Plancot B, Driouich A, Moore JP, Bardor M, Gügi B, et al. Plant Immunity Is Compartmentalized and Specialized in Roots. *Front Plant Sci.* 2018;9:1692. doi:10.3389/fpls.2018.01692.
32. Kesten C, Gámez-Arjona FM, Scholl S, Menna A, Dora S, Huerta AI, et al. Pathogen-induced pH changes regulate the growth-defense balance of plants. *EMBO J.* 2019;e101822. doi:10.1101/550491.
33. Berardini TZ, Reiser L, Li D, Mezheritsky Y, Muller R, Strait E, et al. The Arabidopsis information resource: Making and mining the “gold standard” annotated reference plant genome. *Genesis.* 2015;53:474–85. doi:10.1002/dvg.22877.
34. Edgar R, Domrachev M, Lash AE. Gene Expression Omnibus: NCBI gene expression and hybridization array data repository. *Nucleic Acids Res.* 2002;30:207–10. doi:10.1093/nar/30.1.207.



35. Kumar L, E Futschik M. Mfuzz: a software package for soft clustering of microarray data. *Bioinformation*. 2007;2:5–7. doi:10.6026/97320630002005.
36. The Gene Ontology Consortium. The Gene Ontology Resource : 20 years and still GOing strong. *Nucleic Acids Res*. 2019;47 vember 2018:330–8. doi:10.1093/nar/gky1055.
37. Endler A, Persson S. Cellulose synthases and synthesis in Arabidopsis. *Mol Plant*. 2011;4:199–211. doi:10.1093/mp/ssq079.
38. Schultz CJ, Johnson KL, Currie G, Bacic A. The Classical Arabinogalactan Protein Gene Family of Arabidopsis. *Plant Cell*. 2000;12:1751–67. doi:10.1105/tpc.12.9.1751.
39. Stotz HU, Thomson JG, Wang Y. Plant defensins: defense, development and application. *Plant Signal Behav*. 2009;4:1010–2. doi:10.4161/psb.4.11.9755.
40. Zheng Z, Qamar SA, Chen Z, Mengiste T. Arabidopsis WRKY33 transcription factor is required for resistance to necrotrophic fungal pathogens. *Plant J*. 2006;48:592–605. doi:10.1111/j.1365-313X.2006.02901.x.
41. Anderson JP. Antagonistic Interaction between Abscissic Acid and Jasmonate-Ethylene Signaling Pathways Modulates Defense Gene Expression and Disease Resistance in Arabidopsis. *the Plant Cell Online*. 2004;16:3460–79. doi:10.1105/tpc.104.025833.
42. Ross A, Yamada K, Hiruma K, Yamashita-Yamada M, Lu X, Takano Y, et al. The Arabidopsis PEPR pathway couples local and systemic plant immunity. *EMBO J*. 2014;33:62–75. doi:10.1002/embj.201284303.
43. Daudi A, Cheng Z, O'Brien JA, Mammarella N, Khan S, Ausubel FM, et al. The apoplastic oxidative burst peroxidase in Arabidopsis is a major component of pattern-triggered immunity. *Plant Cell*. 2012;24:275–87. doi:10.1105/tpc.111.093039.
44. Tripathi D, Zhang T, Koo AJ, Stacey G, Tanaka K. Extracellular ATP Acts on Jasmonate Signaling to Reinforce Plant Defense. *Plant Physiol*. 2018;176:511–23. doi:10.1104/pp.17.01477.
45. Pré M, Atallah M, Champion A, De Vos M, Pieterse CMJ, Memelink J. The AP2/ERF Domain Transcription Factor ORA59 Integrates Jasmonic Acid and Ethylene Signals in Plant Defense. *Plant Physiol*. 2008;147:1347–57. doi:10.1104/pp.108.117523.
46. Meng X, Xu J, He Y, Yang K-Y, Mordorski B, Liu Y, et al. Phosphorylation of an ERF Transcription Factor by Arabidopsis MPK3/MPK6 Regulates Plant Defense Gene Induction and Fungal Resistance. *Plant Cell*. 2013;25:1126–42. doi:10.1105/tpc.112.109074.
47. Acosta IF, Gasperini D, Chételat A, Stolz S, Santuari L, Farmer EE. Role of NINJA in root jasmonate signaling. *Proc Natl Acad Sci U S A*. 2013;110:15473–8. doi:10.1073/pnas.1307910110.
48. Gasperini D, Chételat A, Acosta IF, Goossens J, Pauwels L, Goossens A, et al. Multilayered Organization of Jasmonate Signalling in the Regulation of Root Growth. *PLoS Genet*. 2015;11:1–27. doi:10.1371/journal.pgen.1005300.
49. Hernández-Blanco C, Feng DX, Hu J, Sánchez-Vallet A, Deslandes L, Llorente F, et al. Impairment of cellulose synthases required for Arabidopsis secondary cell wall formation

- enhances disease resistance. *Plant Cell*. 2007;19:890–903. doi:10.1105/tpc.106.048058.
50. Miedes E, Vanholme R, Boerjan W, Molina A. The role of the secondary cell wall in plant resistance to pathogens. *Front Plant Sci*. 2014;5 August:1–13. doi:10.3389/fpls.2014.00358.
  51. Xie M, Zhang J, Tschaplinski TJ, Tuskan GA, Chen JG, Muchero W. Regulation of lignin biosynthesis and its role in growth-defense tradeoffs. *Front Plant Sci*. 2018;9 September:1–9. doi:10.3389/fpls.2018.01427.
  52. Sánchez-Rodríguez C, Rubio-Somoza I, Sibout R, Persson S. Phytohormones and the cell wall in *Arabidopsis* during seedling growth. *Trends Plant Sci*. 2010;15:291–301. doi:10.1016/j.tplants.2010.03.002.
  53. Qi PF, Balcerzak M, Rocheleau H, Leung W, Wei YM, Zheng YL, et al. Jasmonic acid and abscisic acid play important roles in host-pathogen interaction between *Fusarium graminearum* and wheat during the early stages of fusarium head blight. *Physiol Mol Plant Pathol*. 2016;93:39–48. doi:10.1016/j.pmpp.2015.12.004.
  54. Park J-H, Halitschke R, Kim HB, Baldwin IT, Feldmann KA. A knock-out mutation in allene oxide synthase results in male sterility and defective wound signal transduction in *Arabidopsis* due to a block in jasmonic acid biosynthesis. *Plant J*. 2002;31:1–12.
  55. Thines B, Katsir L, Melotto M, Niu Y, Mandaokar A, Liu G, et al. JAZ repressor proteins are targets of the SCF(COI1) complex during jasmonate signalling. *Nature*. 2007;448:661–5. doi:10.1038/nature05960.
  56. Wang KLC, Li H, Ecker JR. Ethylene biosynthesis and signaling networks. *Plant Cell*. 2002;14 SUPPL.:131–52. doi:10.1105/tpc.001768.
  57. Alonso JM, Hirayama T, Roman G, Nourizadeh S, Ecker JR. EIN2, a bifunctional transducer of ethylene and stress responses in *Arabidopsis*. *Science*. 1999;284:2148–52. doi:10.1126/science.284.5423.2148.
  58. Guzmán P, Ecker JR. Exploiting the triple response of *Arabidopsis* to identify ethylene-related mutants. *Plant Cell*. 1990;2:513–23. doi:10.1105/tpc.2.6.513.
  59. Zhao C, Wang H, Lu Y, Hu J, Qu L, Li Z, et al. Deep sequencing reveals early reprogramming of *Arabidopsis* root transcriptomes upon *Ralstonia solanacearum* infection. *Mol Plant Microbe Interact*. 2019;31:813–27. doi:10.1094/MPMI-10-18-0268-R.
  60. Morales J, Kadota Y, Zipfel C, Molina A, Torres M-A. The *Arabidopsis* NADPH oxidases *RbohD* and *RbohF* display differential expression patterns and contributions during plant immunity. *Journal of Experimental Botany*. 2016;67:1663–76. doi:10.1093/jxb/erv558.
  61. Penninckx IA, Eggermont K, Terras FR, Thomma BP, De Samblanx GW, Buchala A, et al. Pathogen-induced systemic activation of a plant defensin gene in *Arabidopsis* follows a salicylic acid-independent pathway. *Plant Cell*. 1996;8:2309–23. doi:10.1105/tpc.8.12.2309.
  62. Zhou F, Emonet A, Dénervaud Tendon V, Marhavy P, Wu D, Lahaye T, et al. Co-incidence of Damage and Microbial Patterns Controls Localized Immune Responses in Roots. *Cell*. 2020;180:440–53.e18. doi:10.1016/j.cell.2020.01.013.

63. Digonnet C, Martinez Y, Denancé N, Chasseray M, Dabos P, Ranocha P, et al. Deciphering the route of *Ralstonia solanacearum* colonization in *Arabidopsis thaliana* roots during a compatible interaction: Focus at the plant cell wall. *Planta*. 2012;236:1419–31. doi:10.1007/s00425-012-1694-y.
64. Pedreira J, Herrera MT, Zarra I, Revilla G. The overexpression of AtPrx37, an apoplastic peroxidase, reduces growth in *Arabidopsis*. *Physiol Plant*. 2011;141:177–87. doi:10.1111/j.1399-3054.2010.01427.x.
65. Fernández-Pérez F, Pomar F, Pedreño MA, Novo-Uzal E. The suppression of AtPrx52 affects fibers but not xylem lignification in *Arabidopsis* by altering the proportion of syringyl units. *Physiol Plant*. 2015;154:395–406. doi:10.1111/ppl.12310.
66. Norman-Setterblad C, Vidal S, Palva ET. Interacting signal pathways control defense gene expression in *Arabidopsis* in response to cell wall-degrading enzymes from *Erwinia carotovora*. *Mol Plant Microbe Interact*. 2000;13:430–8. doi:10.1094/MPMI.2000.13.4.430.
67. Berrocal-Lobo M, Molina A. Ethylene response factor 1 mediates *Arabidopsis* resistance to the soilborne fungus *Fusarium oxysporum*. *Mol Plant Microbe Interact*. 2004;17:763–70. doi:10.1094/MPMI.2004.17.7.763.
68. Zhang LL, Ma XF, Zhou BB, Zhao JQ, Fan J, Huang F, et al. EDS1-mediated basal defense and SA-signaling contribute to post-invasion resistance against tobacco powdery mildew in *Arabidopsis*. *Physiol Mol Plant Pathol*. 2015;91:120–30. doi:10.1016/j.pmpp.2015.07.004.
69. Zhang L, Zhang F, Melotto M, Yao J, He SY. Jasmonate signaling and manipulation by pathogens and insects. *J Exp Bot*. 2017;68:1371–85. doi:10.1093/jxb/erw478.
70. Thatcher LF, Manners JM, Kazan K. *Fusarium oxysporum* hijacks COI1-mediated jasmonate signaling to promote disease development in *Arabidopsis*. *Plant J*. 2009;58:927–39. doi:10.1111/j.1365-3113.2009.03831.x.
71. Li C, Shao J, Wang Y, Li W, Guo D, Yan B, et al. Analysis of banana transcriptome and global gene expression profiles in banana roots in response to infection by race 1 and tropical race 4 of *Fusarium oxysporum* f. sp. *cubense*. *BMC Genomics*. 2013;14:1–16. doi:10.1186/1471-2164-14-851.
72. Zhu Q-H, Stephen S, Kazan K, Jin G, Fan L, Taylor J, et al. Characterization of the defense transcriptome responsive to *Fusarium oxysporum*-infection in *Arabidopsis* using RNA-seq. *Gene*. 2013;512:259–66. doi:10.1016/j.gene.2012.10.036.
73. Hermans C, Porco S, Verbruggen N, Bush DR. Chitinase-Like Protein CTL1 Plays a Role in Altering Root System Architecture in Response to Multiple Environmental Conditions. *Plant Physiol*. 2010;152:904–17. doi:10.1104/pp.109.149849.
74. Liu L, Shang-Guan K, Zhang B, Liu X, Yan M, Zhang L, et al. Brittle Culm1, a COBRA-Like Protein, Functions in Cellulose Assembly through Binding Cellulose Microfibrils. *PLoS Genet*. 2013;9. doi:10.1371/journal.pgen.1003704.
75. Ko J-H, Kim JH, Jayanty SS, Howe GA, Han K-H. Loss of function of COBRA, a determinant of oriented cell expansion, invokes cellular defence responses in *Arabidopsis*

*thaliana*. J Exp Bot. 2006;57:2923–36. doi:10.1093/jxb/erl052.

76. Vanholme R, Storme V, Vanholme B, Sundin L, Christensen JH, Goeminne G, et al. A systems biology view of responses to lignin biosynthesis perturbations in *Arabidopsis*. Plant Cell. 2012;24:3506–29. doi:10.1105/tpc.112.102574.

77. Robles LM, Wampole JS, Christians MJ, Larsen PB. *Arabidopsis* enhanced ethylene response 4 encodes an EIN3-interacting TFIID transcription factor required for proper ethylene response, including ERF1 induction. J Exp Bot. 2007;58:2627–39. doi:10.1093/jxb/erm080.

78. Michielse CB, van Wijk R, Reijnen L, Cornelissen BJC, Rep M. Insight into the molecular requirements for pathogenicity of *Fusarium oxysporum* f. sp. *lycopersici* through large-scale insertional mutagenesis. Genome Biol. 2009;10:R4. doi:10.1186/gb-2009-10-1-r4.

79. Takken FLW, Van Wijk R, Michielse CB, Houterman PM, Ram AFJ, Cornelissen BJC. A one-step method to convert vectors into binary vectors suited for *Agrobacterium*-mediated transformation. Curr Genet. 2004;45:242–8. doi:10.1007/s00294-003-0481-5.

80. Huerta AI, Kesten C, Menna A, Sancho Andrés G, Sanchez-Rodriguez C. In-plate quantitative characterization of *Arabidopsis thaliana* susceptibility to the fungal vascular pathogen - *Fusarium oxysporum*. Current Protocols in Plant Biology. 2020;CP-20-0080 Accepted.

81. Monteiro F, Solé M, van Dijk I, Valls M. A chromosomal insertion toolbox for promoter probing, mutant complementation, and pathogenicity studies in *Ralstonia solanacearum*. Mol Plant Microbe Interact. 2012;25:557–68. doi:10.1094/MPMI-07-11-0201.

82. Hatakeyama M, Opitz L, Russo G, Qi W, Schlapbach R, Rehrauer H. SUSHI: an exquisite recipe for fully documented, reproducible and reusable NGS data analysis. BMC Bioinformatics. 2016;17:228. doi:10.1186/s12859-016-1104-8.

83. Bolger AM, Lohse M, Usadel B. Trimmomatic: a flexible trimmer for Illumina sequence data. Bioinformatics. 2014;30:2114–20. doi:10.1093/bioinformatics/btu170.

84. Dodt M, Roehr JT, Ahmed R, Dieterich C. FLEXBAR—Flexible Barcode and Adapter Processing for Next-Generation Sequencing Platforms. Biology . 2012;1:895–905. doi:10.3390/biology1030895.

85. Dobin A, Davis CA, Schlesinger F, Drenkow J, Zaleski C, Jha S, et al. (2012) STAR: ultrafast universal RNA-seq aligner.. Bioinformatics. 2012;29:292–3.

86. Liao Y, Smyth GK, Shi W. featureCounts: an efficient general purpose program for assigning sequence reads to genomic features. Bioinformatics. 2014;30:923–30. doi:10.1093/bioinformatics/btt656.

87. Liao Y, Smyth GK, Shi W. The R package Rsubread is easier, faster, cheaper and better for alignment and quantification of RNA sequencing reads. Nucleic Acids Res. 2019;47:e47. doi:10.1093/nar/gkz114.

88. McCarthy DJ, Chen Y, Smyth GK. Differential expression analysis of multifactor RNA-Seq experiments with respect to biological variation. Nucleic Acids Res. 2012;40:4288–97. doi:10.1093/nar/gks042.

89. Robinson MD, Oshlack A. A scaling normalization method for differential expression analysis of RNA-seq data. *Genome Biol.* 2010;11. doi:10.1186/gb-2010-11-3-r25.
90. Bindea G, Mlecnik B, Hackl H, Charoentong P, Tosolini M, Kirilovsky A, et al. ClueGO: a Cytoscape plug-in to decipher functionally grouped gene ontology and pathway annotation networks. *Bioinformatics.* 2009;25:1091–3. doi:10.1093/bioinformatics/btp101.
91. Shannon P, Markiel A, Ozier O, Baliga NS, Jt JTW. Cytoscape: a software environment for integrated models. *Genome Res.* 2019;13:426. [https://icbi.med.ac.at/courses/bioinformatics\\_ex\\_2020/14597658.pdf](https://icbi.med.ac.at/courses/bioinformatics_ex_2020/14597658.pdf).
92. Ilias IA, Negishi K, Yasue K, Jomura N, Morohashi K, Baharum SN, et al. Transcriptome-wide effects of expansin gene manipulation in etiolated Arabidopsis seedling. *J Plant Res.* 2019;132:159–72. doi:10.1007/s10265-018-1067-0.
93. Zhang H, Yohe T, Huang L, Entwistle S, Wu P, Yang Z, et al. dbCAN2: a meta server for automated carbohydrate-active enzyme annotation. *Nucleic Acids Res.* 2018;46:W95–101. doi:10.1093/nar/gky418.
94. Czechowski T, Stitt M, Altmann T, Udvardi MK, Scheible W-R. Genome-wide identification and testing of superior reference genes for transcript normalization in Arabidopsis. *Plant Physiol.* 2005;139:5–17. doi:10.1104/pp.105.063743.
95. Livak KJ, Schmittgen TD. Analysis of relative gene expression data using real-time quantitative PCR and the 2- $\Delta\Delta CT$  method. *Methods.* 2001;25:402–8. [https://www.researchgate.net/profile/Laurence\\_Dawkins-Hall/post/Could\\_you\\_please\\_help\\_me\\_finding\\_the\\_best\\_way\\_of\\_qPCR\\_analysis\\_when\\_using\\_two\\_reference\\_genes/attachment/59d6328f79197b8077990489/AS:370973569241091@1465458399850/download/Delta+Delta+Ct+analysis\\_Livak.pdf](https://www.researchgate.net/profile/Laurence_Dawkins-Hall/post/Could_you_please_help_me_finding_the_best_way_of_qPCR_analysis_when_using_two_reference_genes/attachment/59d6328f79197b8077990489/AS:370973569241091@1465458399850/download/Delta+Delta+Ct+analysis_Livak.pdf).
96. Schoch GA, Nikov GN, Alworth WL, Werck-Reichhart D. Chemical inactivation of the cinnamate 4-hydroxylase allows for the accumulation of salicylic acid in elicited cells. *Plant Physiol.* 2002;130:1022–31. doi:10.1104/pp.004309.